Monitoring, Diagnosis, and Fault-Tolerant Control of Wind Turbines

Hamed Badihi

A Thesis
In the Department
of
Mechanical and Industrial Engineering

Presented in Partial Fulfillment of the Requirements
For the Degree of
Doctor of Philosophy (Mechanical Engineering) at
Concordia University
Montreal, Quebec, Canada

April 2016

CONCORDIA UNIVERSITY SCHOOL OF GRADUATE STUDIES

This is to certify that the thesis prepared

By: **Hamed Badihi**

Entitled: **Monitoring, Diagnosis, and Fault-Tolerant Control of Wind Turbines**

and submitted in partial fulfillment of the requirements for the degree of

Doctor of Philosophy (Mechanical Engineering)

complies with the regulations of the University and meets the accepted standards with respect to originality and quality.

Signed by the final examining committee:

Dr. P. Pillay, Chair

Dr. G. Joos, External Examiner

Dr. A. Aghdam, External to Program

Dr. W. Xie, Examiner

Dr. B. Gordon, Examiner

Dr. Y. M. Zhang, Thesis Supervisor

Dr. H. Hong, Thesis Co-Supervisor

Approved by

Chair of Department or Graduate Program Director

Dean of Faculty

ABSTRACT

Monitoring, Diagnosis, and Fault-Tolerant Control of Wind Turbines

Hamed Badihi

Concordia University, 2016

Governments across the globe are funding renewable energy initiatives like wind energy to diversify energy resources and promote a greater environmental responsibility. Such an opportunity requires state-of-the-art technologies to realize the required levels of efficiency, reliability, and availability in modern wind turbines. The key enabling technologies for ensuring reliable and efficient operation of modern wind turbines include advanced condition monitoring and diagnosis together with fault-tolerant and efficiency/optimal control. Application of the mentioned technologies in wind turbines constitutes a quite active and, in many aspects, interdisciplinary investigation area that ensures a guaranteed increasing future market for wind energy. In particular, this thesis aims to design and develop novel condition monitoring, diagnosis and fault-tolerant control schemes with application to wind turbines at both individual wind turbine and entire wind farm (i.e., a group of wind turbines) levels. Therefore, the research of the thesis provides advanced levels of monitoring, diagnosis and fault tolerance capabilities to wind turbines in order to ensure their efficient and reliable performance under both fault-free and faulty conditions. Finally, the proposed schemes and strategies are verified by a series of simulations on well-known wind turbine and wind farm benchmark models in the presence of wind turbulences, measurement noises, and different realistic fault scenarios.

List of Publications

- **Journal Papers**

1) H. Badihi**,** Y. M. Zhang, and H. Hong, "**Fault-Tolerant Cooperative Control in an Offshore Wind Farm Using Model-Free and Model-Based Fault Detection and Diagnosis**", Submitted to Applied Energy (Submitted in April 2016).

2) H. Badihi**,** Y. M. Zhang, and H. Hong, "**Active Power Control Design for Supporting Grid Frequency Regulation in Wind Farms**", IFAC Annual Reviews in Control, Vol. 40, pp. 70–81, 12 pages, doi: 10.1016/j.arcontrol.2015.09.005 (2015). (Among List of Popular Articles in 2016).

3) H. Badihi**,** Y. M. Zhang, and H. Hong, "**Wind Turbine Fault Diagnosis and Fault-Tolerant Torque Load Control against Actuator Faults**", IEEE Transactions on Control Systems Technology, Vol. 23, No. 4, pp. 1351-1372, 22 pages, doi: 10.1109/TCST.2014.2364956 (2015). (Among List of Popular Articles in 2015)

4) H. Badihi, Y. M. Zhang, H. Hong, "**Fuzzy Gain-Scheduled Active Fault-Tolerant Control of a Wind Turbine**", Journal of the Franklin Institute (JFI), Vol. 351, No. 7, pp. 3677–3706, 30 pages, doi: 10.1016/j.jfranklin.2013.05.007 (2014). (Among List of Popular Articles in 2014)

5) A. Vargas-Martínez, L. I. Minchala Avila, Y. M. Zhang, L. E. Garza-Castañón, H. Badihi, "**Hybrid Adaptive Fault-Tolerant Control Algorithms for Voltage and Frequency Regulation of an Islanded Microgrid**", International Transactions on Electrical Energy Systems, Vol. 25, No. 5, pp. 827–844 18 pages, doi:10.1002/etep.1875 (2014).

- **Conference Papers**

1) H. Badihi**,** Y. M. Zhang, and H. Hong, "**Model-Free Active Fault-Tolerant Cooperative Control in an Offshore Wind Farm**", Accepted by the 3rd International Conference on Control and Fault-Tolerant Systems, Barcelona, Spain (7-9 September 2016).

2) H. Badihi**,** Y. M. Zhang, and H. Hong, "**Model-Based Active Fault-Tolerant Cooperative Control in an Offshore Wind Farm**", Presented at the Applied Energy Symposium and Forum: Renewable Energy Integration with Mini/Microgrid, Maldives (17-19 April 2016).

3) H. Badihi**,** Y. M. Zhang, and H. Hong, "**Active Fault Tolerant Control in a Wind Farm with Decreased Power Generation Due to Blade Erosion/Debris Build-up**", Proc. of the 9th IFAC Symposium on Fault Detection, Supervision and Safety for Technical Processes, Paris, France (2-4 September 2015).

4) H. Badihi, J. S. Rad, Y. M. Zhang, H. Hong, "**Data-driven Model-based Fault Diagnosis in a Wind Turbine with Actuator Faults**", Proc. of the ASME 2014 International Mechanical Engineering Congress & Exposition, Montreal, Canada (14-20 November 2014).

5) H. Badihi, Y. M. Zhang, H. Hong, "**Design of a Pole Placement Active Power Control System for Supporting Grid Frequency Regulation and Fault Tolerance in Wind Farms**", Proc. of the 19th IFAC World Congress, Cape Town, South Africa (24-29 August 2014).

6) H. Badihi, Y. M. Zhang, H. Hong, "**An Active Fault-Tolerant Control Approach to Wind Turbine Torque Load Control against Actuator Faults**", Proc. of the 32nd ASME Wind Energy Symposium, AIAA Science and Technology Forum and Exposition (SciTech 2014), National Harbor, Maryland, USA (January 2014).

7) H. Badihi, Y. M. Zhang, H. Hong, "**Model Reference Adaptive Fault-Tolerant Control for a Wind Turbine against Actuator Faults**", Proc. of the 2nd International Conference on Control and Fault-Tolerant Systems (SysTol'13), Nice, France (October 2013).

8) H. Badihi, Y. M. Zhang, H. Hong, "**A Review on Application of Monitoring, Diagnosis, and Fault-Tolerant Control to Wind Turbines**", Proc. of the 2nd International Conference on Control and Fault-Tolerant Systems (SysTol'13), Nice, France (October 2013).

9) H. Badihi, Y. M. Zhang, H. Hong, "**Fault-Tolerant Control Design for a Large Off-Shore Wind Turbine Using Fuzzy Gain-Scheduling and Signal Correction**", Proc. of the American Control Conference (ACC), Washington, DC, USA (June 2013).

Contribution of Authors

This thesis is prepared in manuscript format. Except Chapters 1 and 6 that are devoted to the thesis introduction and conclusion, the rest of the chapters are submitted to/published at scientific journals/conferences. The first author of these manuscripts is Mr. Hamed Badihi who is the author of the current thesis. As the first author of the manuscripts, Mr. Hamed Badihi was responsible for designing and development of all the proposed schemes and presentation of the results. In the following, the name of the journals to which the papers are submitted/published will be given in detail. All the following papers are co-authored by Prof. Youmin Zhang and Prof. Henry Hong who are the Ph.D. supervisors of the first author Mr. Hamed Badihi.

Chapter 2 entitled "Fuzzy Gain-Scheduled Active Fault-Tolerant Control of a Wind Turbine" is a published original regular paper in *Journal of the Franklin Institute*, volume 351, number 7, pages 3677–3706, 2014. The paper had been among List of Popular Articles in the journal during 2014.

Chapter 3 entitled "Wind Turbine Fault Diagnosis and Fault-Tolerant Torque Load Control against Actuator Faults" is a published original regular paper in *IEEE Transactions on Control Systems Technology*, volume 23, number 4, pages 1351-1372, 2015.

Chapter 4 entitled "Fault-Tolerant Cooperative Control in an Offshore Wind Farm Using Model-Free and Model-Based Fault Detection and Diagnosis" is submitted to the *Applied Energy*, 2016.

Chapter 5 entitled "Active Power Control Design for Supporting Grid Frequency Regulation in Wind Farms" is a published original regular paper in IFAC *Annual Reviews in Control*, volume 40, pages 70–81, 2015.

To my parents for their unconditional love, continuous encouragement and endless support during my life.

Acknowledgements

I would like to, cordially, express my deep gratitude to my supervisors Prof. Youmin Zhang and Prof. Henry Hong for their helpful supervision, continuous encouragement, support, and valuable comments throughout the progress of my PhD study. They have been wonderful guides and their advice have been priceless during these years, allowing me to grow as a research scientist.

I would also like to acknowledge Natural Sciences and Engineering Research Council of Canada (NSERC) and Concordia University for their financial support to several parts of this PhD research study. I would like to thank Prof. A. Aghdam, Prof. W. Xie, and Prof. B. Gordon for joining my examining committee and providing useful feedback and brilliant comments during my comprehensive exam and research proposal. Also, I would like to thank my colleagues and friends from the Networked Autonomous Vehicles lab for their valuable discussions, friendship, and kind help during the time I was studying at Concordia.

Finally and most importantly, I would like to thank my parents, Ms. Maliheh Geramian and Mr. Ahmad Badihi, without them I could not make it this far. I would also like to thank my dearest, Azadeh Badihi, and Elham Badihi, for their understanding and encouragement in many moments of crisis.

Thank you Lord for being there for me.

This thesis is only the beginning of my journey.

Table of Contents

List of Figures xiii

List of Tables xx

Nomenclature xxiii

Acronyms xxv

Chapter 1 Introduction 1

1.1 Preface 1

1.2 Wind Energy and Wind Turbines 2

1.3 Frequency of Failures in Wind Turbines and Motivation for FDD and FTC 5

1.4 Fault Diagnosis and Fault-Tolerant Control Systems 7

A) Fault and Failure 7

B) Fault-Tolerant Control 8

C) Fault Detection and Diagnosis 9

1.5 Application of Condition Monitoring, Diagnosis and Fault-Tolerant and Efficiency Control to Wind Turbines 10

D) Condition Monitoring and Fault Diagnosis in Wind Turbines 11

E) Fault-Tolerant and Efficiency Control in Wind Turbines 12

F) Wind Farm Control 15

1.6 Simulation Benchmark Models for Wind Turbines and Wind Farms 16

1.7 Thesis Objectives 18

1.8 Thesis Layout and Contributions 19

Chapter 2 Fuzzy Gain-Scheduled Active Fault-Tolerant Control of a Wind Turbine 22

2.1 Introduction 23

2.2 The Wind Turbine Benchmark Model and Fault Scenarios 26

A) Model Description 26
B) Faults Description 27
2.3 Baseline Control System 28
2.4 Fuzzy Gain-Scheduled PI-Controller Design 29
A) Baseline PI-Control System Description 29
B) Fuzzy Gain-Scheduled PI-Controller Design 31
2.5 Remedial Strategy 35
A) Model-Based FDD Approach 36
B) FDD and FTC Design for Fault Scenarios 40
2.6 Simulation Results and Discussion 47
A) Performance of FGS Blade-Pitch PI-Controller in the Fault-Free Case 48
B) Modeling Accuracy for Fuzzy Models 52
C) FDD Results 53
D) Performance of AFTCS against the Faults 55
E) Fault in Generator Speed Sensor 56
F) Fault in Blade-Pitch Angle Sensor 57
G) Robustness 57
2.7 Conclusion 59
Chapter 3 Wind Turbine Fault Diagnosis and Fault-Tolerant Torque Load Control against Actuator Faults 61
3.1 Introduction 62
3.2 The Wind Turbine Benchmark Model 65
A) Baseline Control System 66
B) Fault Scenarios 67
3.3 Fault Analysis 67

3.4 Description of Pitch-Angle Fuzzy Gain-Scheduled PI-Control 70
3.5 Reference Dynamic Model for FDD and FTC Design 71
A) T-S Fuzzy Modeling 72
B) Fuzzy Model Structure 73
C) Data Preprocessing and Parameter Estimation 75
3.6 Design of Fault-Tolerant Control for Torque Regulation 75
A) Design of Torque PFTC Based on FMRAC Strategy 76
B) Design of Torque AFTC Based on an Integrated FDD and ASC Strategy 80
3.7 Simulation Results and Discussion 84
A) Evaluation of Pitch-Angle Fuzzy Gain-Scheduled PI-Control 85
B) Identification and Validation of the Reference Dynamic Model 87
C) Performance of Torque PFTC Scheme Based on FMRAC 89
D) Performance of Torque AFTC Scheme Based on FDD and ASC (FDD-ASC) 90
E) Evaluation of Wind Turbine Structural Dynamics and Loading during Fault Accommodation 92
F) Comparison of Torque FTC Schemes 95
G) Robustness 99
3.8 Conclusion 102
Chapter 4 Fault-Tolerant Cooperative Control in an Offshore Wind Farm Using Model-Free and Model-Based Fault Detection and Diagnosis 103
4.1 Introduction 104
4.2 Overview of the Wind Farm Benchmark Model 106
4.3 Blade Erosion/Debris Build-up Fault 110
4.4 Integrated FDD and FTC Approach 112
4.5 FDD at Wind Farm Level 115
A) Model-Free Monitoring of Power Consistency 119

B) Model-Based Monitoring of Power Consistency 125
4.6 Simulation Results and Discussion 130
A) Identification and Validation of the Fuzzy Dynamic Model 132
B) Performance of FDD System 133
C) Performance of AFTC Schemes Based on Integrated FDD and FTC Approach 134
D) Evaluation of Wind Farm Structural Dynamics and Loading Results 140
E) Robustness 143
4.7 Conclusion 145
Chapter 5 Active Power Control Design for Supporting Grid Frequency Regulation in Wind Farms 147
5.1 Introduction 148
5.2 Wind Farm Benchmark Model 150
5.3 Electrical Grid Frequency and Active Power Control 154
A) APC Based on Fuzzy Gain-Scheduled PI Control Approach 155
B) APC Based on Adaptive Pole Placement Control Approach 158
5.4 Simulation Results and Discussion 164
A) Performance of Active Power/Frequency Control 165
B) Wind Farm Structural Loading/Fatigue 168
C) Tolerance against Frequency Events 169
D) Robustness 171
5.5 Conclusion 172
Chapter 6 Conclusions and Suggestions for Future Work 174
6.1 Summary and Conclusions 174
6.2 Scope for Research and Future Work 176
References 178

List of Figures

Figure 1.1 Wind turbine designs: (a) horizontal axis and (b) vertical axis. 2
Figure 1.2 Wind turbine designs: (a) horizontal axis and (b) vertical axis (Photo courtesy of the National Renewable Energy Laboratory (NREL)) 3
Figure 1.3 Basic components of a modern, three-bladed horizontal-axis wind turbine (Photo courtesy of NREL). 4
Figure 1.4 Wind turbines: (a) onshore (the Castle River wind farm, Alberta, Canada (Photo by Todd Spink courtesy U.S. Energy Dept.)) and (b) offshore (the Sheringham Shoal wind farm (Photo by Alan O'Neill)). 5
Figure 1.5 Reliability characteristics for different components of wind turbine in the WMEP program [7]. 6
Figure 1.6 Fault classification with respect to (a) time characteristics (b) location.....8
Figure 1.7 A general structure for AFTCS (based on [10]) 9
Figure 1.8 A general structure for model-based FDD.....10
Figure 1.9 Illustration of ideal power curve for a typical wind turbine. 13
Figure 1.10 Block diagram showing pitch, torque and yaw control systems in feedback loops. The generator speed measurement $\omega g,m$ and wind yaw error $\Xi e,m$ are extracted from the measured outputs $\boldsymbol{y}$. The other parameters are defined in the provided Nomenclature. 13
Figure 2.1 Block diagram showing wind turbine simulation model and the pitch, torque and yaw control systems in feedback loops. The measured generator speed $\omega g,m$ and wind yaw error $\Xi e,m$ are extracted from the model output vector $\boldsymbol{y}$. 27
Figure 2.2 Illustration of ideal power curve versus wind speed for operation of a typical wind turbine [16].....28
Figure 2.3 Block diagram of the fuzzy gain-scheduled PI control system. The measured generator speed $\omega g,m$ is extracted from the model output vector $\boldsymbol{y}$. 31
Figure 2.4 Membership functions. (a) inputs, (b) outputs.....33
Figure 2.5 Response surfaces. (a) KP' and (b) KI' 34

Figure 2.6 Schematic of AFTCS using FDD module. Based on FDD information $\boldsymbol{I}(k)$, the supervisor applies appropriate signal correction/modification using estimates (wind turbine states and/or fault biases) $\boldsymbol{x}(k)$. 35
Figure 2.7 Model-based fault detection and diagnosis scheme based on fuzzy models. 36
Figure 2.8 Generator/Rotor speed model-based FDD. 42
Figure 2.9 Pitch system model-based FDD. 45
Figure 2.10 Fault accommodation in a pitch system with biased sensor measurement. 46
Figure 2.11 Pitch sensor bias estimation using fuzzy model of pitch system. The estimated bias $\beta bias$ is computed from the difference between measured pitch value βm and estimated pitch value β. 46
Figure 2.12 Wind speed sequence. 48
Figure 2.13 Generator rotational speed regulation with baseline PI-controller and FGS PI-controller. 49
Figure 2.14 Pitch angle rates during turbine operation using baseline PI-controller and FGS PI-controller. 50
Figure 2.15 Measured generated electrical power during turbine operation using baseline PI-controller and FGS PI-controller. 51
Figure 2.16 Measured generator torque during turbine operation using baseline PI-controller and FGS PI-controller. 51
Figure 2.17 Filtered generator torque during turbine operation using baseline PI-controller and FGS PI-controller. 52
Figure 2.18 FDD result for generator speed sensor. (a) Residuals, and (b) fault indicator. 54
Figure 2.19 FDD result for blade-pitch sensor. (a) Residuals, and (b) fault indicator. 54
Figure 2.20 Generator rotational speed regulation with FGS PI-controller and AFTCS during fault-free and faulty operation of the wind turbine. 56
Figure 2.21 Generator rotational speed regulation with FGS PI-controller and AFTCS during fault-free and faulty operation of the wind turbine – time period [120,170] sec. 56
Figure 2.22 Generator rotational speed regulation with FGS PI-controller and AFTCS during fault-free and faulty operation of wind turbine – time period [170,230] sec. 57
Figure 2.23 Wind profiles with mean speeds of 11 and 17 (m/s). 58

Figure 3.1 Block diagram of the wind turbine model in feedback control loops. The model output vector $\boldsymbol{y}$ provides the measured generator speed $\omega g,m$ and wind yaw error $\Xi e,m$ for controllers.....65
Figure 3.2 Ideal power curve versus wind speed characteristic. 66
Figure 3.3 Performance responses during fault-free and faulty operations: (a) Generator speed (b) Generator power. 69
Figure 3.4 Wind turbine control feedback loops including torque FMRAC and pitch FGS systems in the loop. The mesured generator speed $\omega g,m$ and generator power Pg,m are extracted from the plant output vector $\boldsymbol{y}$. 77
Figure 3.5 Membership functions for: (a) two inputs, and (b) two outputs of fuzzy adaptation mechanism. 79
Figure 3.6 Wind turbine control feedback loops including torque control with FDD and ASC and pitch FGS system in the loop. The estimated fault magnitude $\tau g,f$ is extracted from FDD information vector $\boldsymbol{I}$. 81
Figure 3.7 Model-based FDD scheme based on generator power T-S fuzzy model. The measured variables are passed through the low-pass filter (see (3.19)) in order to filter out the noise σ (Note: In practice, the noise effects can never be completely removed). 82
Figure 3.8 The residual evaluation and decision making algorithm used in the FDD system. 83
Figure 3.9 Wind speed profiles. 84
Figure 3.10 Comparison of the measured and model-estimated response of generator power during wind turbine fault-free operation. 89
Figure 3.11 Generator power response under fault-free and faulty conditions - torque PFTC scheme (FMRAC). (a) +1000 Nm torque actuator offset, and (b) +2000 Nm torque actuator offset. 90
Figure 3.12 FDD results. (a) +1000 Nm torque actuator offset, and (b) +2000 Nm torque actuator offset. 91
Figure 3.13 Generator power response under fault-free and faulty conditions - torque AFTC scheme (FDD and ASC). (a) +1000 Nm torque actuator offset, and (b) +2000 Nm torque actuator offset. 92
Figure 3.14 Structural dynamics and loading for torque PFTC scheme (FMRAC) – time period [495,520] sec. (a) tower-top fore-aft and side-to-side accelerations, (b) tower-top fore-

aft and side-to-side deflections, and (c) tower-base fore-aft and side-to-side moments. 93
Figure 3.15 Structural dynamics and loading for AFTC scheme (FDD and ASC) – time period [495,520] sec. (a) tower-top fore-aft and side-to-side accelerations, (b) tower-top fore-aft and side-to-side deflections, and (c) tower-base fore-aft and side-to-side moments. 94
Figure 3.16 Generator power response under fault-free and faulty conditions – time period [495,520] sec. (a) filtered measurement, +1000 Nm torque actuator offset, (b) filtered measurement, +2000 Nm torque actuator offset, (c) true (noise free) measurement, +1000 Nm torque actuator offset, and (d) true (noise free) measurement +2000 Nm torque actuator offset. 97
Figure 3.17 A small (< 500 Nm) intermittent time-dependent torque actuator offset – time period [495,520] sec. 98
Figure 3.18 Generator power response during fault-free and faulty conditions – time period [495,520] sec. 99
Figure 3.19 Generator power response during fault-free and faulty conditions with +1,000 Nm torque actuator offset, and using wind profile with mean speed of 11 m/s. (a) torque PFTC scheme (FMRAC), and (b) torque AFTC scheme (FDD-ASC). 101
Figure 3.20 Generator power response during fault-free and faulty conditions with +1,000 Nm torque actuator offset, and using wind profile with mean speed of 17 m/s. (a) torque PFTC scheme (FMRAC), and (b) torque AFTC scheme (FDD-ASC). 101
Figure 4.1 Wind farm layout (D1=600m, D2=500m, D3=300m). 107
Figure 4.2 Illustration of overall model structure for N turbines. Note that the bold letters stand for sets of variables, for example $\boldsymbol{Pd} = Pd, q$ with $q = 1, 2, \dots, N$ (This figure is based on [112]). 107
Figure 4.3 The qth wind turbine in the farm ($q = 1, 2, \dots, N$). Note that in addition to the generated power Pg, q, the turbine model provides many other measured variables such as coefficient of thrust CT, q, and so on. 109
Figure 4.4 Timeline for the occurance of the considered fault in a designated number of wind turbines in the farm. Note that, the total simulation time is 1000 seconds, and $\mathbf{T}_{\#}$ stands for wind turbine number # with respect to the wind farm layout shown Figure 4.1. .112

Figure 4.5 Generator power response during fault-free and faulty operations of wind turbines: (a) T_1, and (b) T_3 in the farm. 112
Figure 4.6 Schematic of the proposed FDD and FTC approach based on an integrated FDD system and ASC mechanism. Here, $\boldsymbol{Mes}$ is a vector of performance data including measured variables and control commands/references in wind turbines. Based on FDD information $\boldsymbol{I}(k)$, the supervisor applies appropriate signal correction/modification using power loss estimates $\boldsymbol{\mathcal{P}} = \mathcal{P}q$. Note that the farm includes N turbines ($q = 1, 2, \dots, N$). 114
Figure 4.7 FDD system including R modules each for conducting the monitoring of the consistency of the powers generated by any two specific turbines in a wind farm. The module output (MO) signals are analysed and respective decisions are made in the decision making (DM) process. Here, turbine T_Z with ($Z \in \mathbb{N}$ and $1 < Z < N$) represents any turbine except $T1$ and TN. 116
Figure 4.8 Inputs and outputs of example module Mi,j 118
Figure 4.9 Structure of module Mi,j designed using model-free algorithm. 120
Figure 4.10 Input membership functions used in fuzzy inference mechanism: (a) $\Delta Pi,j$, (b) Pri,j, and (c) Pgi,j. 121
Figure 4.11 Output membership functions used in fuzzy inference mechanism. 121
Figure 4.12 Flowchart of post-processing on inconsistency signature Si,j at the time-step k. 123
Figure 4.13 Post-processing of inconsistency signature in an example module. (a) inconsistency signature (b) absolute inconsistency information. 124
Figure 4.14 Structure of module Mi,j designed using model-based algorithm. 126
Figure 4.15 Flowchart of post-processing on residuals r at the time-step k. 127
Figure 4.16 Nacelle wind speed profiles for turbines installed in the wind farm shown in Figure 4.1. (Note: $V_{nac,\,i}$ denotes nacelle wind speed for turbine T_i) 131
Figure 4.17 A typical grid load and total generated active power response by the wind farm under fault free condition. 131
Figure 4.18 Projected membership functions for: (a) $y(k-1)$, and (b) $u(k-1)$ 132
Figure 4.19 The process output and the fuzzy model output (showing the contribution of each local model) – time period [200,250] sec 133
Figure 4.20 FDD results for the model-free FDD system. 135

Figure 4.21 FDD results for the model-based FDD system. 136
Figure 4.22 Generator power response under fault-free and faulty conditions (3% power loss) − integrated model-free FDD and FTC. (a) T_1, (b) T_2, (c) T_3, (d) T_4, (e) T_7, (f) T_8, and (g) T_{10} 138
Figure 4.23 Generator power response under fault-free and faulty conditions (3% power loss) − integrated model-based FDD and FTC. (a) T_1, (b) T_2, (c) T_3, (d) T_4, (e) T_7, (f) T_8, and (g) T_{10}. 139
Figure 4.24 Generator power response under fault-free and faulty conditions (30% power loss) in T_{10} . (a) integrated model-free FDD and FTC, (b) integrated model-based FDD and FTC. 140
Figure 4.25 Drivetrain torsion rate results for wind turbine T_1 in the farm during the: (a) integrated model-free FDD and FTC, (b) integrated model-based FDD and FTC 142
Figure 4.26 Tower bending moment results − integrated model-free FDD and FTC. (a) T_1, (b) T_2, (c) T_3, (d) T_4, (e) T_7, (f) T_8, and (g) T_{10}. 142
Figure 4.27 Tower bending moment results − integrated model-based FDD and FTC. (a) T_1, (b) T_2, (c) T_3, (d) T_4, (e) T_7, (f) T_8, and (g) T_{10}. 143
Figure 5.1 Wind farm layout (D1=600m, D2=500m, D3=300m). 151
Figure 5.2 Illustration of the overall wind farm structure (This figure is based on [112]). 151
Figure 5.3 The qth wind turbine in the farm ($q = 1, 2, \dots, N$). Note that in addition to the generated power Pg, q, the turbine model provides many other measured variables. 153
Figure 5.4 Wind farm control system setup. 154
Figure 5.5 The APC scheme based on the FGS-PI control approach. 156
Figure 5.6 Membership functions for (a) inputs fe and fe, (b) outputs αP and αI 157
Figure 5.7 The APC scheme based on the adaptive pole placement control approach. 159
Figure 5.8 Closed-loop two DOF control system (This figure is based on [132]). 162
Figure 5.9 Nacelle wind speeds for the wind farm shown in Figure 5.1 (Note: $V_{nac,\,i}$ denotes nacelle wind speed for turbine T_i) 164
Figure 5.10 Grid loads – (a) step, and (b) periodic. 166
Figure 5.11 Total active power response during (a) step grid load, and (b) periodic grid load. 167
Figure 5.12 Grid frequency response during (a) step grid load, and (b) periodic grid load. 167
Figure 5.13 A typical grid load. 170

Figure 5.14 Total active power response during the frequency event. 170

List of Tables

Table 1.1 Examples of existing literature on model-based FDD of wind turbines 12
Table 1.2 Modern wind turbine control 14
Table 1.3 Examples of existing literature on control of wind turbines 15
Table 1.4 List of the fault cases 18
Table 2.1 Fault Scenarios 27
Table 2.2 Controller parameters for baseline PI-controller and FGS-PI controller 32
Table 2.3 Fuzzy rules for KP' 33
Table 2.4 Fuzzy rules for KI' 34
Table 2.5 Configuration properties of generator speed T-S fuzzy model (MISO model) 42
Table 2.6 Configuration properties of rotor speed T-S fuzzy model (MISO model) 43
Table 2.7 Configuration properties of pitch system T-S fuzzy model (MISO model) 47
Table 2.8 Quantitative Comparison of blade-pitch PI-controllers - system in normal operation ..50
Table 2.9 Quantitative Comparison of blade-pitch PI-controllers - system in normal operation ..52
Table 2.10 Modeling accuracy of fuzzy models – system in normal operation 53
Table 2.11 Detection time values for sensor faults (in seconds) 55
Table 2.12 Quantitative Comparison of blade-pitch PI-controllers - system in normal operation with wind profile of 11 m/sec mean wind speed 58
Table 2.13 Quantitative Comparison of blade-pitch PI-controllers - system in normal operation with wind profile of 17 m/sec mean wind speed 58
Table 3.1 Fault scenarios 67
Table 3.2 Controller parameters [33] 71
Table 3.3 Configuration properties of generator power T-S fuzzy model (MISO model) 74
Table 3.4 Fuzzy rules for $Kopt'$ and Pg,o' 79
Table 3.5 List of inputs and outputs for MISO fuzzy model used in the FDD system 82
Table 3.6 Quantitative comparison of wind turbine simulation results under wind profile with mean speed of 11 m/s and fault-free conditions, time period [0,630] sec. 86
Table 3.7 Quantitative comparison of wind turbine simulation results under wind profile with mean speed of 14 m/s and fault-free conditions, time period [0,630] sec. 87

Table 3.8 Quantitative comparison of wind turbine simulation results under wind profile with mean speed of 17 m/s and fault-free conditions, time period [0,630] sec. 87
Table 3.9 The estimated consequent parameters for the identified T-S fuzzy reference model 88
Table 3.10 Modeling accuracy for the generator power reference model 88
Table 3.11 Detection time values for the considered fault scenarios (in seconds) 90
Table 3.12 Quantitative comparison of structural dynamics and loading results — torque PFTC scheme – time period [495,520] sec. (a) fault-free operation with nominal torque controller, (b) +1000 Nm torque actuator offset, (c) +2000 Nm torque actuator offset. 94
Table 3.13 Quantitative comparison of structural dynamics and loading results — torque AFTC scheme – time period [495,520] sec. (a) fault-free operation with nominal torque controller, (b) +1000 Nm torque actuator offset, (c) +2000 Nm torque actuator offset. 95
Table 3.14 Quantitative comparison of FTC schemes during fault period [495-520] sec 97
Table 3.15 Quantitative comparison of FTC schemes during fault period [495-520] sec 99
Table 3.16 Available sensors and their white noise parameters 100
Table 3.17 The results of Monte Carlo simulation studies under wind profile with mean speed of 14 m/s. 100
Table 4.1 Formation of R modules for a wind farm with N turbines.....116
Table 4.2 Module output MOi,j results for example module Mi,j 118
Table 4.3 Fuzzy Rules used in fuzzy inference mechanism 121
Table 4.4 Configuration properties of T-S fuzzy model (SISO model). Note that $uk = Pri,j(k)$, and $yk = Pgi,j(k)$, respectively. 129
Table 4.5 Estimated consequent parameters for the identified T-S fuzzy model with the structure given in Table 4.4 132
Table 4.6 Cluster centers 132
Table 4.7 Modeling accuracy and fitting performance of the fuzzy model 133
Table 4.8 Time of fault detection (or detection time) for each FDD system (in seconds).....134
Table 4.9 Quantitative comparison of generator power responses for integrated FDD and FTC schemes during the specified fault periods with 3% power loss 140

Table 4.10 Quantitative comparison of generator power responses for integrated FDD and FTC schemes during the specified fault period with 30% power loss 140
Table 4.11 Quantitative comparison of tower bending moment results during fault periods 143
Table 4.12 The results of Monte Carlo simulation studies under wind field shown in Figure 4.16 144
Table 4.13 Quantitative comparison of generator power responses for integrated FDD and FTC schemes during the specified fault periods with 3% power loss and under wind field with mean speed of 16 m/s, a turbulence intensity of 12%, and over 2000 seconds of run time 145
Table 5.1 Linguistic variables 157
Table 5.2 Fuzzy rules for αP 158
Table 5.3 Fuzzy rules for αI 158
Table 5.4 Parameters used in fuzzy gain-scheduled PI control 165
Table 5.5 Parameters used in adaptive pole placement control 165
Table 5.6 Quantitative comparison of APC schemes in terms of accuracy of active power response 167
Table 5.7 Quantitative comparison of APC schemes in terms of frequency regulation 168
Table 5.8 Fatigue results (DEL – shaft torsion) for APC based on (A) baseline control (B) fuzzy gain-scheduled PI control (C) adaptive pole placement control 169
Table 5.9 Fatigue results (DEL – tower bending) for APC based on (A) baseline control (B) fuzzy gain-scheduled PI control (C) adaptive pole placement control 169
Table 5.10 Frequency events 170
Table 5.11 The results of Monte Carlo simulation studies under variations in wind fields with mean speeds within [13-15] m/s and turbulence intensity values between [10-15] % – (A) fuzzy gain-scheduled PI control (B) adaptive pole placement control 171
Table 5.12 The results of Monte Carlo simulation studies under plant-model uncertainty for adaptive pole placement control 172

Nomenclature

A_i, B_i, C_i	Antecedent fuzzy sets of the *i*th rule
C_p	Power coefficient
e	Error signal
$\dot{e}$	Derivative of error signal
I_{dt}	Drive train inertia
K_D	Derivative gain
K_I	Integral gain
K_P	Proportional gain
K_{opt}	Optimum gain for generator torque control
K_u	Gain of oscillation
N_g	Gearbox ratio
P_{rated}	Wind turbine rated power
P_A	Total available power
P_D	Total active power demand
P_{aer}	Aerodynamic rotor power
$P_{g,o}$	Generator rated power
P_g	Generator power
T_D	Derivative time constant
T_I	Integral time constant
T_u	Period of oscillation
V_{cut-in}	Cut-in wind speed
$V_{cut-out}$	Cut-out wind speed
V_{rated}	Rated wind speed
V_w	Wind speed
b_i	Scalar offset of the *i*th rule
f_c	Corner frequency
f_e	Frequency error
f_m	Measured frequency
f_r	Reference frequency
$\{m, n\}$	Model orders
$\Xi_{e,m}$	Wind yaw error
β_c	Blade-pitch angle control signal
β_m	Measured blade-pitch angle
β_{ref}	Reference blade-pitch angle
η_g	Generator efficiency
μ_i	Degree of fulfillment of *i*th rule
τ_{aer}	Aerodynamic rotor torque
$\tau_{g,c}$	Generator torque control signal
τ_g	Generator torque
$\omega_{g,d}$	Desired generator rotational speed
$\omega_{g,e}$	Generator rotational speed error

$\omega_{g,m}$	Generator speed measurement
ω_g	Generator rotational speed
ω_n	Natural frequency
$\omega_{r,o}$	Rated rotor rotational speed
ω_r	Rotor rotational speed
$\omega_{y,c}$	Yaw motor control signal
J	Rotational inertia of the turbine
L	Load
k	Discrete time-step
α	Low-pass filter coefficient
ζ	Damping ratio
$\boldsymbol{C_T}$	Coefficients of thrust
$\boldsymbol{P_d}$	Power demands
$\boldsymbol{V_{nac}}$	Measured nacelle wind speeds
$\boldsymbol{V_{rot}}$	Effective wind speeds
$\boldsymbol{a_i}$	Parameter vector of the *i*th rule
$\boldsymbol{u_{com}}$	Compensated control inputs
$\boldsymbol{u_{cor}}$	Corrected control inputs
$\boldsymbol{u_{nom}}$	Nominal control inputs
$\boldsymbol{\hat{x}}$	Estimates (wind turbine states and/or fault biases)
$\boldsymbol{\hat{y}}$	Estimated outputs
$\boldsymbol{y_{cor}}$	Corrected measured outputs
$\boldsymbol{I}$	FDD information
$\boldsymbol{Mes}$	A set of measurements
$\boldsymbol{r}$	Reference signal/Residuals
$\boldsymbol{u}$	Inputs
$\boldsymbol{y}$	Measured outputs (Sensor)

Subscripts

com	compensated
corr	corrected
d	demanded/desired
dt	drivetrain
e	error
g	generator/gearbox
m	measured
r	rotor
ref	reference
std	standard deviation

Acronyms

AC	Adaptive Control
AFTC	Active Fault-Tolerant Control
AFTCC	Active Fault-Tolerant Cooperative Control
AFTCS	Active Fault-Tolerant Control Scheme
APC	Active Power Control
ASC	Automatic Signal Correction
DEL	Damage Equivalent Loads
DM	Decision Making
DOFs	Degrees Of Freedom
FAST	Fatigue, Aerodynamics, Structures, and Turbulence
FDD	Fault Detection and Diagnosis
FGS	Fuzzy Gain Scheduled
FMI	Fuzzy Modeling and Identification
FMRAC	Fuzzy Model Reference Adaptive Control
FTC	Fault-Tolerant Control
GK	Gustafson-Kessel clustering algorithm
HAWTs	Horizontal Axis Wind Turbines
LPV	Linear Parameter Varying
LSM	Least Squares Method
MISO	Multi-Input Single-Output
MO	Module Output
MPC	Model Predictive Control

MRAC	Model Reference Adaptive Control
NREL	U.S. National Renewable Energy Laboratory
NRMSE	Normalized Root-Mean-Squared Error
OM	Operation and Maintenance
PCC	Point of Common Coupling
PFTCS	Passive Fault-Tolerant Control Systems
PI	Proportional-Integral
PID	Proportional-Integral-Derivative
RC	Robust Control
RMSE	Root-Mean-Squared Error
RMSPE	Root-Mean-Squared-Percentage Error
SISO	Single-Input Single-Output
STD	Standard Deviation
T-S	Takagi-Sugeno
TSOs	Transmission Systems Operators
TSR	Tip Speed Ratio
UIO	Unknown Input Observer
V&V	Validation & Verification
VAF	Variance Accounted For
WMEP	German Scientific Measurement and Evaluation Program

Chapter 1 Introduction

1.1 Preface

Nowadays, wind as one of the renewable sources of energy has received tremendous attention in the energy market to address the ever-increasing global demand for fossil fuels and subsequent concerns about environmental issues [1]. Wind turbines are complex remotely-installed renewable energy systems driven by wind as a stochastic input, and essentially exhibit highly nonlinear dynamics. They operate in uncertain environments and are exposed to large disturbances. Despite the significant efforts and investments made in the wind-energy industry and subsequent wind power penetration, today's wind turbines are still expensive to install, operate, and maintain [2]. Additionally, the increasing tendency towards larger and more flexible wind turbines is imposing new challenges in reliability and availability [2]. To overcome all these ever increasing requirements and challenges, advanced fault detection, diagnosis, and accommodation schemes together with optimal control constitute the key enabling technologies for ensuring reliable and efficient operation of modern wind turbines and generating electrical energy as cheaply and efficiently as possible [3, 4]. The main objective of the optimal control is to produce the maximum output power while considering the physical constraints and limitations of the system as well as the quality of turbine output power. On the other hand, advanced Fault Detection and Diagnosis (FDD) and Fault-Tolerant Control (FTC) techniques included in a control system use real-time sensor data to early detect and diagnose the faults in the sensing and actuation subsystems of the wind turbine and accommodate the faults when possible. Application of the mentioned technologies in wind turbines constitutes a quite active and, in many aspects, interdisciplinary investigation area that ensures a guaranteed increasing future market for wind energy. In particular, this thesis aims to design and develop novel FDD and FTC schemes/strategies with application to wind turbines at both individual wind turbine and entire wind farm levels. Therefore, the research of the thesis provides advanced levels of monitoring, diagnosis and fault tolerance capabilities to wind turbines in order to ensure their efficient and reliable performance under both fault-free and faulty conditions. There are a wide variety of design configurations for wind turbines, such as: horizontal or vertical axis of rotation, downwind or upwind placement of the rotor, and also

different number of blades. However, this research will only be focused on upwind Horizontal Axis Wind Turbines (HAWTs) because they are predominant utility-scale wind turbines today.

The following sections present some relevant background and motivation with a particular emphasis on wind turbines and FDD-FTC methods. Then, a literature review on the application of monitoring, diagnosis and fault-tolerant and efficiency control to wind turbines is provided. In addition to the presented literature review here, each of the subsequent chapters except the last chapter also includes a relevant review on the available literature.

1.2 Wind Energy and Wind Turbines

Wind Energy is a form of kinetic energy that can be converted into mechanical and then electrical energy using wind turbines. From a design point of view, wind turbines are classified into two different types: vertical axis and horizontal axis (see Figure 1.1). Gradually, the horizontal axis design with three rotor blades came to dominate the commercial market of wind energy due to many advantages such as access to stronger wind because of their tall towers, higher efficiency since the blades always move perpendicularly to the wind, and receiving power through the whole rotation [5].

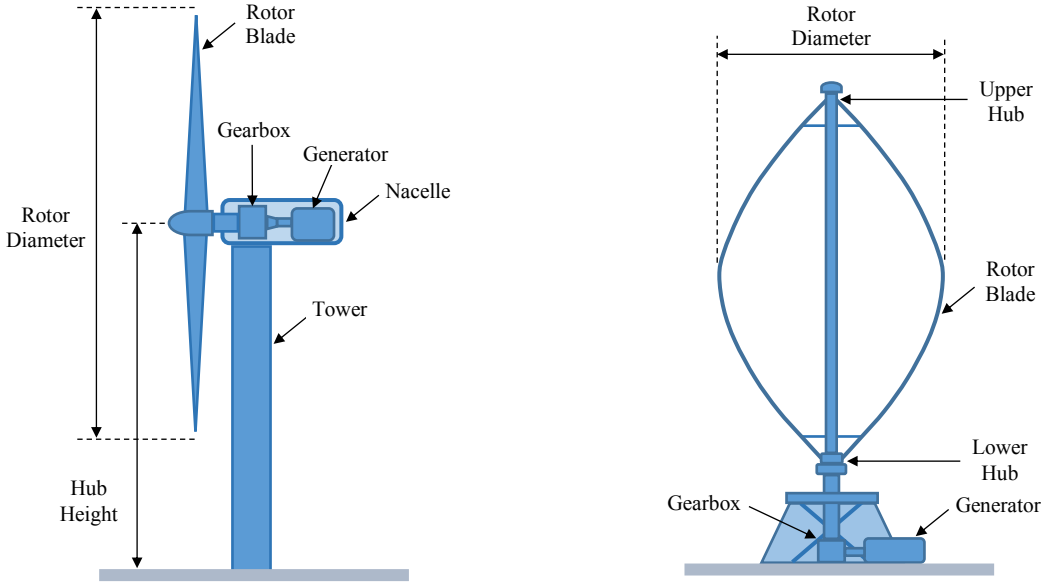

Figure 1.1 Wind turbine designs: (a) horizontal axis and (b) vertical axis.

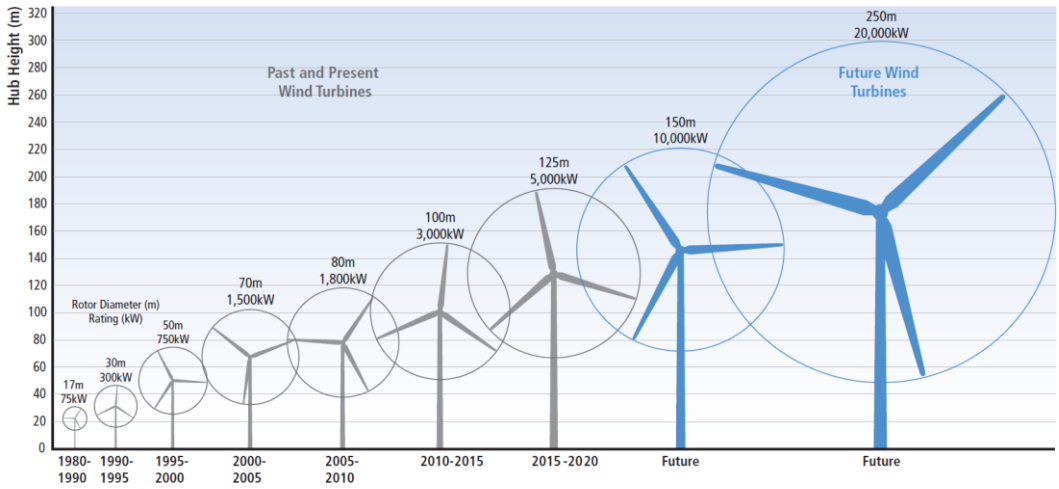

Figure 1.2 Wind turbine designs: (a) horizontal axis and (b) vertical axis (Photo courtesy of the National Renewable Energy Laboratory (NREL))

To minimize the generation cost of wind energy, wind turbine manufacturers have been always interested in increasing turbine size while decreasing usage of materials. As the size of wind turbines increased over time (see Figure 1.2), wind turbine control evolution moved from simple stall control to full-span blade pitch control in which turbine output is controlled by pitching/rotating the blades around their longitudinal axis. Moreover, the reduced cost of power electronics facilitated the variable speed wind turbine operation. Figure 1.3 shows the basic components of a modern three-bladed horizontal axis wind turbine.

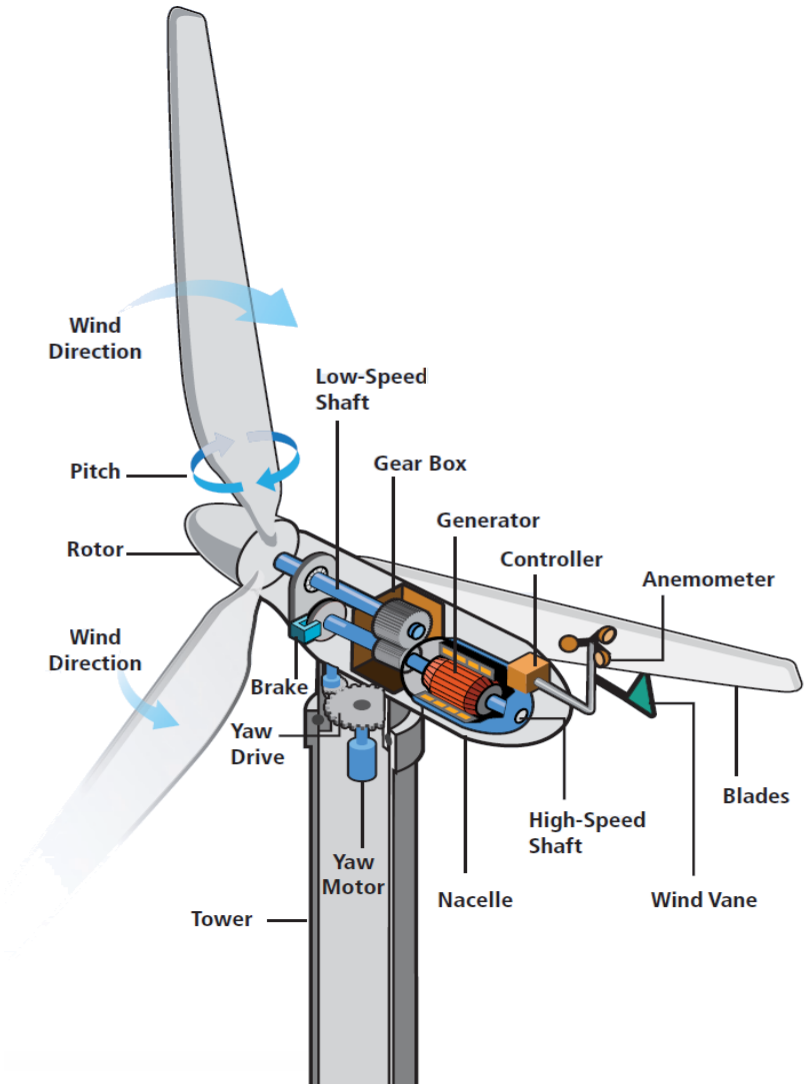

Figure 1.3 Basic components of a modern, three-bladed horizontal-axis wind turbine (Photo courtesy of NREL).

It is worth mentioning that wind turbines can be deployed either onshore or offshore (Figure 1.4). However, it is expected that the offshore wind energy becomes a more significant source of overall wind energy supply in near future. The primary motivation for development of offshore wind energy is to exploit additional and higher-quality wind resources in areas located at sea. Other motivations include: gaining additional economies of scale through deploying even larger wind turbines than onshore turbines; gaining plant-level economies of scale by building larger wind power plants than onshore power plants; and potential reduction in the need for change in land-based transmission infrastructure.

(a)

(b)

Figure 1.4 Wind turbines: (a) onshore (the Castle River wind farm, Alberta, Canada (Photo by Todd Spink courtesy U.S. Energy Dept.)) and (b) offshore (the Sheringham Shoal wind farm (Photo by Alan O'Neill)).

1.3 Frequency of Failures in Wind Turbines and Motivation for FDD and FTC

A wind turbine includes several rotating and non-rotating assemblies, subsystems, and components that may fail over time. A fault or defect even in a component level may propagate in the overall system and deteriorate the performance of other components and eventually cause to overall system failure. The German Scientific Measurement and Evaluation Program (WMEP) is one of the most comprehensive worldwide monitoring surveys on the long-term reliability behavior of wind turbines (onshore) in Europe. The WMEP survey has collected 64,000 reports of maintenance and repair from 1,500 wind turbines within the time period from 1989-2006 [6]. Figure 1.5 presents the failure rates and downtimes for different components of wind turbines in the WMEP survey [6, 7]. Here, the annual failure rate is plotted alongside the downtime per failure, and both highlight the significance of failures in different wind turbine components. As seen in Figure 1.5, the longer periods of downtime per failure are driven by problems with the mechanical subassemblies. However, electrical and control systems fail more frequently than the other components. Moreover, the mean annual downtime for a wind turbine due to component malfunctions varies between minimum of 0.3 day for blades and maximum of 0.88 day for the electrical systems. In summary, faults occurring in electrical and control systems are highly frequent and also responsible for a large portion of the total annual downtime presented in Figure 1.5. Although the presented results in Figure 1.5 are surveyed from modern onshore wind turbines, as offshore wind turbine technology has been directly derived from onshore technology, similar types of faults can be expected; but

under offshore conditions, the mean periods of annual downtime will be exacerbated due to limited accessibility, and it is expected that decreased availability will result. Furthermore, regarding the current tendency to design and use larger and more flexible offshore wind turbines, both the size and complexity factors together with harsh climate conditions come into play and lead to higher failure rates which are particularly noticeable in the electrical system, electronic control, sensors, yaw system, rotor blades, generator and drivetrain [7].

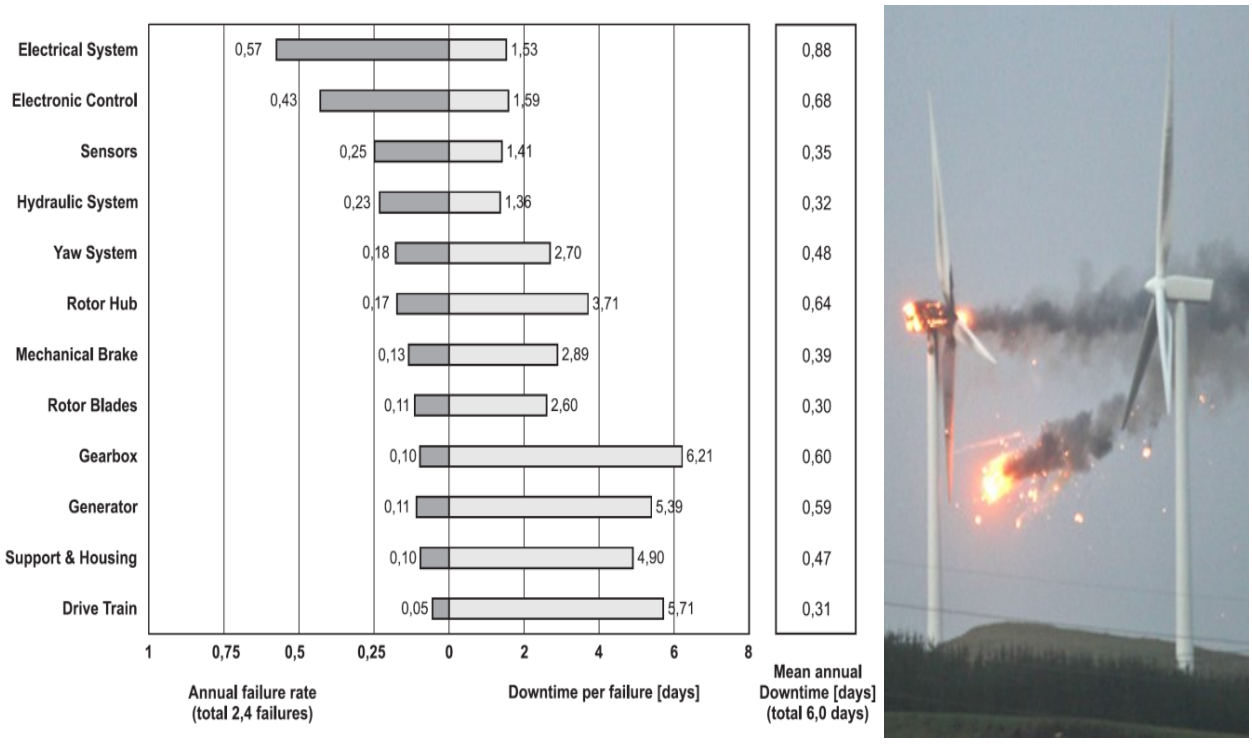

Figure 1.5 Reliability characteristics for different components of wind turbine in the WMEP program [7].

All the above-mentioned results indicate the increasing importance of control system in wind turbine reliability and availability. This can be highlighted as a minor fault in a part of system can propagate to a major fault or severe failure in another part of the wind turbine, while the control system can highly contribute against this fault propagation process. This motivates design and implementation of FDD and FTC techniques for wind turbine condition monitoring and control. Therefore, this thesis aims to propose and investigate novel FDD and FTC techniques for wind turbines to early detect and diagnose the faults in the sensing and actuation subsystems of the turbine and accommodate the faults when possible. Hence, the wind turbine can continue energy generation in spite of faults, although it may experience a graceful degradation in its performance.

This strategy prevents a fault from propagating within the system and leading to a serious failure. Thereby, the reliability, availability and cost effectiveness will be considerably improved.

1.4 Fault Diagnosis and Fault-Tolerant Control Systems

The purpose of this subsection is to provide a brief overview of FDD, and FTC techniques including basic concepts, and available references for further information.

A) Fault and Failure

A *fault* is regarded as an unpermitted change in at least one characteristic property (feature) of a system component which may subsequently result in system instability or performance degradation. Such a fault can occur in any component of the system, such as sensors, actuators or other plant (system) components [8]. In contrast to fault, a *failure* is a much more severe condition which makes a system component completely dysfunctional [8]. In other words, a FTC system may overcome faults and maintain overall system stability and acceptable performance. But failure is an irrecoverable event. As it is shown in Figure 1.6, faults themselves can be classified into different types. From a time characteristics point of view, they can be divided into abrupt faults (with non-smooth time behaviour), incipient faults (with smooth time behaviour), and intermittent faults (with pulsating time behaviour) [9]. Moreover, according to the location of faults acting within a system, the faults are categorized as sensor faults, actuator faults, and process (system) faults. The mentioned classification of faults is widely used in the FTC literature.

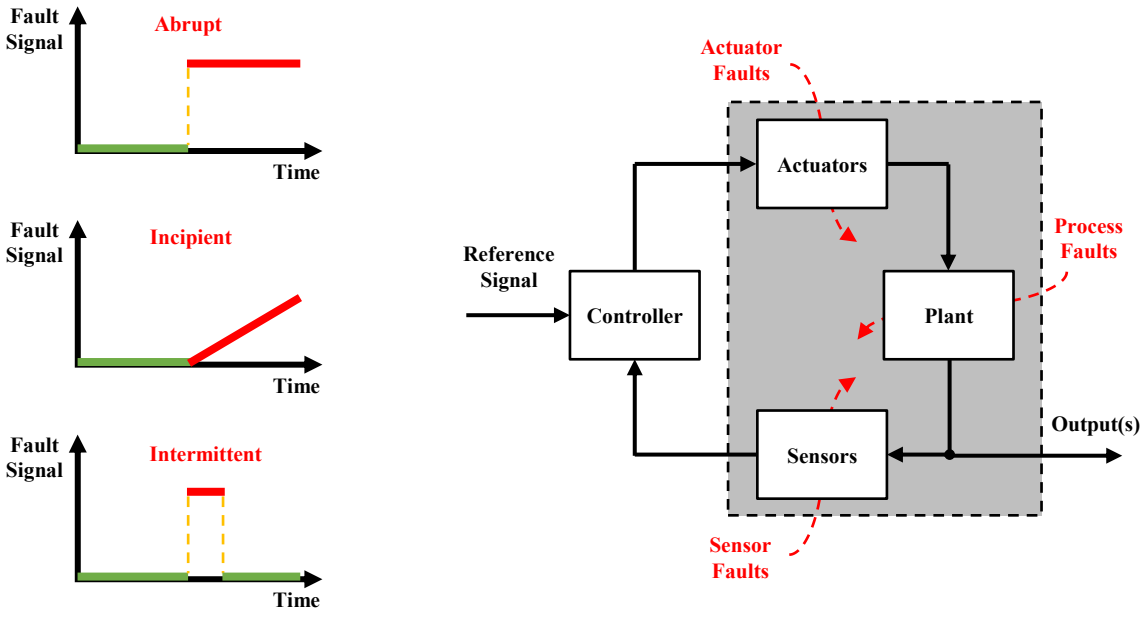

(a) (b)

Figure 1.6 Fault classification with respect to (a) time characteristics (b) location

B) Fault-Tolerant Control

A fault even in a component level may propagate into the overall system and deteriorate the performance of other components and eventually cause to system failure. So, it is of great importance to design control systems which are able to *tolerate* against potential faults in the system. This class of control systems is known as FTC systems [10]. FTC systems can be generally divided into two types, namely, passive (PFTCS) and active (AFTCS) [10]. These two approaches exploit different design methodologies for identical control objective.

PFTCS are fixed control systems designed to be robust against a specified class of faults or some levels of uncertainty in overall system. This approach does not need any kind of FDD scheme or controller reconfiguration algorithm. This implies that the fixed control system is applied for both the *fault-free* as well as the *faulty* system. However, it has limited fault-tolerant capabilities and may cost nominal performance [10]. In contrast to PFTCS, AFTCS react to system component faults (including sensors, actuators, and system itself) by reconfiguring the controller based on the real-time information about the state of the system determined by an FDD scheme (see Figure 1.7) [10]. To be more precise, a reconfiguration mechanism actively exploits the information from the FDD scheme to reconfigure the control system (and also reference governor) for accommodating

faults and maintaining the stability and acceptable performance of the entire system under fault conditions. This implies that the satisfactory performance of AFTCS relies heavily on the speed and accuracy of real-time FDD schemes to provide the most up-to-date information about the true status of the system. Interested readers are referred to a recent review paper [10] for detailed information on reconfigurable FTC systems and the development in this field up to 2008.

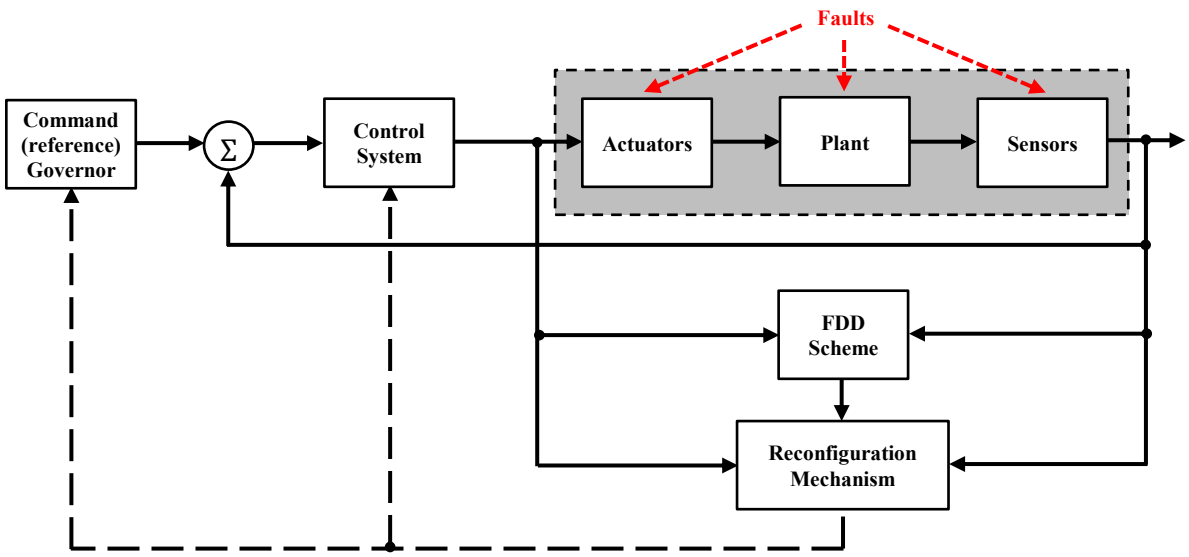

Figure 1.7 A general structure for AFTCS (based on [10])

C) Fault Detection and Diagnosis

FDD scheme used in AFTCS is composed of multiple parts for detection, isolation, and in some cases estimation or identification of faults [8]. Fault *detection* addresses the challenge of real-time monitoring the occurrence of fault in a system. Fault detection can be established in either a passive or an active way. In passive approach the fault detection is done by comparing the observed system behavior with the nominal expected system behavior; hence, the system will be not affected by this method of detection. Conversely, active fault detection relies on injection of auxiliary signals into a system to improve or make possible the fault detection [4]. Fault *isolation* points out faulty components in a system once faults are detected [8]. Note that some faults do not necessarily turn a component on or off, but have an intermediate state. This implies that fault *estimation* (*identification*) is required to determine the magnitude of fault in order to accommodate it.

Figure 1.8 shows a general structure for model-based FDD in which the so-called residuals $\boldsymbol{r}(k)$ are computed as the difference between the plant outputs $\boldsymbol{y}(k)$, and the estimated outputs $\hat{\boldsymbol{y}}(k)$ obtained from a plant model that represents the nominal behavior of the plant. Then, to provide FDD information $\boldsymbol{I}(k)$, the residuals are evaluated, for example, using a threshold test on the instantaneous values of the generated residuals. Further details about FDD process and existing methods in this field can be found in [8] and the references therein.

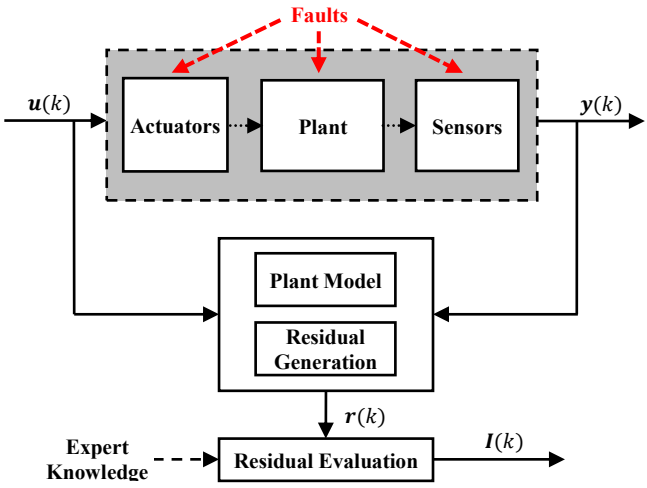

Figure 1.8 A general structure for model-based FDD

1.5 Application of Condition Monitoring, Diagnosis and Fault-Tolerant and Efficiency Control to Wind Turbines

Research in this field has recently been conducted more and more in both academia and industry. There have been a few review papers on wind turbine control and health management in open literature [11-14]. In addition, there are some books available which deal with general aspects of modeling and control of wind turbines [2, 15, 16]. However, given the significance of FDD algorithms and their integration with FTC techniques in an active fault-tolerant architecture, there is very few well-organized, comprehensive survey paper publication about the status of current research in this new and active area along with opportunities for the future. For example, in a recent review of the literature, Badihi *et al.* [17] provide an overall picture of historical, current, and future research and development in monitoring, diagnosis and FTC for wind turbines. In the following subsections the status of the research on condition monitoring and diagnosis as well as fault-tolerant and efficiency control in wind turbines and wind farms is briefly reviewed.

D) Condition Monitoring and Fault Diagnosis in Wind Turbines

The reduction of operational and maintenance costs of wind turbines has always been a key driver for applying low-cost, condition monitoring and diagnosis systems. This allows enhancing the reliability, availability and productivity of wind turbines, and finally realization of condition-based maintenance — defined as a type of preventive maintenance (before a failure) which is based on real-time health monitoring of system's performance metrics.

The condition monitoring methods for wind turbines can be divided into two categories: 1) *offline condition monitoring*, and 2) *online condition monitoring* techniques. The offline condition monitoring techniques concern machine aided periodic inspections in which the machine has to be shut down, and/or the attention of an operator is necessary. The offline techniques are appropriate and cost-effective for design and certification process of new classes of wind turbines [18]. However, they are useless to determine the real-time condition of a wind turbine. A more modern method is to online monitor the machine continuously during operation. Such a method is referred to as online condition monitoring which can automatically report continuous raw measurements, and may incorporate onboard processing for data reduction and analysis. The online condition monitoring techniques can be further divided into three subcategories: 1) hardware sensor-based method, 2) analytical model-based method, and 3) hybrid approach.

The online hardware sensor-based method (also known as signal-based method) mostly requires additional costly sensors for exclusive monitoring and analysis of vibration, torque, temperature, oil/debris, acoustic emission and so on. Although today's industrial wind turbines mostly exploit this condition monitoring method, the method suffers from some disadvantages such as high cost and complexity together with sensor failure [19, 20]. Furthermore, the information collected from these sensors is usually used for condition monitoring (fault detection/isolation) and predictive maintenance purposes only. That is, turbines are turned off and go to downtime even at simple faults to wait for service. More information on hardware sensor-based methods utilized in wind turbines can be found in survey papers [12-14].

More sophisticated online technique that is analytical model-based method (also known as model-based FDD) offers great promise to overcome those shortcomings of hardware sensor-based method, and also establish a suitable framework for development of FTC schemes in wind turbines. Areas where this online condition monitoring techniques can contribute more than the alternatives

include: increased reliability, availability and lifetime of components, together with decreased downtime and maintenance cost. The analytical model-based method, as is evident from its name, monitors a wind turbine continuously using an analytical model of the wind turbine plus information obtained from the main sensors associated with the wind turbine control system excluding vibration and temperature sensors etc. [4]. Obviously, design and implementation of analytical model-based method is not without its challenges. High nonlinearity of the aerodynamic subsystems, wind turbulences, and measurement noises all make wind turbine model-based FDD very difficult and challenging. A list of relevant references on model-based FDD of wind turbines with corresponding FDD approaches is presented in Table 1.1.

Table 1.1 Examples of existing literature on model-based FDD of wind turbines

Design Approaches	**References**
Kalman Filter	[21], [22],[23],[24]
Observer	[23], [25], [26], [27]
Parity Space	[28]
Set Membership Approach	[29], [30]
Support Vector Machines	[31]
Fuzzy Modeling	[32], [33], [34]
Hybrid Modeling	[35]

As a hybrid approach, the online condition monitoring system can be based on a combination of hardware sensor-based and analytical model-based methods. Since information about the control signals and the wind turbine model is added to the information used in hardware sensor-based techniques, the hybrid approach can constitute a promising framework to synthesize the merits of other online methods and improve not only the reliability and performance of the condition monitoring system, but also the feasibility of FTC design in wind turbines.

E) Fault-Tolerant and Efficiency Control in Wind Turbines

A wind turbine consists of several rotating and non-rotating components arranged in an appropriate configuration to provide one of the most efficient forms of renewable power generation. Safe and precise control of such a complex system over the entire operating envelop of the wind turbine which covers four primary regions of operation (see Figure 1.9) creates a significant challenge [16]. As shown in Figure 1.9, Region I represents low wind speeds which are not strong enough to drive the wind turbine. Region II includes mid-range wind speeds which are above the cut-in wind speed V_{cut-in} required for start-up, but still too low to produce *rated* power P_{rated}. So it is also referred to as partial load region. In Region III (full load region), the

wind turbine operates at its rated power due to high wind speeds above the rated wind speed V_{rated}. Finally, when the cut-out wind speed $V_{cut-out}$ is reached (i.e. Region IV), the turbine shuts down to protect itself from mechanical damage.

As it is seen in Figure 1.10, a typical wind turbine control system is developed on the basis of classical control techniques and is composed of three individual controllers for regulating blade-pitch angles, generator torque, and nacelle yaw angle. All controllers commonly use the generator speed feedback, except yaw controller which relies only on yaw error information. The blade-pitch controller typically employs *Proportional-Integral (PI)* control to track a desired generator speed called rated generator speed so that the turbine operates at its rated power P_{rated} in Region III. The torque controller optimizes the power capture through $\tau_{g,c} = K_{opt}\omega_{g,m}$, in which, K_{opt} is a constant gain computed based on wind turbine aerodynamic characteristics for the maximum aerodynamic efficiency. Finally, the yaw controller is an On/Off controller developed to orient the nacelle as wind direction changes.

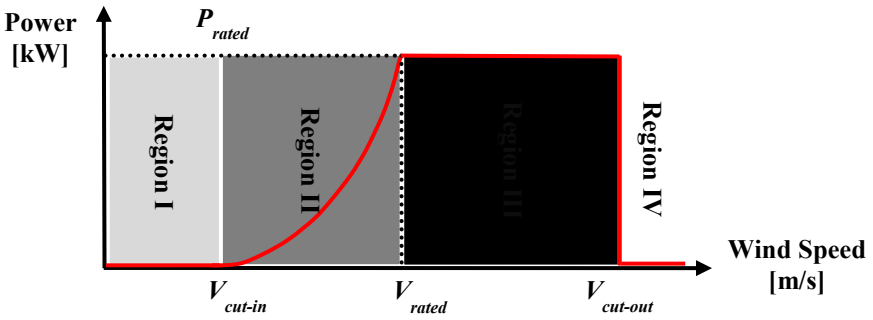

Figure 1.9 Illustration of ideal power curve for a typical wind turbine.

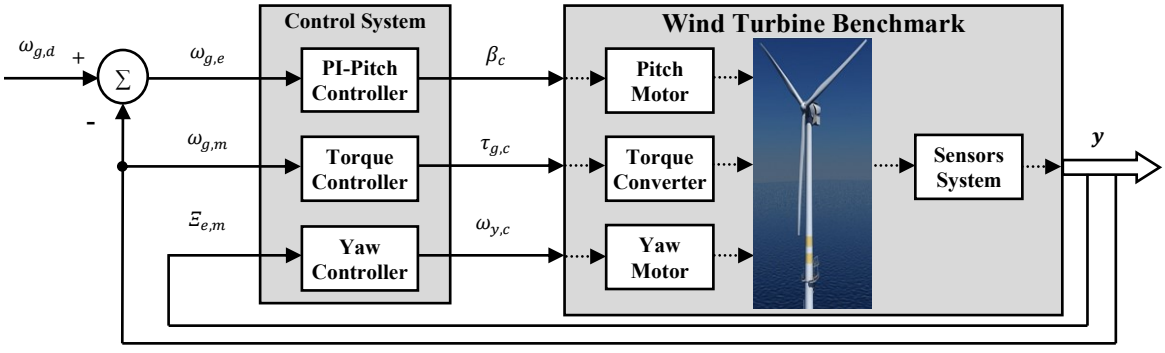

Figure 1.10 Block diagram showing pitch, torque and yaw control systems in feedback loops. The generator speed measurement $\omega_{g,m}$ and wind yaw error $\Xi_{e,m}$ are extracted from the measured outputs $\boldsymbol{y}$. The other parameters are defined in the provided Nomenclature.

Basically, a wind turbine control system relies on a hardware/software subsystem which processes the sensor signals to compute command signals for the actuators. The control system must be able to meet control objectives defined for safe and efficient operation of a wind turbine. An updated list of control objectives and their relevant wind turbine control categories are presented in Table 1.2. Some of these objectives may be closely related, while others may be even conflicting and thus compromise must be considered in design.

As shown in Table 1.2, generally speaking, the literature on control of wind turbines can be divided into three categories, each corresponding to one set of the mentioned control objectives. The first category concerns operational control algorithms which only focus on satisfying the operational control objectives required for each specific regions of wind turbine operation. The second category includes control algorithms which not only consider the operational control objectives, but also take into account the turbine structural fatigue load mitigation. The third category concerns more complete algorithms which consider the operational control objectives together with fault-tolerance properties against probable fault occurrence. Table 1.3 presents a categorized list of relevant references on control of wind turbines with their corresponding control approaches.

Table 1.2 Modern wind turbine control

Control Category	Control Objective
Operational (Efficiency) Control	**Operational Maximum Energy Capture and Power Quality**
	Maintain optimum tip speed ratios in Region II
	Avoid excessive rotational speed in Region III
	Generate smooth output power
Fatigue Load Control	**Structural Load Mitigation**
	Mitigate blade fatigue loads
	Mitigate tower/nacelle loads
	Mitigate drivetrain torsion moments
Fault-Tolerant (Supervisory) Control	**Fault Detection, Diagnosis and Accommodation**
	Detect, isolate, and identify fault(s) as early as possible
	Ensure graceful degradation in performance
	Maintain stability

Table 1.3 Examples of existing literature on control of wind turbines

Control Category		
Operational Control	**Fatigue Load Control**	**Fault-Tolerant Control**
[36] (Linear Model-Based Control)	[41] (Linear Model-Based Control)	[43] (AFTC-LPV)
[37], [38] (Fuzzy Logic)	[42] (Nonlinear MPC)	[44], [45] (AFTC- MRAC)
[39], [40] (LPV)		[46] (AFTC-Adaptive Filters)
		[47] (AFTC- UIO)
		[48] (AFTC – RC)
		[49] (AFTC-Virtual Sensor/Actuator)
		[50] (AFTC-MPC)
		[51] (AFTC-AC)
		[52], [53], [54], [33], [34] (AFTC-Fuzzy Logic)
		[55] (PFTC-Fuzzy Logic)
(Approach)**: AC**: Adaptive Control; **MRAC**: Model Reference Adaptive Control; **MPC**: Model Predictive Control; **LPV**: Linear Parameter Varying; **RC**: Robust Control; **UIO**: Unknown Input Observer		

F) Wind Farm Control

In order to reduce the average cost of wind energy, wind turbines are often installed in groups or clusters called wind farms (or wind power plants) [56, 57]. From a control design perspective, the control of a wind farm is a twofold issue: 1) *coordinated control* of the power generated by each individual turbine such that the negative effects of aerodynamic interactions between the turbines are minimized all over the farm; and 2) *quality control* of the generated power by the wind farm to ensure efficient and reliable integration of the farm into the power grid.

Each turbine located on a wind farm disturbs the wind flow behind it. This disturbed wind flow is called *wake* which is characterized by a mean wind speed deficit and a greater turbulence level. Therefore, the wind turbines operating on a wind farm influence each other through the wakes behind the turbines. This process results in a significant level of aerodynamic interactions between the turbines which in turn upwind turbines will limit power generation and increase fatigue loads on downwind turbines. Due to this fact, coordinated control of all the turbines on a farm is of great importance, and also is more challenging than controlling an individual turbine [57]. In fact, the simple strategy of "each wind turbine on a farm extracts as much power as possible" is not an optimal solution. This strategy can lead to excessive structural loadings, whereas does not necessarily guarantee maximal total overall power capture across the entire farm, because the

turbines on the upwind side of the farm extract too much wind power, slowing the wind significantly before it reaches other turbines on the downwind side of the farm. Thus far, coordinated control problem has received relatively little attention in the literature (see, for example [58-65]). The reason for this lies mainly in the lack of accurate wake models suitable for control design.

With respect to quality control of generated power by a wind farm and electrical interconnection of turbines on the farm, numerous research results are reported in the literature (see [57, 66] and references therein). These researches consider modeling and control of wind farm as a whole, while ignore the aerodynamic interaction among turbines in the farm [56]. As long as only small-scale power units of wind turbines are installed and powering the network, wind power only has a small influence on power fluctuations in the network and in turn can easily be integrated into the power grid. However, the increased penetration of wind power into the grid has challenged the reliable and stable operation of the grid. Therefore, from quality control point of view, wind farms have to behave as active controllable components which embrace more responsibility in grid operation. This means that wind farms have to participate in grid frequency and voltage regulation through control of active and reactive power, respectively.

It is also important to note that the above-mentioned coordinated and quality control functionalities are tightly coupled with fault tolerance and reliability aspects. That is, a wind farm as a whole has to operate in a fault-tolerant framework. Moreover, it should not contribute to grid faults or be damaged by the potential faults in the grid. In fact, most of potential faults can be diagnosed and accommodated efficiently at a wind turbine control level. However, some faults have to be dealt with at the wind farm control level. In reference to the wind farm level, only a few research works on condition monitoring and fault detection of wind farms are reported. Two examples can be found in [67, 68].

1.6 Simulation Benchmark Models for Wind Turbines and Wind Farms

Control design essentially deals with the dynamics of a physical system. Modeling and simulation of wind turbines is an emerging approach in the field of wind turbine controls and health management. Several high-fidelity wind turbine and wind farm simulation models have been developed by various laboratories around the world. Among them, the following Validated and

Verified (V&V) benchmark models are available to meet the increasing interest and need for a common research and development platform in controls and health management research.

- A 4.8 MW wind turbine benchmark model (see [3]) is developed by KK-electronic a/c and Aalborg University for a generic three bladed horizontal-axis variable speed/pitch wind turbine with a full converter coupling.
- A baseline wind turbine model is presented in [69] based on an offshore 5 MW benchmark model proposed by the NREL (see [70]) for supporting concept studies aimed at assessing offshore wind technology. This is a variable speed three-bladed HAWT with full span blade pitch control and generator torque regulation. The baseline wind turbine is itself modeled using FAST (Fatigue, Aerodynamics, Structures, and Turbulence) [71], a comprehensive aeroelastic simulator code which can model a three-bladed HAWT as a combination of rigid and flexible bodies through 24 degrees of freedom, with further details given in [71].
- An advanced wind farm simulation toolbox called *SimWindFarm* is developed as a part of the EU-FP7 project, AEOLUS [17]. The toolbox provides a realistic wind farm simulation benchmark model that allows control designers to develop, implement and investigate farm level control and diagnosis algorithms under different operating conditions for an optional quantity and layout of turbines installed in a wind farm. The wind turbines included in the farm model are simulated using a simple model of the offshore 5 MW benchmark model proposed by the NREL (see [70]).

Both the mentioned wind turbine models contain various fault scenarios and give a possibility to examine different kinds of fault diagnosis and accommodation schemes on a realistic wind turbine model. However, the second model incorporating FAST is a higher-fidelity, more realistic wind turbine model which probably requires more sophisticated FDD and FTC schemes and likely making the results more applicable to the wind energy industry [69]. Table 1.4 presents a detailed list of important faults which are most frequent in wind turbines, and interesting for exploring novel health monitoring, diagnosis and accommodation schemes. Most of these faults are defined and implemented in the mentioned wind turbine models [3, 69]. In contrast to the mentioned wind turbine models, the wind farm model in its original form does not contain any fault scenario. However, it is easily possible to define and implement relevant faults at a wind farm level. These faults may be caused by blade erosion or debris build-up, misalignment of one or more blades

originated at the time of installation of the wind turbines, and change in the drive train damping due to wear and tear, etc. However, the necessity of defining and implementing the fault scenarios as much realistic as possible is an important issue which can and does seriously affect the FDD and FTC results.

Table 1.4 List of the fault cases

Category	Fault	Common Symptom
Sensor Fault	Accelerometer	Offset
	Low speed shaft position encoder	Bit error
	Blade root bending moment measurement	Fixed value / Gain factor
	Pitch angle measurement	
	Rotor speed measurement	
	Generator speed measurement	
	Generator power measurement	
Actuator Fault	Converter torque	Offset
	Pitch actuator	Changed dynamics
	Yaw drive	Offset/Stuck
System Fault	Rotor	Changed dynamics
	Generator	
	Drivetrain	

1.7 Thesis Objectives

This thesis aims to design and develop novel condition monitoring, diagnosis and fault-tolerant control schemes with application to wind turbines at both individual wind turbine and entire wind farm levels. In particular, the thesis is organized around the following research objectives:

i) Designing and developing online FDD techniques which not only can set up a stand-alone cost-effective condition monitoring framework but also can be used for integration with FTC techniques in active fault-tolerant architectures.

ii) Designing and developing FTC schemes/strategies (including PFTCS and AFTCS) to improve the reliability and availability of wind turbines against potential sensor, actuator, and system faults in wind turbines and wind farms. Preferably, these FTC schemes/strategies should not only provide fault tolerance capabilities to the turbines, but also improve the overall performance of the turbines under both fault-free and faulty conditions.

To sum up, the conducted research in this thesis has been primarily expected to synthesize advanced levels of monitoring, diagnosis and fault-tolerant control capabilities in wind turbines which in turn can guarantee the reliable and satisfactory performance at both individual wind turbine and entire wind farm levels. Finally, the proposed schemes and strategies are verified by a series of simulations on well-known wind turbine and wind farm benchmark models in the presence of wind turbulences, measurement noises, and different realistic fault scenarios.

1.8 Thesis Layout and Contributions

This thesis is organized in a manuscript-based format that includes a collection of manuscripts (articles or papers) that are already published, or submitted for publication. However, all components of the thesis are tried to be structured in a coherent and logical order. The thesis consists of 6 chapters starting with Chapter 1 that gives an introduction on the thesis topic including some relevant background and motivation with a particular emphasis on wind turbines, FDD and FTC methods. Moreover, a literature review on the application of monitoring, diagnosis and fault-tolerant and efficiency control to wind turbines is also provided in Chapter 1. Chapters 2-5 present the FDD and FTC schemes proposed at both individual wind turbine (Chapters 2 and 3) and entire wind farm (Chapters 4 and 5) levels. In addition to the provided literature review in Chapter 1, each of Chapters 2-5 also includes a review of the literature that frames the relevant chapter's research area exclusively. Finally, the summary and conclusions of the contents of previous five chapters are drawn in Chapter 6. It also describes possible future research directions arising from this thesis.

With respect to the thesis contributions, following major contributions are made in Chapters 2-5:

- Chapter 2 uses fuzzy modeling, identification and control techniques to propose a novel approach in designing an integrated FDD and FTC scheme which not only provides fault tolerance capabilities to the wind turbine system, but also improves the overall performance of the system in both fault free and faulty conditions. In this regard, firstly, a simple gain-scheduled proportional-integral (PI) controller (the baseline pitch controller) is enhanced to a more sophisticated nonlinear control system based on fuzzy gain scheduling technique for robust and improved regulation of generator speed. Secondly, a model-based FDD system and appropriate automatic signal correction algorithms are designed and integrated to

constitute an AFTCS for accommodation of sensor faults in all operating regions of a wind turbine.

- Chapter 3 extends the work presented in Chapter 2 by introducing novel FTC schemes against actuator faults in a wind turbine. In more details, the main contribution of Chapter 3 is to exploit fuzzy modeling, identification and control techniques to propose two different, novel approaches in designing FTC for reliable regulation of the generator torque load in a wind turbine. The first approach results in a novel fuzzy model reference adaptive control mechanism oriented to the design of a PFTC scheme which has the interesting capability of online adaptation of the control action without any explicit knowledge of the faults and model uncertainties or external disturbances (i.e., no need to employ FDD unit). Conversely, the second approach results in an AFTC scheme which is based on an integrated FDD and automatic signal correction mechanism. The proposed approaches are effective in all operating regions of a wind turbine.

- Chapter 4 presents a novel integrated FDD and FTC approach in a cooperative framework oriented to the design and development of two AFTC schemes for an offshore wind farm against decreased power generation fault caused by turbine blade erosion and debris build-up on the blades over time. The first scheme is based on a model-free FDD system that incorporates a rule-based threshold test technique for residual evaluation. Conversely, the second scheme is based on a model-based FDD system that incorporates data-driven models developed using fuzzy modelling and identification technique. Both schemes are relying on an appropriate automatic signal correction algorithm that employs the provided accurate and timely FDD information for accommodating the possible faults in a wind farm. The proposed schemes are valid for any layouts of a wind farm with any directions of the wind while the fault may occur simultaneously in more than one turbine in the farm.

- Chapter 5 considers active power control at the entire wind farm level and presents two control schemes aimed at tracking various forms of power schedules and loads, while maintaining grid frequency against any sudden imbalance between generation and loads, which is referred to as frequency event. A frequency event is typically caused by sudden variations in electrical loads, new generation allocation, disconnection of generators, and disturbed generation due to faults and failures. The two active power control schemes are developed based on adaptive pole

placement control and fuzzy gain-scheduled PI control approaches. A main advantage of the proposed schemes is their stand-alone structures that do not complicate the wind turbines' conventional control loops for easier acceptance and validation & verification by wind energy industry for commercialization. Furthermore, the proposed schemes can operate in the same range of wind speeds as wind turbines' standard baseline control systems while considering the practical safe operating limits of the turbines.

Chapter 2 Fuzzy Gain-Scheduled Active Fault-Tolerant Control of a Wind Turbine

Abstract

Advanced fault detection and accommodation schemes are required for ensuring efficient and reliable operation of modern wind turbines. This paper presents a novel approach in designing a Fault Detection and Diagnosis (FDD) and Fault-Tolerant Control (FTC) scheme for a wind turbine using fuzzy modeling, identification and control techniques. First, an improved gain-scheduled Proportional-Integral (PI) control system based on Fuzzy Gain Scheduling (FGS) technique for multi-input and multi-output wind turbine system is designed. Then, to accommodate sensor faults and based on a signal correction algorithm, an Active Fault-Tolerant Control System (AFTCS) is developed as an extension of the gain-scheduled PI control system. The AFTCS exploits the fault information from a model-based FDD scheme developed using fuzzy modeling and identification method. The proposed schemes are evaluated by a series of simulations on a well-known large off-shore wind turbine benchmark in the presence of wind turbulences, measurement noises, and different realistic fault scenarios. All results indicate high effectiveness and robustness of the designed control systems in both fault-free and faulty operations of the wind turbine.

2.1 Introduction

Nowadays, wind as one of the renewable sources of energy has received tremendous attention in the energy market to alleviate the ever-increasing global demand for fossil fuels and subsequent concerns about environmental issues [1]. However, lowering the cost of wind energy generation is an essential key to the expansion of wind-energy industry and subsequent wind power penetration in the next decades [72]. In this regard, the future of wind energy industry passes through the use of larger and more flexible wind turbines in remote locations, which are increasingly offshore to benefit stronger and more uniform wind conditions. Hence, both the size and location factors come into play and lead to increased maintenance challenges. Moreover, high mechanical stress is imposed on wind turbines due to highly variable operating conditions and constantly changing loads. This high degree of mechanical stress demands a high degree of maintenance while wind turbines are subjected to high reliability and availability requirements. A promising way to contribute to the mentioned ever increasing requirements and challenges passes through applying low-cost advanced fault detection, diagnosis and accommodation schemes.

A Fault Detection and Diagnosis (FDD) system uses sensor data for detection, isolation and identification of faults in the wind turbine components. The FDD system sends the fault information to a Fault-Tolerant Control (FTC) system to accommodate the faults when possible. Such a FTC system which relies on the fault information obtained from the FDD is called an Active Fault-Tolerant Control System (AFTCS) [10].

Today's industrial wind turbines exploit simple and often conservative hardware redundant fault detection and condition monitoring systems [73]. The information obtained from these systems is usually used for condition monitoring and predictive maintenance purposes only. That is, turbines are turned off and go to downtime even at simple faults to wait for service. A general review on current condition monitoring and fault detection techniques for wind turbines can be found in recent survey papers [12-14].

Recently, numerous studies [27, 30, 74-77] have been conducted to apply analytical redundancy approaches including model-based and data-driven FDD methods as a promising framework not only for low cost fault detection and condition monitoring but also facilitating the realization of concept of active FTC in wind turbines. Odgaard et al. [73] has compared and evaluated a number of papers published on fault detection and isolation of a standard wind turbine

benchmark proposed in [3]. In contrast to FDD, existing literature on wind turbine FTC is still scarce [11]. As an example, Sloth *et al*. [43] present multiple Linear Parameter-Varying (LPV) control schemes for a wind turbine operating over the full load region with a single actuator fault. In fact, a nominal LPV controller is designed to handle the parameter variations along the nominal operating trajectory caused by nonlinear aerodynamics of turbine system. Moreover, it is demonstrated that it is possible to add robustness and fault-tolerance capabilities to the nominal LPV controller provided a sufficiently good model and effective wind speed estimation as the only scheduling variable. However, wind turbines are driven by wind as a stochastic input, and essentially exhibit highly nonlinear dynamics. They are operating in uncertain environments, and are exposed to large disturbances. Describing such a complex nonlinear system accurately by mathematical models is very difficult in practice. Additionally, the increasing tendency towards larger and more flexible wind turbines is making this task even more demanding [16].

From a control standpoint, the lack of rigorous analytical models and large measurement noises in wind turbines have motivated the development of new control strategies capable of securing stability and some performance features despite model uncertainties.

The Takagi-Sugeno (T-S) type dynamic fuzzy model [78] has been recognized as one of the most efficient and successful tools for handling complex nonlinear systems and applications [79]. A T–S fuzzy model consists of a set of fuzzy local models which are combined using a fuzzy inference mechanism corresponding to various operating points. Extensive research efforts have been devoted to the analysis and synthesis problems of T-S fuzzy control systems [79-83]. Moreover, recent researches have been aimed at investigating the reliability considerations in the continuous-time T–S fuzzy systems [84-87].

Although fuzzy logic and other artificial intelligence techniques have been extensively investigated in the literature for modeling and control of wind turbines (see for instance, Refs. [37, 88-91]), there are few results on wind turbine FDD and FTC design using T–S fuzzy modeling method [32, 52-54]. In [32], a diagnosis strategy based on fuzzy prototypes is presented for detection of rotor and converter faults. Kamal et al. [54] propose an observer-based fault-tolerant control design based on T-S fuzzy modeling and multi-sensor scheme (hardware redundant sensors) to handle parameter uncertainties and fault in a generator speed sensor. Authors in [52] propose a T-S fuzzy dynamic output feedback controller which is designed to track the required

optimal rotor speed in the partial load region only. A fuzzy estimator capable of handling the case of time-varying fault signals is employed to compensate the effects of generator and rotor speed sensor faults from the controller inputs. The same authors have presented a similar fuzzy control structure in the second FTC scheme [53]. However, this work describes a simplification of the observer design and also provides an estimation of the effective wind speed in partial load region.

The main contribution of this paper is to exploit fuzzy modeling, identification and control techniques to propose a novel approach in designing an integrated FDD and FTC scheme (FDD-FTC) which not only provides fault tolerance capabilities to the wind turbine system, but also improves the overall performance of the system in both fault free and faulty conditions.

In this regard, the first objective is to enhance a simple gain-scheduled PI-controller (the baseline pitch controller) to a more sophisticated nonlinear control system for robust and improved regulation of generator speed. To this end, a Fuzzy Gain Scheduling (FGS) technique is applied to the baseline pitch controller to tune the controller gains in real-time as operating condition or dynamics of the system varies. This approach is actually a synthesis of the conventional PID control and fuzzy control which combines the simplicity of PID controllers with knowledge representation power of fuzzy controllers. The main advantage of the FGS PI-control technique is that it can be easily implemented by adding to existing hardware PID controllers, and is more likely to gain acceptance from industry [92].

The second objective of the present paper is to propose an AFTCS which exploits the fault information obtained from a model-based FDD system developed using fuzzy modeling and identification method. The AFTCS employs the FGS PI-controller as a platform (baseline) control system which is equipped with appropriate Automatic Signal Correction (ASC) algorithms to accommodate potential faults in the wind turbine system.

An off-shore 5-MW wind turbine benchmark [70] is considered as a testbed for the proposed FDD and control strategies. This is a three-bladed upwind variable-speed variable blade-pitch-to-feather wind turbine. The proposed control schemes are evaluated via the latest available advanced MATLAB/Simulink simulation benchmark model, called “NREL’s FAST 5 MW turbine model” [70, 71]. The simulations are conducted in the presence of wind turbulences, measurement noises, and realistic fault scenarios specified by the benchmark. Two important fault scenarios are investigated: scaling generator speed sensor, and biased blade-pitch angle sensor. The considered

faults are so significant on the effect to the behavior of the wind turbine control system, and therefore, effective FDD and FTC strategies are necessary for maintaining stability and required performance of the wind turbine.

The remainder of the paper is organized as follows: In Section 2, the used wind turbine benchmark model and description about the considered fault scenarios are introduced. The reference/baseline control system of the wind turbine benchmark based on conventional approaches is presented in Section 3. The gain-scheduling approach developed in this paper is described in Section 4. Remedial strategy including the proposed schemes for FDD and FTC of the wind turbine is presented in Section 5. Section 6 presents the simulation results with some comments and discussion. Finally, conclusions are drawn in Section 7.

2.2 The Wind Turbine Benchmark Model and Fault Scenarios

This paper considers an off-shore 5MW baseline turbine proposed by the U.S. National Renewable Energy Laboratory (NREL) [70]. This is a three-bladed Horizontal Axis Wind Turbine (HAWT) containing full generator and converter. The wind turbine is variable speed with full span blade pitch control and generator torque regulation.

A) Model Description

The baseline wind turbine is modeled using FAST (Fatigue, Aerodynamics, Structures, and Turbulence) [71], a comprehensive aeroelastic simulator code developed by NREL for supporting research and development aimed at assessing off-shore wind technology. FAST can model a three-bladed HAWT as a combination of rigid and flexible bodies through 24 Degrees Of Freedom (DOFs), with further details given in [71]. FAST employs another NREL code called AeroDyn subroutine library to predict the aerodynamics of the wind turbine. The AeroDyn itself utilizes realistic wind input files generated in TurbSim which is a stochastic, full-field, turbulent-wind simulator.

A simplified block scheme of the wind turbine benchmark model is shown in Figure 2.1. As shown in the figure, due to some limitations in the FAST code, the dynamics of sensors and actuators are implemented separately from [69] within the Simulink environment.

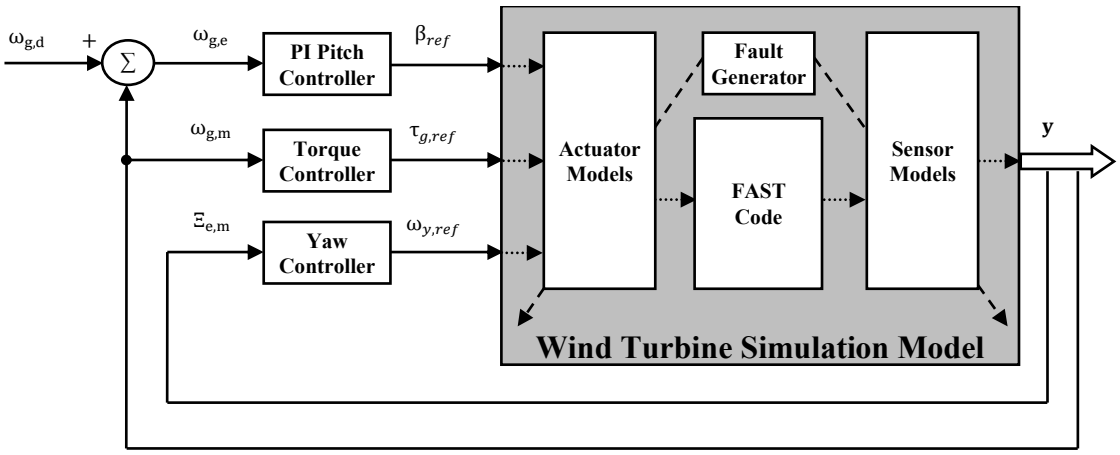

Figure 2.1 Block diagram showing wind turbine simulation model and the pitch, torque and yaw control systems in feedback loops. The measured generator speed $\omega_{g,m}$ and wind yaw error $\Xi_{e,m}$ are extracted from the model output vector $\boldsymbol{y}$.

B) Faults Description

The fault scenarios are implemented within the Sensor Models block (see Figure 2.1) of the benchmark model with sensor faults. Table 2.1 presents the faults considered in this paper [69].

Table 2.1 Fault Scenarios

No.	Fault	Type	Time Period (sec)
1	Generator Speed Sensor	Scaling	130-155
2	Blade-Pitch Angle Sensor	Stuck	185-210

Sensor faults lead to measurements that are mistakenly scaled or stuck from their true values. Fault 1 is a scaling fault which causes the generator sensor to be scaled by a factor of 0.95. This fault is present during [130-155] sec during wind turbine operation. Since this sensor value is fed as an input to both of torque and pitch controllers, this fault can be harmful in the case of bad or slow accommodation.

Fault 2 results in a fixed output value of 1 deg from pitch sensor of one of rotor blades. Fault 2 is active within [185-210] sec. This fault causes a biased pitch angle measurement which affects both the pitch angle sensor and the closed-loop pitch actuator system.

2.3 Baseline Control System

The baseline control system is developed on the basis of classical control techniques. As seen in Figure 2.1, the overall control system is composed of three individual controllers for regulating blade-pitch angles, generator torque, and nacelle yaw angle. All controllers typically use the generator speed feedback, except yaw controller which relies only on yaw error information. To reduce the effects of drive train oscillations on the measured generator speed, a low-pass filter is imposed on it before being fed to the controllers.

In *above rated* wind speeds (full load region or region III, as shown in Figure 2.2), a blade-pitch PI-controller tracks a constant generator speed called rated generator speed so that the turbine operates at its rated power of 5 MW. The controller exploits a simple gain scheduling scheme on the basis of aerodynamic considerations of blade-pitch sensitivity. Actually, the controller uses the blade pitch angle from the previous time step of controller outputs to calculate a gain correction factor at the next time step.

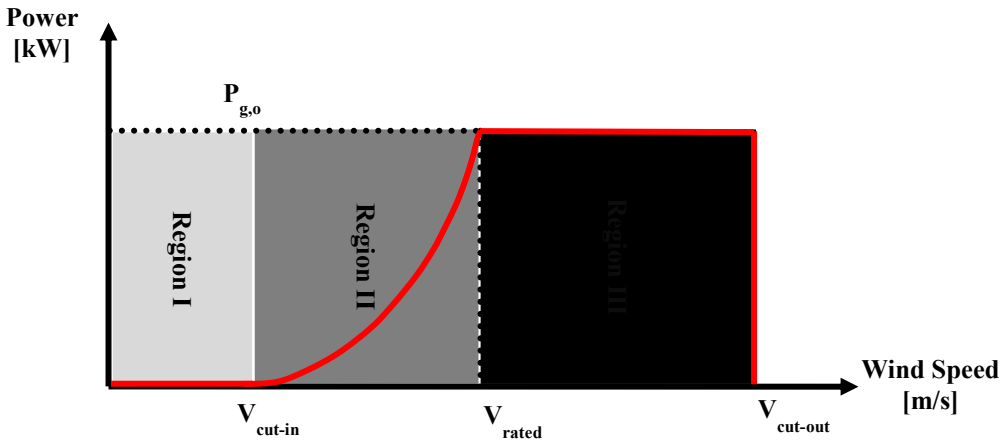

Figure 2.2 Illustration of ideal power curve versus wind speed for operation of a typical wind turbine [16].

The torque controller is designed by varying the generator torque to maximize power capture in the *below rated* wind speeds (partial load region or region II, see Figure 2.2). Furthermore, the torque controller can be set to be active in above rated wind speeds so as to produce constant power output. In this case, the reference generator torque $\tau_{g,ref}$ is calculated using (2.1), where $P_{g,o}$ is the turbine rated power, $\omega_g(t)$ is the filtered generator speed, and η_g is the generator efficiency.

$$\tau_{g,ref}(t) = \frac{P_{g,o}}{\eta_g \omega_g(t)} \tag{2.1}$$

The yaw controller is an On/Off controller developed to orient the nacelle as wind direction changes [69]. However, to avoid dangerous gyroscopic forces, the yaw rate should be typically limited to less than 1°/s. That is, the yaw controller cannot be as fast to react as it is required for investigation of advanced control approaches.

The pitch and torque controllers are faster and much more flexible compared to the yaw controller. However, to avoid any intense commanded signal and its subsequent excessive load on the relevant actuator(s), the appropriate rate limiters and magnitude limiters are imposed on the outputs of each controller. These limiters are kept unchanged throughout this paper.

2.4 Fuzzy Gain-Scheduled PI-Controller Design

In this section, the baseline pitch PI-controller is improved to a Fuzzy Gain-Scheduled (FGS) PI-control system on the basis of proposed method in [93]. The baseline PI-controller has only one input of generator speed tracking error, while the proposed FGS PI-controller has an extra input of change in tracking error (derivative) as well for the purpose of improving control performance of the wind turbine. This derivative input allows for better describing the system's dynamics, and provides some level of passive predictability of system behavior to facilitate control.

A) Baseline PI-Control System Description

In above rated wind speeds, the PI-collective-pitch-control law is represented as:

$$\beta_{ref}(t) = K_P \omega_{g,e}(t) + K_I \int_0^t \omega_{g,e}(\tau) d\tau \tag{2.2}$$

in which, $\beta_{ref}(t)$ is the reference blade-pitch angle, $\omega_{g,e}(t) = \omega_{g,d} - \omega_{g,m}$ is the generator speed error, and the desired generator speed is $\omega_{g,d}$.

Authors in [70] have used the described method in [94] to derive the values of control gains. Using a simple single-DOF model of the wind turbine, and after some simplifying assumptions, [70] derives the following proportional and integral gains for (2.2):

$$K_P(\beta) = K_{P,\beta=0}\,\Phi(\beta) \tag{2.3}$$

$$K_I(\beta) = K_{I,\beta=0}\,\Phi(\beta) \tag{2.4}$$

where $K_{P,\beta=0}$ and $K_{I,\beta=0}$ denote, respectively, the constant uncorrected proportional and integral gains. They are defined in (2.5) and (2.6) respectively, in which the $\frac{\partial P}{\partial \beta}(\beta = 0)$ is pitch sensitivity at rated operating point ($\beta = 0$), the drive train inertia, I_{dt}, rated low-speed shaft rotational speed, $\omega_{r,o}$, and gearbox ratio, N_g, all are constants describing the wind turbine system. The natural frequency, $\omega_{\varphi n}$, and damping ratio, ζ_φ, represent response characteristics with their appropriate constant values recommended in [94].

$$K_{P,\beta=0} = \frac{2I_{dt}\omega_{r,o}\zeta_\varphi\omega_{\varphi n}}{N_g\left[-\frac{\partial P}{\partial \beta}(\beta = 0)\right]} \tag{2.5}$$

$$K_{I,\beta=0} = \frac{I_{dt}\omega_{r,o}{\omega_{\varphi n}}^2}{N_g\left[-\frac{\partial P}{\partial \beta}(\beta = 0)\right]} \tag{2.6}$$

In (2.3) and (2.4), the only adaptive term is the following correction factor (2.7), in which β_c is the blade-pitch angle at which the pitch sensitivity has been doubled from its rated value.

$$\Phi(\beta) = \frac{1}{1 + \frac{\beta}{\beta_c}} \tag{2.7}$$

In the gain scheduling process, the PI-controller applies the blade-pitch angle from the previous control time step $(k-1)$ to calculate the correction factor at the next time step (k).

Since the above method considers some effects of nonlinear aerodynamic characteristics, it is preferred to an ordinary pitch PI-controller with completely constant gains [94]. However, this gain-scheduled system is still a simple PI-controller which is basically derived from a simple single-DOF model of wind turbine and also based on some simplification assumptions (see [70]).

In the next subsection, we propose the design of an effective gain scheduling scheme to improve the performance of the above described baseline PI-controller.

B) Fuzzy Gain-Scheduled PI-Controller Design

The proposed scheduling scheme exploits fuzzy inference mechanism for online adaptation of the proportional and integral gains derived for the baseline PI-controller (see Figure 2.3). As it was shown in the previous subsection, each control gain has its own correction factor which only handles the nonlinearities due to blade-pitch authority (see (2.7)). Here, the correction factors remain unchanged, while the constant uncorrected $K_{P,\beta=0}$ and $K_{I,\beta=0}$ are scheduled to capture other nonlinearities in the wind turbine system.

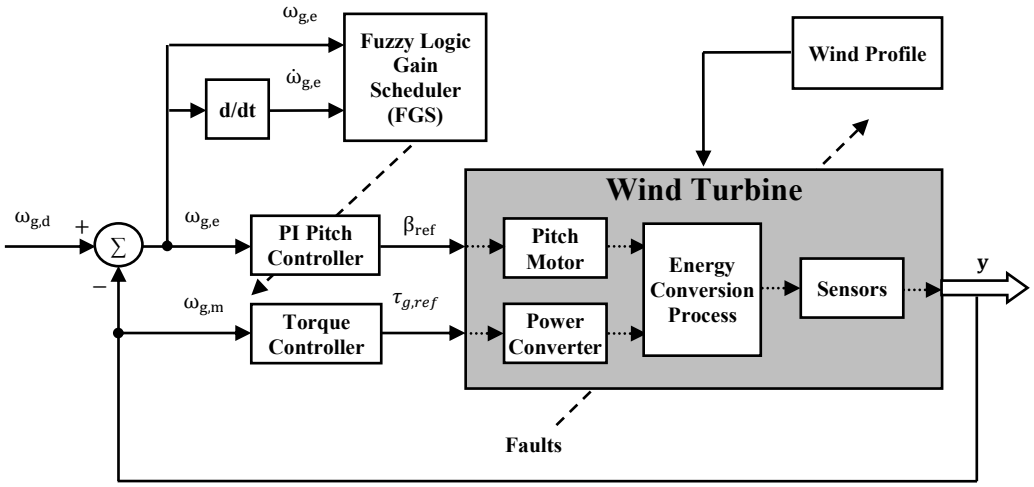

Figure 2.3 Block diagram of the fuzzy gain-scheduled PI control system. The measured generator speed $\omega_{g,m}$ is extracted from the model output vector $\boldsymbol{y}$.

The uncorrected gains can be defined through a simple linear transformation form as follows:

$$K_{P,\beta=0}(k) = \left(K_{P,\beta=0}^{max} - K_{P,\beta=0}^{min}\right)K_P'(k) + K_{P,\beta=0}^{min} \tag{2.8}$$

$$K_{I,\beta=0}(k) = \left(K_{I,\beta=0}^{max} - K_{I,\beta=0}^{min}\right)K_I'(k) + K_{I,\beta=0}^{min} \tag{2.9}$$

where, K_P' and K_I' are respectively normalized values of $K_{P,\beta=0}$ and $K_{I,\beta=0}$ between zero and one. The $\left[K_{P,\beta=0}^{min}, K_{P,\beta=0}^{max}\right]$ and $\left[K_{I,\beta=0}^{min}, K_{I,\beta=0}^{max}\right]$ in (2.8) and (2.9) are prescribed ranges for $K_{P,\beta=0}$ and $K_{I,\beta=0}$ respectively. A rule of thumb for determining the above ranges is given as [93]:

$$K_{P,\beta=0}^{min} = 0.32\, K_u \tag{2.10}$$

$$K_{P,\beta=0}^{max} = 0.6\, K_u \tag{2.11}$$

where K_u denotes the gain of oscillation at the stability limit under P-control [95]. Subsequently, the range of $K_{I,\beta=0}$ can be estimated based on (2.12) in which T_I is the integral time constant [93]:

$$K_{I,\beta=0} = \frac{K_{P,\beta=0}}{T_I} \tag{2.12}$$

Although the above mentioned rule of thumb provides an estimate for each range, more experiments are required to fine tune the ranges and to achieve the favorable control performance. Table 2.2 presents the values of uncorrected gains and the chosen ranges for them.

Table 2.2 Controller parameters for baseline PI-controller and FGS-PI controller

Parameter	Value/Range
$K_{P,\beta=0}$	2×10^{-2}
$[K_{P,\beta=0}^{min}, K_{P,\beta=0}^{max}]$	$[1.05 \times 10^{-2}, 3.8 \times 10^{-2}]$
$K_{I,\beta=0}$	8.07×10^{-3}
$[K_{I,\beta=0}^{min}, K_{I,\beta=0}^{max}]$	$[7.542 \times 10^{-3}, 8.594 \times 10^{-3}]$

The parameters K_P' and K_I' in (2.8) and (2.9) as the normalized values of $K_{P,\beta=0}$ and $K_{I,\beta=0}$ are determined on-line using a set of linguistic *if-then* rules in the form of [93]:

$$\textbf{\textit{Rule i}}\textbf{:}\ \text{If } \omega_{g,e}(k) \text{ is } A_i \text{ and } \dot{\omega}_{g,e}(k) \text{ is } B_i, \text{then } K_P'(k) \text{ is } C_i \text{ and } K_I'(k) \text{ is } D_i \tag{2.13}$$

where A_i, B_i, C_i and D_i (with $i = 1,2, \dots, M$) are fuzzy sets corresponding to $\omega_{g,e}$, $\dot{\omega}_{g,e}$, K_P', and K_I' respectively. The used triangular membership functions for $\omega_{g,e}$ and $\dot{\omega}_{g,e}$ are shown in Figure 2.4(a). In this figure, the fuzzy subset ZO stands for approximately zero, PS for positive-small, PM for positive-medium, and PB for positive-big. Similarly, NS represents negative-small and so on. Figure 2.4(b) shows the selected membership functions for K_P' and K_I'. Both the B (big) and S (small) membership functions are based on generalized bell function in the following form with bell function parameters a, b, and c:

$$\mu(x) = \frac{1}{1 + \left|\frac{x-c}{a}\right|^{2b}} \tag{2.14}$$

The above function provides smooth and nonlinear mapping between the degree of membership function μ and the variable $x = (K_P' \text{ or } K_I')$.

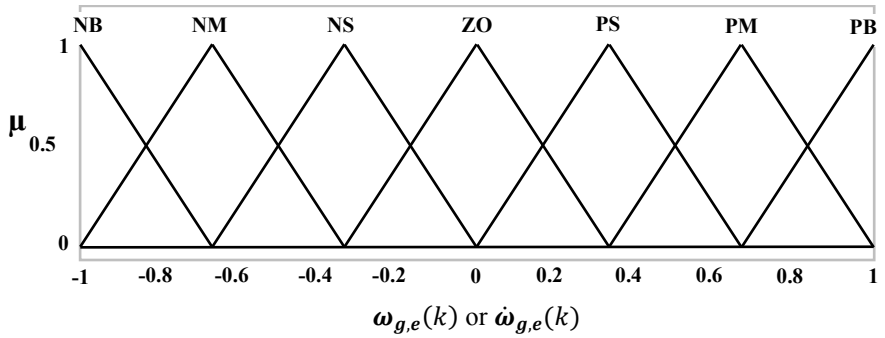

(a)

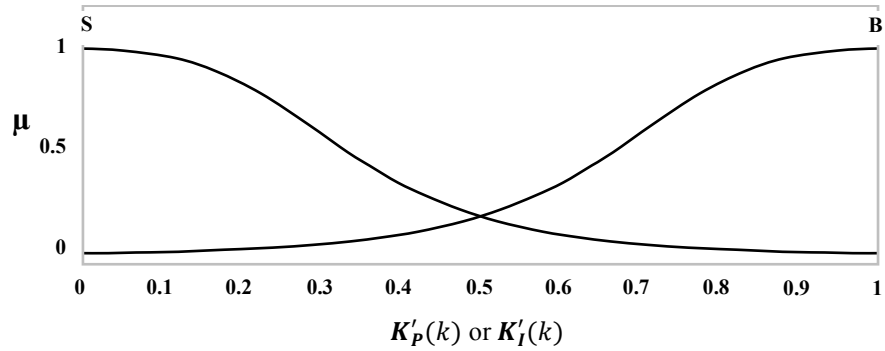

(b)

Figure 2.4 Membership functions. (a) inputs, (b) outputs

Rule bases shown in Tables 2.3 and 2.4 represent rules in (2.13). They are formulated based on expert's knowledge. As a general rule for a PID controller, to produce a big control signal, the controller should use a large proportional gain, a large integral gain, and a small derivative gain.

Table 2.3 Fuzzy rules for K_P'

		$\dot{\omega}_{g,e}(k)$						
		NB	NM	NS	ZO	PS	PM	PB
$\omega_{g,e}(k)$	NB	B	B	B	B	B	B	B
	NM	S	B	B	B	B	B	S
	NS	S	S	B	B	B	S	S
	ZO	S	S	S	B	S	S	S
	PS	S	S	B	B	B	S	S
	PM	S	B	B	B	B	B	S
	PB	B	B	B	B	B	B	B

Table 2.4 Fuzzy rules for K_I'

		$\dot{\omega}_{g,e}(k)$						
		NB	NM	NS	ZO	PS	PM	PB
$\omega_{g,e}(k)$	NB	B	B	B	B	B	B	B
	NM	B	B	S	S	S	B	B
	NS	B	B	B	S	B	B	B
	ZO	B	B	B	S	B	B	B
	PS	B	B	B	S	B	B	B
	PM	B	B	S	S	S	B	B
	PB	B	B	B	B	B	B	B

In this paper, the logic AND has been implemented with the minimum operator, and the defuzzification is based on center of area method as follows [93]:

$$K_P' = \frac{\sum_{i=1}^{M} \mu_i K_{P\,i}'}{\sum_{i=1}^{M} \mu_i} \tag{2.15}$$

$$K_I' = \frac{\sum_{i=1}^{M} \mu_i K_{I\,i}'}{\sum_{i=1}^{M} \mu_i} \tag{2.16}$$

where, $K_{P\,i}'$ and $K_{I\,i}'$ are the values of K_P' and K_I' corresponding to the degree of membership μ_i for the *i*-th rule respectively. Notice that if the fuzzified inputs are normalized to the values between 0 and 1, then the denominator of the above rules will be one.

The eventual input-output surface presentations of the fuzzy gain scheduler for K_P' and K_I' are shown in Figure 2.5.

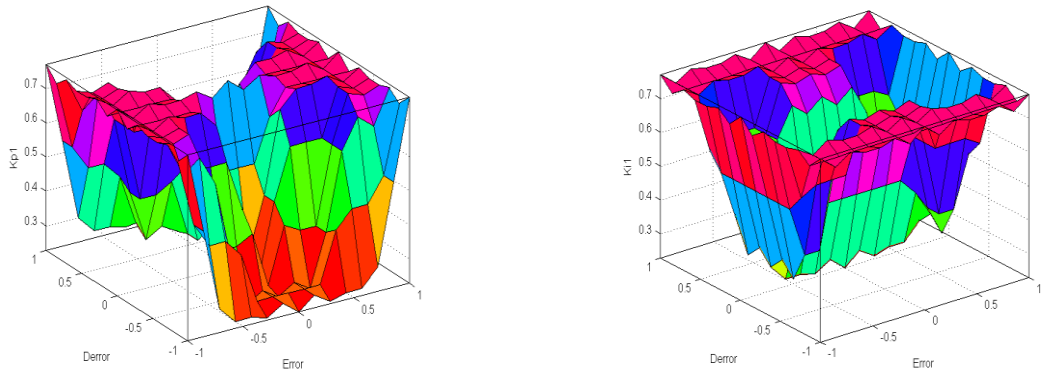

(a) (b)

Figure 2.5 Response surfaces. (a) K_P' and (b) K_I'

2.5 Remedial Strategy

This section presents the strategy that must be taken into consideration to prevent the propagation of faults and system failure. The proposed strategy results in a fault-tolerant control algorithm which is based on signal correction. This FTC algorithm complements the proposed FGS-PI control system, and enhances its functionality to an AFTCS.

Here, signal correction means that the previously developed control system (the pitch FGS PI-controller and the reference torque controller) is not modified; only the inputs and outputs of the controller are corrected according to the faults information. Therefore, the method relies on fault detection and diagnosis scheme to provide the most up-to-date information about the true status of the wind turbine system.

An important feature of AFTCS on the basis of signal correction is its autonomous structure which does not affect the performance of FGS-PI system. So, this property makes it possible to save the robustness and efficiency of the FGS-PI system under the defined fault conditions.

The structure of AFTCS is outlined in Figure 2.6. As shown in the figure, the pitch and torque controllers are kept unchanged themselves; only their inputs and outputs are modified. Here, the supervision process is not described explicitly, because it is very simple in the considered case.

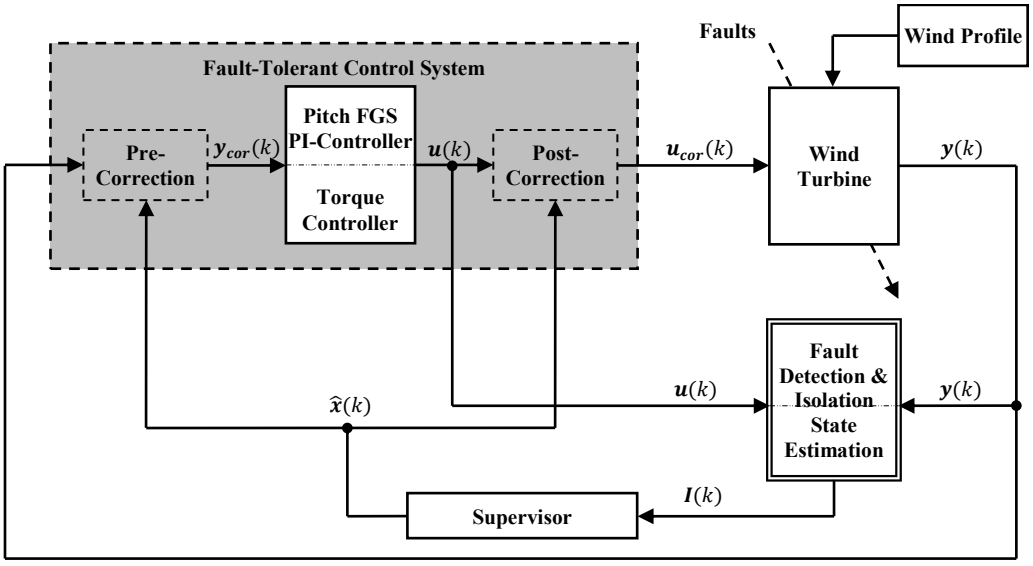

Figure 2.6 Schematic of AFTCS using FDD module. Based on FDD information $\boldsymbol{I}(k)$, the supervisor applies appropriate signal correction/modification using estimates (wind turbine states and/or fault biases) $\hat{\boldsymbol{x}}(k)$.

A) Model-Based FDD Approach

This paper applies a model-based Fault Detection and Diagnosis (FDD) approach using Fuzzy Modeling and Identification (FMI) method (see Figure 2.7).

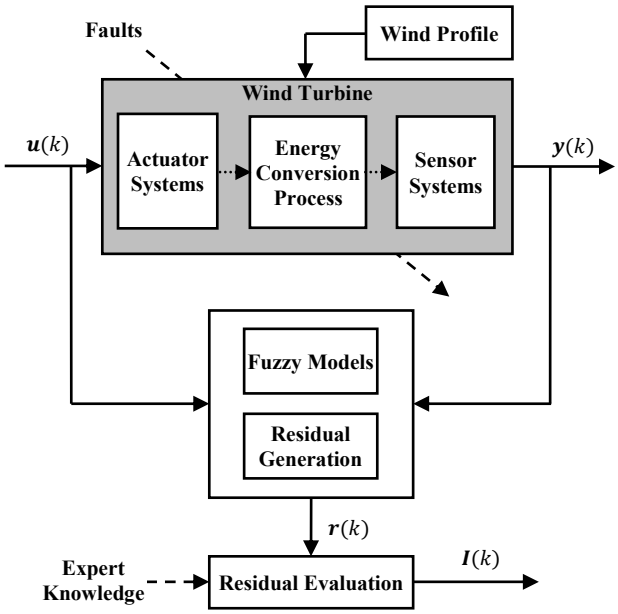

Figure 2.7 Model-based fault detection and diagnosis scheme based on fuzzy models.

As depicted in Figure 2.7, the so-called residuals $\boldsymbol{r}(k)$ are computed as the difference between the actual system outputs $\boldsymbol{y}(k)$, and the estimated outputs $\hat{\boldsymbol{y}}(k)$ obtained from Takagi-Sugeno (T-S) fuzzy models which are identified and developed from measured data during normal operation of wind turbine:

$$\boldsymbol{r}(k) = \hat{\boldsymbol{y}}(k) - \boldsymbol{y}(k) \tag{2.17}$$

A decision-making logic (2.18) can be applied for residual evaluation in Figure 2.7.

$$\begin{cases} (r_m - \gamma r_{std}) \le \boldsymbol{r}(k) \le (r_m + \gamma r_{std}) & No\ Fault \\ \boldsymbol{r}(k) > (r_m + \gamma r_{std}) \quad or \quad \boldsymbol{r}(k) < (r_m - \gamma r_{std}) & Fault \end{cases} \tag{2.18}$$

where r_m and r_{std} denote respectively the mean and the standard deviation values of residuals $\boldsymbol{r}(k)$ during fault-free operation of the wind turbine. The tuning parameter γ represents the modeling error, and should be properly chosen to minimize false detection and missed detection rates.

The accuracy of a model plays an important role in ensuring the performance of a model-based FDD system. The FMI approach is selected in this paper since it has been proved to be an efficient

method for the identification of nonlinear dynamic systems like a wind turbine [32, 96]. An important advantage of local fuzzy model networks is that they can be designed to automatically adapt themselves to the complexity of the problem in a highly efficient way. However, some important problems involved with the identification of dynamic models from real processes are the noise and high frequency excitation in input and output data. In the following section, a filter system is presented to overcome these problems. Subsequently, data-driven modeling and identification scheme based on fuzzy clustering will be presented.

1) Measurement Filter

In this paper, to obtain the appropriate data sets for FMI process and also to obtain precise fuzzy models for the FDD system, a recursive, single-pole low-pass filter with exponential smoothing is used. This type of filter is selected due to its simplicity in implementation and effectiveness in the time domain. The filter is modeled as a discrete-time recursion (difference) equation with discrete time constant T_s and corner frequency f_c [70]:

$$\begin{aligned} y(k) &= (1-\alpha)\,u(k) + \alpha\, y(k-1) \\ \alpha &= e^{-2\pi T_s f_c} \end{aligned} \tag{2.19}$$

where u and y are the unfiltered input measurement and filtered output measurement, respectively, and α denotes low-pass filter coefficient.

By defining the filter state as follows:

$$x(k) = y(k-1) \quad \text{or} \quad x(k+1) = y(k) \tag{2.20}$$

This filter can be presented in discrete-time state-space format as follows:

$$\begin{aligned} x(k+1) &= A_d x(k) + B_d u(k) \\ y(k) &= C_d x(k) + D_d u(k) \end{aligned} \tag{2.21}$$

where $A_d = \alpha$ is the discrete-time state matrix, $B_d = 1-\alpha$ is the discrete-time input matrix, $C_d = \alpha$ is the discrete-time output state matrix, and $D_d = 1-\alpha$ is the discrete-time input transmission matrix. Using the above state-space representation, the filter can be converted into other forms, such as frequency-response form or transfer-function form.

2) Fuzzy Modeling and Identification

Almost all of the physical dynamical systems in real life have a nonlinear nature and cannot be represented only by linear differential equations. In practice, it would be difficult or even impossible to derive a single nonlinear model for all operating conditions of a system. One way to cope with such difficulty is multiple-model approach.

FMI is one of the efficient methods for generating multiple models as a collection of fuzzy if-then rules. A significant fuzzy modeling technique is the Takagi-Sugeno (T-S) method which is a multiple-model approach that can handle uncertain and time-varying situations [78]. It has excellent capability in complex and uncertain system description and is particularly suitable for modeling nonlinear systems using a set of fuzzy local models (sub-models) which are trained based on measured input-output data. These sub-models are combined using a fuzzy inference mechanism corresponding to various operating points, and finally constitute an overall fuzzy model for the system.

a) T-S fuzzy modeling

Without loss of generality, a Single-Input Single-Output (SISO) system can be defined in the following form:

$$\begin{gathered} y(k+1) = f(\psi(k)) + e \\ \boldsymbol{\psi(k)} = \left[y(k), \dots, y\left(k - n_y + 1\right); u(k), \dots, u(k - n_u + 1)\right]^T \end{gathered} \tag{2.22}$$

in which $\boldsymbol{\psi(k)}$ is an information data vector including the past model inputs $u(k)$ and outputs $y(k)$, k is the discrete-time-step, $\{n_u, n_y\} \in \mathbb{Z}$ correspond to the model order which can be defined by the user, and e indicates the modeling error.

As already remarked, the unknown function $f(.)$ Can be approximated by a T-S type fuzzy model described in terms of m rules as [97]:

$$\begin{aligned} \textbf{Rule } \boldsymbol{j}\textbf{:}\quad & \boldsymbol{If}\ y(k)\ is\ A_{j1}\ \boldsymbol{and}\ y(k-1) is\ A_{j2}\ \boldsymbol{and}, \dots, y\left(k - n_y + 1\right) is\ A_{jn_y} \\ & \boldsymbol{and}\ u(k) is\ B_{j1}\ \boldsymbol{and}\ u(k-1) is\ B_{j2}\ \boldsymbol{and}, \dots, u(k - n_u + 1) is\ B_{jn_u} \\ & \boldsymbol{then}\ y(k+1) = F_j\left(y(k), \dots, y\left(k - n_y + 1\right), u(k), \dots, u(k - n_u + 1)\right) \end{aligned} \tag{2.23}$$

where A, B are the antecedent fuzzy sets of the j-th rule ($j = 1,2, \dots, m$) in which each of them are defined by a membership function. Since a T-S fuzzy model represents the rule consequences in the form of crisp functions of the model inputs, so $F_j(.)$ is an arbitrary function which has an identical structure with varying parameters in each rule. One selection for F_j can be a simple but practically efficient affine (linear) form as follows [97]:

$$F_j: \quad y_j(k+1) = \boldsymbol{\chi_j}\boldsymbol{\psi} + \lambda_j \tag{2.24}$$

where $\boldsymbol{\chi_j}$ and λ_j denote the j-th parameter vector and scalar offset of the j-th rule respectively. In this way, an affine T-S model is obtained.

The foresaid approach as a T-S fuzzy model represents the dynamics of a nonlinear system using the following fuzzy fusion over the all model outputs [97]:

$$\hat{y} = \frac{\sum_{j=1}^{m} \mu_j(\boldsymbol{\psi}) y_j}{\sum_{j=1}^{m} \mu_j(\boldsymbol{\psi})} \tag{2.25}$$

where $\hat{y}$ is the aggregated output of the model, μ_j are membership functions each representing the degree of fulfillment of a rule.

b) Identification using fuzzy clustering

The problem of nonlinear system identification emphasizes on identifying the structure of fuzzy model, and then estimating the model parameters. Identifying the structure corresponds to the determination of number and types of membership functions for the input variables and the number of tuning rules and output variables. Estimating the model parameters includes determination of the antecedent fuzzy sets and the consequent parameters of the T-S model. In this paper, the well-established Gustafson-Kessel (GK) clustering algorithm [98] is used to identify fuzzy T-S models. The GK algorithm performs data set partitioning into fuzzy subsets in an iterative way. Then the identification procedure is accomplished by generation of the antecedent membership functions, and the estimation of the parameters of the local linear models through a weighted ordinary least-squares algorithm.

B) FDD and FTC Design for Fault Scenarios

Each of the considered fault scenarios in Section 2.2 has a degree of influence on the wind turbine performance. In the following subsections, the aforementioned remedial strategy including model-based FDD and automatic signal correction algorithms for AFTCS are designed and developed for each type of sensor faults. Additionally, the requirements for the fault diagnosis and accommodation schemes are determined.

1) Generator Speed Sensor Fault Case

Generally, the possible faults that may occur for the generator speed sensor include: scaling (proportional) error on the output, fixed output, and no output. The scaling error is the challenging one which is modeled as follows:

$$\omega_{g,m}(k) = \big(1 + \delta_{se}(k)\big)\omega_g(k) + \sigma_{\omega_g}(k) \tag{2.26}$$

where $\omega_{g,m}(k)$ is the generator speed measurement (rpm) at the instant k, $\delta_{se}(k)$ is the scaling error, and $\sigma_{\omega_g}(k)$ denotes a white noise sequence (rpm).

As already remarked, the considered fault causes the generator speed sensor $\omega_{g,m}$ to be scaled by a factor of 0.95 (i.e., $\delta_{se}(k) = -0.05$). This sensor value is fed as an input to both the pitch and torque controllers. So, the fault must be detected and accommodated in a fast and safe way. This type of fault should be detected before the proportional error equals 50% of the safety margin which is itself 10% of rated generator speed (i.e., 5% of the defined rated generator speed, which would be 1173.7±58.7 rpm) [4]. Then, a switching action is required to feed a corrected generator speed measurement into the controllers and other possible estimators.

Detection of a proportional error on the generator speed sensor is based on the redundant sensor information from the rotor speed sensor and checking of the consistency of both sensor outputs. However, this method relies on the assumption that the generator and rotor speed sensors do not experience fault simultaneously [4]. This assumption by itself is not sufficient for estimation process of scaling error. Because on the one hand, the faulty sensor cannot be isolated by only using information from the two speed sensors; and, on the other hand, the noise power and accuracy of two sensors are different. In other words, knowing the gear ratio, N_g, and then converting the

rotor speed to generator speed does not provide the satisfactory precision required for estimation purpose. Nonetheless, the estimation of true generator speed can be done accurately via a Multi-Input Single-Output (MISO) fuzzy model designed in the form of presented FDD approach in Section 5.1. The suitable inputs for fuzzy model are selected on the basis of relationships between parameters describing wind turbine performance.

There exists a very well-known non-linear relationship between the applied aerodynamic torque, $\tau_{aer}(t)$, to the rotor speed $\omega_{\mathrm{r}}(t)$ and the wind speed $V_w(t)$. Such a relation is given in (2.27), where ρ is the air density, and A is the swept area of the rotor [16].

$$\tau_{aer}(t) = \frac{1}{2\omega_{\mathrm{r}}(t)} \rho\, A\, V_w^3(t)\, C_p(\beta(t), \lambda(t)) \tag{2.27}$$

The coefficient C_p in (2.27) deals with the aerodynamic efficiency of the rotor, and is a nonlinear function of the Tip Speed Ratio (TSR) $\lambda(t)$ and the blade-pitch angle $\beta(t)$. The TSR is given in (2.28), where R is the radius of the rotor.

$$\lambda(t) = \frac{\omega_{\mathrm{r}}(t) R}{V_w(t)} \tag{2.28}$$

The aerodynamic torque in (2.27) is calculated based on estimated value of wind speed and measured values for rotor speed and blade-pitch angles. Then it is used to derive a first-order model of wind turbine, as shown in (2.29), where J is the rotational inertia of the turbine, and τ_g is the generator torque [16].

$$\dot{\omega}_{\mathrm{r}}(t) = \frac{1}{J}(\tau_{aer}(t) - \tau_g(t)) \tag{2.29}$$

As it is seen from (2.29), $\tau_{aer}(t)$ is a key input for modeling of rotating parts in wind turbines. So the measured aerodynamic torque $\tau_{aer,m}$ is selected as an input for the fuzzy model of generator speed. Moreover, despite the aforementioned drawback of rotor speed value in estimation of generator speed, it provides an excellent clue to understand the behavior of the generator speed variation. So, this motivates to consider augmented value of rotor speed ($N_g.\,\omega_{r,m}$) as another input for the fuzzy model. The configuration properties of generator speed model are presented in Table 2.5.

Table 2.5 Configuration properties of generator speed T-S fuzzy model (MISO model)

	Item	No.	Details
Antecedent Part	Number of candidate inputs	4	$\omega_g(k-1);\ \omega_g(k-2);$ $N_g.\omega_{r,m}(k-1);$ $\tau_{aer,m}(k-1)$
	Number of membership functions per input	5	-
Knowledge Base	Number of tuning rules	5	-
Consequent Part	Linear equation form	-	$\omega_g(k) = \chi_1\omega_g(k-1) + \chi_2\omega_g(k-2) + \chi_3 N_g.\omega_{r,m}(k-1) + \chi_4\,\tau_{aer,m}(k-1) + \lambda$
	Defuzzification method	-	$\hat{y} = \frac{\sum_{i=1}^{m}\mu_i(\boldsymbol{\psi})y_i}{\sum_{i=1}^{m}\mu_i(\boldsymbol{\psi})}$

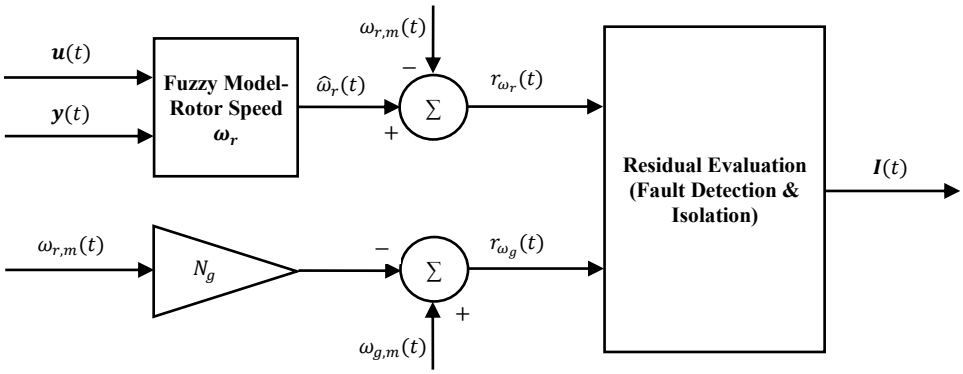

Figure 2.8 Generator/Rotor speed model-based FDD.

As shown in Figure 2.8, using the gearbox ratio N_g, the fault can be seen as an inconsistency in the augmented rotor speed measurement $(N_g.\omega_{r,m})$ and generator speed measurement $\omega_{g,m}$. The fault detection of rotor speed sensor is done separately exploiting a fuzzy model which estimates the rotor speed value $\widehat{\omega_r}$. The FDD system considers both of the obtained residuals simultaneously, and concludes the magnitude and exact place of fault and sends the information to

a supervisor for appropriate decision and possible switch command. Notice that, regardless of whether fault is from the generator or rotor speed sensor, the corrected sensor value obtained from the relevant model must be fed to all controllers and/or estimators to make them tolerant to the fault. The used fuzzy model in Figure 2.8 is identified and developed from the normal operation of wind turbine. Table 2.6 presents the configuration properties for this model.

Table 2.6 Configuration properties of rotor speed T-S fuzzy model (MISO model)

	Item	No.	Details
Antecedent Part	Number of candidate inputs	6	$\omega_r(k-1);\ \omega_r(k-2)$ $\widetilde{\omega_r}(k-1);\ \widetilde{\omega_r}(k-2)$ $;\ \tau_{aer,m}(k-1);\ \tau_{aer,m}(k-2)$
	Number of membership functions per input	5	-
Knowledge Base	Number of tuning rules	5	-
Consequent Part	Linear equation form	-	$\omega_r(k) = \chi_1\omega_r(k-1) + \chi_2\omega_r(k-2) + \chi_3\widetilde{\omega_r}(k-1) + \chi_4\widetilde{\omega_r}(k-2) + \chi_5\,\tau_{aer,m}(k-1) + \chi_6\,\tau_{aer,m}(k-2) + \lambda$
	Defuzzification method	-	$\hat{y} = \frac{\sum_{i=1}^{m}\mu_i(\psi)y_i}{\sum_{i=1}^{m}\mu_i(\psi)}$

In Table 2.6, $\widetilde{\omega_r}$ is defined with the following equation, where P_g is the turbine power, and η_g is the generator efficiency.

$$\widetilde{\omega_r}(t) = \frac{P_g(t)}{N_g\eta_g\tau_g(t)} \tag{2.30}$$

Theoretically, the above expression exists to directly estimate the generator and rotor speeds. But, due to time-varying nature of power system efficiency, it is not accurate enough in practice. Nonetheless, $\widetilde{\omega_r}$ acts as a candidate input which has precious information about behavior of the rotor speed during wind turbine operation. Hence, the fuzzy model exploits this information besides

the other inputs to accurately estimate the rotor speed. As it is seen from Table 2.6, the model is not directly dependent on the output of generator speed sensor. So, in the case of any fault in the speed sensors, the model will be fast and robust enough to indicate any possible deviation of rotor speed from its true value.

2) Pitch Sensor Fault Case

Generally speaking, an internal fault in a pitch sensor system may result in a biased output. This biased output is a sensor fault, but it is also located inside a closed-loop pitch actuator system. That is, the fault affects both the pitch angle measurement and the pitch actuator through its closed-loop servo controller.

In this paper, the considered pitch sensor fault results in a fixed-value output from pitch sensor of one of rotor blades. However, due to time-varying behavior of reference pitch angle $\beta_{ref}(t)$ the fault magnitude would be time-varying and results in a pitch angle bias value β_{bias} located on the closed-loop servo controller. With the occurrence of this fault, the model of pitch actuator as a second-order closed-loop system is modified as shown in (2.31) in which ω_n and ξ represent the constant natural frequency and damping ratio of the pitch system respectively [4]. Furthermore, the modified sensor measurement can be modeled as seen in (2.32), where, β_{bias} denotes the pitch angle bias value and $\sigma_\beta(k)$ represents the noise term.

$$\ddot{\beta}(t) = -2\xi\omega_n\dot{\beta}(t) - \omega_n^2\big(\beta(t) + \beta_{bias}(t)\big) + \omega_n^2\beta_{ref}(t) \tag{2.31}$$

$$\beta_m(k) = \big(\beta(k) + \beta_{bias}(k)\big) + \sigma_\beta(k) \tag{2.32}$$

A bias on a single pitch sensor causes unbalanced rotation of the rotor and leads to adverse tower acceleration and change of aerodynamic torque. These symptoms may be used to detect and isolate the fault, and also estimate the magnitude of the bias (see [4]). However, in this paper a simpler and more reliable method (Figure 2.9) is proposed for the model-based FDD. As shown in Figure 2.9, a fault detection and isolation system constituting of three autonomous fuzzy models for each of the pitch actuators is designed. The generated residuals are computed as the difference between measured and estimated pitch angle values. Analysis of these residuals based on simple threshold logic allows detection and isolation of the faulty sensor. Then, the concluded information will be used for an appropriate remedial action.

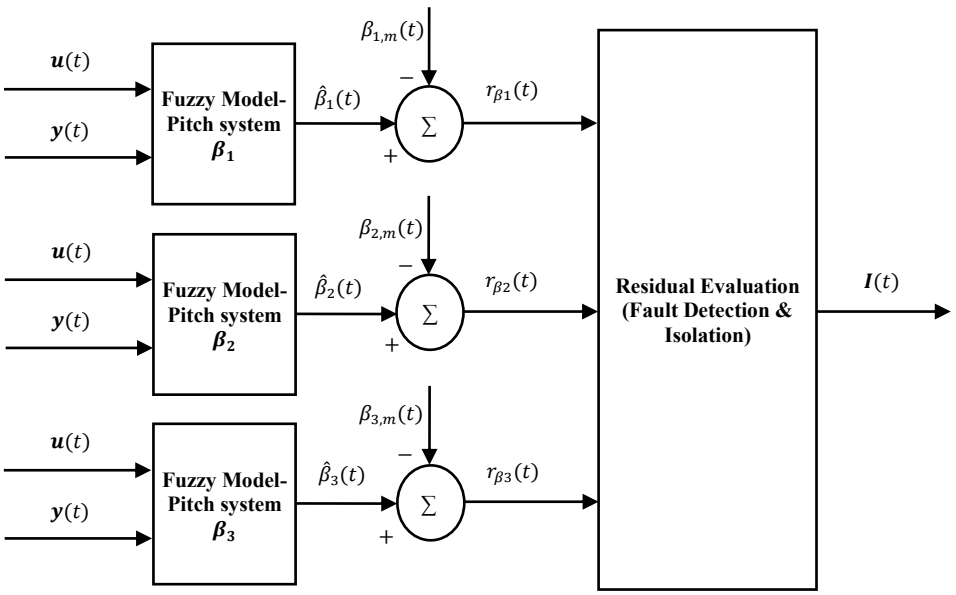

Figure 2.9 Pitch system model-based FDD.

From a practical point of view, the pitch system is a closed system which cannot be influenced through the subtraction of the bias from the measured pitch angle. So, the only way to modify the system would be through the pitch reference signal. An accommodation design for single pitch sensor bias is depicted in Figure 2.10 [4]. This method compensates the sensor bias β_{bias} using signal correction by adding the estimated bias $\hat{\beta}_{bias}$ to the pitch reference signal β_{ref}. Additionally, the corrected pitch measurement $\hat{\beta}$ must be fed to the other active estimators in the overall FDD-FTC system. This is essential to make them tolerant to the fault. Note that the modeling uncertainty may degrade the performance of wind turbine in fault-free operation if the accommodation scheme shown in Figure 2.10 is kept permanently active. Therefore, the accommodation scheme will be activated only after detection of fault through the presented FDD system in Figure 2.9.

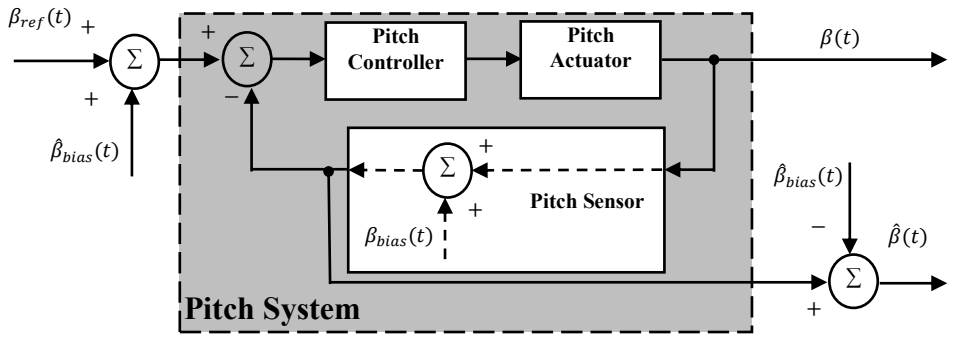

Figure 2.10 Fault accommodation in a pitch system with biased sensor measurement.

The proposed structure of bias estimation system is illustrated in Figure 2.11. To have an accurate estimation for pitch system measurement, the manipulated reference signal is fed to the fuzzy model through a filter. The filter includes a simple integral action with an appropriate state identifier. Hence, the compensated reference signal $(\beta_{ref} + \hat{\beta}_{bias})$ is converted to a normal reference signal $\beta_{ref,n}$ which should be followed by a normal pitch system. Therefore, the pitch system fuzzy model estimates correctly the value of pitch angle during the fault occurrence.

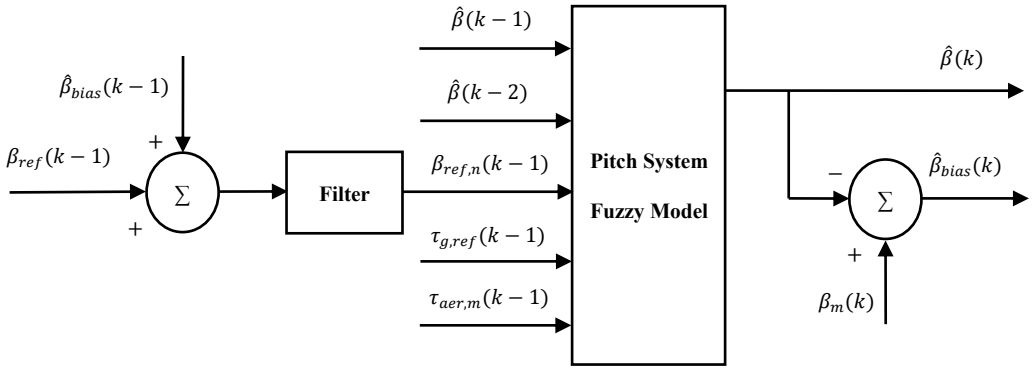

Figure 2.11 Pitch sensor bias estimation using fuzzy model of pitch system. The estimated bias $\hat{\beta}_{bias}$ is computed from the difference between measured pitch value β_m and estimated pitch value $\widehat{\beta}$.

Table 2.7 presents the structure properties of applied MISO fuzzy models for pitch systems in Figures 2.9 and 2.11. Similar to the presented fuzzy models in Section 5.2.1, the aerodynamic torque is used as an input for the model. Moreover, the command/reference control signals are also used as two additional inputs based on the presented pitch system model in (2.31), and the changing nature of generator torque over the entire operation envelop of wind turbine.

Table 2.7 Configuration properties of pitch system T-S fuzzy model (MISO model)

	Item	No.	Details
Antecedent Part	Number of candidate inputs	5	$\beta(k-1); \beta(k-2);$ $\tau_{g,ref}(k-1);\ \tau_{aer,m}(k-1);$ $\beta_{ref}(k-1)$
	Number of membership functions per input	4	-
Knowledge Base	Number of tuning rules	4	-
Consequent Part	Linear equation form	-	$\beta(k) = \chi_1\beta(k-1) + \chi_2\beta(k-2) + \chi_3\beta_{ref}(k-1) + \chi_4\tau_{g,ref}(k-1) + \chi_5\ \tau_{aer,m}(k-1) + \lambda$
	Defuzzification method	-	$\hat{y} = \frac{\sum_{i=1}^{m}\mu_i(\boldsymbol{\psi})y_i}{\sum_{i=1}^{m}\mu_i(\boldsymbol{\psi})}$

2.6 Simulation Results and Discussion

This section presents the performance evaluation of proposed FGS-PI and FDD and FTC schemes. Simulations were performed in MATLAB/Simulink environment using the nonlinear model presented in Section 2. In order to compare between different control systems, the described baseline control system in Section 3 was used as a frame of reference. Simulations were conducted for a realistic wind speed sequence with mean speed of 14 m/s, and over 630 seconds of run time. This wind speed sequence is illustrated in Figure 2.12. The rated and cutout wind speeds are 11.4 m/s and 25 m/s, respectively.

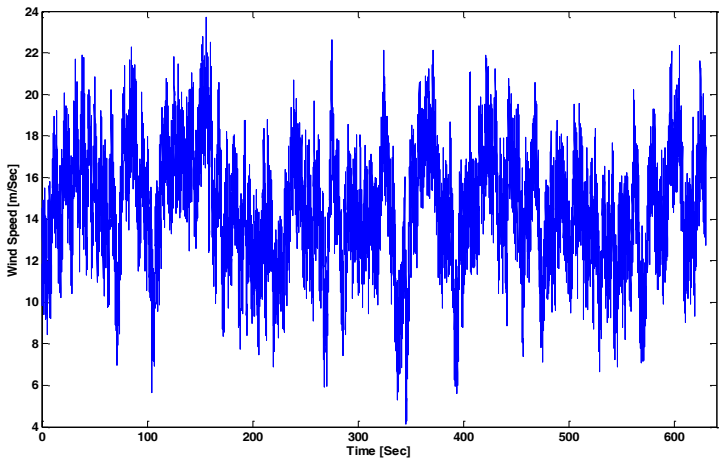

Figure 2.12 Wind speed sequence.

As shown in Figure 2.12, the wind profile covers different regions above and below the rated wind speed. Therefore both the blade-pitch control and torque control systems are in working condition. Additionally, the torque controller is set to be active for changing the torque in above rated wind speeds too. In the following subsections, different sets of simulations and numerical results for fuzzy modeling, fuzzy gain scheduled PI-control, FDD, and AFTCS are presented.

A) Performance of FGS Blade-Pitch PI-Controller in the Fault-Free Case

First, the high performance of the FGS PI-controller is demonstrated in fault-free operation of the wind turbine. Here, various properties indicating performance and safety considerations are chosen to present a complete comparison between FGS and baseline PI-controllers.

Figure 2.13 displays the time history of generator rotational speed for the two controllers. Additionally, the mean and standard deviation values obtained from this figure are stated in Table 2.8.

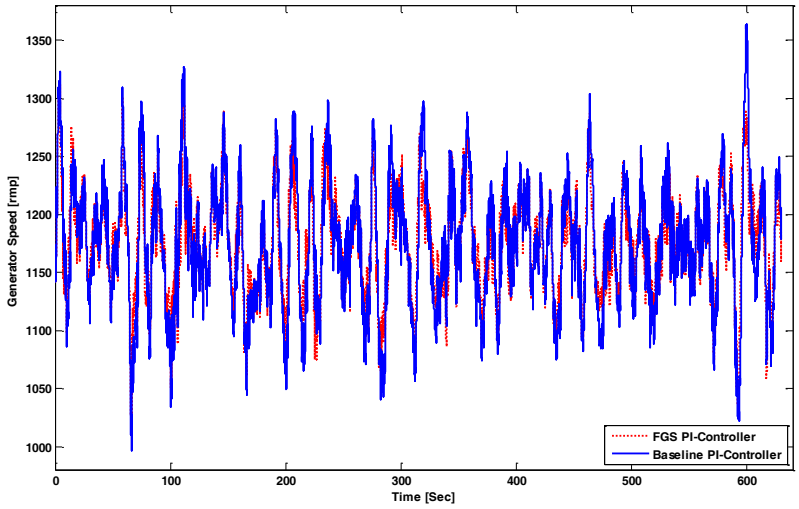

Figure 2.13 Generator rotational speed regulation with baseline PI-controller and FGS PI-controller.

Based on the simulation results, reflected in Figure 2.13 and Table 2.8, the FGS PI-controller is faster and more successful in tracking the rated generator speed of 1173.7 rpm. In particular, the FGS PI-controller has regulated the generator speed below its recommended maximum value which is about 1320 rpm. This is due to improved adaptation of control gains and also related to the fact that the FGS PI-controller evaluates not only the speed tracking error but also the rate of this error. In order to consider safe loadings on the actuators, both the control output reference signals $\beta_{ref}(t)$ are passed through prescribed rate and magnitude limiters. Figure 2.14 displays the measured pitch rates during wind turbine simulation with each controller. As can be seen from the figure, the values of pitch rates are well within the safe range (±10 deg/sec) for the pitch system. Additionally, the figure indicates higher but safe variation in pitch rate for pitch angle regulation under the FGS PI-control. This implies that the FGS PI-controller has realized the unused potential of the pitch actuators to improve the tracking performance.

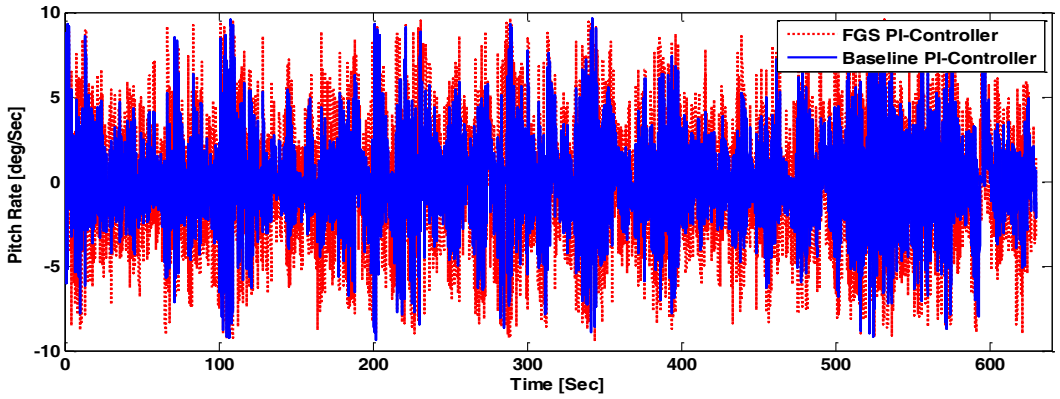

Figure 2.14 Pitch angle rates during turbine operation using baseline PI-controller and FGS PI-controller.

The tower-top fore-aft (x) and side-to-side (y) accelerations are also monitored. As can be seen from Table 2.8, both control approaches result in almost the same acceleration values for the tower-top.

Table 2.8 Quantitative Comparison of blade-pitch PI-controllers - system in normal operation

Blade-Pitch Control System	**Generator Speed [rpm]**		**Tower-Top Acceleration (X-Dir.) [m/s^2]**		**Tower-Top Acceleration (Y-Dir.) [m/s^2]**	
	Mean	**STD**	**Mean**	**STD**	**Mean**	**STD**
Baseline PI-Controller	1175.03	53.15	0.012	0.51	-0.001	0.85
FGS PI-Controller	1174.90	43.24	0.012	0.52	-0.001	0.84

The generated electrical power is shown in Figure 2.15 to indicate the capability of each controller in tracking the rated power value of 5 MW.

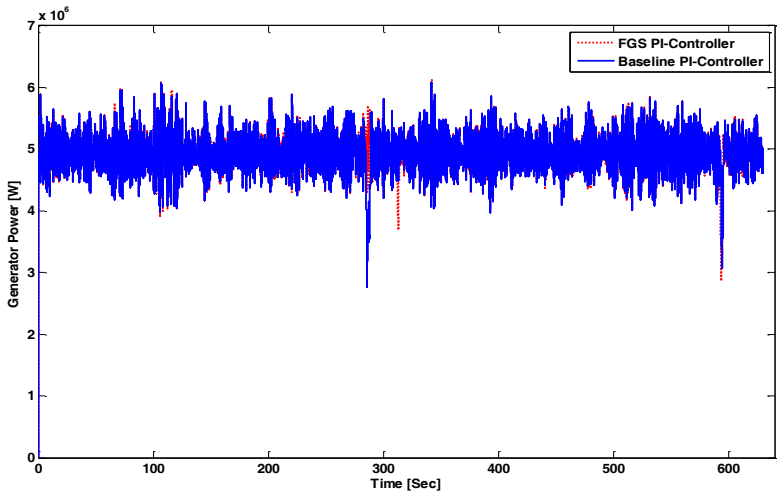

Figure 2.15 Measured generated electrical power during turbine operation using baseline PI-controller and FGS PI-controller.

As seen in Figure 2.15, there are some distinctive moments of power drop (transition from region III to II) even if there is sufficient wind available to produce the rated power continuously. This can be due to the present turbulence in vicinity of above rated wind speed. Hence, the rotor speed may vary somewhat around the reference rated RPM and might sometimes even deviate below the RPM for maximum generator power capture (region II). As it can be seen from the figure, although both the curves exhibit some points of power drop, the tracking of rated power has been more satisfactory for the wind turbine operating with the FGS PI-controller. The available information in Table 2.9 also confirms the excellence of FGS PI-controller.

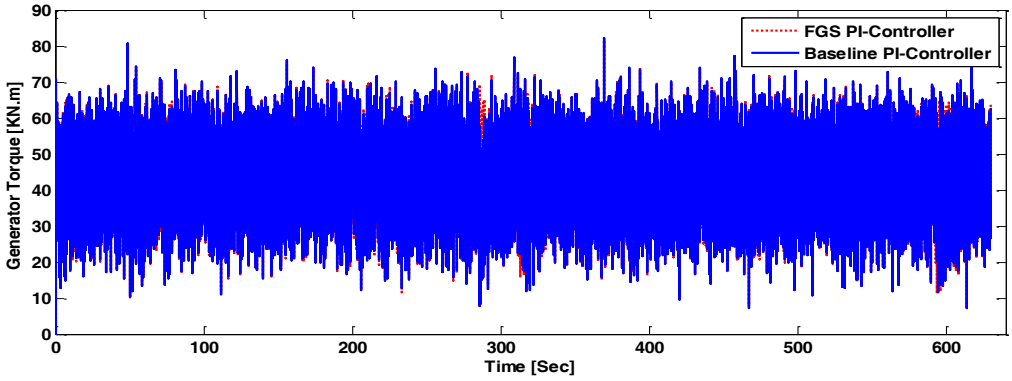

Figure 2.16 Measured generator torque during turbine operation using baseline PI-controller and FGS PI-controller.

Figure 2.16 shows the measured generator torque which is highly noisy signal. The described low-pass filter in Section 5 can be applied to mitigate the high-frequency excitation of the measured signal as shown in Figure 2.17.

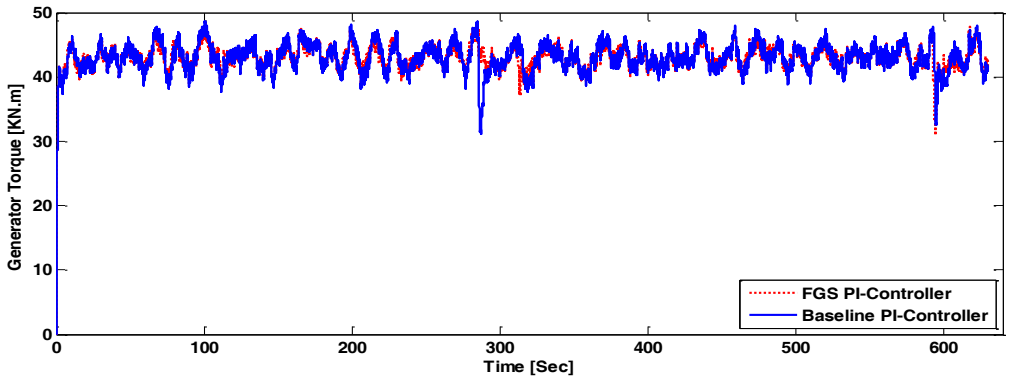

Figure 2.17 Filtered generator torque during turbine operation using baseline PI-controller and FGS PI-controller.

From Figure 2.17 and Table 2.9, both the controllers are tracking the rated generator torque of 43 KN. However, the FGS PI-controller has demonstrated better tracking performance compared to the baseline PI-controller.

Table 2.9 Quantitative Comparison of blade-pitch PI-controllers - system in normal operation

Blade-Pitch Control System	**Generator Torque [KN]**		**Generator Power [W]**	
	Mean	**STD**	**Mean**	**STD**
Baseline PI-Controller	42.982	2.296	4937416	178409
FGS PI-Controller	43.003	1.975	4942745	161858

B) Modeling Accuracy for Fuzzy Models

In order to train and evaluate each fuzzy model, a set of 50,400 measured data for each of inputs and outputs were used. The data were obtained from the simulation of wind turbine benchmark model under normal operation with FGS PI-controller and with a sampling rate of 80 Hz. Note that each set of the measured data was split into equal halves; one half for training and the other half for validation.

To measure modeling accuracy and fitting performance of the fuzzy models, the Root-Mean-Squared Error (RMSE) and the Variance Accounted For (VAF) index are used respectively. The RMSE is defined as:

$$RMSE = \sqrt{\frac{1}{N}\sum_{k=1}^{N}(y_k - \hat{y}_k)^2} \tag{2.33}$$

in which, y_k and $\hat{y}_k$ are the k-th true output of the system and estimated output of the model, respectively. The percentile VAF is computed by:

$$VAF = \left[1 - \frac{cov(y_k - \hat{y}_k)}{cov(y_k)}\right] 100\% \tag{2.34}$$

where *cov* denotes the covariance of the respective vector. The obtained results are presented in Table 2.10. From the table, it is clear that the fuzzy models are considerably accurate for approximating the process under diagnosis.

Table 2.10 Modeling accuracy of fuzzy models – system in normal operation

Fuzzy Model	VAF (%)	RMSE
Generator Rotational Speed	99.7	0.17
Rotor Rotational Speed	91.0	0.14
Pitch System	98.7	0.35

C) FDD Results

The proposed FDI architectures in this paper were able to detect and isolate both the considered sensor faults specified in Section 2.2. Each fault results in deviation of the defined residual from vicinity of zero. The residual signals of the faults in generator speed sensor and blade-pitch sensor are shown in Figure 2.18(a) and 2.19(a), respectively.

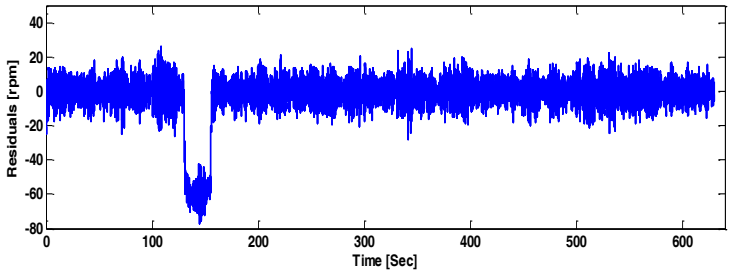

(a)

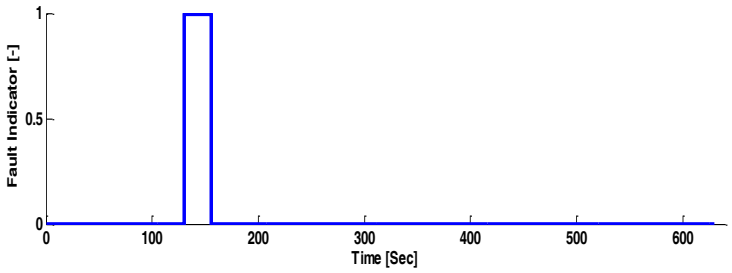

(b)

Figure 2.18 FDD result for generator speed sensor. (a) Residuals, and (b) fault indicator.

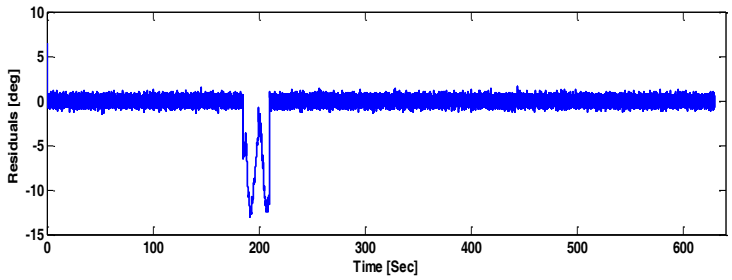

(a)

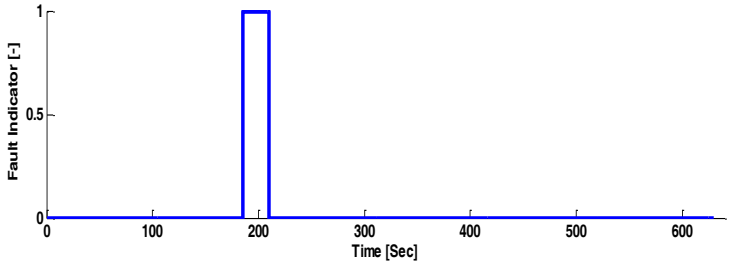

(b)

Figure 2.19 FDD result for blade-pitch sensor. (a) Residuals, and (b) fault indicator.

To evaluate the obtained residuals, the described decision-making logic in (2.18) was applied. In Figures 2.18(b) and 2.19(b), the fault indicator signals are generated when the residual signal

exceeds its relevant threshold by more than 5 consecutive samples. The thresholds were obtained with a trial and error procedure to minimize the possibility of false detection and missed detection. The time of detection for each fault is presented in Table 2.11. The blade-pitch sensor fault is rapidly detected, but the fault in generator speed sensor requires more time to be detected. This is mainly due to the type of each fault.

Table 2.11 Detection time values for sensor faults (in seconds)

Fault	Type	Detection time (sec)
Generator speed sensor	Scaling	0.37
Pitch angle sensor	Stuck	0.02

D) Performance of AFTCS against the Faults

The performance of AFTCS is highly dependent on the speed and accuracy of the FDD scheme. Generally speaking, in practice, it may be difficult to measure or obtain the instant precise value of a fault in a system. That is the FDD system can only determine an online estimate for the magnitude of fault after its occurrence. In addition, the time-delays present in the FDD process and subsequent real-time control reconfiguration (signal correction) cause the AFTCS to accept a continued operation with graceful degradation in overall system performance under the fault conditions, rather than complete failure.

In this subsection, the investigation of active fault-tolerant control algorithm is performed. A series of simulations have been conducted in which the described fault scenarios (see Section 2.2) were applied. The generator speed is selected to be investigated as the most important response of the control system. Furthermore, the fault-free simulation with FGS PI-controller is used as a frame of reference to investigate the tolerance of control system against faults. All simulation results are presented in Figure 2.20. In the following, this figure is re-plotted for more details in zoom-in views containing time period of each fault scenario (see Figures 2.21 and 2.22).

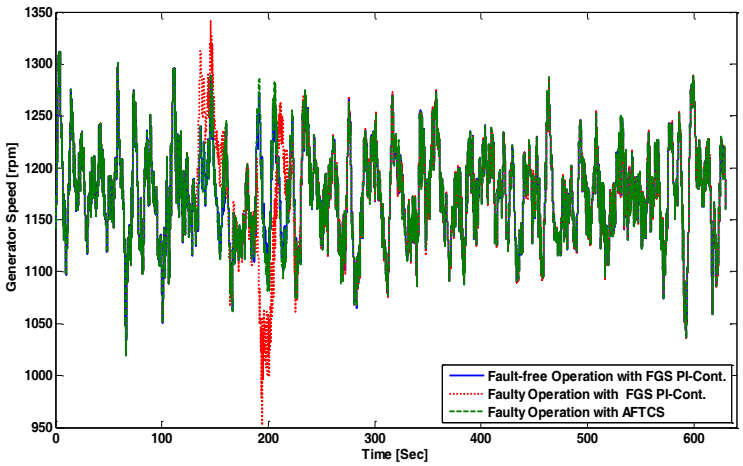

Figure 2.20 Generator rotational speed regulation with FGS PI-controller and AFTCS during fault-free and faulty operation of the wind turbine.

E) Fault in Generator Speed Sensor

Figure 2.21 plots the generator speed during this fault. It can be seen that the AFTCS has successfully kept the generator speed at the same trajectory as in the fault-free case. This implies that the FDD and subsequent signal correction processes were performed properly. This is not the case for the FGS-PI system which only relies on the information from the faulty sensor of generator speed (see Figure 2.21).

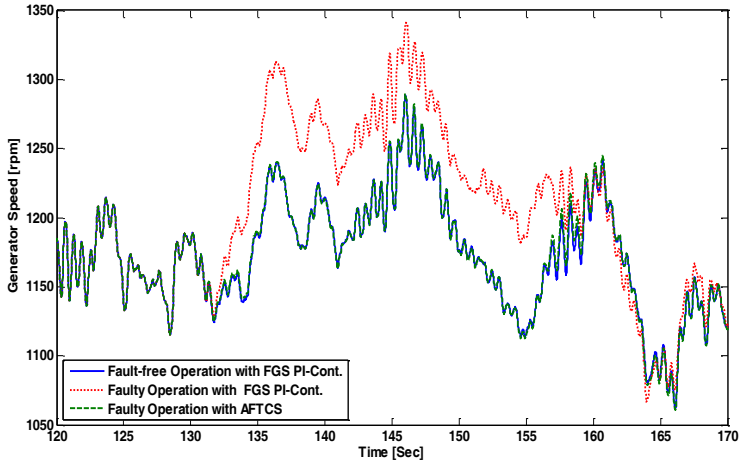

Figure 2.21 Generator rotational speed regulation with FGS PI-controller and AFTCS during fault-free and faulty operation of the wind turbine – time period [120,170] sec.

F) Fault in Blade-Pitch Angle Sensor

A biased blade-pitch angle measurement results in unbalanced rotation of the rotor, which in turn affects the generator speed too. The outcome of this fault is shown on the generator speed in Figure 2.22. As can be seen in the figure, the FGS-PI system cannot handle this fault, and the fault has a significant influence on the system behavior. In contrast, the AFTCS utilizes the information obtained from FDD system, and accommodates the fault based on described signal correction approach in Section 5.2.2. However, some less serious deviations still exist due to the common pitch offset.

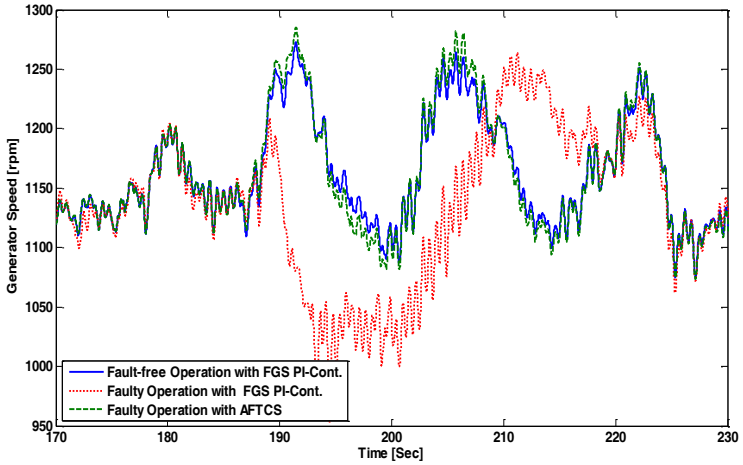

Figure 2.22 Generator rotational speed regulation with FGS PI-controller and AFTCS during fault-free and faulty operation of wind turbine – time period [170,230] sec.

G) Robustness

As mentioned in Section 5, an important feature of the described AFTCS on the basis of signal correction is its autonomous structure which does not affect the performance of FGS PI-controller. So the robustness of AFTCS depends on the robustness of FGS PI-controller, and the accuracy of FDD system. The accuracy of FDD system was validated in Sections 6.2 and 6.3. Hence, the robustness of the FGS PI-controller will be examined here.

The applied wind input profile for testing the control systems is highly turbulent, and covers variety of wind speeds over operating regions of the wind turbine. To further investigate the robustness of controller to external disturbances (e.g., wind changes), two different wind speed profiles with mean wind speeds of 11 and 17 m/s (see Figure 2.23) are used. For each wind profile,

similar simulations as described in Section 6.1 are conducted. The obtained performance measures are stated in Tables 2.12 and 2.13 (the simulation plots are not shown here for the sake of brevity). All results confirm that the FGS PI-controller is not only robust in the presence of wind disturbances, but also secures safe and improved performance compared to the baseline PI-controller.

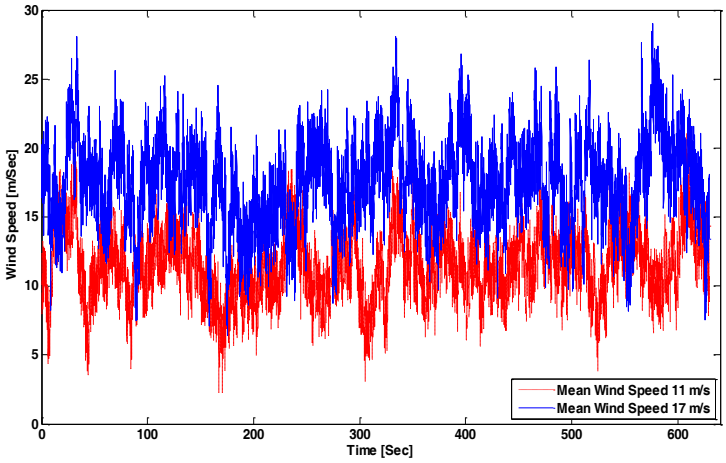

Figure 2.23 Wind profiles with mean speeds of 11 and 17 (m/s).

Table 2.12 Quantitative Comparison of blade-pitch PI-controllers - system in normal operation with wind profile of 11 m/sec mean wind speed

Blade-Pitch Control System	Generator Speed [rpm]		Tower-Top Acceleration (X-Dir.) [m/s^2]		Tower-Top Acceleration (Y-Dir.) [m/s^2]		Generator Torque [N]		Generator Power [W]	
	Mean	STD	Mean	STD	Mean	STD	Mean	STD	Mean	STD
Baseline	1165.8	40.97	0.013	0.53	-7.27E-5	0.80	40773.2	3873.6	4658106.9	489293.2
FGS	1166.5	36.10	0.012	0.54	-2.28E-5	0.79	40803.0	3693.3	4664677.2	470518.8

Table 2.13 Quantitative Comparison of blade-pitch PI-controllers - system in normal operation with wind profile of 17 m/sec mean wind speed

Blade-Pitch Control System	Generator Speed [rpm]		Tower-Top Acceleration (X-Dir.) [m/s^2]		Tower-Top Acceleration (Y-Dir.) [m/s^2]		Generator Torque [N]		Generator Power [W]	
	Mean	STD	Mean	STD	Mean	STD	Mean	STD	Mean	STD
Baseline	1175.3	60.55	0.011	0.53	3.4E-4	0.95	43113.5	2439.9	4950721.9	145854.1
FGS	1175.4	52.05	0.011	0.54	2.3E-4	0.96	43092.7	2195.7	4951790.1	143836.4

2.7 Conclusion

This paper addressed the design of a novel Fault Detection and Diagnosis (FDD) and Fault-Tolerant Control (FTC) scheme for efficient and reliable control of a large off-shore wind turbine operating in full and partial load regions, and in the presence of wind turbulences, measurement noises, and different realistic fault scenarios. First, a Fuzzy Gain Scheduling (FGS) technique was used to enhance a simple gain-scheduled PI-controller (the baseline pitch controller) to a FGS PI-control system for robust and improved regulation of generator speed. Then, to add active fault tolerance capabilities to the FGS PI-control system, a model-based FDD scheme has been developed using fuzzy modeling and identification method. The FDD system provides fault information to be used in an Active Fault-Tolerant Control System (AFTCS) based on a signal correction approach.

All simulations have been conducted in 630 seconds using NREL's FAST 5 MW turbine benchmark model. Numerical results and simulation studies on various performance and safety parameters clearly indicate the effectiveness of the proposed schemes over the entire range of the tested wind speeds and in both the fault-free and faulty conditions. Compared to the baseline PI-controller, the developed FGS PI-controller has been able to improve the overall performance of wind turbine. In the case of sensor faults, the accommodation has been done using FDD information, and based on signal correction algorithms by the developed AFTCS.

Simulations and verifications indicate that the AFTCS does not affect the nominal performance of FGS PI-control system and provides acceptable performance in the presence of sensor faults, which cannot be achieved with baseline PI-controller and even FGS PI-control system alone.

Since the architecture of AFTCS is based on signal correction approach which is applied to the FGS PI-control system, the robustness of FGS PI-control system results in robustness of the AFTCS. However, accuracy of the FDD system has a large impact on the overall performance of AFTCS. Even though both the FGS PI-controller and AFTCS showed almost the same performance during normal operation of wind turbine, the fault tolerance provided by AFTCS makes it superior to FGS PI-controller.

Extending the presented FTC method to accommodation of other types of faults like actuator or system component faults remains one of the future research topics. Moreover, the AFTCS has been developed under the assumption of perfect communication links without network-induced

limitations such as packet dropouts and/or quantization effects etc. However, to achieve a practical AFTCS, the FDD scheme and real-time control system reconfiguration should be designed along with techniques in fault-tolerant computing, and fault-tolerant communication networks.

Chapter 3 Wind Turbine Fault Diagnosis and Fault-Tolerant Torque Load Control against Actuator Faults

Abstract

Wind turbines are designed to generate electrical energy as efficiently and reliably as possible. Advanced fault detection, diagnosis and accommodation schemes are necessary to realize the required levels of reliability and availability in modern wind turbines. This paper presents two novel approaches oriented to the design of fault-tolerant control schemes for reliable regulation of generator torque in a wind turbine which can be affected by both model uncertainties and actuator faults in its generator/converter. The first approach is based on fuzzy model reference adaptive control in which a fuzzy inference mechanism is used for parameter adaptation without any explicit knowledge of the potential faults in the system. The second approach exploits fuzzy modeling and identification method to develop an integrated model-based fault detection and diagnosis and automatic signal correction mechanism to accommodate potential faults in the system based on online diagnostic information. Finally, the effectiveness of the proposed fault-tolerant control schemes are illustrated and compared by a series of simulations on a well-known large offshore wind turbine benchmark in the presence of wind turbulences, measurement noises, and realistic fault scenarios in the generator/converter torque actuator.

3.1 Introduction

It is becoming a real challenge today to meet the world's power demands with optimal reliability, quality and cost, while addressing the environmental concerns. Wind as one of the renewable sources of energy has received a great deal of attention in recent years [72]. However, the reduction of relatively high cost of Operation and Maintenance (OM) is a key issue for the successful deployment of wind energy systems over the next decades [72]. Advanced control solutions constitute a promising approach to lower the cost of wind energy generation by improving the efficiency, and thus the net captured energy, or by extending the lifetime of wind turbine components and structures through reducing structural loading [99]. Furthermore, as wind energy becomes a higher proportion of worldwide electricity generation, and wind turbines become larger, more expensive, and increasingly offshore, advanced fault detection, diagnosis and accommodation schemes play crucial roles in ensuring the reliability and availability (and thereby power generation) of modern wind turbines while reducing the cost of unscheduled maintenance.

Wind turbines are complex aero-electromechanical energy systems driven by wind as a stochastic input, and essentially exhibit highly nonlinear dynamics. They operate in uncertain environments and are exposed to large aerodynamic, gravitational, centrifugal, and gyroscopic loads. Obviously, precise control and health management of such a system is quite challenging [99, 100]. A wind turbine consists of several rotating and non-rotating assemblies, subsystems, and components that may fail. A fault even in a component level may propagate in the overall system and deteriorate the performance of other components and eventually cause to system failure. There exist several different types of faults which are most frequent in wind turbines, and each can result in unsatisfactory performance and/or significant component failure rates (see, e.g., [69]). Among them, the torque offset faults in generator/converter are classified into actuator faults that originate from either an internal fault in the converter electronics or an offset in the converter torque estimate which itself can be due to design/manufacturing defects [69, 101]. This type of fault disturbs the torque control action with high severity. Consequently, serious problems arise with successful tracking of the maximum power point and rated power in partial and full load regions, respectively. Accordingly, the unexpected overshoots and fluctuations in the turbine dynamics and generated power by the wind turbine will cause higher fatigue loads as well as significant power quality problems at the wind farm level (including a group of wind turbines), and then at the whole

connected electrical grid. In this regard, the present study is motivated by the emerging need for a Fault-Tolerant Control (FTC) approach that is capable of tolerating the potential torque offset faults in generator/converter of a wind turbine system in order to improve the reliability and availability of the system, while providing a desirable performance.

Generally speaking, the FTC methods can be divided into two types, namely, passive (PFTC) and active (AFTC) [10]. The PFTC deals with fixed control systems designed to be robust against a specified class of faults or some levels of uncertainty in overall system. In fact, PFTC does not need any kind of Fault Detection and Diagnosis (FDD) scheme or controller reconfiguration algorithm. This implies that the fixed control system is applied for both the fault-free as well as the faulty system. However, it has limited fault-tolerance capabilities and may cost nominal performance [10]. In contrast to PFTC, AFTC concerns reconfigurable control systems that react to system component faults (including sensors, actuators, and system itself) by reconfiguring the control action based on the real-time information about the state of the system determined by an FDD scheme [10].

In terms of FDD for wind turbines, the number of publications has been increasing exponentially over the past three years. For example, Odgaard et al. [101] presents a standard wind turbine benchmark model, and reviews some newly published methods for fault detection and isolation in the standard model. The wind turbine FTC has also been studied in the literature, and is currently the subject of intensive research worldwide. For example, authors in [44] propose a FTC scheme which is a combination of model reference adaptive control with neural network compensation. Sloth et al. [43] presents four Linear Parameter Varying (LPV) control schemes for a wind turbine operating in the full load region and under a single fault in the dynamics of pitch system. In [46], an AFTC scheme which exploits a robust actuator fault estimation approach based on adaptive filters is proposed.

With respect to the high degree of nonlinearity and uncertainty present in wind turbines, modeling of such systems is a rather difficult task. Also, the increasing tendency towards larger and more flexible wind turbines makes this task even more demanding [16]. Additionally, the available models are too detailed for direct use in control design purposes. The mentioned difficulties have motivated the development of new control strategies based on fuzzy modeling and control methods to guarantee robustness and performance features despite model uncertainties.

The Takagi-Sugeno (T-S) type dynamic fuzzy model [78] is regarded as a highly efficient tool for handling complex nonlinear systems and applications [79]. For the specific application of wind turbines, the design of FDD and FTC strategies based on T-S fuzzy modeling has been an active area of research recently [32, 33, 52, 53, 102]. In [32], a data-driven diagnosis strategy based on T-S fuzzy prototypes is presented for detection of rotor and converter faults. Kamal et al. [102] propose a fuzzy scheduler fault-tolerant control scheme based on multiple sensors–observers with a switching mechanism for detection, isolation, and accommodation of sensor faults in a hybrid wind–diesel system. Two FTC schemes based on T-S fuzzy modeling and control are presented in [52, 53]. More recent work by Badihi et al. [33] exploits fuzzy modeling, identification and control techniques to propose an integrated FDD and FTC scheme which not only provides fault-tolerance capabilities against sensor faults in a wind turbine, but also considerably improves the overall performance of the turbine in both fault-free and faulty conditions. The present paper aims to extend authors' work presented in [33] by introducing novel FTC schemes against actuator faults. In more detail, the main contribution of this paper is to exploit fuzzy modeling, identification and control techniques to propose two different, novel approaches in designing FTC for reliable regulation of the generator torque load in a wind turbine which can be affected by both model uncertainties and actuator faults in its generator/converter. The first approach proposes a novel Fuzzy Model Reference Adaptive Control (FMRAC) mechanism oriented to the design of a PFTC scheme which has the interesting capability of online adaptation of the control action without any explicit knowledge of the faults and model uncertainties or external disturbances (i.e., no need to employ FDD unit). Conversely, the second approach results in an AFTC scheme which is based on an integrated FDD and Automatic Signal Correction (ASC) mechanism. The proposed FDD system employs a fault detection and estimation algorithm based on fuzzy modeling and identification method to provide the most up-to-date information about true status of the wind turbine system. The proposed AFTC scheme based on FDD and ASC will not disturb the nominal performance of the torque control system under normal (fault-free) operating conditions. This feature is particularly favorable in the case of wind turbine torque control system whose fixed-structure is well defined for optimizing power capture in the partial load region, and improving output power quality in the full load region.

The proposed FTC schemes are implemented and evaluated via an advanced and realistic simulation benchmark model presented in [69]. The simulations are conducted in the presence of

wind turbulences, measurement noises, and realistic fault scenarios to demonstrate the fault-tolerance, as well as the reference (nominal) tracking capabilities.

The remainder of the paper is organized as follows: In Section 3.2, the wind turbine plant model, its baseline control system, and the considered fault scenarios are introduced briefly. A fault analysis about the effects of the considered faults on the wind turbine system is presented in Section 3.3. A gain-scheduling approach for pitch controller is briefly recalled in Section 3.4. Section 3.5 presents a reference dynamic model of wind turbine with application to FDD and FTC design for the wind turbine. Design of FTC schemes for torque regulation is addressed in Section 3.6. Section 3.7 presents and discusses the simulation results. Finally, conclusions are drawn in Section 3.8.

3.2 The Wind Turbine Benchmark Model

This paper considers the wind turbine benchmark model presented in [69]. The benchmark model is basically built upon FAST (Fatigue, Aerodynamics, Structures, and Turbulence) aeroelastic wind turbine simulator code [71], and represents an offshore 5 MW three-bladed horizontal axis wind turbine proposed by the U.S. National Renewable Energy Laboratory (NREL) [70]. Figure 3.1 shows the wind turbine benchmark model together with baseline controllers in feedback loops. In the following, basic details of the baseline controllers are briefly recalled, followed by the considered fault scenarios. A more complete description of the wind turbine benchmark model can be found in [69].

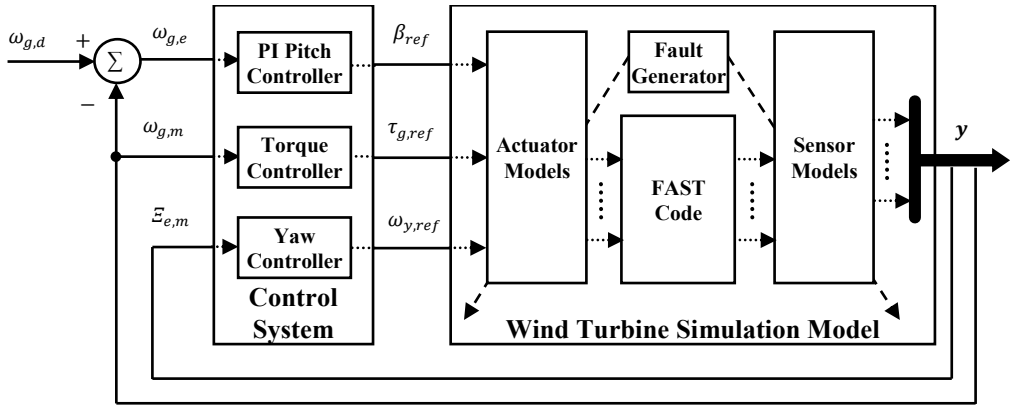

Figure 3.1 Block diagram of the wind turbine model in feedback control loops. The model output vector $\boldsymbol{y}$ provides the measured generator speed $\omega_{g,m}$ and wind yaw error $\Xi_{e,m}$ for controllers.

A) Baseline Control System

The baseline control system includes three individual controllers for regulating blade-pitch angles, generator torque, and nacelle yaw angle (see Figure 3.1). As shown in Figure 3.1, the blade-pitch controller employs PI (Proportional-Integral) control to track a constant generator speed called rated generator speed so that the turbine operates at its rated power $P_{g,o}$ in above rated wind speeds (i.e., full load region or region III, see Figure 3.2).

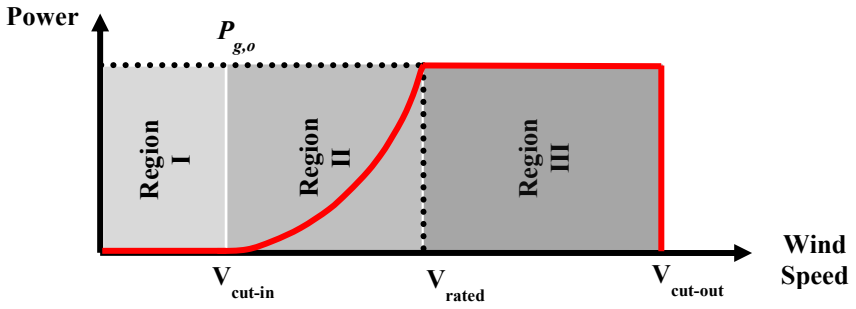

Figure 3.2 Ideal power curve versus wind speed characteristic.

In *below rated* wind speeds (i.e., *partial load region* or *region II*, see Figure 3.2), a torque controller is designed by varying the generator torque to maximize power capture. In this region, the reference generator torque τ_{ref} is defined as:

$$\tau_{ref}(t) = K_{opt}\,{\omega_r}^2(t) \tag{3.1}$$

in which ω_r is the rotor angular speed (i.e., measured generator speed divided by a gearbox ratio), and the gain K_{opt} is given by:

$$K_{opt} = \left(\frac{1}{2\lambda_o^3}\right)\rho\pi R^5 C_{p,max} \tag{3.2}$$

where R is the rotor radius, ρ is the air density, and λ_o is the tip-speed ratio at which the maximum power coefficient $C_{p,max}$ occurs. The general definition of tip-speed ratio will be given later in Section 3.3 (see (3.7)).

Furthermore, in above rated wind speeds, the quality of constant output power can be improved using the reference generator torque given in (3.3), where $P_{g,0}$ is the turbine rated power, $\omega_g(t)$ is the filtered generator speed, and η_g is the generator efficiency. For further details, see [70].

$$\tau_{ref}(t) = \frac{P_{g,0}}{\eta_g \omega_g(t)} \tag{3.3}$$

It is worth mentioning that, the yaw controller is a slow On/Off controller designed to orient the turbine nacelle as wind direction varies [69]. In order to avoid any intense commanded signal and extreme loading on the actuator(s), the appropriate rate and magnitude limiters are imposed on the output of controllers. Due to the importance of these limiters for practical implementation of the controllers in industrial applications, the limiters are kept unchanged and active throughout this paper.

B) Fault Scenarios

The wind turbine benchmark model considered in this paper can simulate a number of realistic malfunctions including different kinds of possible faults in wind turbines [69]. However, Table 3.1. only presents the fault scenarios considered in this paper. The faults have identical features but different magnitudes. They are implemented within the Actuator Models block of the benchmark model (see Figure 3.1). Note that each fault scenario corresponds to an individual simulation and is present within [495-520] sec during wind turbine operation.

Table 3.1 Fault scenarios

Fault No.	Type and Magnitude	Position	Time Period (sec)
1	+1000 Nm torque offset	Generator/Converter	495 - 520
2	+2000 Nm torque offset		

3.3 Fault Analysis

The generator/converter faults considered in Subsection 3.2B result in a torque offset which can originate from either an internal fault in the converter electronics or an offset in the converter torque estimate which itself can be due to design/manufacturing defects [69, 101]. This type of fault disturbs the torque control action with high severity. Consequently, serious problems arise with

successful tracking of the maximum power point and rated power in partial and full load regions, respectively.

To analyze the effects of the considered faults on performance of the wind turbine, there exists a well-known relation between generator power P_g, speed ω_g, and torque τ_g as follows:

$$\frac{P_g(t)}{\omega_g(t)} = \eta_g \cdot \tau_g(t) \tag{3.4}$$

The above relation implies that a change in generator torque (due to faults or uncertainties) can cause a change in both the generator speed and power. In other words, with respect to the considered actuator faults in the generator/converter, the torque offset values directly result in undesirable changes in generator speed and power which can be sensed through the measured generator speed $\omega_{g,m}(t)$ and power $P_{g,m}(t)$, respectively.

Basically, the generator speed ω_g is related to the rotor speed ω_r through a constant gearbox ratio. In reference to the first order model of wind turbine (see (3.5), [16]) and considering the rotational inertia of the turbine J, basically, the changes in generator speed arise from changes in generator torque τ_g and aerodynamic torque τ_{aer} as well.

$$\dot{\omega_r}(t) = \frac{1}{J}(\tau_{aer}(t) - \tau_g(t)) \tag{3.5}$$

As mentioned in Section 3.2, the generator torque is controlled using (3.1) and (3.3), respectively, in partial and full load regions. However, the aerodynamic torque mainly relies on the effective wind speed V_w, rotor speed ω_r and blade-pitch angle β which is itself controlled by the pitch control system as wind speed varies in full load region. The aerodynamic torque τ_{aer} is given in (3.6), where ρ is the air density, A is the swept area of the rotor, and C_p is the power coefficient [16].

$$\tau_{aer}(t) = \frac{1}{2\omega_r(t)} \rho\, A\, V_w^3(t)\, C_p(\beta(t), \lambda(t)) \tag{3.6}$$

The power coefficient deals with the aerodynamic efficiency of the rotor and is a nonlinear function of the blade-pitch angle β and tip-speed ratio λ. The tip-speed ratio is given in (3.7), where R is the radius of the rotor.

$$\lambda(t) = \frac{\omega_r(t)R}{V_w(t)} \tag{3.7}$$

Since the potential torque uncertainties and offset values in a large wind turbine generator/converter constitute only a small proportion of the total generator torque τ_g, their subsequent effects on the total magnitude of torque difference in (3.5) will be inconsiderable, particularly in the full load region in which the blade pitch controller is also active and generator speed regulation is basically conducted through pitching the blades and varying the aerodynamic torque τ_{aer} in (3.5). In other words, the changes in generator speed due to the mentioned torque uncertainties and offset values in generator/converter are almost negligible. This is also confirmed by simulation results shown in Figure 3.3. This figure illustrates filtered measurements of the generator speed and power under the considered torque offset values (see Table 3.1) during a wind sequence with a mean speed of 11 m/s which covers both the partial and full load operation regions. As can be seen in Figure 3.3, the fault effects on the measured generator speed response are minimal (i.e., the percentage error is less than 1% of the true value). However, due to the direct relation between generator power and torque (see (3.4)), the measured generator power reflects well the undesirable changes in the generator torque in both the full and partial load regions. Therefore, the measured generator power can be considered as a well-suited performance index for investigation and verification of FTC schemes against actuator faults in the turbine generator/converter.

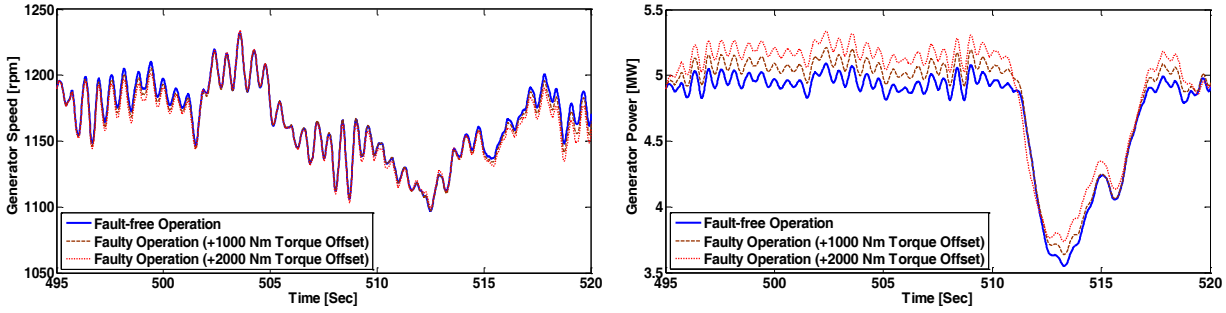

(a) (b)

Figure 3.3 Performance responses during fault-free and faulty operations: (a) Generator speed (b) Generator power.

3.4 Description of Pitch-Angle Fuzzy Gain-Scheduled PI-Control

Blade-pitch control is an essential element in above rated wind speeds. The wind turbine benchmark model presented in Section 3.2 employs the following simple PI-controller (see (3.8)) for regulating blade-pitch angles.

$$\beta_{ref}(t) = K_P \omega_{g,e}(t) + K_I \int_0^t \omega_{g,e}(\tau) d\tau \tag{3.8}$$

in which $\beta_{ref}(t)$ is the reference blade-pitch angle, $\omega_{g,e}(t) = \omega_{g,d} - \omega_{g,m}$ is the generator speed error, and the desired generator speed is $\omega_{g,d}$.

Although the present paper is addressing the important issue of generator torque control in a wind turbine and the proposed torque FTC methodologies in next sections are completely general and do not involve any assumption about the type and characteristics of pitch control system, it is more useful to exploit an improved gain-scheduled PI control system instead of the baseline blade-pitch PI controller given in (3.8). In fact, despite autonomous structure of the blade-pitch control and generator torque control systems (see Figure 3.1 and Section 3.2), it is obvious that the overall wind turbine performance depends on the functionality of both control systems.

A recent work by Badihi et al. [33] proposes a fuzzy gain scheduling technique for real-time tuning of the parameters of blade-pitch PI controller in (3.8) as operating condition or dynamics of the wind turbine varies. With respect to the control performance, this Fuzzy Gain-Scheduled (FGS)-PI control system is proved to be superior to the baseline PI controller designed using classical methods [33]. In the following, a brief description of the FGS-PI control system reported in [33] is recalled.

The proportional and integral control gains in (3.8) can be defined in the following forms:

$$K_P(\beta) = K_{P,\beta=0}\, \Phi(\beta) \tag{3.9}$$

$$K_I(\beta) = K_{I,\beta=0}\, \Phi(\beta) \tag{3.10}$$

where $K_{P,\beta=0}$ and $K_{I,\beta=0}$ denote, respectively, the constant uncorrected proportional and integral gains, and $\Phi(\beta)$ represents a correction factor which is solely a function of turbine blade-pitch angle β as described in [70].

The proposed pitch gain scheduling scheme in [33] exploits fuzzy inference mechanism for online adaptation of the constant uncorrected $K_{P,\beta=0}$ and $K_{I,\beta=0}$ to capture nonlinearities in the wind turbine system (see pitch FGS system in Figure 3.4). The uncorrected gains can be defined through a simple linear transformation form as follows [33]:

$$K_{P,\beta=0} = \left(K_{P,\beta=0}^{max} - K_{P,\beta=0}^{min}\right)K_P' + K_{P,\beta=0}^{min} \tag{3.11}$$

$$K_{I,\beta=0} = \left(K_{I,\beta=0}^{max} - K_{I,\beta=0}^{min}\right)K_I' + K_{I,\beta=0}^{min} \tag{3.12}$$

where K_P' and K_I' are, respectively, normalized values of $K_{P,\beta=0}$ and $K_{I,\beta=0}$ between zero and one. The $\left[K_{P,\beta=0}^{min}, K_{P,\beta=0}^{max}\right]$ and $\left[K_{I,\beta=0}^{min}, K_{I,\beta=0}^{max}\right]$ in (3.11) and (3.12) are prescribed ranges for $K_{P,\beta=0}$ and $K_{I,\beta=0}$, respectively. Table 3.2 presents the values of uncorrected gains and the chosen ranges for them. The parameters K_P' and K_I' in (3.11) and (3.12) are determined online using a set of linguistic if-then rules within the framework of rule-based fuzzy logic control with further details provided in [33].

Table 3.2 Controller parameters [33]

Parameter	Value/Range
$K_{P,\beta=0}$	2×10^{-2}
$\left[K_{P,\beta=0}^{min}, K_{P,\beta=0}^{max}\right]$	$[1.05 \times 10^{-2}, 3.8 \times 10^{-2}]$
$K_{I,\beta=0}$	8.07×10^{-3}
$\left[K_{I,\beta=0}^{min}, K_{I,\beta=0}^{max}\right]$	$[7.542 \times 10^{-3}, 8.594 \times 10^{-3}]$

3.5 Reference Dynamic Model for FDD and FTC Design

Wind turbines are relatively complex structures comprising flexible mechanical systems immersed in a fully-stochastic wind field. Modeling of such a nonlinear system is a rather difficult task. In practice, it is often difficult, or even impossible to derive a single nonlinear model for the system over its entire operational envelope. One way to address this difficulty is to use multiple-model approach. Because of these considerations, this paper suggests a data-driven modeling scheme using Fuzzy Modeling and Identification (FMI) method. The FMI method generates multiple models as a collection of fuzzy if-then rules. One of the most famous fuzzy modeling techniques

is the Takagi-Sugeno (T-S) modeling which is a multiple-model approach that can handle uncertain and time-varying conditions of the system over its operating range [78].

With respect to the FMI method presented in this section, the reference (nominal) dynamic model of the wind turbine plant can be represented by a T-S type dynamic fuzzy model to be identified from input/output plant measurements obtained from simulation of the wind turbine benchmark model under normal (fault-free) operation. The reference dynamic model presented here is intended to be used as a nominal model in FDD and FTC schemes designed in Section 3.6.

A) T-S Fuzzy Modeling

Consider a Multi-Input Single-Output (MISO) nonlinear dynamic system with m inputs: $\boldsymbol{u} \in U \subset \mathbb{R}^m$, and one output $y \in Y \subset \mathbb{R}$. This system can be represented by an input-output NARX type model (Nonlinear Auto Regressive model with eXogenous inputs [103]),

$$y(k+1) = f(\boldsymbol{\psi}(k)) + e \tag{3.13}$$

where $f(.)$ represents a nonlinear function, k is the discrete time instants (samples), and e denotes the modeling error. The regression vector $\boldsymbol{\psi}(k)$ in (3.13) includes the past inputs and outputs as follows:

$$\boldsymbol{\psi}(k) = [y(k), \dots, y(k-n_y+1), u_i(k), \dots, u_i(k-n_{u,i}+1)] \ , \qquad i = 1,2, \dots, m \tag{3.14}$$

in which $n_{u,i}$ and n_y are integers corresponding to the system's order.

The unknown function $f(.)$ in (3.13) can be approximated by a T-S type fuzzy model described in terms of R rules which are characterized by linear function rule consequents (i.e., a collection of local linear models) as follows [97]:

$$\begin{aligned} &\textbf{Rule } \boldsymbol{j}\textbf{:} \quad \textbf{If } y(k) \text{ is } A_{j,1} \textbf{ and } \dots y(k-n_y+1) \text{ is } A_{j,n_y} \textbf{ and} \\ &u_1(k) \text{ is } B_{j,1,1} \textbf{ and } \dots u_1(k-n_{u,1}+1) \text{ is } B_{j,1,n_{u,1}} \textbf{ and } \dots \\ &u_m(k) \text{ is } B_{j,m,1} \textbf{ and } \dots u_m(k-n_{u,m}+1) \text{ is } B_{j,m,n_{u,m}} \textbf{ then} \\ &\hat{y}_j(k+1) = \sum_{l=1}^{n_y} a_{j,l}\, y(k-l+1) + \sum_{i=1}^{m} \sum_{l=1}^{n_{u,i}} b_{j,i,l}\, u_i(k-l+1) + c_j \end{aligned} \tag{3.15}$$

In (3.15), $\boldsymbol{Rule\ j}$ means the jth rule ($j = 1,2, \dots, R$), A and B are the antecedent fuzzy sets, $\hat{y}_j$ is the output from the jth rule, and a, b, and c are the consequent parameters, associated with the jth rule.

The output of the model can be inferred as following weighted average of the rule contributions [97],

$$\hat{y} = \frac{\sum_{j=1}^{R} \mu_j(\boldsymbol{\psi}) \hat{y}_j}{\sum_{j=1}^{R} \mu_j(\boldsymbol{\psi})} \tag{3.16}$$

in which $\hat{y}$ is the aggregated output of the model, μ_j are membership functions with each representing the degree of fulfillment of a rule.

For developing T-S models of a complex real system, it is necessary to address the nonlinear system identification problem which is the process of identifying the structure of fuzzy model, and then estimating the model parameters. These two steps are presented in the following subsections.

B) Fuzzy Model Structure

A suitable structure needs to be determined to represent the dynamics of the process (e.g., an input-output regression model, and the number of tuning rules). Generally, as much available knowledge of the system as possible should be incorporated in this step. With respect to the fault analysis presented in Section 3.3 and the importance of generator power as a performance index with application to FDD and FTC design against the considered faults, the reference dynamic model needs to serve as an accurate numerical predictor of the nominal generator power response. Therefore, the model is represented by a MISO fuzzy model with single output of the generator power. The inputs for the fuzzy model can be determined using the physical knowledge about generator power in a wind turbine. In general, in addition to the mentioned equation in (3.4), the generator power can also be expressed as:

$$P_g(t) = \eta_g \eta_m P_{aer}(t) \tag{3.17}$$

in which η_m is the efficiency of transmission system, and $P_{aer}(t)$ is the aerodynamic rotor power given by [99]:

$$P_{aer}(t) = \tau_{aer}(t)\, \omega_r(t) \tag{3.18}$$

where ω_r is the rotor rotational speed (i.e. the generator speed divided by gearbox ratio), and τ_{aer} is the aerodynamic torque (see (3.6)).

Equations (3.4) and (3.17) define the generator power, respectively, based on generator-side dynamic properties (i.e., the generator torque and the generator speed, see (3.4)) and rotor-side dynamic properties (i.e., the aerodynamic torque and the rotor speed; see (3.17) and (3.18)). Among the rotor-side dynamic properties, the aerodynamic torque cannot be computed exactly by (3.6) because of the lack of the effective wind speed over the whole rotor plane. The accurate estimation of aerodynamic torque requires an individual model which will bring with itself some model uncertainty anyway. Therefore, based on the relation shown in (3.4), to represent the operating conditions of the wind turbine system, it is decided here to employ the generator-side dynamic properties including generator torque and generator speed as two of candidate inputs for MISO fuzzy model. However, the nominal reference generator torque signal obtained from the nominal torque control system is preferred to the measured generator torque which is a highly noisy signal that may also contain the torque actuator offset values. The detailed configuration properties of the MISO fuzzy model are presented in Table 3.3.

Table 3.3 Configuration properties of generator power T-S fuzzy model (MISO model)

	Item	No.	Details
Antecedent Part	Candidate inputs	6	$\hat{P}_g(k-1);\ \hat{P}_g(k-2)$ $\omega_g(k-1);\ \omega_g(k-2)$ $\tau_{ref}(k-1);\tau_{ref}(k-2)$
	Membership functions per input	6	-
Knowledge Base	Tuning rules	6	$j = 1,2,\dots,R$ $R = 6$
Consequent Part	Linear equation form in *j*th rule	-	$\hat{P}_{g_j}(k) = a_{j,1}\hat{P}_g(k-1) + a_{j,2}\hat{P}_g(k-2)$ $+ b_{j,1,1}\omega_g(k-1) + b_{j,1,2}\omega_g(k-2)$ $+ b_{j,2,1}\,\tau_{ref}(k-1) + b_{j,2,2}\,\tau_{ref}(k-2)$ $+ c_j$
	Defuzzification method	-	$\hat{P}_g = \frac{\sum_{j=1}^{R}\mu_j(\boldsymbol{\psi})\hat{P}_{g_j}}{\sum_{j=1}^{R}\mu_j(\boldsymbol{\psi})}$

C) Data Preprocessing and Parameter Estimation

Once the structure is determined, the estimation problem should be solved to obtain the model parameters including the antecedent fuzzy sets and the consequent parameters of the fuzzy model. However, process data corrupted by noise and high frequency excitations have detrimental effects on the performance of parameter estimation. To deal with such a problem, it is suggested that the original data be preprocessed using a recursive, single-pole low-pass filter with exponential smoothing. The filter is modeled as a discrete-time recursive (difference) equation with discrete time constant T_s and corner frequency f_c [70]:

$$y(k) = (1-\alpha)u(k) + \alpha y(k-1)$$
$$\alpha = e^{-2\pi T_s f_c} \tag{3.19}$$

where u and y are the measurements of unfiltered input and filtered output, respectively, and α denotes low-pass filter coefficient.

The obtained preprocessed data can be used by the parameter estimation algorithm to obtain the model parameters. In this paper, fuzzy clustering based on the well-established Gustafson-Kessel (GK) algorithm [98] is employed to identify the fuzzy T-S model. The GK algorithm performs data set partitioning into fuzzy subsets in an iterative way. Then the identification procedure is accomplished by generation of the antecedent membership functions, and the estimation of the parameters of the local linear models through a weighted ordinary least-squares algorithm.

3.6 Design of Fault-Tolerant Control for Torque Regulation

The purpose of this section is to explain the design of two proposed FTC schemes for regulation of generator torque load in a wind turbine. Both FTC schemes are basically model-based and exploit the reference dynamic model presented in Section 3.5. In more detail, the first scheme is a PFTC scheme based on model reference adaptive control approach in which a fuzzy inference mechanism is used for parameter adaptation without any explicit knowledge of the potential faults in the system. Conversely, the second scheme is an AFTC scheme which exploits an automatic signal correction approach which relies on a fault detection and diagnosis system to provide the

most up-to-date information about true status of the wind turbine system. In the following subsections, each scheme is described in detail.

A) Design of Torque PFTC Based on FMRAC Strategy

This subsection presents a Fuzzy Model Reference Adaptive Control (FMRAC) strategy oriented to upgrade the baseline torque control system from a simple control system with fixed-parameters to a real-time adaptive control system. The proposed strategy results in a PFTC scheme which enables fault-tolerant regulation of generator torque in the presence of both model uncertainties and actuator faults. In fact, this scheme has the interesting capability of online adaptation of the control action without any explicit knowledge of the potential faults and model uncertainties or external disturbances. A block diagram illustrating the structure of torque FMRAC system in the loop is given in Figure 3.4. Associated with Figure 3.4, the FMRAC exploits a fuzzy adaptation mechanism to process information collected in real-time in order to tune the torque controllers for achieving and maintaining the desired performance specified by the reference dynamic model presented in Section 3.5.

An important point about the fixed-structure torque controllers in (3.1) and (3.3) is that they are, respectively, well-defined for optimizing power capture in the partial load region, and for improving output power quality in the full load region. So, the FMRAC system has to maintain the torque reference signal as close to its nominal values as possible during fault-free conditions and under large and nonlinear operation regions. With reference to this consideration, as seen in Figure 3.4, the reference dynamic model receives the nominal reference torque control signal $\tau_{ref,n}$ obtained from a fixed-structure torque control system as defined in (3.1) and (3.3). Furthermore, the reference model uses the measured generator speed $\omega_{g,m}$ to improve prediction of future desired values of the plant output.

In Figure 3.4, the fuzzy adaptation mechanism exploits fuzzy inference for online adaptation of parameters in the adjustable torque controllers. With respect to the mentioned considerations in Section 3.3, the measured generator power (i.e., filtered $P_{g,m}$) is selected as a *performance index* for the FMRAC system. This performance index will be compared to the estimated nominal (desired) performance index $\hat{P}_{g,n}$ and their difference is called the *plant-model error* $P_{g,e}(k)$, defined as shown in (3.20), where k is the discrete-time-step.

$$P_{g,e}(k) = P_{g,m}(k) - \hat{P}_{g,n}(k) \tag{3.20}$$

Using the above plant-model error and its derivative $\dot{P}_{g,e}(k)$, the adaptation mechanism modifies parameters of the adjustable torque controllers in order to maintain the measured generator power $P_{g,m}(k)$ close to its estimated nominal values $\hat{P}_{g,n}(k)$ obtained from the reference dynamic model.

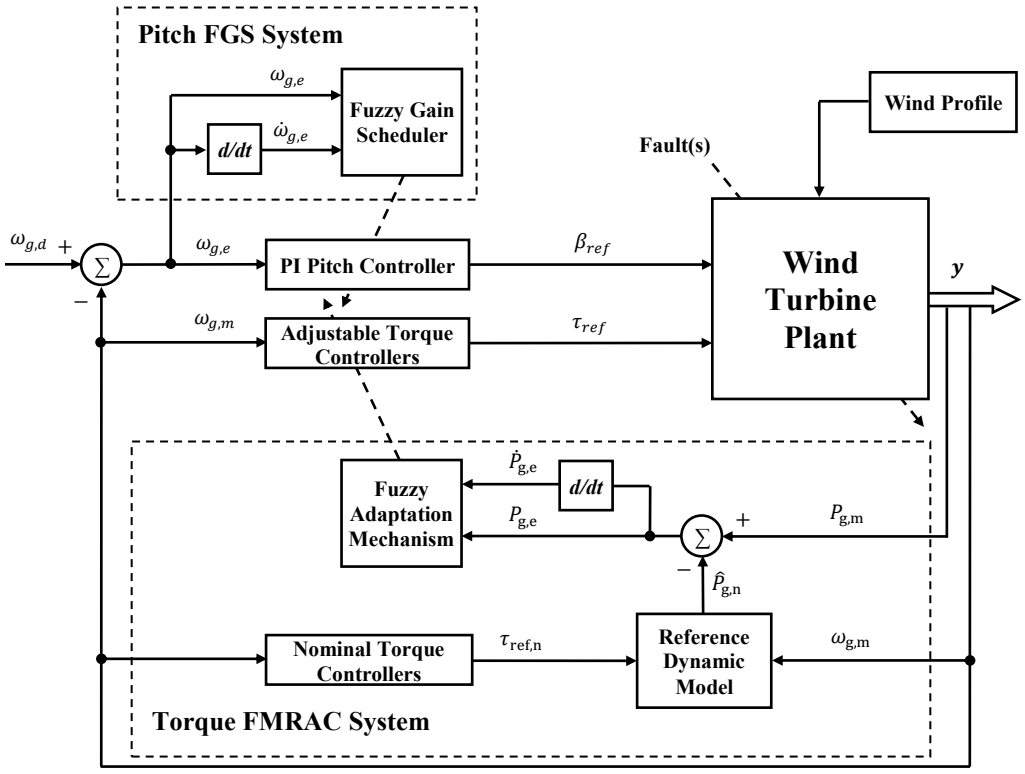

Figure 3.4 Wind turbine control feedback loops including torque FMRAC and pitch FGS systems in the loop. The mesured generator speed $\omega_{g,m}$ and generator power $P_{g,m}$ are extracted from the plant output vector $\boldsymbol{y}$.

As it was shown in Section 3.2, with respect to the wind turbine operation region, the reference generator torque is calculated using two fixed-parameter torque controllers presented in (3.1) and (3.3). To achieve the adjustable structure for the torque controllers, it is required to define tunable parameters for each of the controllers (3.1) and (3.3). The selected tunable parameters include the gain $K_{opt}(k)$ and the turbine rated power $P_{g,o}(k)$ which can be given within two symmetric ranges (see (3.21) and (3.22)) around the originally fixed parameters K_{opt} and $P_{g,o}$ in (3.1) and (3.3), respectively.

$$(1-\delta)K_{opt} \leq K_{opt}(k) \leq (1+\delta)K_{opt} \tag{3.21}$$

$$(1-\gamma)P_{g,o} \leq P_{g,o}(k) \leq (1+\gamma)P_{g,o} \tag{3.22}$$

where γ and δ are two positive scaling factors with values between zero and one. Using the given ranges in (3.21) and (3.22), the tunable parameters can be defined based on a linear transformation form as follows:

$$K_{opt}(k) = K_{opt}\big(2\delta K'_{opt}(k) + 1 - \delta\big) \tag{3.23}$$

$$P_{g,o}(k) = P_{g,o}\big(2\gamma P'_{g,o}(k) + 1 - \gamma\big) \tag{3.24}$$

where $K'_{opt}(k)$ and $P'_{g,o}(k)$ are normalized values between zero and one for $K_{opt}(k)$ and $P_{g,o}(k)$, respectively.

The parameters $K'_{opt}(k)$ and $P'_{g,o}(k)$ in (3.23) and (3.24) are determined online using a set of linguistic *if-then* rules in the form of:

***Rule i*:** If $P_{g,e}(k)$ is A_i and $\dot{P}_{g,e}(k)$ is B_i, then $K'_{opt}(k)$ is C_i and $P'_{g,o}(k)$ is D_i (3.25)

where A_i, B_i, C_i and D_i (with $i = 1,2,\dots,M$) are fuzzy sets corresponding to $P_{g,e}(k)$, $\dot{P}_{g,e}(k)$, $K'_{opt}(k)$, and $P'_{g,o}(k)$, respectively. In Figure 3.5(a), the used triangular-type membership functions for $P_{g,e}$ and $\dot{P}_{g,e}$ are scaled from -1 to 1. In this figure, the fuzzy subset ZO stands for approximately zero, PS for positive-small, PM for positive-medium, and PB for positive-big. Similarly, NS represents negative-small and so on. For the sake of simplicity, the membership functions are symmetrically around the origin and each one overlaps the adjacent functions by 50 percent, except the ZO membership function which has a smaller base in order to cover a smaller domain around the origin. This enables the adaptation mechanism for both the fine and coarse control. The VS (very small), MS (medium small), M (medium), MB (medium big), and VB (very big) in Figure 3.5(b) show the selected membership functions for $P'_{g,o}$ and K'_{opt} scaled from 0 to 1.

The complete set of rules ($i = 1,2,\dots,M;\ M = 49$) for each of K'_{opt} and $P'_{g,o}$ is given in Table 3.4. Each of the 49 rules represents a desired adaptation response to a particular situation. The rules are formulated based on expert's knowledge and understanding of the desired effect of the adaptation mechanism. For example, consider the rule:

If $P_{g,e}(k)$ is ZO and $\dot{P}_{g,e}(k)$ is NS, then $K'_{opt}(k)$ is M and $P'_{g,o}(k)$ is M

The above rule recommends that the desired operating point will be reached soon and corrective adaptation is no longer necessary. That is, the tunable parameters in (3.23) and (3.24) should attain values close to the originally fixed parameters used in controllers (3.1) and (3.3) (i.e., the constants K_{opt} and $P_{g,o}$). This is represented by the membership function 'M' in the conclusion part of the rule. As can be seen in Figure 3.5(b), the triangular-type membership function 'M' has a very small base which suggests values close to 0.5 for K'_{opt} and $P'_{g,o}$ in (3.23) and (3.24).

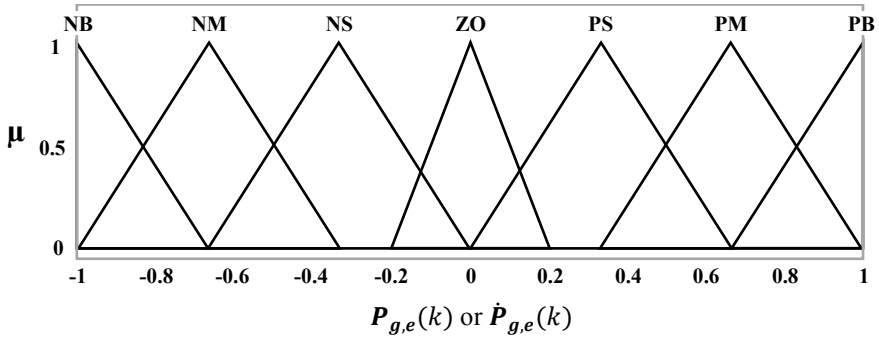

(a)

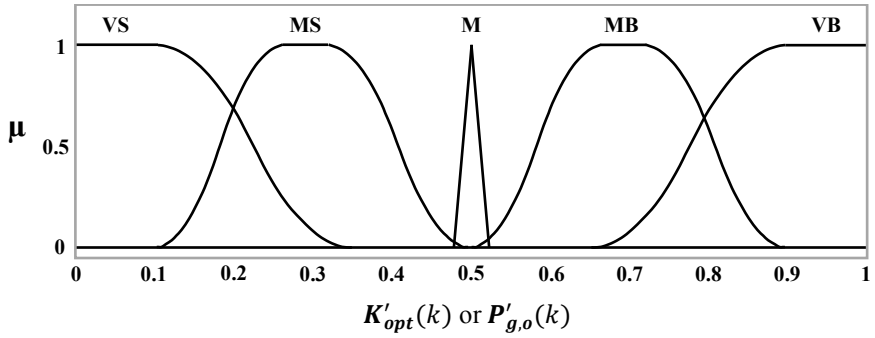

(b)

Figure 3.5 Membership functions for: (a) two inputs, and (b) two outputs of fuzzy adaptation mechanism.

Table 3.4 Fuzzy rules for K'_{opt} and $P'_{g,o}$

		$\dot{P}_{g,e}$						
		NB	**NM**	**NS**	**ZO**	**PS**	**PM**	**PB**
$P_{g,e}$	**NB**	VB	VB	VB	VB	MB	MB	MB
	NM	VB	VB	VB	MB	MB	MB	MB
	NS	VB	VB	MB	MB	MB	MB	M
	ZO	VB	MB	M	M	M	MS	VS
	PS	M	MS	MS	MS	MS	VS	VS
	PM	MS	MS	MS	MS	VS	VS	VS
	PB	MS	MS	MS	VS	VS	VS	VS

In all the rules, the logic AND has been implemented with the minimum operator, and the defuzzification is based on center of area method as follows:

$$K'_{opt} = \left(\sum_{i=1}^{M} \mu_i K'_{opt_i}\right) / \left(\sum_{i=1}^{M} \mu_i\right) \tag{3.26}$$

$$P'_{g,o} = \left(\sum_{i=1}^{M} \mu_i P'_{g,o_i}\right) / \left(\sum_{i=1}^{M} \mu_i\right) \tag{3.27}$$

where K'_{opt_i} and P'_{g,o_i} are, respectively, the values of K'_{opt} and $P'_{g,o}$ corresponding to the degree of membership μ_i for the *i*th rule.

Although the developed fuzzy adaptation mechanism in this section is applied to the torque controllers, the mechanism is generic and easily applicable to other adaptive control applications.

B) Design of Torque AFTC Based on an Integrated FDD and ASC Strategy

This section presents the strategy that must be taken into consideration to detect, diagnose and accommodate the actuator faults in generator/converter system. The proposed strategy results in an AFTC scheme which is based on Automatic Signal Correction (ASC) mechanism. Here, signal correction means that the nominal fixed-structure torque controllers in (3.1) and (3.3) are kept unchanged; only the outputs of the controllers are corrected according to the real-time fault information. Therefore, the AFTC scheme also relies on a Fault Detection and Diagnosis (FDD) system to provide the most up-to-date information about the true status of the wind turbine system. The ASC mechanism and FDD system are described in the following two subsections, respectively.

1) ASC Mechanism

An important feature of the AFTC on the basis of ASC is its autonomous structure which does not affect the nominal performance of the torque controllers, a favorable strategy for acceptance and easy Validation & Verification (V&V) by engineering applications and commercialization. This feature is particularly favorable in the case of wind turbine torque control whose fixed-structure is well defined for optimizing power capture in the partial load region, and for improving output power quality in the full load region. The proposed AFTC structure is outlined in Figure 3.6.

As shown in Figure 3.6 and mentioned before, the torque control system (including (3.1) and (3.3)) is kept unchanged itself; only the control output is modified. Here, the FDD system not only detects the actuator faults in generator/converter, but also estimates the fault magnitude $\hat{\tau}_{g,f}$ which can take either positive or negative values. Then, the estimated fault magnitude will act upon the reference torque control signal τ_{ref} in order to maintain the nominal system performance through a compensated reference torque control signal $\tau_{ref,com}$ given by:

$$\tau_{ref,com} = \tau_{ref} + \hat{\tau}_{g,f} \tag{3.28}$$

The next subsection describes the design of FDD system shown in Figure 3.6.

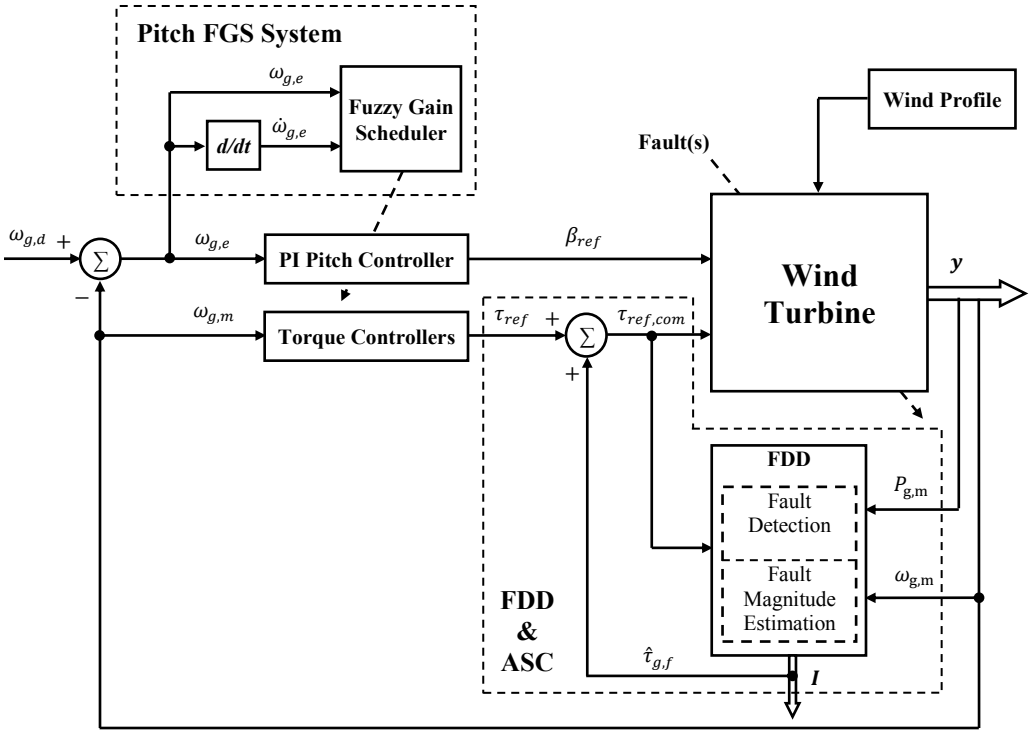

Figure 3.6 Wind turbine control feedback loops including torque control with FDD and ASC and pitch FGS system in the loop. The estimated fault magnitude $\hat{\tau}_{g,f}$ is extracted from FDD information vector $\boldsymbol{I}$.

2) FDD System

The purpose of this subsection is to provide an explanation of the designed FDD system in Figure 3.6. The FDD system can be used both for condition monitoring purpose and in an AFTC

scheme to provide the most up-to-date information about the true status of the system that will enable the reconfiguration of control action whenever there are faults in the system.

Here, it is intended to create a model-based FDD system which exploits the developed MISO fuzzy model in Section 3.5 as a reference model to carry out FDD in real-time. The detailed structure of the FDD system is shown in Figure 3.7. Moreover, the complete list of inputs and output for the MISO fuzzy model is presented in Table 3.5.

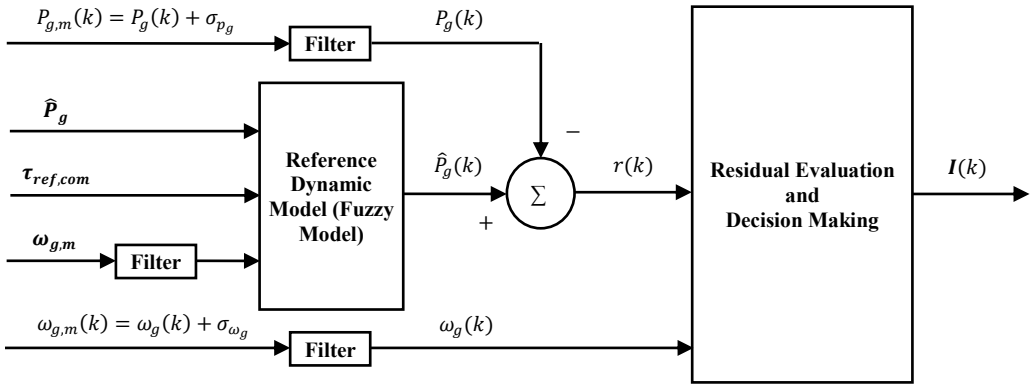

Figure 3.7 Model-based FDD scheme based on generator power T-S fuzzy model. The measured variables are passed through the low-pass filter (see (3.19)) in order to filter out the noise σ (Note: In practice, the noise effects can never be completely removed).

Table 3.5 List of inputs and outputs for MISO fuzzy model used in the FDD system

Inputs	**Output**
$\widehat{\boldsymbol{P}}_{\boldsymbol{g}} = [\hat{P}_g(k-1), \hat{P}_g(k-2)]^T$	
$\boldsymbol{\omega}_{\boldsymbol{g,m}} = [\omega_{g,m}(k-1), \omega_{g,m}(k-2)]^T$	$\hat{P}_g(k)$
$\boldsymbol{\tau}_{\boldsymbol{ref,com}} = [\tau_{ref,com}(k-1), \tau_{ref,com}(k-2)]^T$	

In Figure 3.7, since the MISO fuzzy model is identified and developed from measured data during normal operation of wind turbine system, the model simulates the nominal performance of the system. In other words, the model acts again as a reference model which estimates the nominal values of generator output power for fault-free operation of the wind turbine under compensated reference torque control signal (i.e., $\boldsymbol{\tau}_{\boldsymbol{ref,com}}$). The so-called residuals r are computed in (3.29) as the difference between actual values of output power P_g from wind turbine generator and estimated values of output power $\hat{P}_g$ from the reference model.

$$r\,(k) = \hat{P}_g(k) - P_g(k) \tag{3.29}$$

As shown in Figure 3.7, the residual evaluation and decision making will be conducted on the residuals in order to detect and then help in the diagnosis/estimation of the actuator faults in generator/converter system. The proposed algorithm for real-time residual evaluation and decision making is outlined in the flowchart shown in Figure 3.8. As can be seen from the flowchart (see Figure 3.8), the algorithm basically relies on the magnitude of the residuals. The fault detection is conducted using a threshold test on the instantaneous values of the generated residuals. In the fault-free operation, the residuals are only due to noise and model uncertainties. However, their magnitudes are close to zero and lower than the threshold value. Thereby, there is no need to modify/compensate the nominal reference torque control signal. That is, the estimated fault magnitude $\hat{\tau}_{g,f}$ is assigned to be exactly zero in order to maintain the nominal performance of wind turbine in fault-free operation. Conversely, in the presence of torque actuator faults, the residuals show sensitivity and move out of the threshold range. Then, the fault magnitude will be estimated using the generated residuals accordingly.

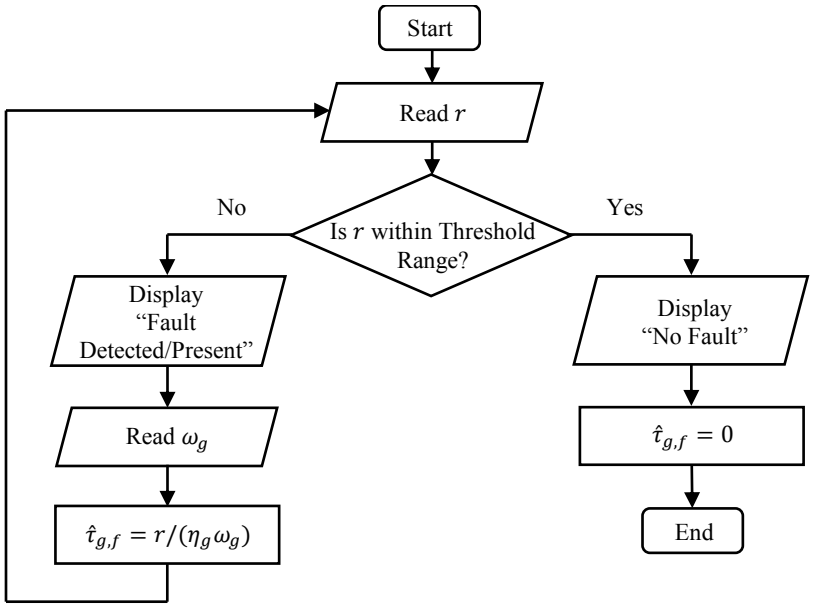

Figure 3.8 The residual evaluation and decision making algorithm used in the FDD system.

With respect to (3.4) and aforementioned considerations in Section 3.3, the residuals that represent changes in generator power due to actuator faults can be used in (3.30) to estimate the magnitudes of faults (torque offsets). This method of estimation is fairly accurate because the fault

effects on generator speed response are minimal. Hence, the changes in generator power can be directly correlated with torque offsets in generator/converter.

$$\hat{\tau}_{g,f}\,(k) = \frac{r(k)}{\eta_g \omega_g(k)} \tag{3.30}$$

It is clear from (3.29) and (3.30) that depending on the sign of potential offset faults in the torque actuator, the estimates of fault magnitude will attain positive or negative values, respectively, for negative or positive actuator offsets. Therefore, the obtained estimates of fault magnitude will be used directly in (3.28) for signal correction and fault accommodation.

3.7 Simulation Results and Discussion

In this section, simulation study is conducted to investigate the performance of proposed schemes under both fault-free and faulty conditions. Simulations have been performed in MATLAB/Simulink environment using the nonlinear offshore wind turbine benchmark model presented in Section 3.2. Three realistic wind speed profiles with hub-height mean speeds of 11 m/s, 14 m/s, and 17 m/s are used separately for simulations in this section. The wind speed profiles are shown in Figure 3.9. The cut-in, rated, and cut-out wind speeds are 3 m/s, 11.4 m/s, and 25 m/s, respectively. It is also worth remarking that the torque control system is set to be active for changing the torque in both the below and above rated wind speeds.

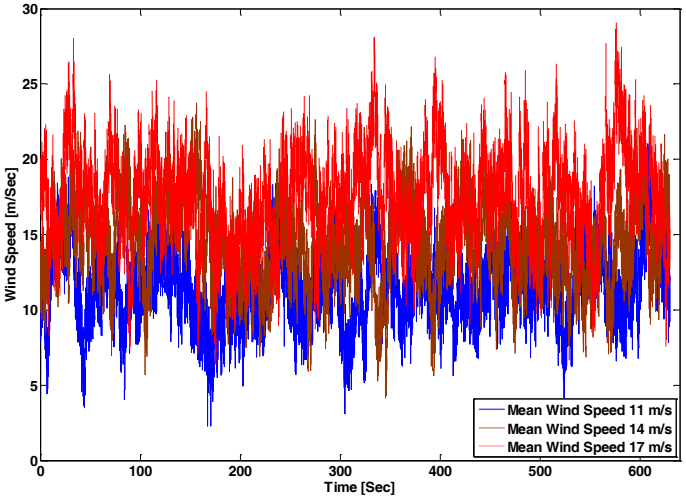

Figure 3.9 Wind speed profiles.

In Figure 3.9, the wind profile with mean speed of 11 m/s has a turbulence intensity of 20.14% and generally corresponds to the operating points in the below rated wind speeds. Conversely, the wind profile with mean speed of 17 m/s has a turbulence intensity of 17.27% and generally corresponds to the operating points in the above rated wind speeds. However, the wind profile with mean speed of 14 m/s has a turbulence intensity of 18.4% and fully covers a wide speed range from below rated wind speeds to above rated wind speeds over its 630 seconds of run time. Therefore, unless otherwise stated, the wind profile with mean speed of 14 m/s is used as a reference wind profile for conducting the main part of the simulation and evaluation process presented in this section. The wind profiles with mean speeds of 11 and 17 m/s are mainly used for conducting further simulation trials in order to test the robustness in performance of the proposed schemes in terms of external disturbances (e.g., wind changes).

In the following subsections, different sets of simulations and numerical results for the proposed wind turbine system modeling and control are presented. The fault-free simulation with pitch FGS-PI controller and nominal fixed-structure torque controllers (i.e., equations (3.1) and (3.3)) is used as a frame of reference to evaluate the overall performance and fault-tolerance property of the proposed FTC schemes against the considered actuator faults. Furthermore, with respect to the considerations given in Section 3.3, the generator power response is chosen as a well-suited performance index in order to investigate the performance of proposed FTC schemes. Both the true (before noise) and filtered measurements (sensor outputs) of the generator power are considered and assessed in this regard. In more detail, the true measurement is used to present the numerical results in tables, while the filtered measurement is used here to show the plots of power response since it is found to be clearer (immediately obvious to readers) with less signal excitations compared to the true measurement.

A) Evaluation of Pitch-Angle Fuzzy Gain-Scheduled PI-Control

As it was mentioned in Section 3.4, the proposed torque FTC methodologies are completely general and do not involve any assumption about the type and characteristics of pitch control system. However, it is decided to employ the improved gain-scheduled PI control system given in (3.9-3.12) instead of the baseline blade-pitch PI controller given in (3.8). This subsection extends and further discusses the earlier results of performance evaluation between the above mentioned two blade-pitch controllers already presented in [33].

The performance evaluation is conducted under the fault-free operation of the wind turbine. The numerical comparison is made based on the simulation results obtained employing each of the baseline and FGS-PI blade-pitch controllers. Three different wind speed profiles with mean speeds of 11, 14 and 17 m/s (see Figure 3.9) are applied. For each wind profile, similar simulations and evaluations are conducted. In particular, the mean and standard deviation (STD) values are computed for the important performance and structural dynamics and loading measures. The obtained results for performance measures are summarized in Tables 3.6-3.8. With respect to the considered benchmark model, the rated performance properties including rated generator speed, torque and power are 1173.7 rpm, 43,093.5 Nm, and 5.0 MW, respectively [70]. As it is seen from Tables 3.6-3.8, by comparing the mean and STD results, the FGS-PI controller demonstrate better performance than the baseline PI controller. Furthermore, Tables 3.6-3.8 present the obtained results for structural dynamics and loading affecting the wind turbine. As it is seen from the tables, the structural dynamics and loading measures show almost the same values for both the baseline and FGS-PI blade-pitch controllers. Here, the simulation plots are not shown for the sake of brevity.

It is worth mentioning that, although the FGS-PI controller performs better than the baseline PI controller on the benchmark model and thereby shows a relevant potential for an industrial wind turbine, it is necessary to conduct much more evaluation of different wind load cases as well as to take into account different extreme and fatigue structural loads before installation as an industrial wind turbine controller.

Table 3.6 Quantitative comparison of wind turbine simulation results under wind profile with mean speed of 11 m/s and fault-free conditions, time period [0,630] sec.

Blade-Pitch Control System	**Performance**											
	Generator Speed (rpm) (from [33])				**Generator Torque (Nm)** (from [33])				**Generator Power (W)** (from [33])			
	Mean		**STD**		**Mean**		**STD**		**Mean**		**STD**	
Baseline PI	1,165.8		40.97		40,773		3,873		4,658,106		489,293	
FGS-PI	1,166.5		36.10		40,803		3,693		4,664,677		470,518	
	Structural Dynamics and Loading											
	Tower-top Fore-Aft Acceleration (m/sec^2) (from [33])		**Tower-top Side-to-Side Acceleration (m/sec^2)** (from [33])		**Tower-top Fore-Aft Deflection (m)**		**Tower-top Side-to-Side Deflection (m)**		**Tower-base Fore-Aft Moment (kNm)**		**Tower-base Side-to Side Moment (kNm)**	
	Mean	**STD**	**Mean**	**STD**	**Mean**	**STD**	**Mean**	**STD**	**Mean**	**STD**	**Mean**	**STD**
Baseline PI	0.013	0.53	-7.27E-5	0.80	0.2267	0.2082	-0.0465	0.2700	37862	42076	4031.6	46598
FGS-PI	0.012	0.54	-7.28E-5	0.79	0.2257	0.2137	-0.0467	0.2609	37710	43115	4070.5	45248

Table 3.7 Quantitative comparison of wind turbine simulation results under wind profile with mean speed of 14 m/s and fault-free conditions, time period [0,630] sec.

Blade-Pitch Control System	**Performance**					
	Generator Speed (rpm) (from [33])		**Generator Torque (Nm)** (from [33])		**Generator Power (W)** (from [33])	
	Mean	**STD**	**Mean**	**STD**	**Mean**	**STD**
Baseline PI	1,175.03	53.15	42,982	2,296	4,937,416	178,409
FGS-PI	1,174.90	43.24	43,003	1,975	4,942,745	161,858

	Structural Dynamics and Loading											
	Tower-top Fore-Aft Acceleration (m/sec^2) (from [33])		**Tower-top Side-to-Side Acceleration (m/sec^2)** (from [33])		**Tower-top Fore-Aft Deflection (m)**		**Tower-top Side-to-Side Deflection (m)**		**Tower-base Fore-Aft Moment (kNm)**		**Tower-base Side-to Side Moment (kNm)**	
	Mean	**STD**	**Mean**	**STD**	**Mean**	**STD**	**Mean**	**STD**	**Mean**	**STD**	**Mean**	**STD**
Baseline PI	0.012	0.51	-0.001	0.85	0.1452	0.1926	-0.0542	0.2384	24379	41658	5188.5	43022
FGS-PI	0.012	0.52	-0.001	0.84	0.1443	0.1947	-0.0541	0.2376	24239	41966	5165.7	42937

Table 3.8 Quantitative comparison of wind turbine simulation results under wind profile with mean speed of 17 m/s and fault-free conditions, time period [0,630] sec.

Blade-Pitch Control System	**Performance**					
	Generator Speed (rpm) (from [33])		**Generator Torque (Nm)** (from [33])		**Generator Power (W)** (from [33])	
	Mean	**STD**	**Mean**	**STD**	**Mean**	**STD**
Baseline PI	1,175.3	60.55	43,113	2,439	4,950,721	145,854
FGS-PI	1,175.4	52.05	43,092	2,195	4,951,790	143,836

	Structural Dynamics and Loading											
	Tower-top Fore-Aft Acceleration (m/sec^2) (from [33])		**Tower-top Side-to-Side Acceleration (m/sec^2)** (from [33])		**Tower-top Fore-Aft Deflection (m)**		**Tower-top Side-to-Side Deflection (m)**		**Tower-base Fore-Aft Moment (kNm)**		**Tower-base Side-to Side Moment (kNm)**	
	Mean	**STD**	**Mean**	**STD**	**Mean**	**STD**	**Mean**	**STD**	**Mean**	**STD**	**Mean**	**STD**
Baseline PI	0.011	0.53	3.4E-4	0.95	0.1085	0.1792	-0.0560	0.2323	18324	44191	5453.5	44677
FGS-PI	0.011	0.54	2.3E-4	0.96	0.1079	0.1868	-0.0560	0.2356	18229	45335	5461.6	45448

B) Identification and Validation of the Reference Dynamic Model

In order to identify and validate the fuzzy reference model, a set of 100,800 measured data for each of inputs and output were used. The data were obtained with a sampling rate of 80 Hz from simulation of the wind turbine benchmark model under normal operation with FGS-PI controller for pitch-angle regulation and nominal fixed-structure torque control system for torque load regulation. Note that each set of the measured data was split into equal halves; one half for identification and the other half for validation. Using the determined structure for the fuzzy

reference model (see Table 3.3), the parameter estimation algorithm obtains the consequent parameters of the model, which are presented in Table 3.9.

Table 3.9 The estimated consequent parameters for the identified T-S fuzzy reference model

Rule No. (j)	$a_{j,1}$	$a_{j,2}$	$b_{j,1,1}$	$b_{j,1,2}$	$b_{j,2,1}$	$b_{j,2,2}$	c_j
1	$1.47 \cdot 10^{0}$	$-4.77 \cdot 10^{-1}$	$1.98 \cdot 10^{1}$	$-1.94 \cdot 10^{1}$	$-8.24 \cdot 10^{-3}$	$1.91 \cdot 10^{-2}$	$-4.43 \cdot 10^{2}$
2	$5.22 \cdot 10^{-1}$	$4.52 \cdot 10^{-1}$	$6.99 \cdot 10^{1}$	$-6.87 \cdot 10^{1}$	$-1.28 \cdot 10^{-3}$	$3.19 \cdot 10^{-2}$	$-1.49 \cdot 10^{3}$
3	$1.52 \cdot 10^{0}$	$-5.30 \cdot 10^{-1}$	$1.99 \cdot 10^{1}$	$-1.95 \cdot 10^{1}$	$-3.01 \cdot 10^{-2}$	$4.22 \cdot 10^{-2}$	$-6.05 \cdot 10^{2}$
4	$7.05 \cdot 10^{-1}$	$2.71 \cdot 10^{-1}$	$5.76 \cdot 10^{1}$	$-5.66 \cdot 10^{1}$	$-1.48 \cdot 10^{-4}$	$2.43 \cdot 10^{-2}$	$-9.59 \cdot 10^{2}$
5	$9.63 \cdot 10^{-1}$	$1.72 \cdot 10^{-2}$	$4.28 \cdot 10^{1}$	$-4.19 \cdot 10^{1}$	$-8.10 \cdot 10^{-3}$	$3.03 \cdot 10^{-2}$	$-9.40 \cdot 10^{2}$
6	$1.01 \cdot 10^{0}$	$-2.70 \cdot 10^{-2}$	$3.24 \cdot 10^{1}$	$-3.18 \cdot 10^{1}$	$-2.01 \cdot 10^{-1}$	$2.22 \cdot 10^{-1}$	$-7.40 \cdot 10^{2}$

To measure modeling accuracy and fitting performance of the fuzzy reference model, the Root-Mean-Squared-Percentage Error (RMSPE) and the Variance Accounted For (VAF) index are used, respectively. The RMSPE is defined as:

$$RMSPE = \sqrt{\frac{1}{N}\sum_{k=1}^{N}\left(\frac{y_k - \hat{y}_k}{y_k}\right)^2}\,100\% \tag{3.31}$$

in which, y_k and $\hat{y}_k$ are the kth true output of the system and estimated output of the model, respectively. The percentile VAF is computed by:

$$VAF = \left[1 - \frac{cov(y_k - \hat{y}_k)}{cov(y_k)}\right]100\% \tag{3.32}$$

where *cov* denotes the covariance of the respective vector. The obtained results are presented in Table 3.10. From the table, it is clear that the fuzzy reference model is considerably accurate for approximating the process under diagnosis. For example, the response of fuzzy reference model during a fault-free operation of the wind turbine is illustrated in Figure 3.10. In this figure, the filtered measurement of generator power is used to be compared with the model response. Furthermore, the zoomed view in Figure 3.10 shows the transition period between regions III and II which is accurately simulated by the developed fuzzy model.

Table 3.10 Modeling accuracy for the generator power reference model

VAF (%)	RMSPE (%)
99.0	0.32

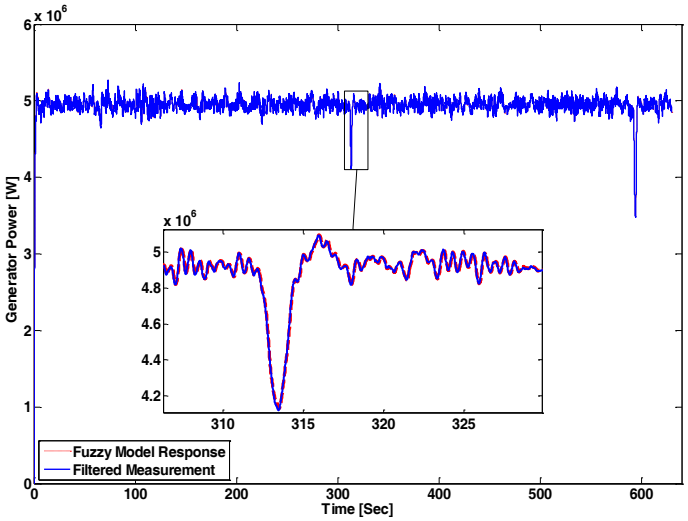

Figure 3.10 Comparison of the measured and model-estimated response of generator power during wind turbine fault-free operation.

C) Performance of Torque PFTC Scheme Based on FMRAC

In this subsection, the investigation of torque FMRAC system is performed. The scaling factors $\delta = 0.03$ in (3.21) and $\gamma = 0.05$ in (3.22) are considered for the tunable parameters of adjustable torque control system. Figure 3.11(a) demonstrates the generator power during the considered 1000 Nm torque actuator offset in [495-520] sec. As seen in the figure, the torque FMRAC system has successfully maintained the generator power at the same trajectory as in the fault-free case. Another interesting observation about Figure 3.11(a) is that there are some distinctive instants of power drop which correspond to transition from full load region to partial load region due to variations in wind speed. This implies that the proposed scheme can operate well in both operating regions.

Figure 3.11(b) displays the generator power under similar assumptions but with 2000 Nm torque actuator offset. As can be seen in the figure, the torque FMRAC system is still able to reduce the fault effects on the generator power response. However, its fault-tolerance capability has been limited due to its predefined properties for fuzzy adaptation mechanism (e.g., the scaling factors δ and γ). In fact, there is a tradeoff between the fault-tolerance capability and nominal tracking performance of the developed torque FMRAC system. For example, increasing the scaling factors results in higher fault-tolerance capability but at the same time causes the torque FMRAC system to be more sensitive to small variations due to plant-model error and disturbances and

results in poor nominal tracking performance under fault-free conditions. The selected values for δ and γ not only enable the FMRAC system to maintain the torque reference signal as close to its nominal values as possible under fault-free conditions (with VAF fitting performance index of more than 90%), but also provide enough fault-tolerance capability to completely accommodate torque actuator offsets up to 1500 Nm.

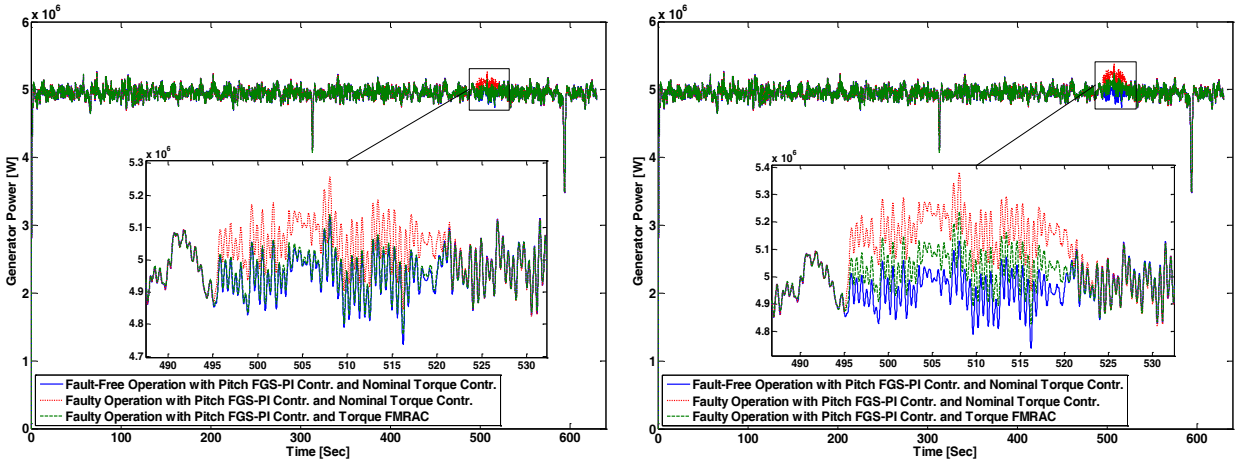

(a) (b)

Figure 3.11 Generator power response under fault-free and faulty conditions - torque PFTC scheme (FMRAC). (a) +1000 Nm torque actuator offset, and (b) +2000 Nm torque actuator offset.

D) Performance of Torque AFTC Scheme Based on FDD and ASC (FDD-ASC)

The proposed FDD system in this paper is able to detect and diagnose both the considered torque offset faults specified in Section 3.2. Each fault results in deviation of the defined residuals from the vicinity of zero. The time of detection for each fault is presented in Table 3.11. As can be inferred from the table, the greater the magnitude of offset faults, the lower the required time for detection.

Table 3.11 Detection time values for the considered fault scenarios (in seconds)

Fault No.	Type	Detection Time (sec)
1	+1000 Nm torque actuator offset	0.53
2	+2000 Nm torque actuator offset	0.31

As mentioned before, the proposed model-based FDD system provides not only the fault detection but also the fault diagnosis (estimation). The estimated torque offset values in the generator/convertor and their relevant detection signals are shown in Figure 3.12(a) and (b), respectively, for +1000 and +2000 Nm torque offsets. The estimated offset values have negative sign due to positive offset faults in the generator/converter. Therefore, the obtained estimates can be used directly in (3.28) for signal correction and fault accommodation accordingly. Moreover, due to time-varying behavior of the reference torque control signal, the estimated offset values are basically time-varying with mean values of -1000 Nm and -2000 Nm shown in Figure 3.12(a) and (b), respectively.

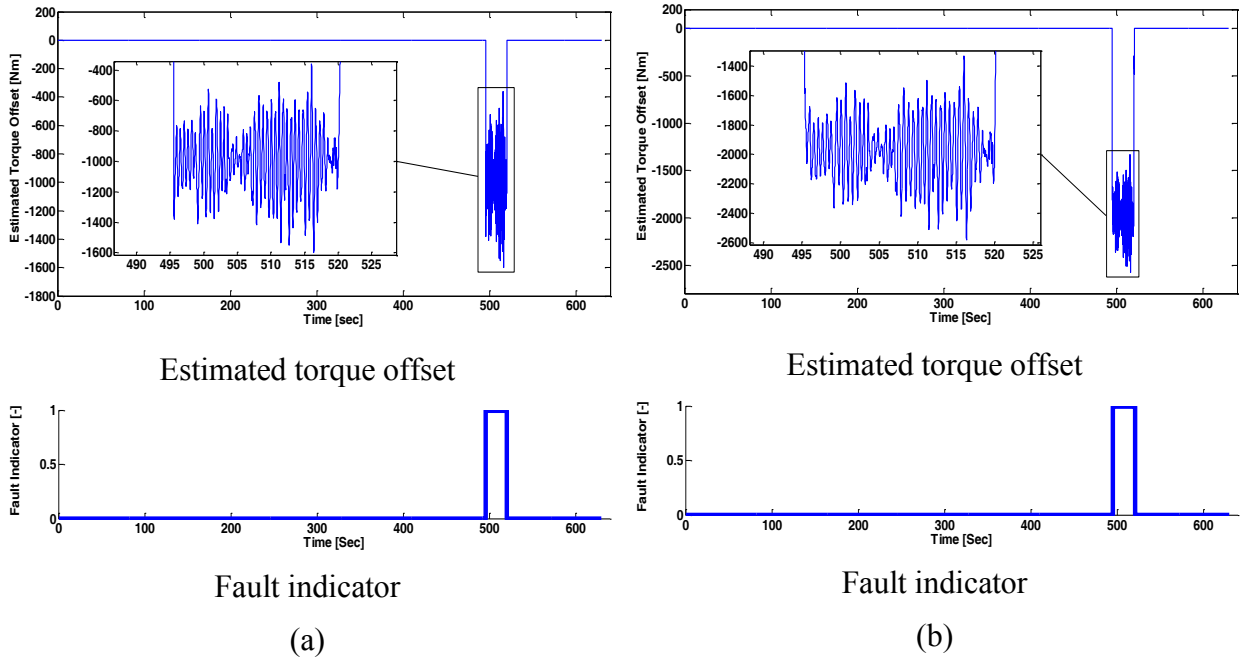

Figure 3.12 FDD results. (a) +1000 Nm torque actuator offset, and (b) +2000 Nm torque actuator offset.

As already mentioned, the estimated torque offset values act upon the reference torque control signal (see (3.28)) in order to maintain the nominal wind turbine system performance under the faulty conditions. As illustrated in Figure 3.13(a), the fault accommodation is successfully conducted during the considered 1000 Nm torque actuator offset. As foreseen, since the control reconfiguration (signal correction) is only activated during the fault period, the nominal performance of the torque controllers will be unaffected during fault-free conditions.

Another interesting feature of this AFTC scheme is that the signal correction can be carried out for large values of torque offset in generator/converter system with satisfactory performance. This is confirmed by the generator power response (see Figure 3.13(b)) obtained from the wind turbine simulation under 2000 Nm torque actuator offset in [495-520] sec. As can be seen in the figure, in contrast to the FMRAC system, the torque AFTC scheme with FDD and ASC is apparently able to accommodate the fault effects on the generator power response under 2000 Nm torque actuator offset.

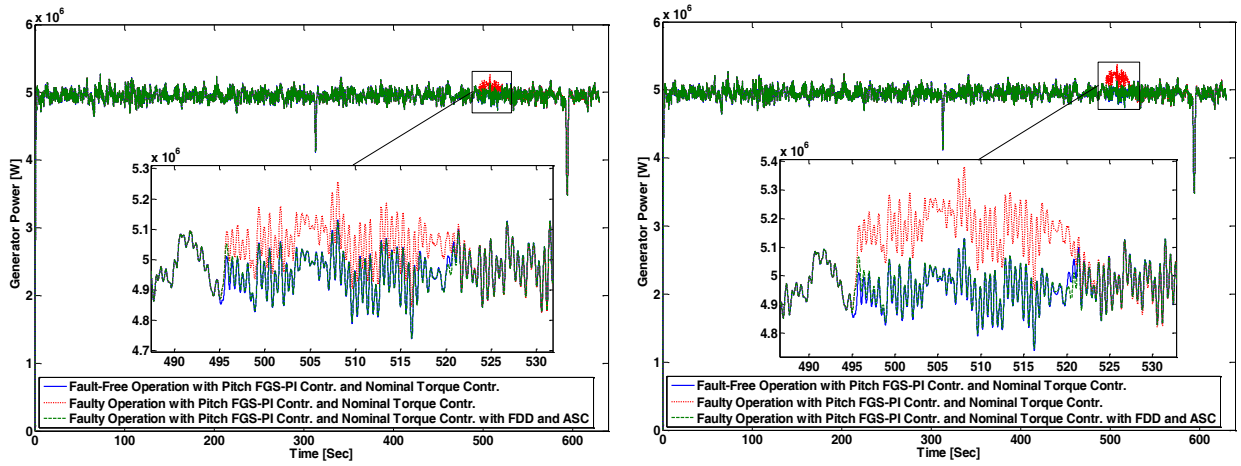

(a) (b)

Figure 3.13 Generator power response under fault-free and faulty conditions - torque AFTC scheme (FDD and ASC). (a) +1000 Nm torque actuator offset, and (b) +2000 Nm torque actuator offset.

E) Evaluation of Wind Turbine Structural Dynamics and Loading during Fault Accommodation

In addition to the evaluation of the wind turbine performance under the proposed FTC schemes, it is also required to evaluate the functionality of the FTC schemes in terms of wind turbine structural dynamics and loading. Actually, different structural safety measures including those related to allowable loading on the actuators and wind turbine structure have been evaluated in this study and found to be well within their safe ranges. However, this subsection presents some of the important structural dynamics and loading results during fault accommodation using each of the proposed passive and active FTC schemes. In particular, the tower-top fore-aft and side-to-side accelerations and deflections, as well as tower-base fore-aft and side-to-side moments are

considered and evaluated. Figure 3.14 displays the mentioned structural dynamics and loading results for the torque PFTC scheme during the considered 1000 Nm and 2000 Nm torque actuator offsets in [495-520] sec. In connection with Figure 3.14, a quantitative comparison in terms of mean and STD for each of the considered results is also presented in Table 3.12. Similarly, Figure 3.15 and Table 3.13 present the structural dynamics and loading results for the torque AFTC scheme. The results shown in Figure 3.14 and Figure 3.15 together with the numerical results presented in Tables 3.12 and 3.13 all demonstrate that both the torque FTC schemes have minimal impact on the wind turbine structural dynamics and loading during fault accommodation.

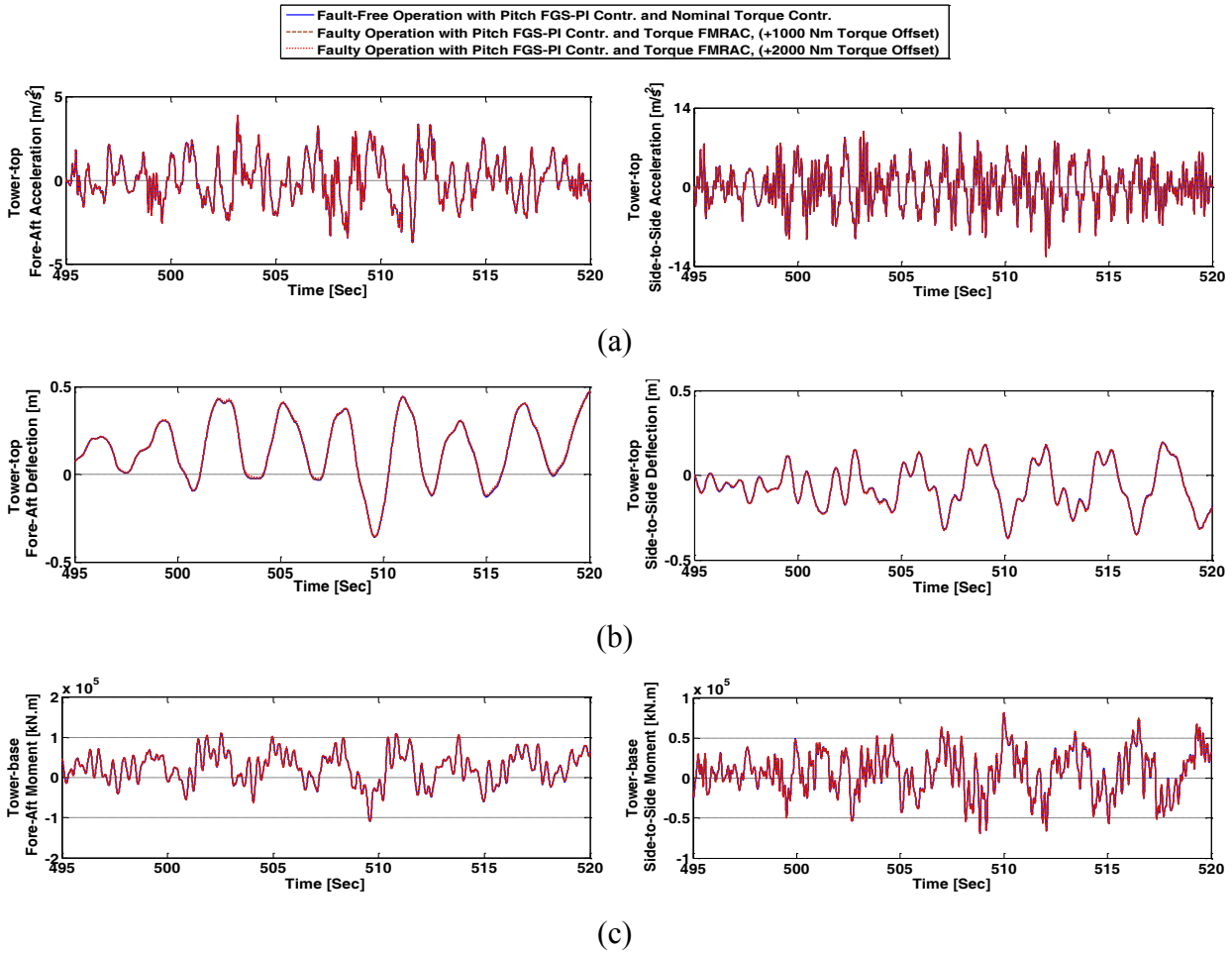

Figure 3.14 Structural dynamics and loading for torque PFTC scheme (FMRAC) – time period [495,520] sec. (a) tower-top fore-aft and side-to-side accelerations, (b) tower-top fore-aft and side-to-side deflections, and (c) tower-base fore-aft and side-to-side moments.

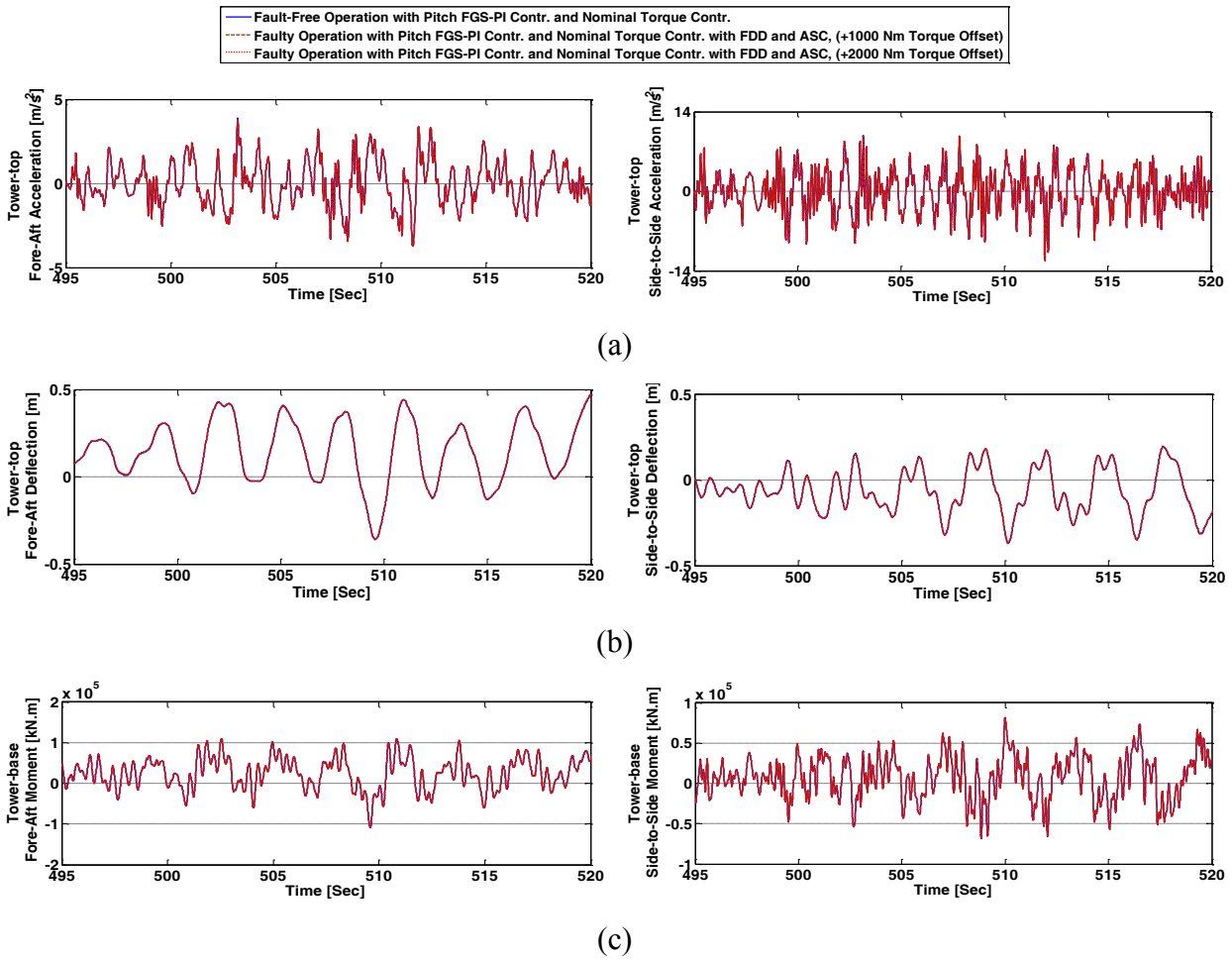

Figure 3.15 Structural dynamics and loading for AFTC scheme (FDD and ASC) – time period [495,520] sec. (a) tower-top fore-aft and side-to-side accelerations, (b) tower-top fore-aft and side-to-side deflections, and (c) tower-base fore-aft and side-to-side moments.

Table 3.12 Quantitative comparison of structural dynamics and loading results — torque PFTC scheme – time period [495,520] sec. (a) fault-free operation with nominal torque controller, (b) +1000 Nm torque actuator offset, (c) +2000 Nm torque actuator offset.

Case	Tower-top Fore-Aft Acceleration (m/sec^2)		Tower-top Side-to-Side Acceleration (m/sec^2)		Tower-top Fore-Aft Deflection (m)		Tower-top Side-to-Side Deflection (m)		Tower-base Fore-Aft Moment (kNm)		Tower-base Side-to Side Moment (kNm)	
	Mean	STD	Mean	STD	Mean	STD	Mean	STD	Mean	STD	Mean	STD
(a)	0.0004462	0.2589	0.001004	0.7110	0.1455	0.1783	-0.0662	0.1278	24611	38077	6975.5	26553
(b)	0.0004392	0.2585	0.000997	0.7117	0.1467	0.1775	-0.0664	0.1299	24799	38017	7001.8	26871
(c)	0.0004488	0.2584	0.001004	0.7098	0.1515	0.1777	-0.0676	0.1294	25583	38050	7121.9	26754

Table 3.13 Quantitative comparison of structural dynamics and loading results — torque AFTC scheme – time period [495,520] sec. (a) fault-free operation with nominal torque controller, (b) +1000 Nm torque actuator offset, (c) +2000 Nm torque actuator offset.

Case	Tower-top Fore-Aft Acceleration (m/sec^2)		Tower-top Side-to-Side Acceleration (m/sec^2)		Tower-top Fore-Aft Deflection (m)		Tower-top Side-to-Side Deflection (m)		Tower-base Fore-Aft Moment (kNm)		Tower-base Side-to Side Moment (kNm)	
	Mean	**STD**	**Mean**	**STD**	**Mean**	**STD**	**Mean**	**STD**	**Mean**	**STD**	**Mean**	**STD**
(a)	0.0004462	0.2589	0.001004	0.7110	0.1455	0.1783	-0.0662	0.1278	24611	38077	6975.5	26553
(b)	0.0004503	0.2589	0.001006	0.7105	0.1457	0.1784	-0.0663	0.1276	24637	38088	6979.9	26543
(c)	0.0004488	0.2584	0.001004	0.7098	0.1457	0.1777	-0.0663	0.1273	24647	37993	6977.8	26499

F) Comparison of Torque FTC Schemes

To compare the performance of the proposed FTC schemes, simulation plots for the already shown filtered measurement of the generator power under the considered +1000 Nm and +2000 Nm actuator faults are recalled in Figure 3.16(a) and (b), respectively. Moreover, in order to have an idea of what exactly the true measurement of the generator power looks like, the relevant simulation plots under the mentioned +1000 Nm and +2000 Nm actuator faults are also shown in Figure 3.16(c) and (d), respectively. In connection with Figure 3.16(c) and (d), Table 3.14 presents a precise quantitative comparison between the passive and active FTC schemes in terms of RMSPE during the period of considered fault scenarios. Note that, the lower the RMSPE, the better the fault-tolerance has scored.

In addition to the presented discussions in subsections 3.7C and 3.7D, the simulation plots shown in Figure 3.16 together with the results presented in Table 3.14 can be considered to explore and summarize the pros and cons of using the proposed FTC schemes for regulation of generator torque load.

The torque PFTC scheme based on FMRAC has the interesting capability of online adaptation of the control action without any explicit knowledge of the potential faults in the generator/converter system. This feature makes the FMRAC system a very powerful tool for the accommodation of various types of faults and model uncertainties or external disturbances. Since the FMRAC system is independent of FDD information, it does not deal with FDD uncertainties and time-delays with respect to fault detection/isolation process (see Figure 3.16(a) and (c)).

However, as can be seen in Figure 3.16(b) and (d), the PFTC scheme has limited fault-tolerance capability against large values of torque offset (see also Table 3.14 for +2000 Nm torque offset scenario). In contrast to the torque PFTC scheme, the torque AFTC scheme with FDD and ASC can satisfactorily accommodate large values of torque offset as well (see Figure 3.16(b) and (d) and Table 3.14). Furthermore, in this scheme, the proposed ASC approach does not disturb the nominal performance of the torque controllers under normal (fault-free) operating conditions. This feature is particularly favorable in the case of wind turbine torque control whose fixed-structure is well defined for optimizing power capture in the partial load region and for improving output power quality in the full load region in order to achieve fault-tolerance capability without scarifying best performance of the wind turbine under different normal operation conditions for handling well also the system's nonlinearity. However, it is worth mentioning that, the performance of ASC scheme is highly dependent on the speed and accuracy of the FDD system. It may be difficult in practice to measure or obtain the instant precise values of faults in the system. Therefore, the FDD system can only determine an online estimate for the magnitude of offset faults after their occurrence. Furthermore, the time delays present in the FDD process and subsequent real-time control reconfiguration (signal correction) result in a temporary graceful degradation in overall wind turbine performance under the faulty conditions (see Figure 3.16).

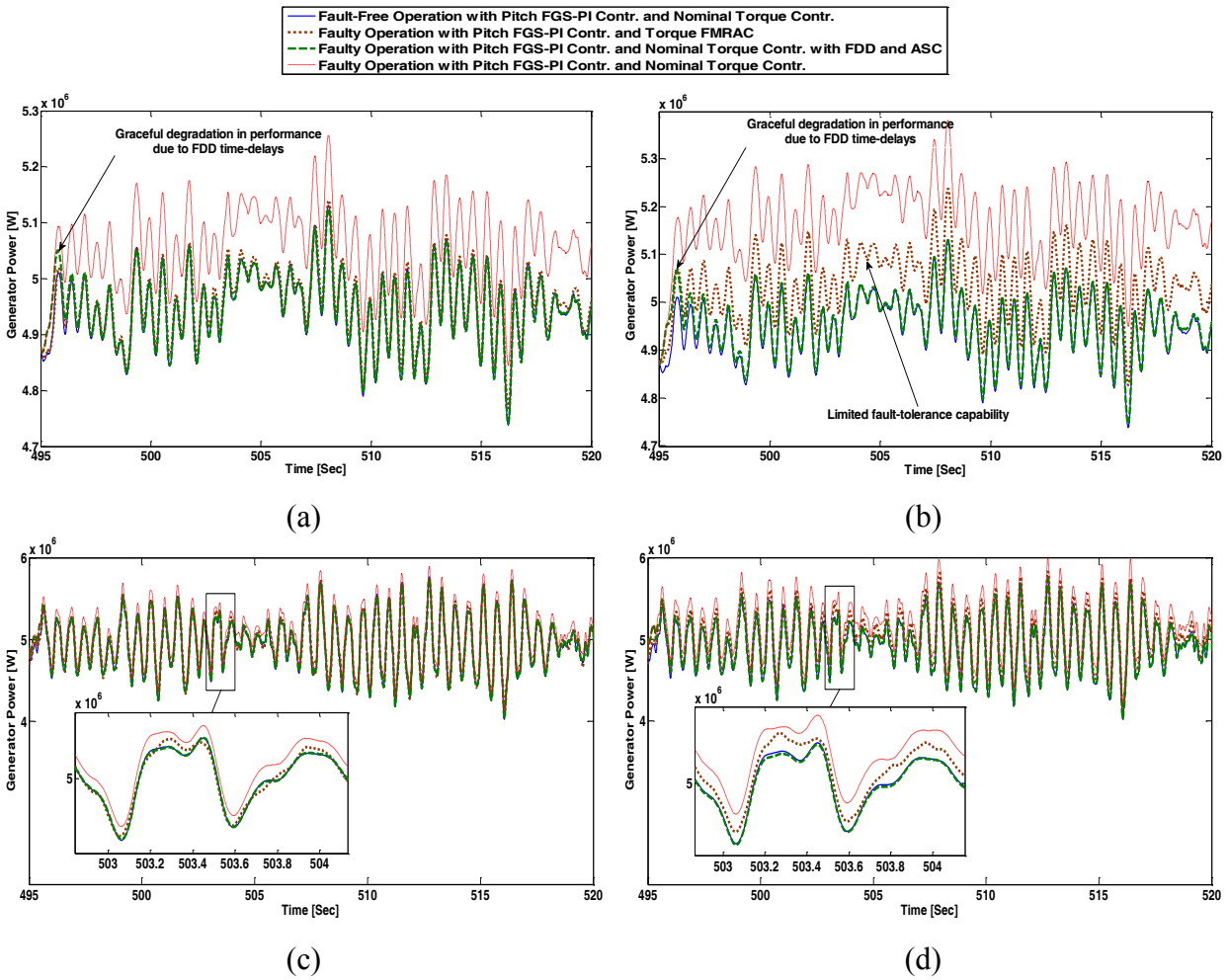

Figure 3.16 Generator power response under fault-free and faulty conditions – time period [495,520] sec. (a) filtered measurement, +1000 Nm torque actuator offset, (b) filtered measurement, +2000 Nm torque actuator offset, (c) true (noise free) measurement, +1000 Nm torque actuator offset, and (d) true (noise free) measurement +2000 Nm torque actuator offset.

Table 3.14 Quantitative comparison of FTC schemes during fault period [495-520] sec

Fault No.	Type	RMSPE (%)	
		AFTC Scheme (FDD-ASC)	PFTC Scheme (FMRAC)
1	+1000 Nm torque actuator offset	0.406	0.958
2	+2000 Nm torque actuator offset	0.667	1.911

To sum up, the presented results in Figure 3.16 and Table 3.14 show that the AFTC scheme has superior performance compared to the PFTC scheme under large values of torque offset (severe fault cases), even though the speed and accuracy of the FDD system play an important role in this regard. More precisely, the AFTC scheme with FDD and ASC can demonstrate a highly effective

fault accommodation as long as the FDD information is timely and accurate. However, in the case of small values of torque offset (mild fault cases) such as intermittent system uncertainties, both the FDD uncertainties and time-delays make it difficult for the AFTC scheme to outperform the PFTC scheme which is basically independent of FDD information. For instance, by considering an intermittent time-dependent torque offset such as the fault signal shown in Figure 3.17 which corrupts the generator/converter torque actuator during the same period of [495,520] sec, the fault accommodation gives the interesting results shown in Figure 3.18 and Table 3.15. The results reflected in Figure 3.18 and Table 3.15 confirms the already mentioned fact that, unlike the AFTC scheme, the passive scheme demonstrates better performance against the small values of torque offset that are difficult to be detected and identified in a timely and accurate manner. In this particular wind turbine application, the PFTC scheme provides satisfactory fault-tolerance capability to completely accommodate torque actuator offsets with absolute values up to 1500 [Nm], while the AFTC scheme provides such a capability for accommodation of torque actuator offsets with absolute values greater than 500 [Nm].

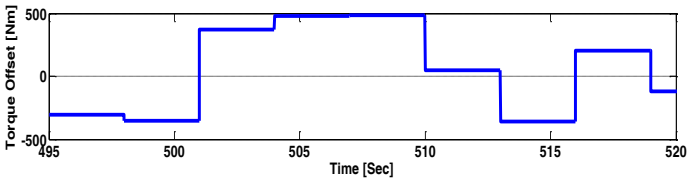

Figure 3.17 A small (< 500 Nm) intermittent time-dependent torque actuator offset – time period [495,520] sec.

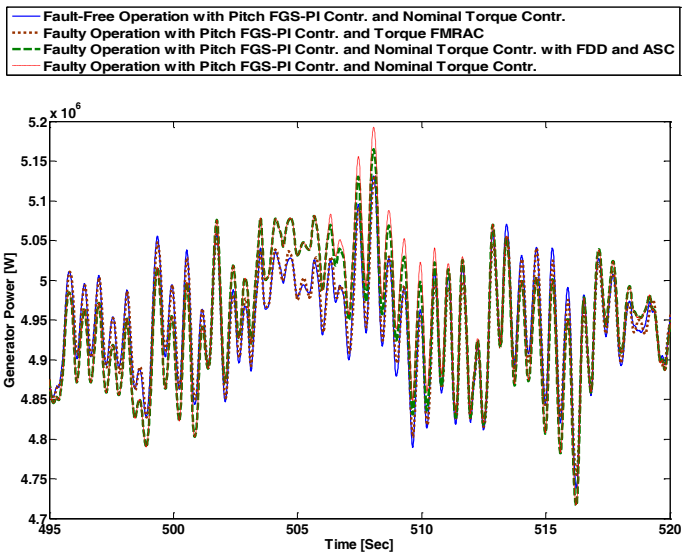

Figure 3.18 Generator power response during fault-free and faulty conditions – time period [495,520] sec.

Table 3.15 Quantitative comparison of FTC schemes during fault period [495-520] sec

Fault Type	RMSPE (%)	
	AFTC Scheme (FDD-ASC)	PFTC Scheme (FMRAC)
Intermittent time-dependent torque actuator offset in Figure 3.17	0.757	0.311

G) Robustness

The purpose of this subsection is to evaluate the robustness of the designed FTC schemes with respect to modeling errors, disturbances and measurement uncertainties. The robustness evaluation consists of extensive Monte Carlo simulations using different noise parameters (e.g., starting seeds, noise power) affecting the stochastic features of the signals in order to model process parameter errors and measurement uncertainties. In the benchmark model, sensors are modeled as noise-contaminated, uncertain measurement systems. The measurement noise in each sensor model is generated as band limited white noise parameterized by a noise power and starting seed value. Table 3.16 presents a list of available sensors and their noise parameters considered in the Monte Carlo simulations. In total, 100 Monte Carlo simulations have been carried out for each of the active and passive FTC schemes, and the best, average and worst values of performance characteristics are reported in Table 3.17.

Table 3.16 Available sensors and their white noise parameters

Sensor	Unit	Noise Power		Starting Seed
		Nominal	Error	
Anemometer – Wind speed at hub height	m/s	0.0071	50%	Stochastic values
Rotor speed	rad/s	10^{-4}		
Generator speed	rad/s	$2 \cdot 10^{-4}$		
Generator torque	Nm	0.9		
Generated electrical power (Generator power)	W	10		
Pitch angle of *i*-th blade	deg	$1.5 \cdot 10^{-3}$		
Azimuth angle low speed side	rad	10^{-3}		
Blade root moment of *i*-th blade	Nm	10^{3}		
Tower-top acceleration (x and y direction)	m/s^2	$5 \cdot 10^{-4}$		
Yaw error	deg	$5 \cdot 10^{-2}$		

Table 3.17 The results of Monte Carlo simulation studies under wind profile with mean speed of 14 m/s.

Fault Type	MCS Results	AFTCS		PFTCS
		Detection Time (sec)	RMSPE (%)	RMSPE (%)
+1000 Nm torque actuator offset	Best Case	0.5125	0.3873	0.9449
	Average Case	0.5320	0.4094	0.9583
	Worst Case	0.5500	0.4325	1.0116
+2000 Nm torque actuator offset	Best Case	0.2875	0.6630	1.9055
	Average Case	0.3085	0.6799	1.9241
	Worst Case	0.3375	0.7081	1.9618

Although the wind profile with mean speed of 14 m/s (see Figure 3.9) used for the above mentioned Monte Carlo study has high turbulence intensity and covers a wide speed range from below rated wind speeds to above rated wind speeds, two additional simulation trials are also made in order to test the robustness in performance of the FTC schemes in terms of external disturbances (e.g., wind changes). In this regard, the wind profiles with mean speeds of 11 m/s, and 17 m/s are used here (see Figure 3.9). For each wind profile, similar simulations as described in subsections 3.7C and 3.7D are conducted. However, only simulation results for the +1000 Nm torque offset fault scenario are presented here for the sake of brevity. The generator power response obtained from the first simulation trial is shown in Figure 3.19(a) and (b) for PFTC scheme and AFTC scheme, respectively. As can be seen in these figures, the generated power is mostly below its rated value of 5 MW, mainly due to the used wind speed profile which has a below rated hub-height mean speed of 11 m/s. Similarly, the generator power response obtained from the second simulation trial is shown in Figure 3.20(a) and (b) for PFTC scheme and AFTC scheme, respectively. In this simulation trial, since the used wind profile has an above rated hub-height mean speed of 17 m/s, the wind turbine generates full power of 5 MW.

With respect to the results of Monte Carlo study reported in Table 3.17 and the generator power responses shown in Figure 3.19 and Figure 3.20, all results confirm that both the active and passive FTC schemes are not only robust in the presence of modeling errors, measurement uncertainties, and disturbances, but also can successfully maintain reliable wind turbine performance under faulty conditions in both below and above rated wind speeds.

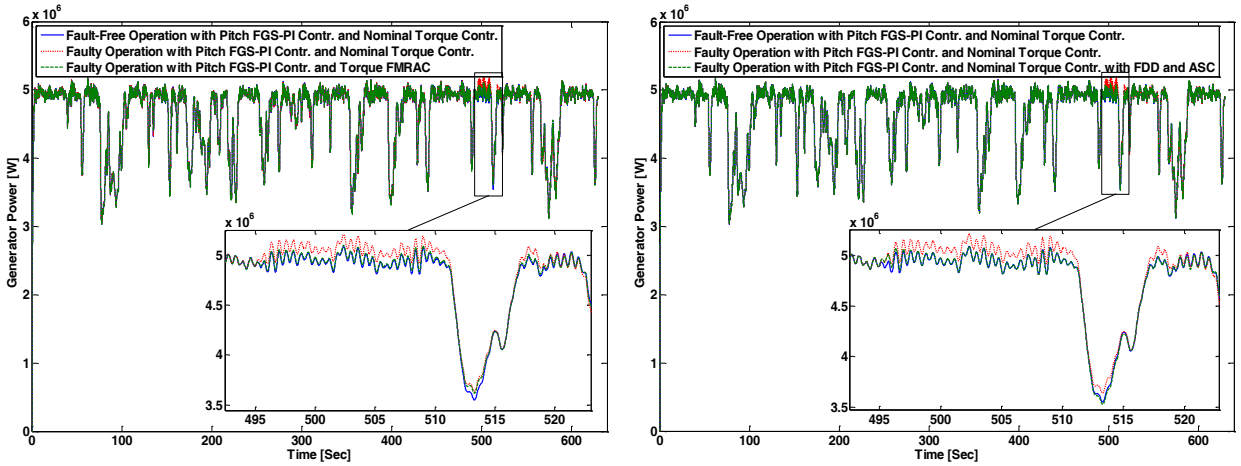

(a) (b)

Figure 3.19 Generator power response during fault-free and faulty conditions with +1,000 Nm torque actuator offset, and using wind profile with mean speed of 11 m/s. (a) torque PFTC scheme (FMRAC), and (b) torque AFTC scheme (FDD-ASC).

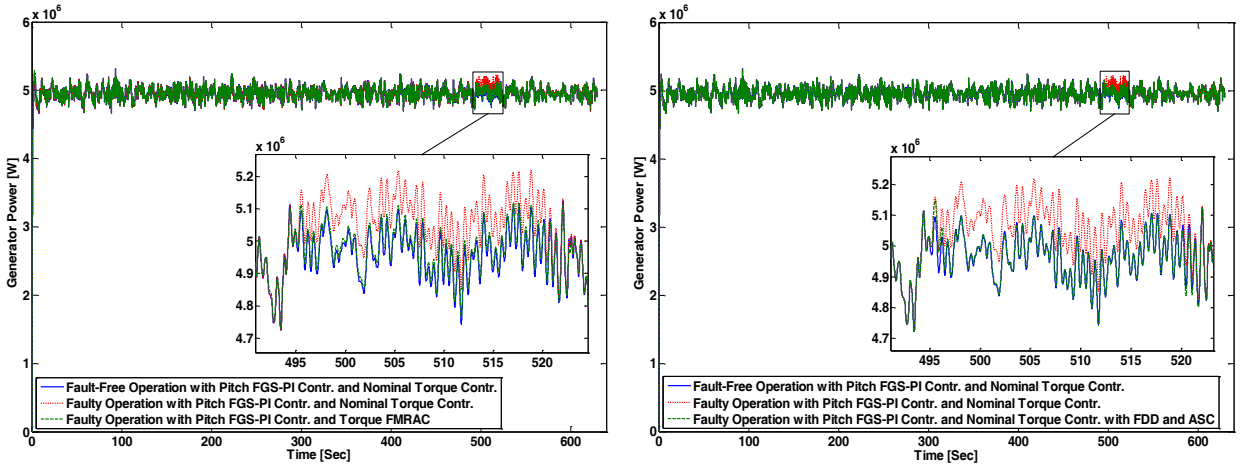

(a) (b)

Figure 3.20 Generator power response during fault-free and faulty conditions with +1,000 Nm torque actuator offset, and using wind profile with mean speed of 17 m/s. (a) torque PFTC scheme (FMRAC), and (b) torque AFTC scheme (FDD-ASC).

3.8 Conclusion

This paper addressed the design of two fault-tolerant control schemes for reliable regulation of generator torque load in a wind turbine which can be affected by both model uncertainties and actuator faults in its generator/converter system. The first scheme is a passive fault-tolerant control scheme based on a fuzzy model reference adaptive control approach in which a fuzzy inference mechanism is used for parameter adaptation without any explicit knowledge of the potential faults in the system and without the need of a fault detection and diagnosis system. The second scheme is an active fault-tolerant control scheme which exploits an automatic signal correction approach that itself relies on a fault detection and diagnosis system.

Simulations have been conducted using a well-known large offshore wind turbine benchmark model in the presence of wind turbulences, measurement noises, and realistic fault scenarios in the generator/converter torque actuator. Numerical results and simulation studies clearly indicate the effectiveness and robustness of the proposed schemes over the entire range of tested wind profiles for both the fault-free and faulty conditions.

Although both the fault-tolerant control schemes are superior to a reference torque control system designed using classical methods, the fault-tolerance and nominal performance provided by the active scheme will make it a practical choice if the faults change the system's behavior significantly. The passive scheme should be favored when faults are difficult to diagnose (e.g., due to their small impact on system performance), or there is no tolerance for false decisions in the fault detection and diagnosis system.

Extending the presented fault-tolerant control methodologies to accommodation of other types of faults like new actuator or system component faults as well as their integration with other control schemes tolerant to sensor faults remain as interesting future research topics. Furthermore, in order to achieve a practical fault-tolerant control scheme, the fault detection and diagnosis system as well as real-time control system reconfiguration/adaptation should be designed along with techniques in fault-tolerant computing, and fault-tolerant communication networks followed by hardware-in-the-loop testing for thorough evaluation before real system tests.

Chapter 4 Fault-Tolerant Cooperative Control in an Offshore Wind Farm Using Model-Free and Model-Based Fault Detection and Diagnosis

"Reprinted from paper [Hamed Badihi, Youmin Zhang, Henry Hong, "Fault-Tolerant Cooperative Control in an Offshore Wind Farm Using Model-Free and Model-Based Fault Detection and Diagnosis", submitted to the Applied Energy, 2016."

Abstract

Given the importance of reliability and availability in wind farms, this paper focuses on the development of fault diagnosis and fault-tolerant control schemes in a cooperative framework (referred to as active fault-tolerant cooperative control) at wind farm level against the decreased power generation caused by turbine blade erosion and debris build-up on the blades over time. In more details, the paper presents a novel integrated fault detection and diagnosis and fault-tolerant control approach oriented to the design and development of two active fault-tolerant control schemes for an offshore wind farm. Each of the schemes employs a fault detection and diagnosis system to provide accurate and timely diagnosis information to be used in an appropriate automatic signal correction algorithm for accommodation of faults in the wind farm. The effectiveness and performance of the proposed schemes are evaluated and compared by different simulations on a high-fidelity offshore wind farm benchmark model in the presence of wind turbulences, measurement noises and realistic fault scenarios.

4.1 Introduction

Wind energy has remarkable potential for fulfilling the increasing world's energy demand in a sustainable and clean way. In order to reduce the average cost of wind energy, large wind turbines are often installed in clusters called wind farms, particularly in offshore locations. As more and more offshore wind farms are developed, further from shore, both the factors of complexity and limited accessibility together with harsh climate conditions come into play and result in higher failure rates and maintenance challenges. This motivates the design and development of advanced fault detection and diagnosis (FDD) as well as fault-tolerant control (FTC) schemes in wind farms to improve their reliability and availability. The FTC schemes can be designed in either passive or active ways. A passive FTC (PFTC) scheme employs the robustness of the closed-loop control system to accommodate faults, while an active FTC (AFTC) scheme reconfigures the closed-loop control system after fault occurrence. AFTC schemes usually require FDD information in the process of control reconfiguration.

In general, the FDD and FTC schemes can be applied at both individual wind turbine and entire wind farm levels. Recently, research works have been more focused on the application of such methods at wind turbine level (for example see, [30, 33, 43, 46, 104]). Most of these works try to address the FDD and FTC problems in two standard wind turbine benchmark models presented in [3] and [69]. A recent review of the literature in [17] provides more references on FDD and FTC for wind turbines. Actually, some faults are easier to be detected, diagnosed, and accommodated at wind farm level through comparing the performance of turbines operating under almost the same wind conditions. With respect to the FDD and FTC at wind farm level that is a very recent field of research, only a few research works are reported in the literature. Most of these works are only focused on condition monitoring and fault detection in wind farms. In [67, 68], various data-mining algorithms are applied to develop models for predicting possible faults in wind farms. In [105], the relationship between the wind speed and the generated power in a wind farm is estimated using three different machine learning models. The models can detect anomalous functioning conditions of the wind farm. But, they are unable to isolate and identify faults. More recently, researchers have studied the FDD and FTC problems in a standard benchmark model presented in [106] that represents a wind farm with nine turbines subjected to different fault scenarios. For example, authors in [107] present a fault detection and isolation approach based on

a set of piecewise affine Takagi–Sugeno models that are identified from the noisy measurements obtained from the simulated benchmark model. Duviella et al. [108] propose an evolving classification algorithm for detection and isolation of faults due to debris build-up on the wind turbine blades is presented. In [109], the fault diagnosis is conducted using interval nonlinear parameter-varying parity equations assuming unknown but bounded description of the noise and modeling errors. Another work reported in [110] presents a fault detection system relying on dynamical cumulative sum for residual evaluation, and a load distributing controller for accommodating the possible faults. Moreover, an active fault-tolerant control scheme based on a model-based FDD approach is also presented in [111]. The above cited research works are common in two aspects. First, they have assumed that only one fault can occur at a time in a farm. Second, they mostly rely on wind speed or its estimation that itself, normally, depends on the layout of the wind farm and direction of the wind as well. For example, the algorithms proposed in [108-110] are only developed for one or two specific wind directions.

Given the importance of FDD and FTC at wind farm level and by recognizing the differences in controlling a wind farm from a single wind turbine, this paper presents a novel integrated FDD and FTC approach in a cooperative framework referred to as active fault-tolerant cooperative control (AFTCC) in this paper, where the term of “active” is due to the integrated design by combining both FDD and FTC schemes [10], while the term of “cooperative” is due to the cooperative design for multiple wind turbines (wind farm) which is beyond a design for single wind turbine as will be demonstrated in the later parts of this paper for both FDD and FTC schemes. The proposed AFTCC approach is oriented to the design and development of two AFTC schemes for an offshore wind farm against decreased power generation fault caused by turbine blade erosion and debris build-up on the blades over time. The first scheme is based on a model-free FDD system that incorporates a rule-based threshold test technique for residual evaluation. Conversely, the second scheme is based on a model-based FDD system that incorporates data-driven models developed using fuzzy modelling and identification (FMI) technique. Both schemes are relying on an appropriate automatic signal correction (ASC) algorithm that employs the provided accurate and timely FDD information for accommodating the possible faults in a wind farm. To sum up, the proposed schemes not only provide necessary FDD information for condition monitoring purposes, but also provide the effective possibility of accommodation of faults in a wind farm. To further highlight the contribution of this paper compared to the other relevant works in the existing

literature, it is worth mentioning that the proposed schemes in this paper are designed and developed in a way to be valid for any layouts of a wind farm with any directions of the wind while the considered fault may occur simultaneously in more than one turbine in the farm.

The effectiveness and performance of the proposed FDD and FTC schemes are evaluated and compared by different simulations on a high-fidelity offshore wind farm benchmark model in the presence of wind turbulences, measurement noises and realistic fault scenarios. Moreover, extensive Monte Carlo simulations are performed to evaluate the robustness of the proposed schemes with respect to modelling errors, disturbances and measurement uncertainties.

The remainder of the paper is organized as follows: In Section 4.2, the wind farm benchmark model used in this paper is briefly described. The considered fault is described and analysed in Section 4.3. Section 4.4 presents an integrated FDD and FTC approach against the fault discussed in Section 4.3. The details of the FDD at wind farm level is presented in Section 4.5. Section 4.6 presents the simulation results with some comments and discussions. Finally, conclusions are drawn in Section 4.7.

4.2 Overview of the Wind Farm Benchmark Model

This paper considers an advanced wind farm simulation toolbox called *SimWindFarm* developed as a part of the EU-FP7 project, AEOLUS [112]. The toolbox provides a realistic wind farm simulation benchmark model that allows control designers to develop, implement and investigate farm level control and diagnosis algorithms under different operating conditions for an optional quantity and layout of turbines installed in a wind farm. In the benchmark model, sensor models are updated to represent noise-contaminated, uncertain measurement systems. The recommended rate and magnitude limiters are also applied on any reference signal to the actuator models. In addition, to facilitate the assessment of the robustness features of any control solution under external disturbances, different wind fields with arbitrary mean wind speeds and turbulence intensities can be generated and applied in the benchmark model. Figure 4.1 shows the default layout for the considered wind farm with ten turbines. The overall structure of the simulation benchmark model under consideration is illustrated in Figure 4.2.

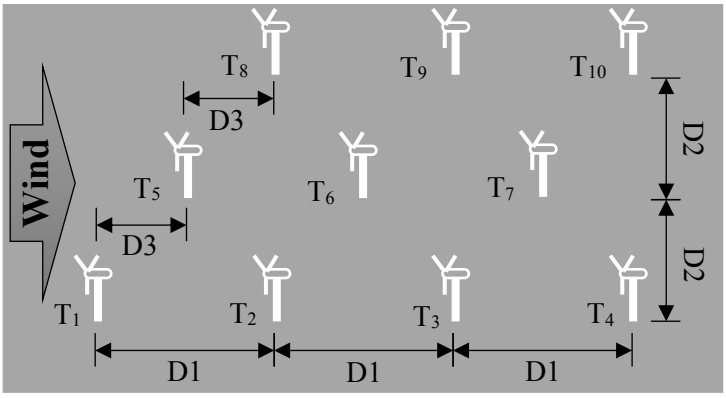

Figure 4.1 Wind farm layout (D1=600m, D2=500m, D3=300m).

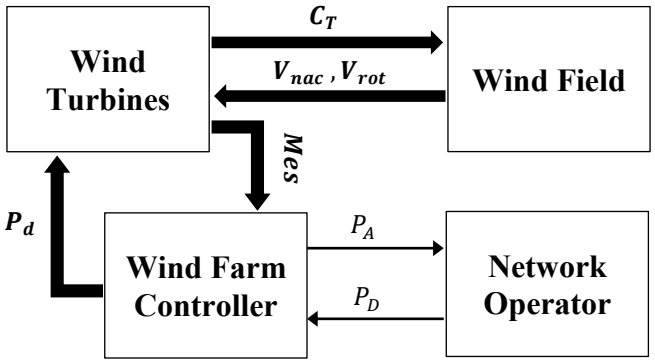

Figure 4.2 Illustration of overall model structure for N turbines. Note that the bold letters stand for sets of variables, for example $\boldsymbol{P_d} = [P_{d,q}]$ with $q = 1, 2, \dots, N$ (This figure is based on [112]).

As it is shown in Figure 4.2, the wind farm simulation benchmark model is composed of four major components in the top level that operate in a closed loop:

Network Operator: The network operator is responsible to determine the total active power demand P_D (also called operator's total demanded power) required for reliable connection of the wind farm to the electrical grid. This can be performed in different modes such as: absolute, delta, and frequency regulation modes. This paper employs the frequency regulation mode in which the measured grid frequency f_m is used as a feedback signal to set up *active power control* in real-time. The objective is to maintain the necessary balance between power generation and load, which in turn regulates the grid frequency to its reference value f_r, despite a changing grid load. The baseline model for the network operator in the frequency regulation mode includes a dead-band proportional gain control which employs frequency error $f_e(k)$ in (4.1) to determine the total

demanded power $P_D(k)$ at the time-step k in (4.2). Such a simple control scheme regulates the grid frequency to any specified reference value, for example, 50 Hz in large areas of the world.

$$f_e(k) = f_m(k) - f_r \tag{4.1}$$

$$P_D(k) = \begin{cases} 0.5(P_1) & -d \le f_e(k) \le d \\ 0.5(P_1 - P_2) & f_e(k) \ge c \\ 0.5(P_1 + P_2) & f_e(k) \le -c \\ 0.5(P_1) - 0.5(P_2)\left(\dfrac{f_e(k) - d}{c - d}\right) & d < f_e(k) < c \\ 0.5(P_1) - 0.5(P_2)\left(\dfrac{f_e(k) + d}{c - d}\right) & -c < f_e(k) < -d \end{cases} \tag{4.2}$$

In (4.2), the constants c and d are, respectively, the control band and the dead band defined by user ($c > d$). Moreover, the power parameters P_1 and P_2 are defined in (4.3) and (4.4), respectively. Here, P_{min} and P_{max} denote the prescribed minimum and maximum limits for the total power generated by the wind farm, respectively.

$$P_1 = P_{max} + P_{min} \tag{4.3}$$

$$P_2 = P_{max} - P_{min} \tag{4.4}$$

Wind Farm Controller: As it is shown in Figure 4.2, the wind farm controller acts as an interface between the network operator and wind turbines. Its main functionality is to ensure the appropriate distribution of operator's total demanded power P_D among wind turbines in the farm. It also provides an estimate of total available power P_A in the wind farm to the operator (e.g., in the case of delta mode operator). The baseline wind farm controller employs the proportional distribution algorithm in (4.5) which provides a set of power demands $P_{d,q}(k)$ at the time-step k (i.e., $\boldsymbol{P_d}$ in Figure 4.2) to each of N individual wind turbines. Here, $P_{a,q}(k)$ and $P_A(k)$ are the estimated available power from turbine q and the total available power from the wind farm, respectively.

$$P_{d,q}(k) = P_D(k)\frac{P_{a,q}(k)}{P_A(k)} \quad , \qquad q = 1, 2, \dots, N \tag{4.5}$$

Wind Turbines: As it is shown in Figure 4.2, this component is devoted to the simulation of dynamics of N turbines installed in the wind farm based on their measured nacelle wind speeds $\boldsymbol{V_{nac}} = [V_{nac,q}]$, effective wind speeds $\boldsymbol{V_{rot}} = [V_{rot,q}]$, and power demands $\boldsymbol{P_d} = [P_{d,q}]$

with $q = 1, 2, \dots, N$. With respect to the outputs, the component generates a set of outputs including a set of measurements $\boldsymbol{Mes}$ required for use by the wind farm controller as well as a set of coefficients of thrust $\boldsymbol{C_T} = [C_{T,q}]$ for turbines, necessary to calculate the wake effects (i.e., low speed turbulent air flows behind turbine) by wind field component. In the component of wind turbines, each turbine is simulated using a simple model of an offshore 5 MW turbine that has been already proposed by the U.S. National Renewable Energy Laboratory (NREL) (see [70]). The baseline control system used in each individual wind turbine is shown in Figure 4.3. As it is shown in the figure, the control system acts upon the power demand $P_{d,q}$ in (4.5). This control system is basically composed of a blade-pitch controller and a torque controller to compute appropriate reference blade-pitch angle $\beta_{r,q}$ and reference generator torque $\tau_{r,q}$, respectively. The blade-pitch controller is basically a Proportional-Integral (PI) controller that tracks a constant generator speed (rated generator speed) so that the turbine operates at its rated power in the *full-load region*. The torque controller is designed to optimize power capture in the *partial-load region*, and to improve output power quality in the full-load region both by varying the generator torque. More precisely, the torque controller is set to be active for varying the torque during both the below and above rated wind speeds. A more complete description of the wind turbine benchmark model is available in [70].

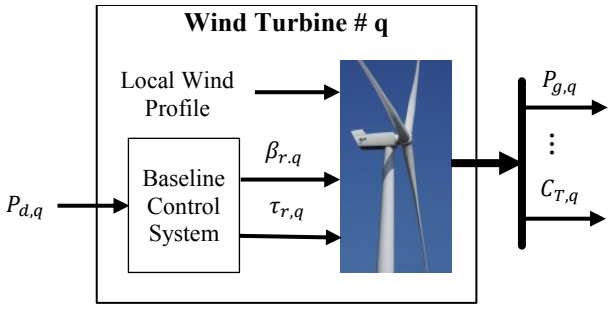

Figure 4.3 The qth wind turbine in the farm ($q = 1, 2, \dots, N$). Note that in addition to the generated power $P_{g,q}$, the turbine model provides many other measured variables such as coefficient of thrust $C_{T,q}$, and so on.

Wind Field: The wind field model represents the interactions between the wind turbines installed in a wind farm. This model includes models of ambient field and wake phenomenon for simulating wakes meandering behind turbines and their effects on the ambient wind field. So, the wind speed throughout the farm is obtained.

4.3 Blade Erosion/Debris Build-up Fault

Basically, decreased power generation in a wind farm may be due to several different malfunctions. However, blade erosion along with debris build-up on the blades due to dirt, ice, etc. constitute the most probable fault which results in a lower power generation because of changes in the aerodynamics of the wind turbine, and thereby lowering the maximally obtained power. In more detail, the aerodynamic torque τ_{aer} applied to the rotor by the wind is defined in (4.6), in which ω_{rot} is the rotor angular speed, ρ is the air density, A is the swept area of the turbine rotor, and V_w is the wind speed [99].

$$\tau_{aer}(t) = \frac{1}{2\omega_{rot}(t)} \rho\, A\, V_w^3(t)\, C_p(\beta(t), \lambda(t)) \tag{4.6}$$

In (4.6), the power coefficient $C_p(\beta, \lambda)$ is a three dimensional surface as a function of the tip-speed ratio λ and the blade pitch angle β in which the latter two terms determine the operating condition of a variable speed wind turbine. For variable-speed wind turbines, the turbine is ideally operated at the peak of the C_p surface in order to capture as much power as possible. However, over time, the blade erosion and debris build-up fault shifts the turbine's C_p surface downward, resulting in lower energy capture through not only a decrease in the peak value of the C_p surface but also a change in the location of the peak of the C_p surface. The sensitivity of energy loss to the changes at the peak of the C_p surface due to this fault is considered and quantified in [113], which concludes that the fault can lead to a substantial off optimal operation and power loss. Given the importance of the blade erosion and debris build-up fault in wind turbines, it is necessary to detect, diagnose, and accommodate such a fault in a timely and effective manner. However, it is difficult to handle this fault at a wind turbine control level, mainly because of the fact that a lower generated power may be due to either debris build-up on the blades or simply that the true wind speed is lower than the measured/estimated wind speed. Conversely, at a wind farm level, it is possible to compare the performance and operation features of the different wind turbines in a given wind farm.

The described benchmark model in Section 4.2, in its original form, does not include any faults. However, it is possible to fairly model a realistic scenario for the blade erosion and debris

build-up fault and incorporate it in the benchmark model. In the following lines, the modeling of the considered fault in this paper is described.

In general, the generator power P_g can be expressed as:

$$P_g(t) = \eta_g \eta_m P_{aer}(t) \tag{4.7}$$

in which η_g is the generator efficiency, η_m is the efficiency of transmission system, and P_{aer} is the aerodynamic rotor power given by [99]:

$$P_{aer}(t) = \tau_{aer}(t)\ \omega_{rot}(t) \tag{4.8}$$

Now, substituting (4.8) into (4.7) and using (4.6) yields:

$$P_g(t) = \frac{(\eta_g . \eta_m)}{2} \rho\ A\ V_w^3(t)\ C_p(\beta(t), \lambda(t)) \tag{4.9}$$

Equation (4.9) shows that the generated power P_g is a direct function of the power coefficient C_p which itself can be changed due to the blade erosion and debris build-up fault. With respect to this fact, the fault can be simply modeled by scaling the generated power in a wind turbine. Therefore, a realistic scaling factor of 0.97 (3% power loss) is used. In this case, the benchmark model is modified with a generic fault scenario representing occurrence of 3% power loss in a designated number of turbines in the wind farm shown in Figure 4.1. The detailed timeline for the occurrence of the considered fault scenario is shown in Figure 4.4. As it is obvious from the figure, during some periods of the simulation time, the considered decreased power generation fault has occurred simultaneously in more than one turbine in the farm. For example, Figure 4.5 shows the power loss effect due to occurrence of the fault in wind turbines T1 and T3 in the farm.

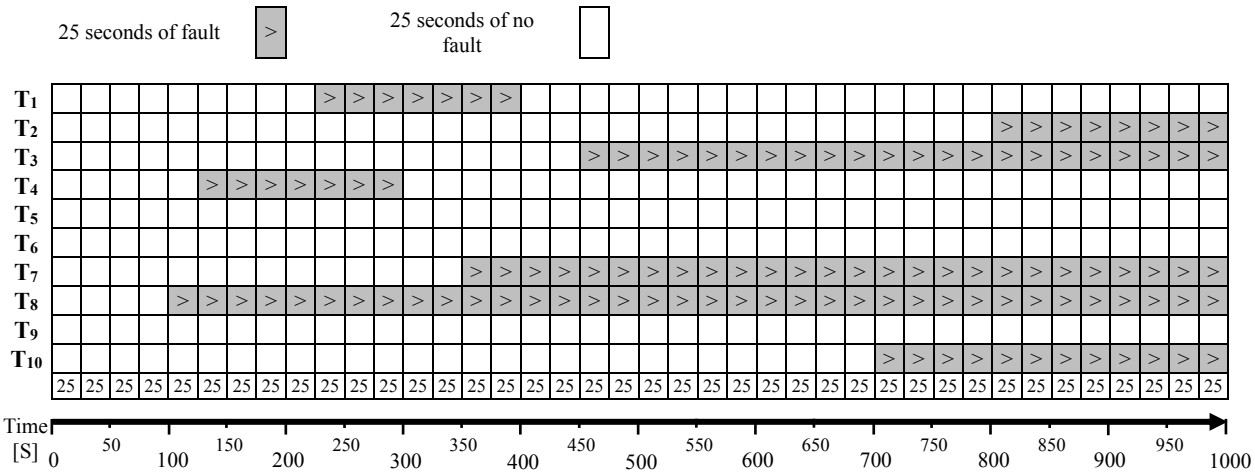

Figure 4.4 Timeline for the occurance of the considered fault in a designated number of wind turbines in the farm. Note that, the total simulation time is 1000 seconds, and $T_{\#}$ stands for wind turbine number # with respect to the wind farm layout shown Figure 4.1.

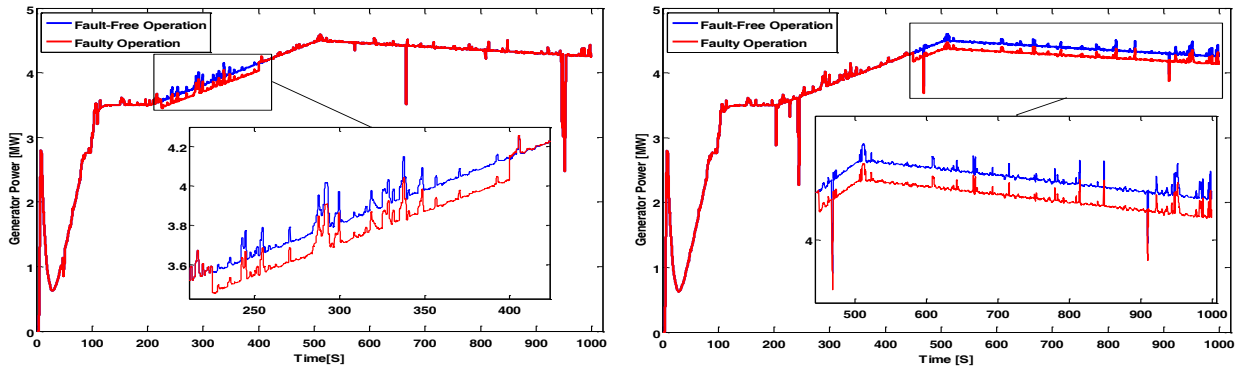

(a) (b)

Figure 4.5 Generator power response during fault-free and faulty operations of wind turbines: (a) T_1, and (b) T_3 in the farm.

4.4 Integrated FDD and FTC Approach

This section presents an integrated FDD and FTC approach aimed at improving the reliability and availability of wind farms against the fault discussed in Section 4.3. Here, it is assumed that the fault(s) may occur at any time and in any turbine installed in a farm. Simultaneous faults in more than one turbine are also possible.

As already mentioned in Section 4.3, the considered fault results in a lower power generation that negatively affects the total active power generated by all wind turbines in a farm as a whole.

Generally speaking, when such a fault occurs in one or more turbines in a wind farm, the wind farm controller still has to follow the operator's total demanded power P_D using the proportional distribution algorithm described in (4.5), no matter which turbine(s) is/are faulty. Whereas, to compensate the power loss caused by the faulty turbine(s), it is necessary to avoid overloading the remaining healthy turbines but only correcting the reference power signal(s) to the faulty turbine(s) and thereby accommodating the fault effects. In fact, overloading the healthy wind turbines may lead to high structural loading and fatigue.

The integrated FDD and FTC approach proposed in this paper is shown in Figure 4.6. As it is observed in this figure, the proposed approach basically relies on an integrated FDD system and ASC mechanism that covers the entire farm with any layouts and any wind directions. The FDD system in Figure 4.6 provides the most up-to-date information about true status of the wind farm system. As it is further discussed in Section 4.5, the FDD system can be developed based on either model-free or model-based monitoring of power consistency in a wind farm. Basically, the main idea behind the FDD process is to monitor the consistency of generated powers from any individual wind turbine and all other remaining turbines in the farm in real-time. Then, any inconsistencies in the generated powers should be detected, isolated and identified to generate FDD information. Finally, the FDD information is used for ASC and accommodation of the faults in faulty turbines. The ASC mechanism means that the nominal controllers at both wind turbine and wind farm levels are kept unchanged; only the output of the torque controller in any faulty turbine is corrected according to the real-time fault information from the FDD system. Here, the supervision process shown in Figure 4.6 is not described explicitly, because it is very simple in the considered case. In fact, according to the provided information from the FDD system, the supervisor only identifies the faulty turbines in the farm together with their relevant estimated power losses (fault magnitudes) due to the faults. Then, to accommodate the fault effects in each faulty turbine, the estimated fault magnitude is used to correct the nominal reference generator torque control signal $\tau_{r,q}$ computed by the torque controller that is itself active in both partial- and full-load regions. This signal correction is defined below for the qth wind turbine in the farm.

$$\tau_{r,q,corr}(k) = \tau_{r,q}(k) + \frac{\hat{\mathcal{P}}_q(k)}{\omega_{g,q}(k)} \quad , \qquad q = 1, 2, \dots, N \tag{4.10}$$

In (4.10), $\tau_{r,q,corr}$ is the corrected reference generator torque and $\hat{\mathcal{P}}_q$ is the estimated fault magnitude (power loss due to fault) both in the qth wind turbine in the farm. It is worth mentioning that the fault magnitude provided by the FDD system is assigned to be exactly zero ($\hat{\mathcal{P}}_q = 0$) under fault-free operation. In other words, to maintain the nominal performance of the system there is no need to modify/compensate the nominal reference torque control signal $\tau_{r,q}$ in (4.10) under fault-free operation. Finally, to avoid any intense commanded signal and extreme loading on the actuator(s), the recommended rate and magnitude limiters are also applied on the corrected reference generator torque $\tau_{r,q,corr}$ computed by (4.10).

As already mentioned, the faulty turbine and its relevant fault magnitude all are determined by the FDD system which itself can be developed based on either model-free or model-based monitoring of power consistency in a wind farm. Therefore, two AFTC schemes based on the integrated FDD and FTC approach are designed and developed. The first scheme is based on a model-free FDD system while the second scheme is based on a model-based FDD system. The following section presents the development of the FDD systems in detail.

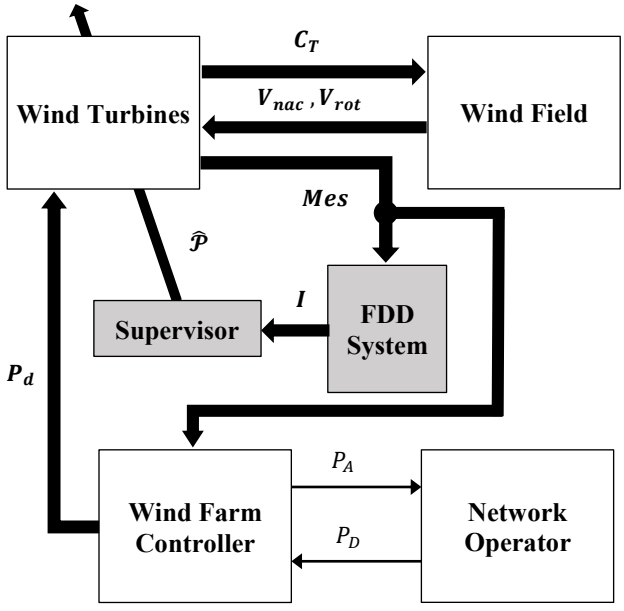

Figure 4.6 Schematic of the proposed FDD and FTC approach based on an integrated FDD system and ASC mechanism. Here, $\boldsymbol{Mes}$ is a vector of performance data including measured variables and control commands/references in wind turbines. Based on FDD information $\boldsymbol{I}(k)$, the supervisor applies appropriate signal correction/modification using power loss estimates $\hat{\boldsymbol{\mathcal{P}}} = [\hat{\mathcal{P}}_q]$. Note that the farm includes N turbines ($q = 1, 2, \dots, N$).

4.5 FDD at Wind Farm Level

The FDD system is to provide the most up-to-date information about true status of a wind farm. With respect to the facts discussed in Section III, the considered fault is difficult to be detected and identified at a wind turbine level. Therefore, as already mentioned, the FDD system in the proposed approach in Figure 4.6 addresses the considered fault at a wind farm level through monitoring the consistency of generated powers from all turbines in a given wind farm in real-time. Then, any inconsistencies in the generated powers will be detected, isolated and identified to generate FDD information. Such a monitoring can be achieved by either a model-free algorithm or a model-based algorithm that are presented in the following of this section. Therefore, each individual algorithm can be used in the FDD system and thereby either a model-free or a model-based FDD system can be established.

It should be noted that a real-time monitoring of the consistency of generated powers from different turbines in a wind farm is not a straightforward process even in the case of adjacent turbines where wind condition may be almost similar. In fact, the reference power signals are not necessarily similar for the turbines in a farm, and hence the turbines' generated powers may be different even under fault-free condition. Therefore, in order to monitor the consistency of generated powers from any two arbitrary wind turbines, it is required to consider not only the generated power responses from the turbines, but also the turbines' reference power signals. In this regard, an efficient approach is to monitor in real-time the consistency of generated powers from any individual wind turbine and all other remaining turbines in the farm simultaneously. More precisely, considering a wind farm with N turbines that are arbitrarily labeled as $T_1, T_2, \dots, T_N$, the consistency of generated powers needs to be monitored through R similar modules:

$$R = 1 + 2 + 3 + \cdots + (N-1) = \frac{N(N-1)}{2} \tag{4.11}$$

Table 4.1 shows the formation of modules (each denoted by an M) for such a wind farm with N turbines. Here, each particular module monitors the consistency of the powers generated by two different wind turbines in the farm (e.g., $M_{i,j}$ represents a module that monitors the consistency of the powers generated by turbine T_i and turbine T_j in a farm ($i \neq j$). For example, in a wind farm with ten working turbines (N=10), 45 modules (R=45) are required to monitor the consistency of generated powers among all turbines in the entire wind farm.

Table 4.1 Formation of R modules for a wind farm with N turbines

	T_1	T_2	T_3	T_4	T_5	T_6	T_7	T_8	T_9	T_{10}	⋯	T_{N-1}	T_N
T_1		$M_{1,2}$	$M_{1,3}$	$M_{1,4}$	$M_{1,5}$	$M_{1,6}$	$M_{1,7}$	$M_{1,8}$	$M_{1,9}$	$M_{1,10}$	⋯	$M_{1,N-1}$	$M_{1,N}$
T_2			$M_{2,3}$	$M_{2,4}$	$M_{2,5}$	$M_{2,6}$	$M_{2,7}$	$M_{2,8}$	$M_{2,9}$	$M_{2,10}$	⋯	$M_{2,N-1}$	$M_{2,N}$
T_3				$M_{3,4}$	$M_{3,5}$	$M_{3,6}$	$M_{3,7}$	$M_{3,8}$	$M_{3,9}$	$M_{3,10}$	⋯	$M_{3,N-1}$	$M_{3,N}$
T_4					$M_{4,5}$	$M_{4,6}$	$M_{4,7}$	$M_{4,8}$	$M_{4,9}$	$M_{4,10}$	⋯	$M_{4,N-1}$	$M_{4,N}$
T_5						$M_{5,6}$	$M_{5,7}$	$M_{5,8}$	$M_{5,9}$	$M_{5,10}$	⋯	$M_{5,N-1}$	$M_{5,N}$
T_6							$M_{6,7}$	$M_{6,8}$	$M_{6,9}$	$M_{6,10}$	⋯	$M_{6,N-1}$	$M_{6,N}$
T_7								$M_{7,8}$	$M_{7,9}$	$M_{7,10}$	⋯	$M_{7,N-1}$	$M_{7,N}$
T_8									$M_{8,9}$	$M_{8,10}$	⋯	$M_{8,N-1}$	$M_{8,N}$
T_9										$M_{9,10}$	⋯	$M_{9,N-1}$	$M_{9,N}$
T_{10}											⋯	$M_{10,N-1}$	$M_{10,N}$
⋮												⋮	⋮
T_{N-1}													$M_{N-1,N}$

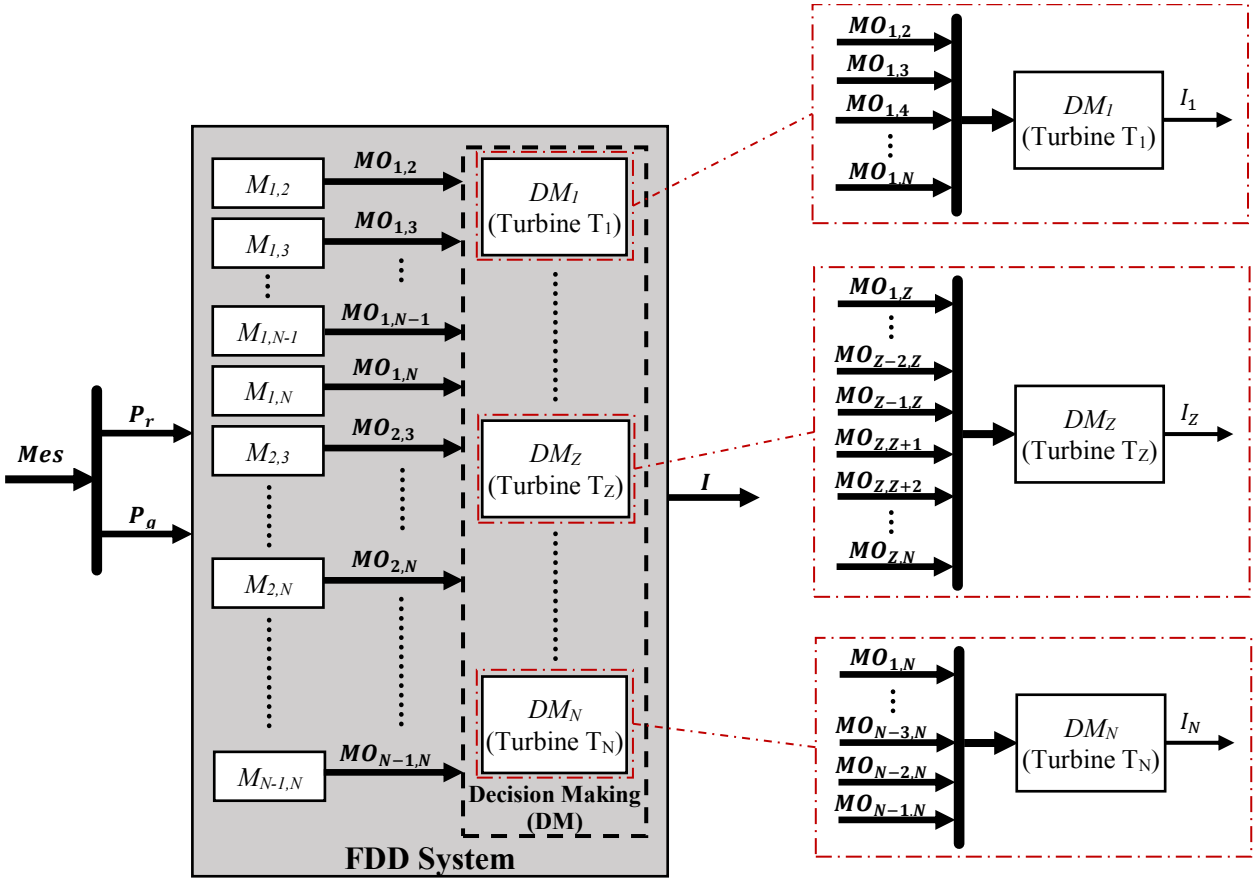

Figure 4.7 FDD system including R modules each for conducting the monitoring of the consistency of the powers generated by any two specific turbines in a wind farm. The module output (MO) signals are analysed and respective decisions are made in the decision making (DM) process. Here, turbine T_Z with ($Z \in \mathbb{N}$ and $1 < Z < N$) represents any turbine except T_1 and T_N.

Figure 4.7 shows the general structure of the FDD system that is composed of R modules (already presented in Table 4.1) and a set of decision making (DM) blocks ($DM_1, DM_2, \dots, DM_N$) that each corresponds to an individual turbine and is used for analysing the module output (MO) signals and making decision about the real-time status of the turbine. In Figure 4.7, $\boldsymbol{Mes}$ is a vector of performance data including measured variables and control commands/references in wind turbines. However, the FDD system only needs the sets of reference powers and generated powers defined in (4.12) and (4.13), respectively.

$$\boldsymbol{P_r}(k) = [P_{r,q}(k)] \quad , \qquad q = 1, 2, \dots, N \tag{4.12}$$

$$\boldsymbol{P_g}(k) = \left[P_{g,q}(k)\right] \quad , \qquad q = 1, 2, \dots, N \tag{4.13}$$

The reference powers $P_{r,q}$ in (4.12) are computed as:

$$P_{r,q}(k) = \tau_{r,q}(k) \cdot \omega_{g,q}(k) \tag{4.14}$$

in which $\tau_{r,q}$ and $\omega_{g,q}$ are the reference generator torque and generator angular speed for qth wind turbine in the farm, respectively. Each particular module in the FDD system shown in Figure 4.7 has its relevant inputs and outputs. For example, Figure 4.8 shows the relevant inputs and outputs for example module $M_{i,j}$ that monitors the consistency of the powers generated by turbine $\mathrm{T_i}$ and turbine $\mathrm{T_j}$ in a farm ($i \neq j$). In this figure, the inputs include the reference powers and generated powers corresponding to turbines $\mathrm{T_i}$ and T_j that the module is monitoring their power consistency, while, the module output $\boldsymbol{MO_{i,j}}$ includes inconsistency detection ($ID_{i,j}$) and inconsistency magnitude ($IM_{i,j}$) signals as the outputs of the module. The inconsistency detection signal and inconsistency magnitude signal indicate, respectively, the occurrence and magnitude of any possible inconsistency in the generated powers by turbines $\mathrm{T_i}$ and T_j. More precisely, regardless of details of monitoring process conducted in the module that are presented in two next subsections, the module output $\boldsymbol{MO_{i,j}}$ can attain the values described in Table 4.2 under two possibilities for the consistency of power generation by turbines.

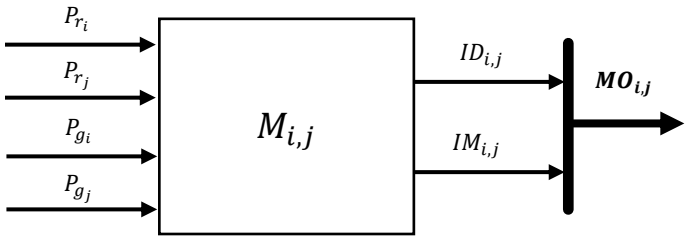

Figure 4.8 Inputs and outputs of example module $M_{i,j}$

Table 4.2 Module output $MO_{i,j}$ results for example module $M_{i,j}$

$\boldsymbol{T_i}$ **and** $\boldsymbol{T_j}$ **Power Consistency**	**Module Output** $\boldsymbol{MO_{i,j}}$	
	$ID_{i,j}$	$IM_{i,j}$
Consistent	0	0
Inconsistent	i	$\lvert\overline{\Delta P}_{i,j}\rvert$
	j	$\lvert\overline{\Delta P}_{i,j}\rvert$

As it is observed in Table 4.2, when power generation is inconsistent between T_i and T_j, the inconsistency detection and inconsistency magnitude signals indicate the faulty turbine and the absolute value of estimated power loss $\lvert\overline{\Delta P}_{i,j}\rvert$, respectively. Conversely, when power generation is consistent between T_i and T_j, both inconsistency detection and inconsistency magnitude signals are zero. This does not necessarily mean that both turbines are healthy. In fact, when power generation is consistent between two turbines T_i and T_j, they are either both healthy or both faulty. Therefore, as it is shown in Figure 4.7, the DM blocks are required to analyse the output results of modules all together in real-time, and determine faulty turbine(s), consequently. In particular, Figure 4.7 shows the distribution and contribution of MO signals in the decision making process in each particular DM block. As already mentioned, each DM block corresponds to an individual turbine and is exclusively used for analysing the MO signals related to that specific turbine, and then, making an appropriate decision about the real-time status of the turbine. Such a decision is simply made based on the logic that states that as long as at least one of the relevant modules detects a turbine as a faulty turbine, then that turbine is faulty and its power loss due to the fault (i.e., $\hat{\mathcal{P}}_q$ in (4.10)) is conservatively the maximum power loss estimated by the modules. In connection with Figure 4.7 and mentioned information about Figure 4.8 and Table 4.2, the mentioned logic of

decision making is formulated in (4.15)-(4.17) for T_1, T_Z and T_N, respectively. Note that turbine T_Z with ($Z \in \mathbb{N}$ and $1 < Z < N$) represents any turbine except T_1 and T_N.

$$\begin{gathered}\boldsymbol{If}\ \left(ID_{1,2}=1\right)\boldsymbol{OR}\left(ID_{1,3}=1\right)\boldsymbol{OR}\left(ID_{1,4}=1\right)\boldsymbol{OR}\ldots\boldsymbol{OR}\left(ID_{1,N}=1\right),\\ \boldsymbol{Then}\ T_1\ is\ faulty\ \boldsymbol{and}\ its\ power\ loss\ is\ maximum\ of\ \left\{IM_{1,2},IM_{1,3},IM_{1,4},\ldots,IM_{1,N}\right\}\end{gathered} \tag{4.15}$$

$$\begin{gathered}\boldsymbol{If}\ \left(ID_{1,Z}=Z\right)\boldsymbol{OR}\ldots\boldsymbol{OR}\left(ID_{Z-2,Z}=Z\right)\boldsymbol{OR}\left(ID_{Z-1,Z}=Z\right)\boldsymbol{OR}\left(ID_{Z,Z+1}=Z\right)\boldsymbol{OR}\left(ID_{Z,Z+2}=Z\right)\boldsymbol{OR}\ldots\boldsymbol{OR}\left(ID_{Z,N}=Z\right),\\ \boldsymbol{Then}\ T_Z\ is\ faulty\ \boldsymbol{and}\ its\ power\ loss\ is\\ maximum\ of\ \left\{IM_{1,Z},\ldots,IM_{Z-2,Z},IM_{Z-1,Z},IM_{Z,Z+1},IM_{Z,Z+2}\ldots,IM_{Z,N}\right\}\end{gathered} \tag{4.16}$$

$$\begin{gathered}\boldsymbol{If}\ \left(ID_{1,N}=N\right)\boldsymbol{OR}\ldots\boldsymbol{OR}\left(ID_{N-3,N}=N\right)\boldsymbol{OR}\left(ID_{N-2,N}=N\right)\boldsymbol{OR}\left(ID_{N-1,N}=N\right),\\ \boldsymbol{Then}\ T_N\ is\ faulty\ \boldsymbol{and}\ its\ power\ loss\ is\ maximum\ of\ \left\{IM_{1,N},\ldots,IM_{N-3,N},IM_{N-2,N},IM_{N-1,N}\right\}\end{gathered} \tag{4.17}$$

Results obtained from DM blocks in Figure 4.7 constitute FDD information vector $\boldsymbol{I}$ as follows:

$$\boldsymbol{I}(k)=[I_1(k),I_2(k),\ldots,I_N(k)] \tag{4.18}$$

The FDD system discussed here is highly dependent on the monitoring process in each module. From a design point of view, all modules used in the FDD system shown in Figure 4.7 are essentially the same but each corresponds a particular group of two turbines. As already mentioned, each module (e.g., module $M_{i,j}$) monitors the consistency of the powers generated by two different wind turbines (e.g., T_i and T_j in a farm ($i \neq j$)). To address such a monitoring process, this paper proposes two different algorithms. The first one is basically a model-free algorithm based on a rule-based threshold test technique. While, the second one is a model-based algorithm based on an FMI technique. As it is shown in the following subsections, each individual algorithm can be used in the FDD system and thereby either a model-free or a model-based FDD system can be established.

A) Model-Free Monitoring of Power Consistency

From R modules used in the FDD system shown in Figure 4.7, consider an example module $M_{i,j}$ as shown in Figure 4.8 that monitors the consistency of the powers generated by turbines T_i

and T_j in a farm ($i \neq j$). This subsection addresses the design of such a module using a model-free algorithm based on a rule-based threshold test technique. A block diagram illustrating the overall structure of the module designed using the mentioned model-free algorithm is shown in Figure 4.9.

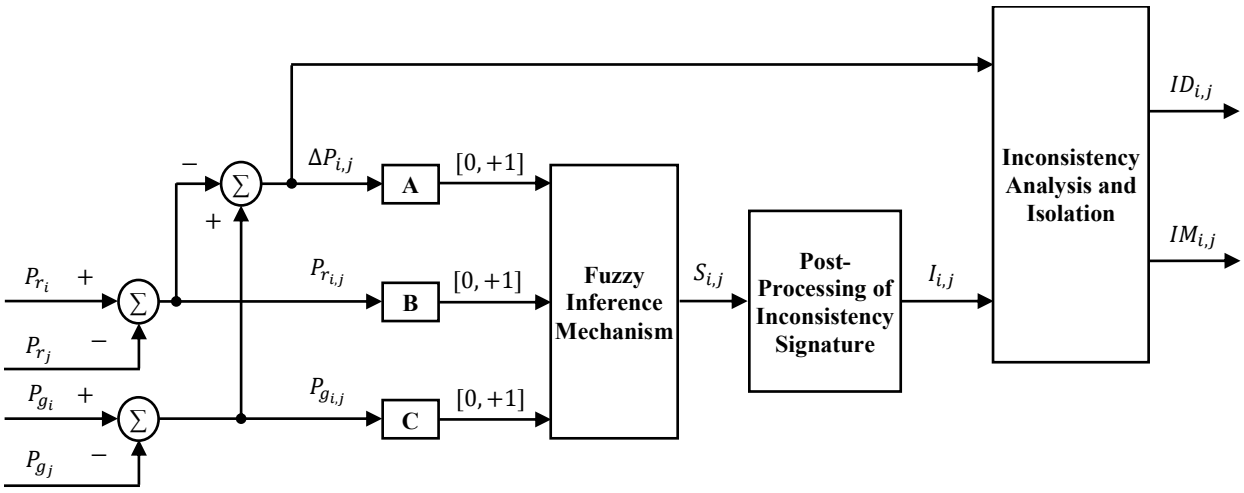

Figure 4.9 Structure of module $M_{i,j}$ designed using model-free algorithm.

As it is shown in Figure 4.9, a fuzzy inference mechanism is used for conducting the rule-based threshold testing over three different inputs including the difference of reference powers $P_{r_{i,j}}$, the difference of generated powers $P_{g_{i,j}}$, and their difference denoted by $\Delta P_{i,j}$. Appropriate scaling gains A, B, and C are applied to normalize the mentioned inputs between $[0,+1]$. The fuzzy inference mechanism provides an output indicating inconsistency signature $S_{i,j}$ that includes all traces of inconsistency in generated powers. As it is shown in Figure 4.10 and Figure 4.11, trapezoidal membership functions and singleton membership functions are used for the mentioned inputs and output, respectively.

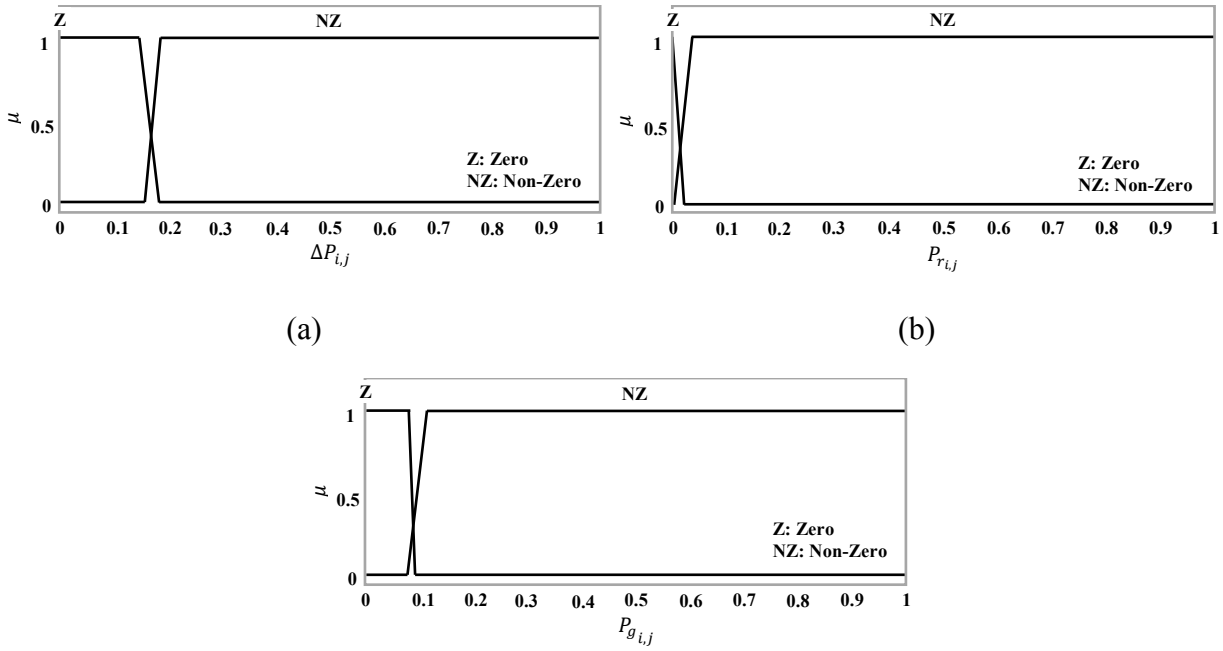

Figure 4.10 Input membership functions used in fuzzy inference mechanism: (a) $\Delta P_{i,j}$, (b) $P_{r_{i,j}}$, and (c) $P_{g_{i,j}}$.

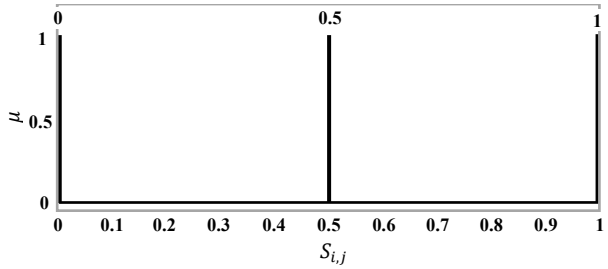

Figure 4.11 Output membership functions used in fuzzy inference mechanism.

Table 4.3 Fuzzy Rules used in fuzzy inference mechanism

Rule No.	***If***	$\Delta P_{i,j}$ *is*	***and***	$P_{r_{i,j}}$ *is*	***and***	$P_{g_{i,j}}$ *is*	***then***	$S_{i,j}$ *is*
1		Z		Z		Z		0
2		Z		NZ		Z		0.5
3		Z		NZ		NZ		0.5
4		Z		Z		NZ		1
5		NZ		Z		Z		1
6		NZ		Z		NZ		1
7		NZ		NZ		Z		1
8		NZ		NZ		NZ		1

With respect to the shown membership functions in Figure 4.10 and Figure 4.11, the complete set of rules used in the fuzzy inference mechanism is presented in Table 4.3. The rules are formulated based on expert's knowledge obtained through observing and understanding the relation between the consistency of generated powers and variations in the inputs. Each rule corresponds to a particular condition. In total, three different possibilities are considered: (1) consistent power generation represented by $S_{i,j} = 0$, (2) inconsistent power generation represented by $S_{i,j} = 1$, and (3) either consistent or inconsistent power generation represented by $S_{i,j} = 0.5$. More precisely, when $S_{i,j}$ attains values of 0 or 1 (i.e., rule 1 or rules 4-8 in Table 4.3), the power generation is directly determined as consistent or inconsistent, respectively. Conversely, when $S_{i,j}$ attains value of 0.5 (i.e., rules 2 and 3 in Table 4.3), the power generation cannot be directly determined as consistent or inconsistent. In fact, rules 2 and 3 in Table 4.3 are related to the so-called response time of the whole wind farm system. That is the time the wind farm system takes to react to its given inputs. In other words, the wind farm system takes a short period of time (i.e., the response time) for $P_{g_{i,j}}$ and $\Delta P_{i,j}$ to react to any change in $P_{r_{i,j}}$ by the reference power signal(s) commanded from the wind farm control system. During such a short response time it is not possible to directly determine the consistency of generated powers in a model-free way. Therefore, as it is shown in Figure 4.9, the output of fuzzy inference mechanism (i.e., inconsistency signature $S_{i,j}$) needs to be post-processed in order to obtain absolute inconsistency information $I_{i,j}$ that can be either 0 (consistent power generation) or 1 (inconsistent power generation). The post-processing conducted on $S_{i,j}$ at the time-step k is coded based on the flowchart shown in Figure 4.12.

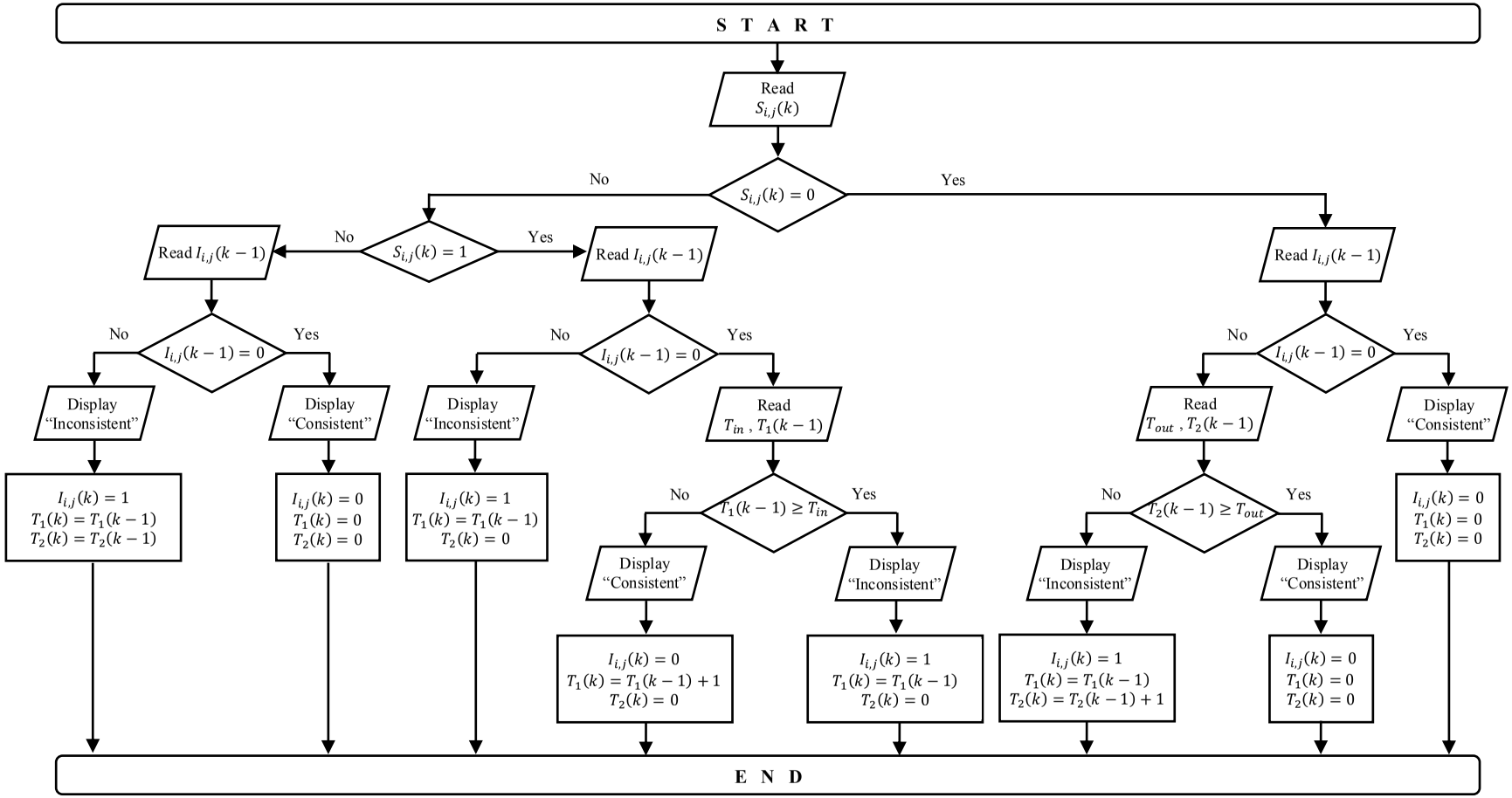

Figure 4.12 Flowchart of post-processing on inconsistency signature $S_{i,j}$ at the time-step k.

As it is shown in the flowchart in Figure 4.12, to achieve a more reliable conclusion on $I_{i,j}$, in response to any possible occurrence of inconsistency in power generation, $I_{i,j}$ changes from 0 to 1, when $S_{i,j}$ stays at its relevant values presented in the flowchart for T_{in} consecutive sample-times (i.e., the number of repetitions satisfies $T_1 \geq T_{in}$). Similarly, $I_{i,j}$ changes from 1 to 0, when $S_{i,j}$ stays at its relevant values presented in the flowchart for T_{out} consecutive sample-times (i.e., the number of repetitions satisfies $T_2 \geq T_{out}$). The appropriate values for T_{in} and T_{out} are determined by the user through considering that the greater the values of T_{in} and T_{out}, the higher the required time for changing $I_{i,j}$ from 0 to 1, and 1 to 0 (i.e., higher conservatism). As it is shown in the flowchart in Figure 4.12, when $S_{i,j}$ attains value of 0.5 (i.e., during short periods of response time of the wind farm system described by rules 2 and 3 in Table 4.3), $I_{i,j}$ stays at its previous value obtained in the previous time-step (i.e., $I_{i,j}(k) = I_{i,j}\ (k-1)$). With respect to the flowchart shown in Figure 4.12, an example inconsistency signature and its absolute inconsistency information are shown in Figure 4.13. The figure corresponds to module $M_{1,4}$ for turbines T_1 and T_4 while considering the fault scenario shown in Figure 4.4. As it is shown in Figure 4.13, $S_{i,j}$ only attains value of 0.5 for very short periods of time when the inputs of fuzzy inference mechanism activate rules 2 and 3 in Table 4.3.

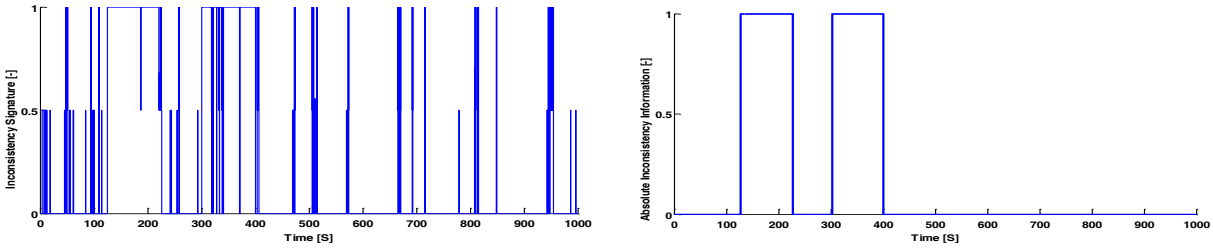

(a) (b)

Figure 4.13 Post-processing of inconsistency signature in an example module. (a) inconsistency signature (b) absolute inconsistency information.

The absolute inconsistency information $I_{i,j}$ obtained from the post-processing of inconsistency signature $S_{i,j}$ only determines the presence of consistency or inconsistency in the generated powers by turbines T_i and T_j. However, in the case of inconsistency in the generated powers, $I_{i,j}$ does not provide any information about isolation of faulty turbine and magnitude of fault (power loss). Therefore, it is required to further analyse $I_{i,j}$ through inconsistency analysis and isolation block as shown in Figure 4.9. The functionality of this block is very simple in comparison with the already

mentioned post-processing block. In fact, by the occurrence of any inconsistency in the generated powers (i.e., $I_{i,j} = 1$), the inconsistency analysis and isolation block computes in real-time the running mean of $\Delta P_{i,j}$ (see Figure 4.9). Then, the block determines (isolates) the faulty turbine based on the sign of the computed mean. That is, if the mean attains positive values, T_j is faulty while if it attains negative values it means that T_i is faulty. Moreover, the absolute magnitude of this running mean $\left|\overline{\Delta P}_{i,j}\right|$ is used as the estimated power loss in the faulty turbine (see Table 4.2).

It should be noted that the module $M_{i,j}$ designed here only determines whether powers generated from turbines T_i and T_j are consistent or inconsistent. When power generation is inconsistent, the module provides relevant information about detection and diagnosis of the faulty turbine. However, as already mentioned at the beginning of Section 4.5, when power generation is consistent between turbines T_i and T_j, they are either both healthy or both faulty. More precisely, if the fault happens simultaneously in both turbines T_i and T_j, the module $M_{i,j}$ still shows consistent power generation. For example, this is shown in Figure 4.13 for module $M_{1,4}$ while both turbines T_1 and T_4 are faulty during [225,300] seconds. Therefore, as it was already shown in Figure 4.7, and formulated in (4.15)-(4.17), the DM blocks are required to analyse the output results of modules all together in real-time, and to detect and diagnose faulty turbine(s), consequently.

B) Model-Based Monitoring of Power Consistency

From R modules used in the FDD system shown in Figure 4.7, consider an example module $M_{i,j}$ that monitors the consistency of the powers generated by turbines T_i and T_j in a farm ($i \neq j$). This subsection addresses the design of such a module using a model-based algorithm based on an FMI technique. A block diagram illustrating the overall structure of the module designed using the mentioned model-based algorithm is shown in Figure 4.14. As it is shown in Figure 4.14, the module employs a nominal dynamic model of the system that is developed using a data-driven modelling approach based on FMI technique. The model estimates the nominal relative performance between turbines T_i and T_j in a farm. In fact, powers generated from turbines T_i and T_j are consistent as long as $\hat{P}_{g_{i,j}}$ and $P_{g_{i,j}}$ are (ideally) equal. However, they cannot be equal in practice due to the presence of noise and uncertainties inherent in real data. Therefore, a post-processing

including a threshold testing is necessary to obtain absolute inconsistency information $I_{i,j}$ that can be either 0 (consistent power generation) or 1 (inconsistent power generation).

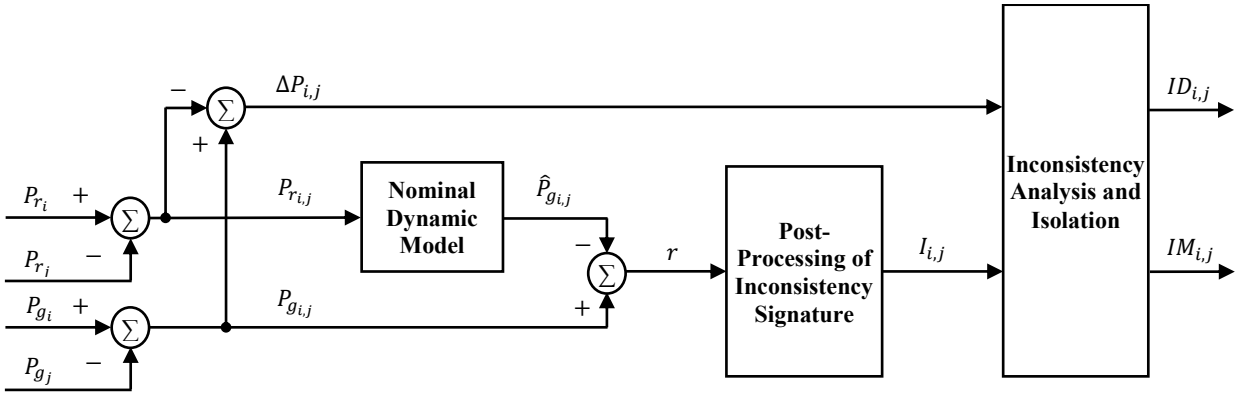

Figure 4.14 Structure of module $M_{i,j}$ designed using model-based algorithm.

The post-processing at the time-step k is coded based on the flowchart shown in Figure 4.15. Similar to what mentioned in the previous subsection, to achieve a more reliable conclusion on $I_{i,j}$, in response to any possible occurrence of inconsistency in power generation, $I_{i,j}$ changes from 0 to 1, when residuals r stays outside of its threshold for T_{in} consecutive sample-times (i.e., the number of repetitions satisfies $T_1 \geq T_{in}$). Similarly, $I_{i,j}$ changes from 1 to 0, when residuals r stays within its threshold for T_{out} consecutive sample-times (i.e., the number of repetitions satisfies $T_2 \geq T_{out}$). The appropriate values for the thresholds T_{in} and T_{out} are determined by the user. To isolate the faulty turbine and obtain its magnitude of the fault (power loss), $I_{i,j}$ obtained from the post-processing is further analysed by the shown inconsistency analysis and isolation block in Figure 4.14. The functionality of this block is completely similar to what already mentioned in the previous subsection for the module designed using the model-free algorithm. It is also worth reminding that module $M_{i,j}$ proposed here provides relevant information about detection and diagnosis of the faulty turbine only when power generation is inconsistent. However, as already mentioned, when power generation is consistent between turbines T_i and T_j, they are either both healthy or both faulty. Therefore, as it was already shown in Figure 4.7, and formulated in (4.15-4.17), the DM blocks are required to analyse the output results of modules all together in real-time, and to detect and diagnose faulty turbine(s), consequently.

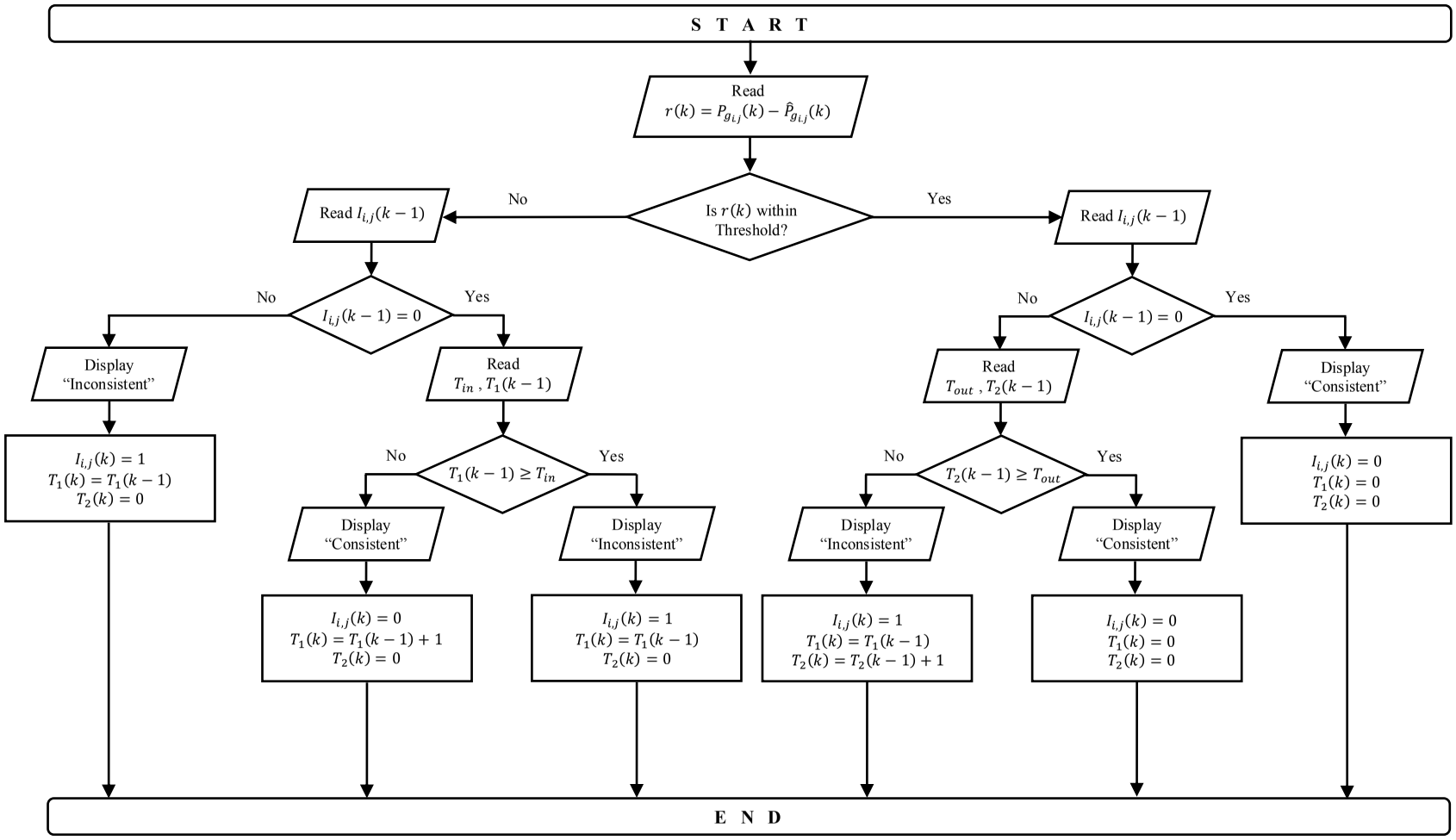

Figure 4.15 Flowchart of post-processing on residuals r at the time-step k.

Obviously, the performance and effectiveness of the model-based module $M_{i,j}$ proposed here highly depends on the nominal dynamic model of the system (see Figure 4.14) that, as already mentioned, is developed using the data-driven modelling approach based on FMI technique. The FMI technique generates multiple models as a collection of fuzzy if-then rules. In detail, the nominal dynamic model can be represented by a Takagi-Sugeno (T-S) type dynamic fuzzy model identified from input/output system's measurements obtained from the simulation of the system under normal (fault-free) operation. Such a method of modelling is particularly suitable for wind turbines that are relatively complex structures comprising flexible mechanical systems immersed in a fully-stochastic wind field. In practice, it is often demanding, or even impossible to derive a single nonlinear model for wind energy systems over their entire operational envelope. In the following lines, the used FMI technique is described briefly.

Without loss of generality, a single-input single-output (SISO) nonlinear system can be expressed by:

$$y(k) = f(\boldsymbol{\Phi}(k-1)) + e \tag{4.19}$$

where $\boldsymbol{\Phi}(k-1)$ as defined in (4.20) is an information data vector including the past model inputs u and outputs y, k is the discrete-time-step, $\{m, n\} \in \mathbb{Z}$ denote the model order that are defined by the user, and e denotes the modelling error.

$$\boldsymbol{\Phi}(k-1) = \begin{bmatrix} y(k-1) \\ \vdots \\ y(k-m) \\ u(k-1) \\ \vdots \\ u(k-n) \end{bmatrix} \tag{4.20}$$

A T-S type fuzzy model can approximate the unknown function $f(.)$ in (4.19) using L rules (local models) as follows [97]:

$$\textbf{Rule}_{\boldsymbol{i}}: \quad \textbf{If } \boldsymbol{\Phi}(k-1) \text{ is } \boldsymbol{A}_i \textbf{ then } \hat{y}_i(k) = F_i\big(\boldsymbol{\Phi}(k-1)\big) \ , \qquad i = 1,2,\dots,L \tag{4.21}$$

where $\boldsymbol{A_i}$ are the antecedent fuzzy sets of the ith rule. A simple but efficient linear form for $F_i(.)$ is defined by [97]:

$$F_i(.): \quad \hat{y}_i(k) = \boldsymbol{a_i}\boldsymbol{\Phi}(\mathrm{k}-1) + b_i \tag{4.22}$$

where $\boldsymbol{a_i}$ and b_i denote the parameter vector and scalar offset of the ith rule, respectively.

The following fuzzy fusion over all rule outputs provides the dynamics of a nonlinear system [97]:

$$\hat{y} = \left(\sum_{i=1}^{L} \mu_i(\boldsymbol{\Phi})\hat{y}_i\right) / \left(\sum_{i=1}^{L} \mu_i(\boldsymbol{\Phi})\right) \tag{4.23}$$

where $\hat{y}$ is the aggregated output of the fuzzy model, and μ_i denotes the degree of fulfilment of *i*th rule in (4.21).

To develop the mentioned T-S model for a real system, it is necessary to perform the nonlinear system identification that is the process of identifying the structure of fuzzy model, and then estimating the parameters in the model. The detailed structure of the fuzzy model developed for application in the module in Figure 4.14 is presented in Table 4.4. It is worth mentioning that, in order to identify the T-S model, the well-established Gustafson–Kessel clustering algorithm [98] is used here.

Table 4.4 Configuration properties of T-S fuzzy model (SISO model). Note that $u(k) = P_{r_{i,j}}(k)$, and $\hat{y}(k) = \hat{P}_{g_{i,j}}(k)$, respectively.

	Item	No.	Details
Antecedent Part	Candidate inputs	2	$u(k-1)\,, n=1$ $\hat{y}(k-1)\,,\ m=1$
	Membership functions per input	2	Figure 4.18
Knowledge Base	Tuning rules	2	$i = 1,2,\ldots,L$ $L = 2$
Consequent Part	Linear equation form in *i*th rule	-	$\hat{y}_i(k) = a_{i,1}\hat{y}(k-1) + a_{i,2}u(k-1) + b_i$
	Defuzzification method	-	$\hat{y} = \frac{\sum_{i=1}^{L} \mu_i(\boldsymbol{\Phi})\hat{y}_i}{\sum_{i=1}^{L} \mu_i(\boldsymbol{\Phi})}$

4.6 Simulation Results and Discussion

This section presents and discusses different simulation results for investigation of the performance of proposed schemes under both fault-free and faulty conditions. The simulations in this work have been carried out in MATLAB/Simulink environment using the nonlinear offshore wind farm benchmark model presented in Section 4.2. In more details, an offshore wind farm including ten 5MW-turbines ($N = 10$) is created with the layout as shown in Figure 4.1. A realistic wind field with mean speed of 15 m/s and a turbulence intensity of 10% is simulated over 1000 seconds of run time. The obtained wind speed profiles for each of the ten turbines in the farm are shown in Figure 4.16. Moreover, a typical electrical grid load is applied to the wind farm over the simulation time. Figure 4.17 shows the applied time-varying grid load as well as the relevant total generated active power response obtained from the wind farm under fault-free condition.

In the following subsections, various simulations and numerical results for the proposed schemes are presented and discussed. The fault-free simulation with the baseline wind farm controller in (4.5) is used as a frame of reference to evaluate the overall performance, effectiveness and fault-tolerance properties of the proposed FDD and FTC schemes against the considered decreased power generation faults that are already described in Figure 4.4. In this regard, with respect to the considerations given in Section 4.3, the generator power response is chosen as a well-suited performance index to illustrate the performance of each turbine in the wind farm.

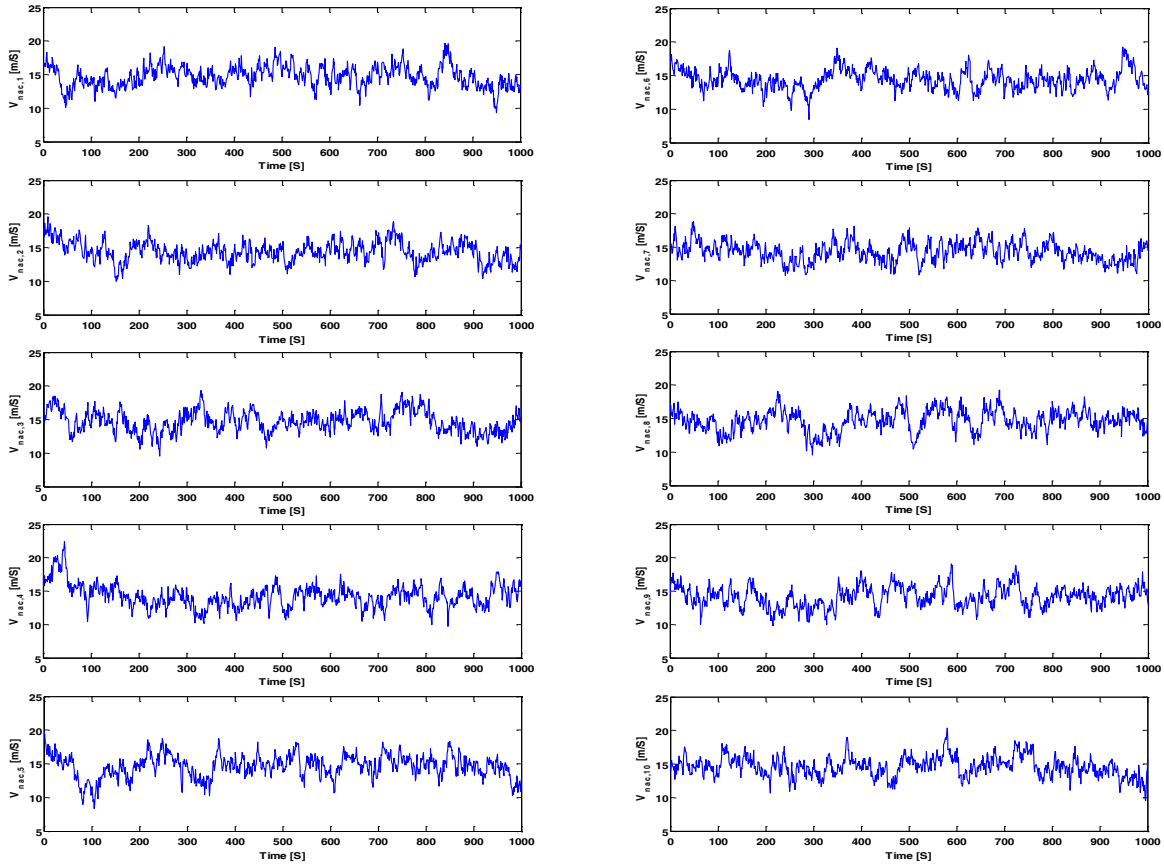

Figure 4.16 Nacelle wind speed profiles for turbines installed in the wind farm shown in Figure 4.1. (Note: $V_{nac,\,i}$ denotes nacelle wind speed for turbine T_i)

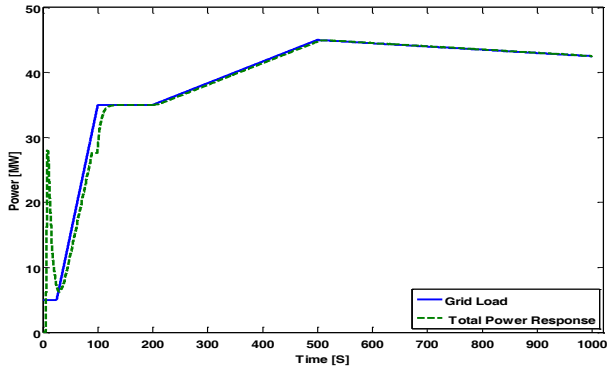

Figure 4.17 A typical grid load and total generated active power response by the wind farm under fault free condition.

A) Identification and Validation of the Fuzzy Dynamic Model

As already mentioned, the nominal dynamic model used in the modules of the model-based FDD system is designed and developed using the FMI technique described in Section 4.5B. In more details, to train and evaluate a model, a set of 80,000 measured data for each of inputs and output were used. The data were obtained with a sampling rate of 80 Hz from the fault-free simulation of the wind farm with its baseline control system. It is worth mentioning that each set of the data was split into equal halves; one half for training and the other one for validation. The structure for the fuzzy model is already determined in Table 4.4. In connection to the mentioned table and the performed nonlinear system identification process, the projected membership functions (two membership functions per input) are shown in Figure 4.18. The consequent parameters of the model as well as the cluster centers are also presented in Table 4.5 and Table 4.6, respectively. In addition, for example, Figure 4.19 shows the output of a fuzzy model during a fault-free operation of the wind farm including the contribution of each local model (rule) in the developed model over a 50 seconds of simulation time. In this figure, the noise-free measurement of process output is used to be compared with the model output.

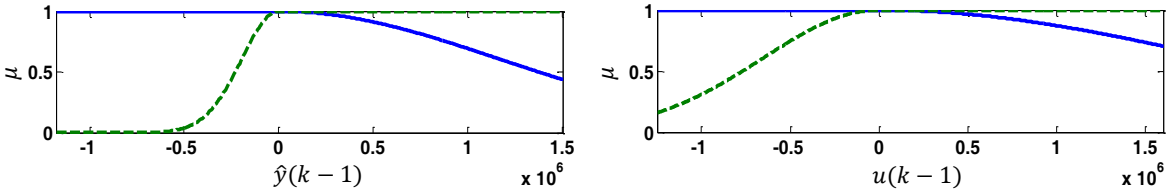

(a) (b)

Figure 4.18 Projected membership functions for: (a) $\hat{y}(k-1)$, and (b) $u(k-1)$

Table 4.5 Estimated consequent parameters for the identified T-S fuzzy model with the structure given in Table 4.4

Rule No. (i)	$a_{i,1}$	$a_{i,2}$	b_i
1	$+8.9 \cdot 10^{-1}$	$+1.0 \cdot 10^{-1}$	$+3.9 \cdot 10^{2}$
2	$+9.0 \cdot 10^{-1}$	$+9.1 \cdot 10^{-2}$	$-4.2 \cdot 10^{2}$

Table 4.6 Cluster centers

Rule No. (i)	$\hat{y}(k-1)$	$u(k-1)$
1	$-9.8 \cdot 10^{+3}$	$-7.6 \cdot 10^{+3}$
2	$-5.2 \cdot 10^{+3}$	$-8.0 \cdot 10^{+3}$

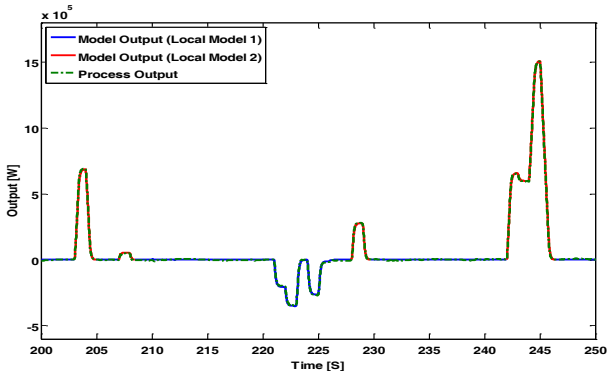

Figure 4.19 The process output and the fuzzy model output (showing the contribution of each local model) – time period [200,250] sec

To assess the quality of the developed fuzzy model in terms of modeling accuracy and fitting performance, the *normalized root-mean-squared error (NRMSE)* and the *variance accounted for (VAF)* index are used, respectively. The NRMSE is defined as:

$$NRMSE = \frac{\sqrt{\frac{1}{N}\sum_{k=1}^{N}(y_k - \hat{y}_k)^2}}{y_{max} - y_{min}} \tag{4.24}$$

where y_k and $\hat{y}_k$ are the *k*th true output of the system (process), and the *k*th estimated output of the model, respectively. The denominator in (4.24) represents the range of the true output defined as the maximum value y_{max} minus the minimum value y_{min}. The percentile VAF is computed by:

$$VAF = \left[1 - \frac{cov(y_k - \hat{y}_k)}{cov(y_k)}\right] 100\% \tag{4.25}$$

where *cov* denotes the covariance of the respective vector. Table 4.7 presents the obtained results. From the table, it is obvious that the fuzzy model is considerably accurate for approximating the process under diagnosis.

Table 4.7 Modeling accuracy and fitting performance of the fuzzy model

VAF (%)	NRMSE
99.2	0.004

B) Performance of FDD System

As it was already presented in Section 4.5, the FDD system can be developed based on either model-free or model-based monitoring of power consistency in the wind farm. Both model-free

FDD system and model-based FDD system are investigated under both fault-free and faulty conditions. As it is shown by the FDD results in Figure 4.20 and Figure 4.21, the proposed model-free and model-based FDD systems both are able to detect and diagnose all the considered faults based on the scenario defined in Figure 4.4. The FDD results are shown in terms of both fault detection indicators/signals and estimated fault magnitudes that can be used for ASC and accommodation of the faults in faulty turbines. Faulty turbines include T_1, T_2, T_3, T_4, T_7, T_8, and T_{10} (see Figure 4.1) that are affected by the considered fault in Section 4.3.

The time of fault detection (i.e., the time required for detecting a fault after its occurrence) for each FDD system is presented in Table 4.8. The time of fault detection reflected in this table is directly related to the T_{in} consecutive sample-times considered in the design process of each FDD system. As can be seen from Table 4.8, the model-based FDD system requires lower time for detection of faults. The lower the detection time, the better the fault detection has scored. With respect to the identification of faults, both FDD systems provide almost similar estimates for fault magnitudes in each particular faulty turbine that they are accurate enough to be used for fault accommodation process. This fact is quantitatively shown in the next subsection while the obtained estimates are used directly in (4.10) for signal correction and fault accommodation in the framework of integrated FDD and FTC schemes.

Table 4.8 Time of fault detection (or detection time) for each FDD system (in seconds)

FDD system type	Detection time (sec)
Model-free	2.2125
Model-based	1.5000

C) Performance of AFTC Schemes Based on Integrated FDD and FTC Approach

As already mentioned, the estimated fault magnitudes act upon the reference torque control signal (see (4.10)) to accommodate the fault effects in each faulty turbine in the farm. Based on the integrated FDD and FTC approach presented in Section 4.4, two AFTC schemes are designed and developed using the model-free and model-based FDD systems in Section 4.5.

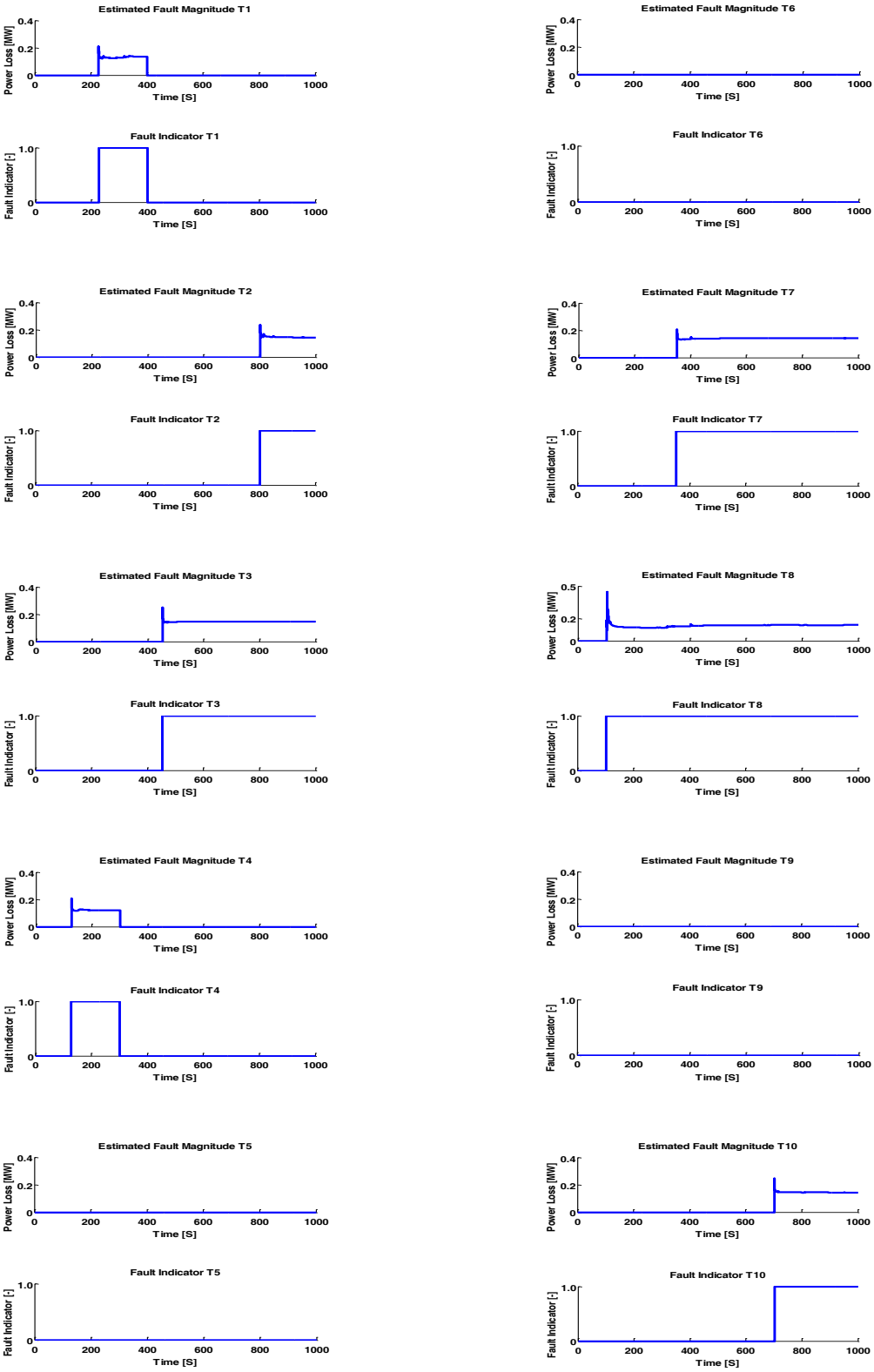

Figure 4.20 FDD results for the model-free FDD system.

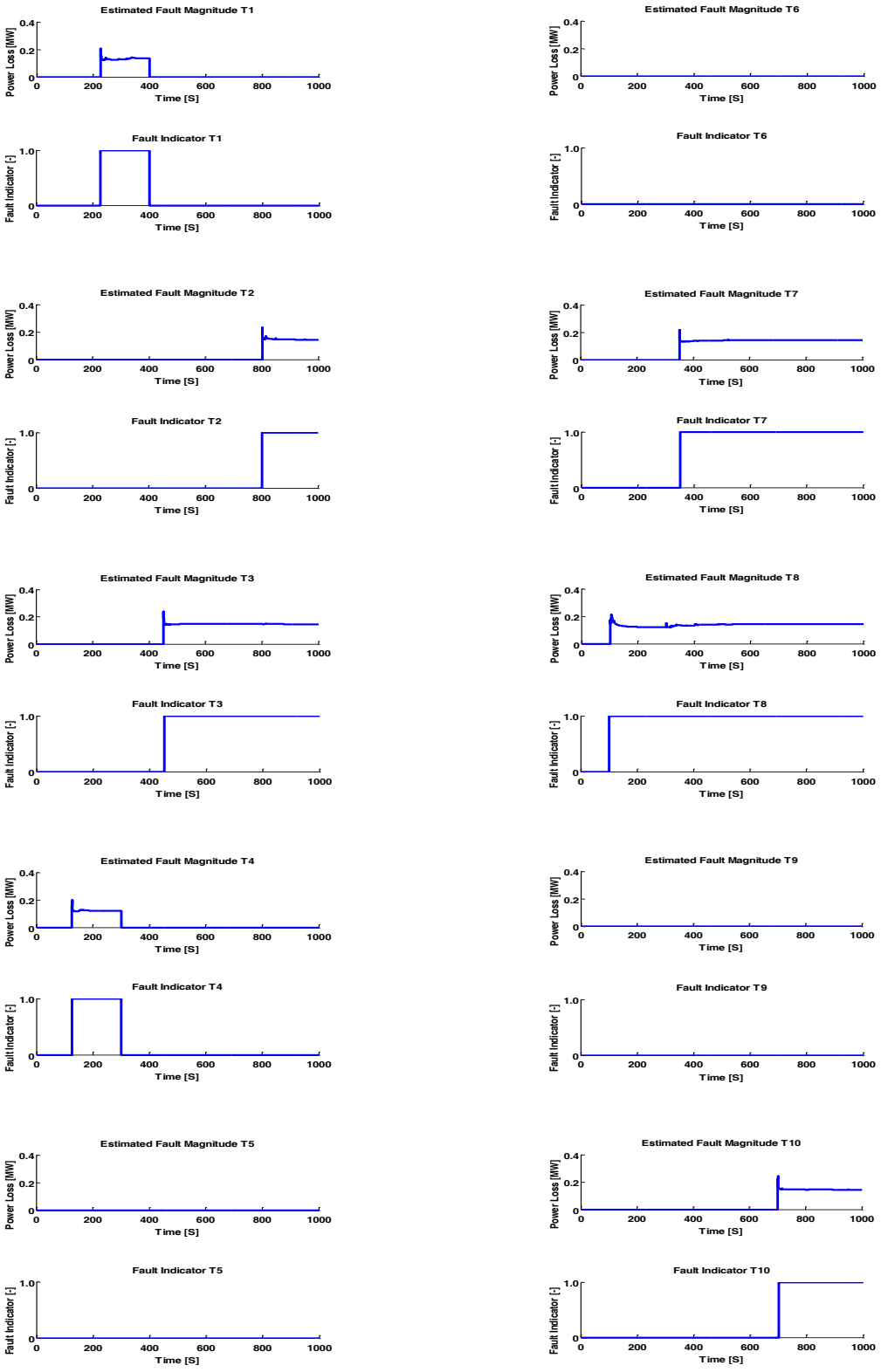

Figure 4.21 FDD results for the model-based FDD system.

In the following figures and tables, the AFTC scheme using the model-free FDD system is denoted by "integrated model-free FDD and FTC" scheme, and the AFTC scheme using the model-based FDD system is denoted by "integrated model-based FDD and FTC" scheme. Based on the FDD results presented in the preceding subsection, the fault accommodation is performed in the faulty turbines that include T_1, T_2, T_3, T_4, T_7, T_8, and T_{10}. Figure 4.22 and Figure 4.23 show the generator power responses in the mentioned turbines under both fault-free and faulty conditions. Figure 4.22 corresponds to the performance of integrated model-free FDD and FTC scheme, while Figure 4.23 corresponds to the performance of integrated model-based FDD and FTC scheme. Both figures illustrate that the accommodation of faults is successfully performed in the faulty turbines and during all periods of fault activity. As foreseen, since the control reconfiguration (signal correction) is only activated during the periods of fault activity, the nominal performance of wind turbines in the farm will be unaffected under fault-free conditions.

To further investigate the performance of the proposed schemes in a comparative perspective, Table 4.9 presents a precise quantitative comparison between both schemes in terms of NRMSE during the periods of fault activity in the faulty wind turbines. Note that, the lower the NRMSE, the better the fault-tolerance has scored. Based on the results presented in Table 4.9, the integrated model-based FDD and FTC scheme provides more efficient accommodation of faults compared with the integrated model-free FDD and FTC scheme. Basically, this is due to the fact that the performance of each scheme is highly dependent on the speed and accuracy of its FDD system. As already discussed in the previous subsection, the model-based FDD system demonstrates better performance compared with the model-free FDD system that does not employ any dynamic model of the system. However, this superior performance of the model-based FDD system may be subjected to modeling uncertainties while the model-free system does not deal with any difficulties related to system modeling.

In addition to the presented results, Figure 4.24 together with the numerical results presented in Table 4.10 show the fault-tolerance capability of the proposed integrated FDD and FTC schemes against a fault with 30% power loss in turbine T_{10}, for example. This demonstrates that both the schemes can also satisfactorily accommodate large magnitudes of the considered type of fault in turbines as long as their FDD information is timely and accurate.

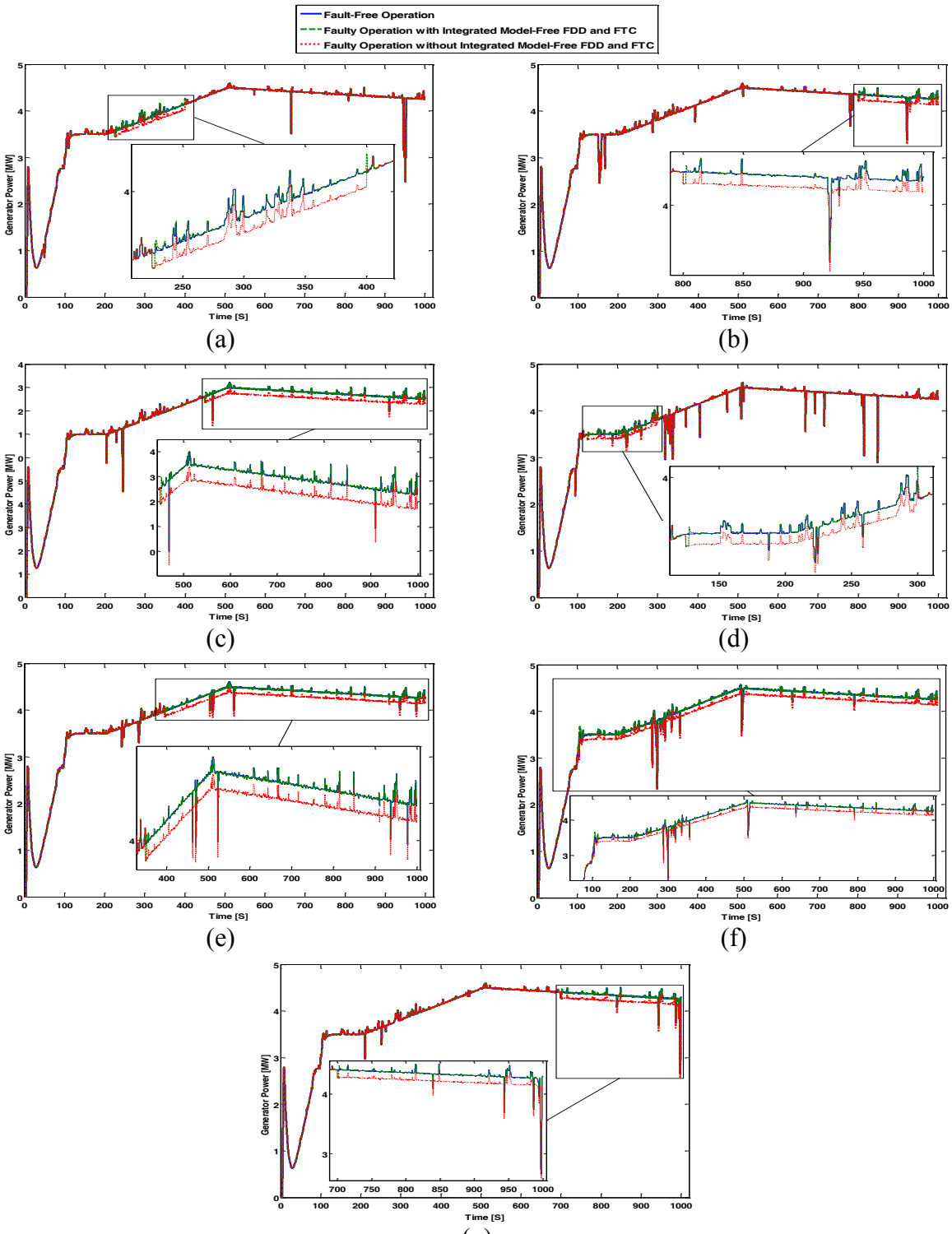

Figure 4.22 Generator power response under fault-free and faulty conditions (3% power loss) – integrated model-free FDD and FTC. (a) T_1, (b) T_2, (c) T_3, (d) T_4, (e) T_7, (f) T_8, and (g) T_{10}.

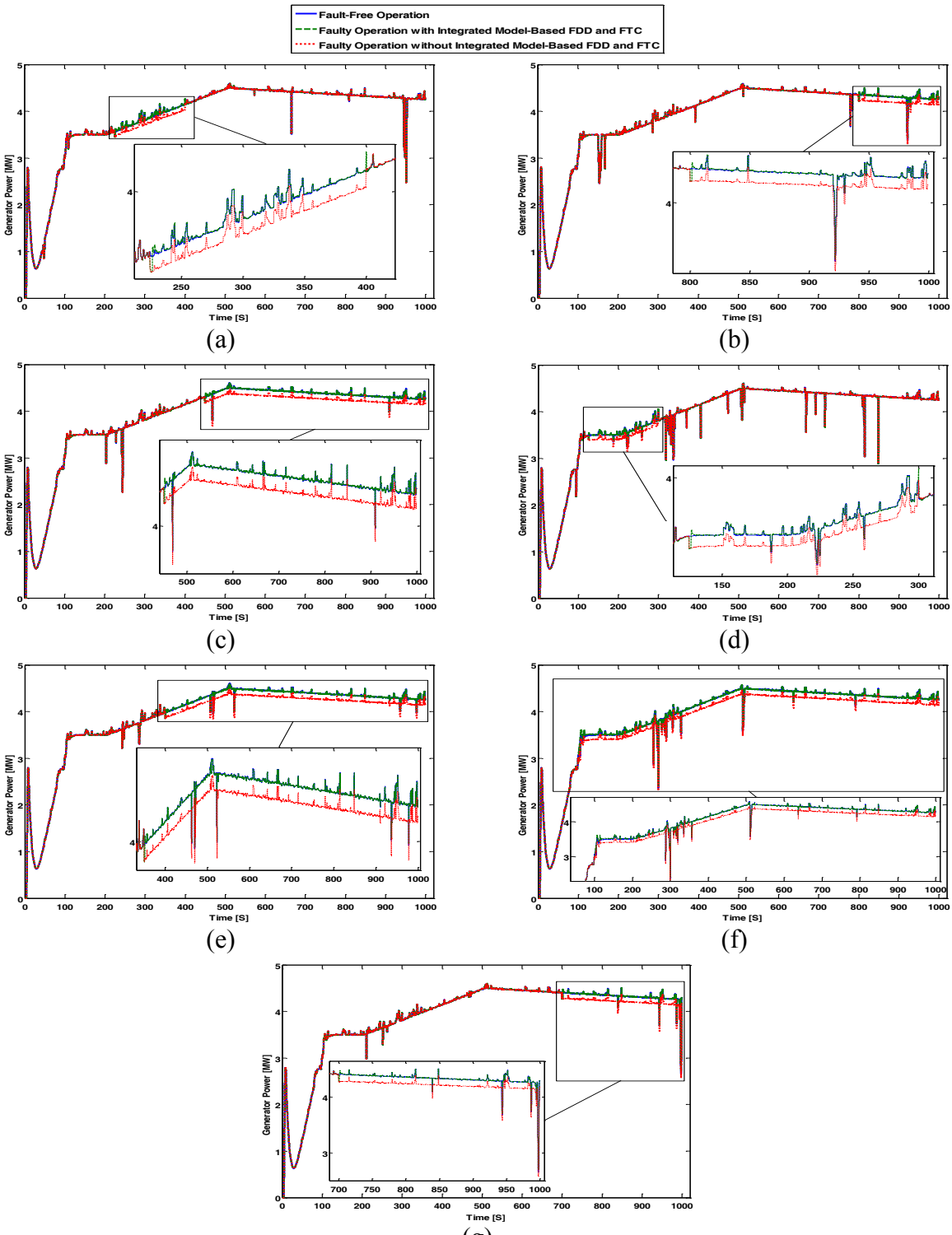

Figure 4.23 Generator power response under fault-free and faulty conditions (3% power loss) – integrated model-based FDD and FTC. (a) T_1, (b) T_2, (c) T_3, (d) T_4, (e) T_7, (f) T_8, and (g) T_{10}.

Table 4.9 Quantitative comparison of generator power responses for integrated FDD and FTC schemes during the specified fault periods with 3% power loss

Faulty Turbine	Fault Period [S]	NRMSE [-]	
		Model-Based	Model-Free
T_1	[225,400]	0.0031	0.0037
T_2	[800,1000]	0.0030	0.0035
T_3	[450,1000]	0.0018	0.0021
T_4	[125,300]	0.0032	0.0038
T_7	[350,1000]	0.0015	0.0017
T_8	[100,1000]	0.0023	0.0033
T_{10}	[700,1000]	0.0025	0.0030

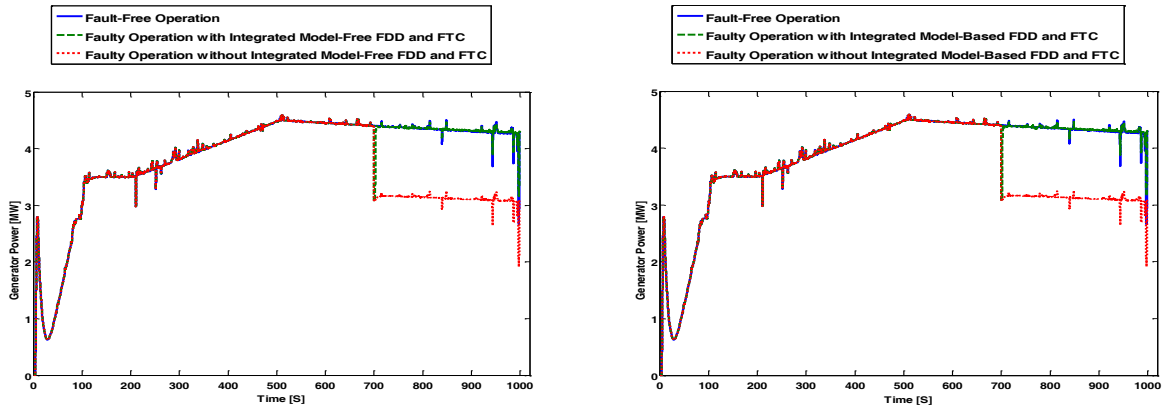

(a) (b)

Figure 4.24 Generator power response under fault-free and faulty conditions (30% power loss) in T_{10} . (a) integrated model-free FDD and FTC, (b) integrated model-based FDD and FTC.

Table 4.10 Quantitative comparison of generator power responses for integrated FDD and FTC schemes during the specified fault period with 30% power loss

Faulty Turbine	**Fault Period [S]**	**NRMSE [-]**	
		Model-Based	**Model-Free**
T_{10}	[700,1000]	0.0266	0.0304

D) Evaluation of Wind Farm Structural Dynamics and Loading Results

In continuation of evaluating the performance and effectiveness of the proposed schemes, it is also necessary to evaluate the functionality of the proposed schemes in terms of wind farm structural dynamics and loading. With respect to the implementation of control schemes, the recommended rate and magnitude limiters are employed in the benchmark model under consideration. Such an implementation aims to avoid intense control command and thereby extreme structural loading on the wind turbines' actuators. Different structural safety measures

such as blade root bending moments, nacelle acceleration, drivetrain torsion, and tower bending moments have been considered and evaluated in this study and found to be well within their safe ranges. However, some of the evaluated structural dynamics and loading results are presented in this subsection. In particular, the drivetrain torsion rates and tower bending moments under both fault-free and faulty conditions are presented here. Figure 4.25 shows the results of drivetrain torsion rate in turbine T_1 for both the proposed model-free and model-based schemes. This figure also includes the zoomed-in views of the torsion rate response around the time instants in which the fault accommodation begins and finishes. Based on the scenario defined in Figure 4.4, the fault period for T_1 is [225,400] sec. However, as already discussed, the accommodation of fault is delayed by the fault detection time related to the FDD process. As it is seen in the zoomed-in views, in reference to the torsion rate response under fault-free condition, the process of fault accommodation has been conducted safely although the beginning and end of the fault accommodation show minor deviations because of activating and deactivating of the ASC process, respectively. Similar results for drivetrain torsion rates from other turbines in the farm have also been obtained that are not shown here for the sake of brevity.

Figure 4.26 and Figure 4.27 show the tower bending moment results for the integrated model-free FDD and FTC scheme and integrated model-based FDD and FTC scheme, respectively. In connection with these figures, a quantitative comparison in terms of mean and standard deviation (STD) for each of the considered results is also presented in Table 4.11.

The results shown in Figures 4.25, 4.26 and 4.27 together with the numerical results presented in Table 4.11 all demonstrate that both the integrated FDD and FTC schemes have minimal impact on the wind turbine structural dynamics and loading during fault accommodation.

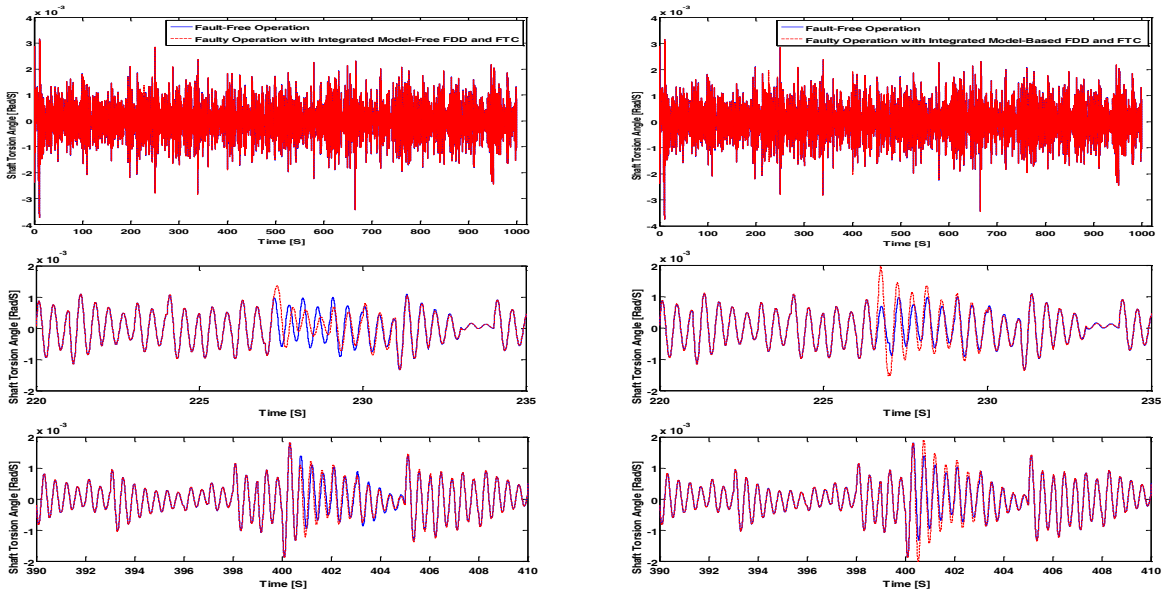

(a) (b)

Figure 4.25 Drivetrain torsion rate results for wind turbine T_1 in the farm during the: (a) integrated model-free FDD and FTC, (b) integrated model-based FDD and FTC

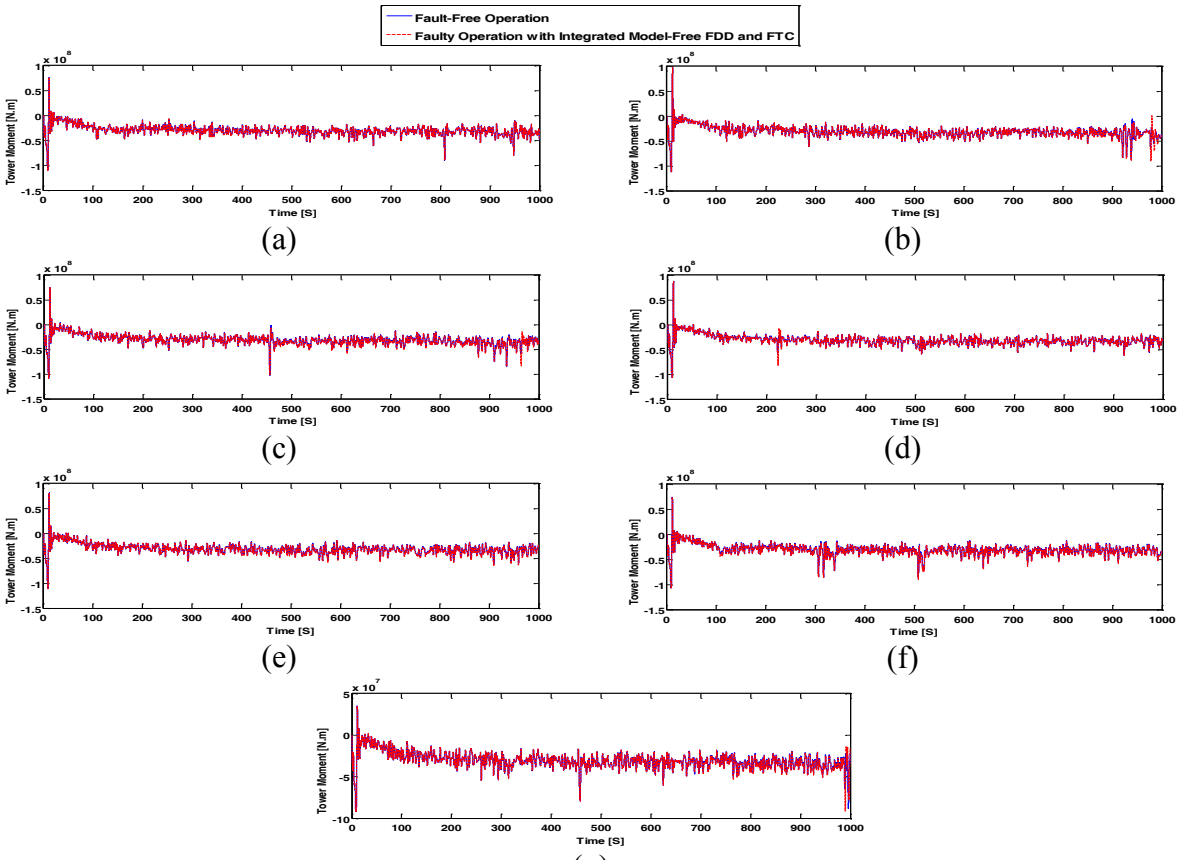

(a) (b) (c) (d) (e) (f) (g)

Figure 4.26 Tower bending moment results − integrated model-free FDD and FTC. (a) T_1, (b) T_2, (c) T_3, (d) T_4, (e) T_7, (f) T_8, and (g) T_{10}.

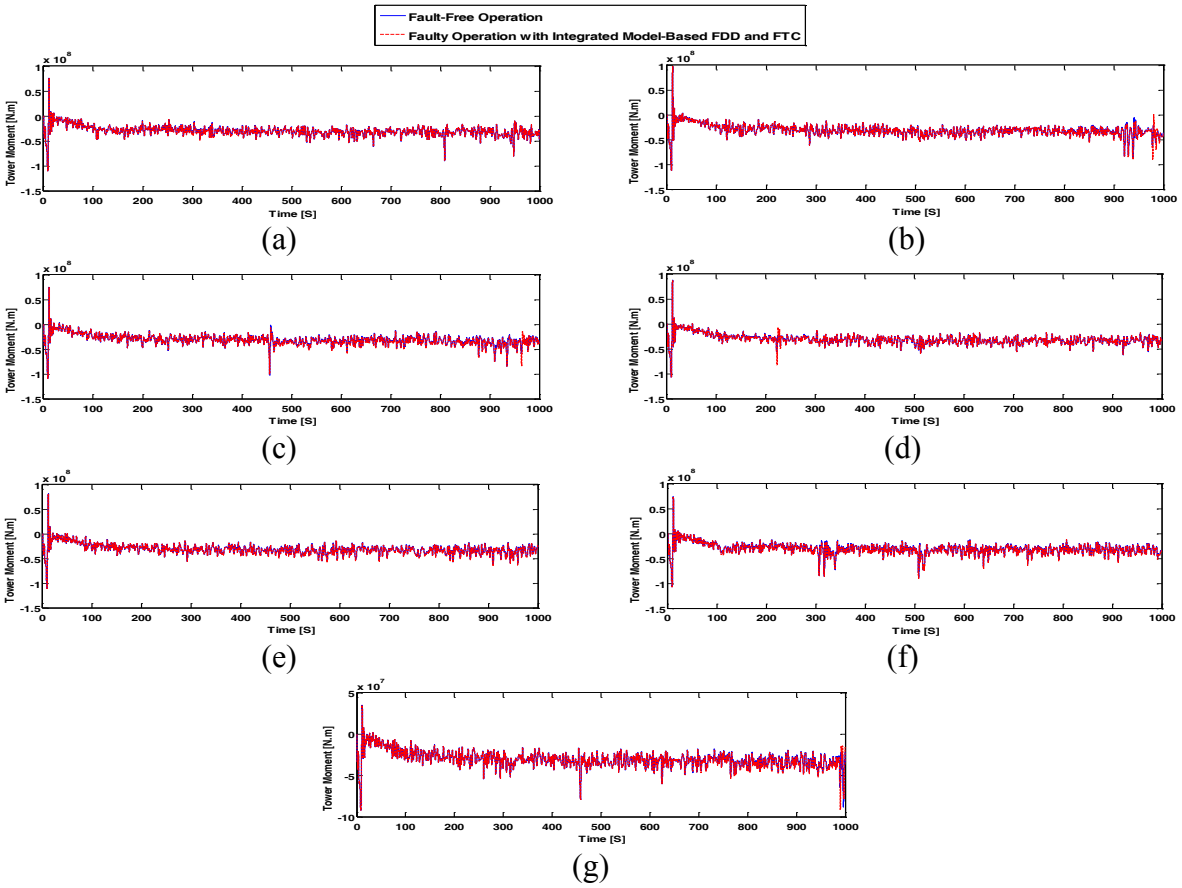

Figure 4.27 Tower bending moment results − integrated model-based FDD and FTC. (a) T_1, (b) T_2, (c) T_3, (d) T_4, (e) T_7, (f) T_8, and (g) T_{10}.

Table 4.11 Quantitative comparison of tower bending moment results during fault periods

Faulty Turbine	Fault Period [sec]	Fault-Free Operation		Faulty Operation with Integrated FDD and FTC			
				Model-Based		Model-Free	
		Mean [kNm]	STD [kNm]	Mean [kNm]	STD [kNm]	Mean [kNm]	STD [kNm]
T_1	[225,400]	-28574	6166.2	-29453	6291.4	-29453	6294.6
T_2	[800,1000]	-36041	10278	-37320	11379	-37317	11376
T_3	[450,1000]	-34570	8555.2	-35740	8989.5	-35739	9000.6
T_4	[125,300]	-28807	5243.3	-29794	7000.1	-29794	7000.9
T_7	[350,1000]	-33755	7202.2	-34824	7414.3	-34825	7412.5
T_8	[100,1000]	-31985	8473.4	-33005	8623.4	-33008	8629.5
T_{10}	[700,1000]	-33837	7426.5	-34977	8229.8	-34975	8227.2

E) Robustness

This subsection deals with further evaluation of the proposed integrated FDD and FTC schemes in terms of robustness to disturbances and measurement uncertainties. Extensive Monte Carlo simulations have been performed using the wind farm nonlinear benchmark model that was modified to include the stochastic features of the signals used for modelling of the process

parameter variations and measurement uncertainties. In this regard, sensors are modeled as noise-contaminated uncertain measurement systems and some model parameters in turbines' drivetrain and aerodynamic models are stochastically varied around their nominal values. In total, 100 Monte Carlo simulations have been performed for each of the integrated FDD and FTC schemes under both fault-free and faulty (3% power loss) conditions. The best, average and the worst values of NRMSE are presented in Table 4.12.

Table 4.12 The results of Monte Carlo simulation studies under wind field shown in Figure 4.16

Faulty Turbine	Fault Period [S]		NRMSE [-] Model-Based Integrated FDD and FTC	NRMSE [-] Model-Free Integrated FDD and FTC
T_1	[225,400]	Best Case	0.00308	0.00369
		Average Case	0.00323	0.00385
		Worst Case	0.00331	0.00396
T_2	[800,1000]	Best Case	0.00296	0.00348
		Average Case	0.00321	0.00364
		Worst Case	0.00331	0.00375
T_3	[450,1000]	Best Case	0.00164	0.00209
		Average Case	0.00171	0.00221
		Worst Case	0.00191	0.00246
T_4	[125,300]	Best Case	0.00285	0.00351
		Average Case	0.00311	0.00364
		Worst Case	0.00323	0.00384
T_7	[350,1000]	Best Case	0.00144	0.00168
		Average Case	0.00152	0.00182
		Worst Case	0.00159	0.00191
T_8	[100,1000]	Best Case	0.00215	0.00328
		Average Case	0.00226	0.00334
		Worst Case	0.00231	0.00339
T_{10}	[700,1000]	Best Case	0.00235	0.00286
		Average Case	0.00248	0.00298
		Worst Case	0.00257	0.00312

Although the wind speed profiles with mean speed of 15 m/s and a turbulence intensity of 10% over 1000 seconds of run time (see Figure 4.16) was used for the above mentioned Monte Carlo study, an additional simulation trial is also made in order to test the robustness in performance of the proposed schemes in terms of external disturbances (e.g., wind changes). In this regard, a new wind field with mean speed of 16 m/s and a turbulence intensity of 12% is simulated over 2000 seconds of run time. For the mentioned wind field, similar simulations as described in Section 4.6C are conducted with the exception of fault activity periods that are extended by an extra 1000 seconds of run time. Table 4.13 presents the quantitative comparison between the proposed schemes in terms of NRMSE during the mentioned periods of fault activity in the faulty wind turbines (the simulation plots are not shown here for the sake of brevity).

All results presented in Table 4.12 and Table 4.13 confirm that both model-free and model-based integrated FDD and FTC schemes are not only robust in the presence of modeling errors, measurement uncertainties, and external disturbances, but also can successfully maintain reliable wind farm performance under faulty conditions.

Table 4.13 Quantitative comparison of generator power responses for integrated FDD and FTC schemes during the specified fault periods with 3% power loss and under wind field with mean speed of 16 m/s, a turbulence intensity of 12%, and over 2000 seconds of run time.

Faulty Turbine	Fault Period [S]	NRMSE [-]	
		Model-Based	Model-Free
T_1	[225,1400]	0.0015	0.0018
T_2	[800,2000]	0.0019	0.0021
T_3	[450,2000]	0.0017	0.0019
T_4	[125,1300]	0.0020	0.0023
T_7	[350,2000]	0.0015	0.0017
T_8	[100,2000]	0.0016	0.0018
T_{10}	[700,2000]	0.0018	0.0023

4.7 Conclusion

This paper proposed a novel integrated fault detection and diagnosis (FDD) and fault-tolerant control (FTC) approach oriented to the design and development of two active fault-tolerant cooperative control (AFTCC) schemes for an offshore wind farm. The designed AFTCC schemes can address decreased power generation faults caused by turbine blade erosion and debris build-up on the blades over time. Each of the designed schemes employs a FDD system to provide accurate and timely diagnosis information to be used in an appropriate automatic signal correction algorithm for accommodation of faults in the farm. The first scheme is based on a model-free FDD system that incorporates a rule-based threshold test technique for residual evaluation. Conversely, the second scheme is based on a model-based FDD system that incorporates data-driven models developed using fuzzy modelling and identification technique.

Different simulations have been performed using a high-fidelity offshore wind farm benchmark model in the presence of wind turbulences, measurement noises, and realistic fault scenarios. Moreover, extensive Monte Carlo simulations are performed to evaluate the robustness of the designed schemes with respect to modelling errors, disturbances and measurement uncertainties. All simulation studies and numerical results clearly indicate the effectiveness and

robustness of the schemes over the entire range of tested wind profiles for both the fault-free and faulty conditions.

Both active fault-tolerant cooperative control schemes are superior to the baseline wind farm control system designed using classical methods. The fault-tolerance and nominal performance provided by the schemes make them an efficient and practical choice for wind farms. In particular, the fact that the proposed schemes employ an automatic signal correction algorithm for fault accommodation, and hence they do not disturb the nominal performance of a wind farm under normal (fault-free) operating conditions is a remarkable feature. This feature is particularly favorable in the case of any already designed wind farm control systems whose structures are well defined for optimizing power capture in a farm while achieving fault-tolerance capability without scarifying best performance of the wind farm. However, it is worth mentioning that, the performance of the proposed AFTCC schemes is highly dependent on the speed and accuracy of their FDD systems. Obviously, it may be impossible in practice to measure or obtain the instant precise values of faults in a system. Actually, the FDD systems only determine an online estimate for the magnitude of faults after their occurrence while accepting a detection time delay.

With respect to the future research topics related to this presented work, it can be promising to extend the presented integrated FDD and FTC approach (AFTCC) to accommodation of other frequent faults in wind farms such as misalignment of one or more blades originated at the time of installation and/or change in the drivetrain damping due to wear and tear. Moreover, it should be noted that in order to practically implement and benefit from such a fault-tolerant control approach, the FDD system and real-time control system reconfiguration as a whole needs to be designed and developed along with the so-called techniques related to fault-tolerant computing and fault-tolerant communication networks that are followed by hardware-in-the-loop testing for complete evaluation before real system tests.

Chapter 5 Active Power Control Design for Supporting Grid Frequency Regulation in Wind Farms

Abstract

Among renewable energy sources, wind power is expected to contribute a larger and rapidly growing portion of the world's energy portfolio. However, the increased penetration of wind power into the power grid has challenged the reliable and stable operation of the grid. This motivates new opportunities in the design and development of novel control schemes capable of actively maintaining the necessary balance between power generation and load, which in turn regulates the grid frequency when plenty of winds are available. This paper presents two active power control schemes that are developed based on adaptive pole placement control and fuzzy gain-scheduled proportional-integral control approaches. The active power control is conducted collectively across a wind farm to provide rapid power response while maintaining safe structural loading on turbines' components. The proposed active power control schemes are evaluated and compared by a series of simulations on an advanced wind farm benchmark model in the presence of wind turbulences, measurement noises, and grid load variations. It is further demonstrated that the mentioned schemes are able to tolerate probable occurrence of sudden imbalance between generation and load due to relevant faults/failures in the wind farm or electric grid.

5.1 Introduction

Renewable energy technologies are clean and sustainable sources of energy that can serve as alternatives to meet the world's increasing demand for efficient, reliable and affordable energy needs in the years ahead. Among renewable energy sources, wind power is expected to contribute a larger and rapidly growing portion of the world's energy portfolio. Over the past few decades, much research and development have been done on wind power in order to minimize the cost of wind energy. In this regard, larger and more flexible wind turbines have been designed and installed in remote locations such as offshore regions. Moreover, to lower the high costs of operation and maintenance due to high rate of failures of wind turbine components, advanced condition monitoring, diagnosis, and fault-tolerant and efficiency control solutions have been proposed recently. For example, in [33] and [104], the authors employ fuzzy modelling, identification, and control techniques to design and develop integrated fault diagnosis and fault-tolerant control schemes for addressing sensor faults and actuator faults in a wind turbine, respectively. In [114], an observer-based fault tolerant control scheme within a linear parameter varying framework is proposed for an offshore wind turbine system. Another work presented in [115] proposes a sensor fault-tolerant control approach based on fault estimation and compensation for an offshore wind turbine described via Takagi-Sugeno multiple models. In [46], a fault-tolerant control scheme that employs a robust actuator fault estimation approach using adaptive filters is proposed.

Based on international statistics, many large wind farms have already been installed and more in all forms of onshore and offshore are planned to be integrated into the power grids throughout the world [116]. Since wind energy is naturally a fluctuating source of power which relies on the prevailing wind, the efficient and reliable connection/integration of wind turbines and wind farms to the grid has always been an important issue for grid operation. As long as only small-scale power units of wind turbines are installed and powering the network, wind power only has a small influence on power fluctuations in the network and in turn can easily be integrated. However, the increased penetration of wind power into the power grid has challenged the reliable and stable operation of the grid. This situation has required some transmission systems operators (TSOs) to formulate grid code requirements exclusively for countries and regions with relatively isolated grids and high levels of wind power penetration. Basically, these grid codes require wind farms to behave as active and controllable components which embrace more responsibility in grid operation.

This means that wind farms have to participate in grid frequency and voltage regulation through control of active and reactive power, respectively. So, the codes provide specific information such as operational ranges for voltage and frequency as well as control requirements for active and reactive power. For example, in Canada, Hydro-Québec grid code for wind farm interconnection requires that wind farms with installed capacity of more than 10 MW shall have active power control capability for at least 10 seconds to provide power/frequency regulation in response to grid frequency deviations higher than 0.5 Hz [117].

In order to meet the ever evolving grid code requirements on frequency variations and to support efficient and reliable integration of wind power, active power control (APC) strategies are essential for actively maintaining the necessary balance between power generation and loads, which in turn regulates the grid frequency when plenty of winds are available. Research related to APC of wind energy generation has been focused on control approaches that are able to meet the grid code requirements and satisfactory response time for tracking power commands without exceeding the safe operating limits of the turbines. Most of the APC approaches rely on modification of generator torque with respect to measurements of the variations in grid frequency and possibly the rate of these variations. In [118-120], the wind turbine operates at a higher than optimal tip-speed ratio to provide an overhead power reserve for addressing possible deviations in frequency. The authors in [121] present an augmented control approach that employs two proportional control loops based on variations in grid frequency and the rate of these variations for modifying the generator torque command. In addition to the modification of generator torque, the blade pitch angles can also be modified for providing APC. An integrated torque and blade pitch control approach is developed in [122]. Here, the change in grid frequency is used by a proportional torque controller while a blade pitch controller assists in primary response by regulating pitch angle as needed to avoid large variations in mechanical power during frequency transients. Droop curves are typically used to characterize the change in active power output of a generator governor caused by a change in grid frequency. The application of droop curves to APC of wind turbines has also been studied in the literature, for example see [123-126].

From a control system development viewpoint, APC in wind turbines can be developed at both individual turbine and entire wind farm levels. Prior research on wind turbine APC has been mostly focused on APC at individual turbine level that means performing active power control on

individual turbines separately. However, performing APC collectively across a wind farm can be advantageous in terms of faster response and recovery to grid frequency deviations [66]. Therefore, considering APC at the entire wind farm level, this paper presents two control schemes aimed at tracking various forms of power schedules and loads, while maintaining grid frequency against any sudden imbalance between generation and loads, which is referred to as *frequency event*. A frequency event is typically caused by sudden variations in electrical loads, new generation allocation, disconnection of generators, and disturbed generation due to faults and failures. The two APC schemes are developed based on adaptive pole placement control and fuzzy gain-scheduled proportional-integral (PI) control approaches. A main advantage of the proposed schemes is their stand-alone structures that do not complicate the wind turbines' conventional control loops for easier acceptance and validation & verification by wind energy industry for commercialization. Furthermore, the proposed schemes can operate in the same range of wind speeds as wind turbines' standard baseline control systems while considering the practical safe operating limits of the turbines.

The effectiveness of the proposed APC schemes is evaluated by a series of simulations on an advanced wind farm benchmark model [112], in the presence of wind turbulences, measurement noises, and grid loads variations. It is also demonstrated that the mentioned schemes are able to tolerate probable occurrence of realistic frequency events.

The remainder of the paper is organized as follows: In Section 5.2, the used wind farm benchmark model is briefly overviewed. The overall framework used for electrical grid frequency regulation and active power control based on fuzzy gain-scheduled PI control and adaptive pole placement control are described in Section 5.3. Section 5.4 presents the simulation results with some comments and discussions. Finally, conclusions are drawn in Section 5.5.

5.2 Wind Farm Benchmark Model

This paper considers an advanced wind farm simulation benchmark model developed in the EU-FP7 project, AEOLUS [112]. The model allows control designers to develop and investigate farm level control solutions under various operating conditions for an optional quantity and layout of wind turbines installed in a wind farm. In the benchmark model, sensor models are updated as noise-contaminated, uncertain measurement systems. Moreover, different wind fields with

arbitrary mean wind speeds and turbulence intensities can be generated and applied in order to facilitate the assessment of the robustness features of any control solution under external disturbances. The default wind farm layout is shown in Figure 5.1.

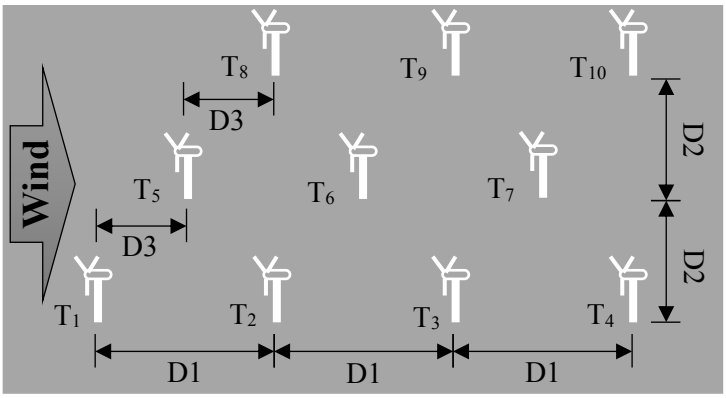

Figure 5.1 Wind farm layout (D1=600m, D2=500m, D3=300m).

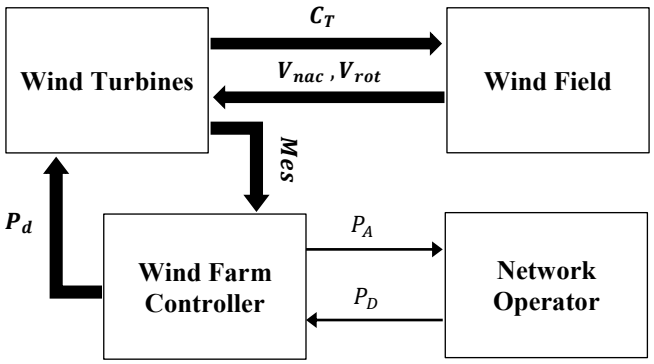

Figure 5.2 Illustration of the overall wind farm structure (This figure is based on [112]).

Figure 5.2 illustrates the overall structure of the wind farm under consideration. As it is shown in Figure 5.2, this benchmark model is composed of four major components:

Network Operator: The network operator determines the active power demand P_D required for safe and reliable connection of wind farm to the electrical grid. The baseline model for network operator can function in different modes such as: absolute, delta, and frequency regulation modes. Basically, in the frequency regulation mode used in this paper, the measured grid frequency $f_m(k)$ is used as a feedback signal to set up *active power control* in real-time and maintain the necessary balance between power generation and loads, which in turn regulates the grid frequency to its reference value f_r, despite a changing grid load. As presented in the following equations (5.1) and

(5.2), the baseline model includes a dead-band proportional gain control which employs frequency error $f_e(k)$ in (5.1) to determine the total demanded power $P_D(k)$ at the time step k in (5.2). This simple control scheme regulates the grid frequency to its reference value (e.g., 50 Hz in large areas of the world or any other frequencies).

$$f_e(k) = f_m(k) - f_r \tag{5.1}$$

$$P_D(k) = \begin{cases} 0.5(P_1) & -d \le f_e(k) \le d \\ 0.5(P_1 - P_2) & f_e(k) \ge c \\ 0.5(P_1 + P_2) & f_e(k) \le -c \\ 0.5(P_1) - 0.5(P_2)\left(\dfrac{f_e(k) - d}{c - d}\right) & d < f_e(k) < c \\ 0.5(P_1) - 0.5(P_2)\left(\dfrac{f_e(k) + d}{c - d}\right) & -c < f_e(k) < -d \end{cases} \tag{5.2}$$

In (5.2), the used c and d are two constants ($c > d$) defined by user to represent control and dead bands, respectively. Moreover, P_1 and P_2 are power parameters defined in (5.3) and (5.4), respectively.

$$P_1 = P_{max} + P_{min} \tag{5.3}$$

$$P_2 = P_{max} - P_{min} \tag{5.4}$$

The power range $[P_{min}, P_{max}]$ in (5.3) and (5.4) denotes, respectively, the prescribed minimum and maximum limits for the total power generated by the wind farm.

Wind Farm Controller: As can be seen in Figure 5.2, the wind farm controller plays an interface role which ensures appropriate distribution of total demanded power P_D among wind turbines in the farm while providing an estimate of total available power P_A in the wind farm to the operator (e.g., in the case of delta mode operator). The baseline wind farm controller in (5.5) carries out operations using a proportional distribution algorithm which sends a set of power demands $P_{d,q}(k)$ at the time step k (i.e., $P_{d,q}$ in Figure 5.2) to each of N individual turbines based on a simple estimate of their currently available powers $P_{a,q}(k)$ and the total available $P_A(k)$ and total demanded $P_D(k)$ powers in the wind farm.

$$P_{d,q}(k) = P_D(k)\frac{P_{a,q}(k)}{P_A(k)} \quad , \qquad q = 1, 2, \dots, N \tag{5.5}$$

Wind Turbines: This component simulates the dynamics of the wind turbines installed in the farm based on the measured nacelle wind speed V_{nac}, effective wind speed V_{rot}, and power demands $P_{d,q}$ at each individual turbine. Each turbine is represented using a simple model of an offshore 5 MW baseline turbine proposed by the U.S. National Renewable Energy Laboratory (NREL) (see [70]). As it is shown in Figure 5.3, the baseline control system in each individual wind turbine basically acts upon the power demand $P_{d,q}$ in (5.5) specified by the wind farm controller. To this end, the turbine's baseline control system employs a blade-pitch controller as well as a torque controller to compute appropriate blade-pitch reference $\beta_{r,q}$ and generator torque reference $\tau_{r,q}$, respectively. The blade-pitch controller is basically a PI (proportional-integral) controller to track a constant generator speed called rated generator speed so that the turbine operates at its rated power in the *full-load region*. The torque controller is designed by varying the generator torque to optimize power capture in the *partial-load region*, and to improve output power quality in the full-load region. In other words, the torque controller is set to be active for changing the torque in both the below and the above rated wind speeds. A more complete description of the wind turbine benchmark model can be found in [70].

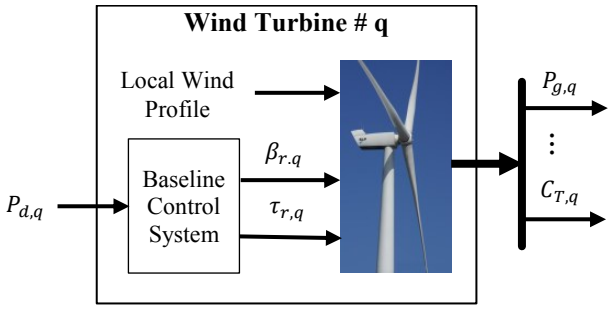

Figure 5.3 The qth wind turbine in the farm ($q = 1, 2, \ldots, N$). Note that in addition to the generated power $P_{g,q}$, the turbine model provides many other measured variables.

With respect to the outputs, the components of wind turbines in Figure 5.2 generate a set of outputs including a set of measurements $\boldsymbol{Mes}$ required for use by the wind farm controller along with a set of coefficients of thrust $\boldsymbol{C_T}$ for turbines, necessary to calculate the wake effects (i.e., low speed turbulent air flows behind turbine) by wind field component.

Wind Field: The interactions between the wind turbines installed in a wind farm can be represented through the wind field model. This model simulates the wind speed throughout the farm based on

an ambient field model together with a wake model which describes wakes meandering behind turbines and their effects on the ambient wind field.

5.3 Electrical Grid Frequency and Active Power Control

Imbalances between the generation and consumption of active power lead to frequency fluctuations in the grid. To maintain a desired level of frequency, it is required to balance the total active power generated with the total power consumed by loads and losses on the grid. This balance must be actively maintained through APC against frequency events that are typically caused by sudden variations in electrical load, new generation allocation, disconnection of generators, and disturbed generation due to faults and failures. In essence, the better the balance between power generation and consumption, the smaller the frequency fluctuations, and consequently the higher the electricity quality. This paper considers APC at an entire wind farm level within the general structure shown in Figure 5.4 that includes a typical large wind farm including N wind turbines. In this figure, every individual wind turbine is equipped with an exclusive standard torque/pitch control system that can follow the instructions (power references) provided by an APC system.

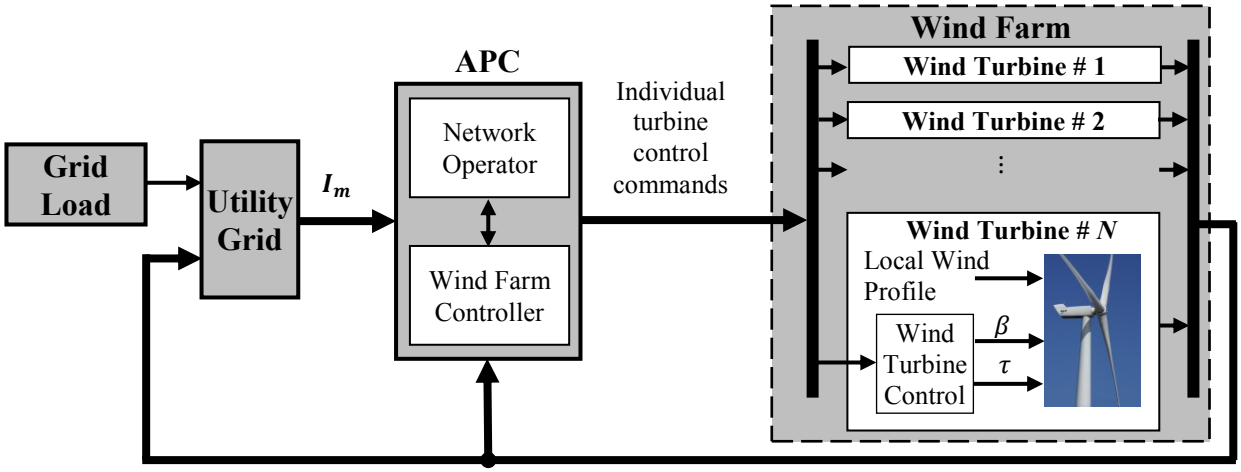

Figure 5.4 Wind farm control system setup.

Basically, APC in wind turbines can be conducted at both individual turbine and entire wind farm levels. However, as it is shown in Figure 5.4, performing APC collectively across a wind farm can be advantageous in terms of faster response and recovery to grid frequency deviations [66]. Therefore, the APC system shown in Figure 5.4 controls collectively the power production from the whole wind farm based on the set of measurements $\boldsymbol{I_m}$ at the point of common coupling (PCC) of the wind farm with the utility grid (e.g., measured grid frequency) and on the received

information from the wind turbines about the maximum amount of available power at each turbine location. In more details, the network operator determines the active power demand required to maintain the necessary balance between wind farm generation and grid loads, which in turn can regulate the grid frequency. Then, the wind farm controller distributes the demanded active power from network operator to the local wind turbines for achieving the desired generation and frequency level.

The proposed APC schemes in this paper are developed based on the fuzzy gain-scheduled PI control and adaptive pole placement control approaches. In reference to Figure 5.4, the mentioned approaches are used to address the development of two adaptive control schemes for implementation in the network operator module, while the wind farm controller module still employs the baseline proportional distribution algorithm described in Section 5.2. In the following two subsections, each APC scheme is described in detail.

A) APC Based on Fuzzy Gain-Scheduled PI Control Approach

Conventional proportional-integral-derivative (PID) controllers with their simple structure are the most widely used control systems in industrial applications. Although the conventional PID controllers are simple and particularly adequate in the control of first and second order systems, their performance is often limited for systems with more complicated dynamics, changing parameters or strong nonlinearities [127]. Basically, wind energy conversion systems are aero-electromechanical energy systems with strong nonlinear dynamic characteristics which need to be considered in their control design. To address this problem, different types of modified PID control designs such as adaptive and auto-tuning PID controllers are proposed [33, 38, 128, 129]. Among the online adaptive PID controllers, some designs incorporate fuzzy logic for performing the tuning of the controller parameters. For example, in [33, 38, 129], fuzzy rules and reasoning are utilized on-line to determine the controller parameters.

A general PID gain-scheduling approach based on fuzzy rules and reasoning is presented in [93]. This subsection presents a similar approach but for a PI controller that employs fuzzy rules to represent human expertise on the PI gains scheduling with application to APC in wind farms. Figure 5.5 shows the detailed structure of the APC scheme based on the fuzzy gain-scheduling (FGS) PI control approach implemented in the network operator module shown in Figure 5.4.

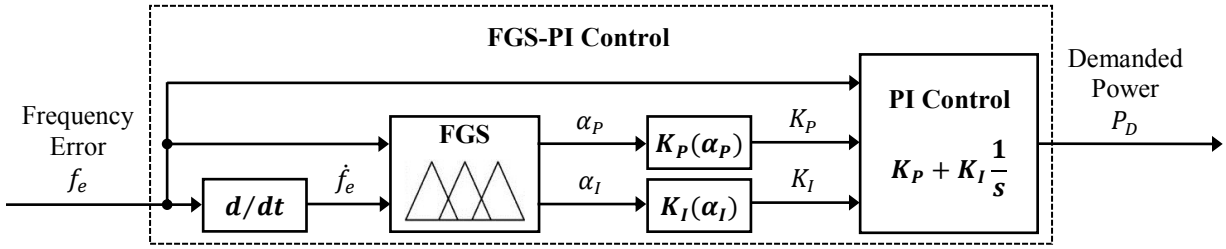

Figure 5.5 The APC scheme based on the FGS-PI control approach.

As it is shown in Figure 5.5, the APC scheme employs two inputs of frequency error f_e defined in (5.1) and its derivative $\dot{f}_e$ to determine the total demanded active power P_D for regulating the grid frequency. Note that the derivative input $\dot{f}_e$ can be approximated through numerical differentiation and any state variable filters if needed. As it is shown in (5.6) and (5.7), the proportional and integral gains have linear and quadratic dependence on scheduling variables $-1 \leq \alpha_P \leq +1$, and $-1 \leq \alpha_I \leq +1$, respectively.

$$K_P(\alpha_P) = K_{P_1}\alpha_P + K_{P_0} \tag{5.6}$$

$$K_I(\alpha_I) = K_{I_2}{\alpha_I}^2 + K_{I_1}\alpha_I + K_{I_0} \tag{5.7}$$

In (5.6) and (5.7), the positive tunable coefficients K_{P_1}, K_{I_1}, and K_{I_2} are defined by user to determine the relevant ranges of variations for constant proportional and integral gains, K_{P_0} and K_{I_0}, respectively. The constant gains K_{P_0} and K_{I_0} represent a conventional PI controller that provides a good but not optimum system response. This conventional PI controller can be obtained using any available general tuning methods for PID controllers such as the Ziegler Nichols, Lambda or Amigo tuning methods [127, 130].

The scheduling variables α_P, and α_I in (5.6) and (5.7) are determined online by the FGS system in Figure 5.5 using a set of linguistic *if-then* rules in the form of:

$$\textbf{\textit{Rule i:}}\ \text{If } f_e \text{ is } A_i \text{ and } \dot{f}_e \text{ is } B_i, \text{then } \alpha_P \text{ is } C_i \text{ and } \alpha_I \text{ is } D_i \tag{5.8}$$

where A_i, B_i, C_i and D_i (with $i = 1,2,\dots,M$) represent fuzzy membership functions corresponding to f_e, $\dot{f}_e$, α_P, and α_I, respectively. Figure 5.6(a) and (b) show the triangular membership functions used for the inputs f_e and $\dot{f}_e$, and outputs α_P and α_I, respectively. The vertical axes represent the

degree of membership μ that is within the range of $[0, +1]$. Moreover, Table 5.1 presents the meaning of linguistic variables used in the both figures.

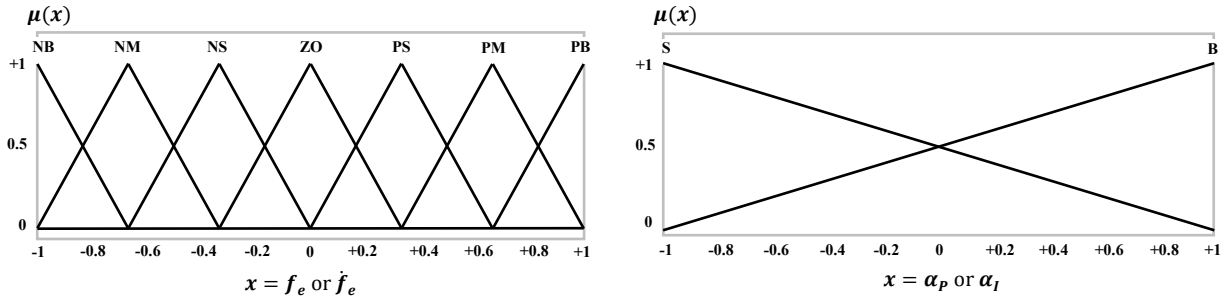

(a) (b)

Figure 5.6 Membership functions for (a) inputs f_e and $\dot{f}_e$, (b) outputs α_P and α_I

Table 5.1 Linguistic variables

Linguistic Variables	Meaning
S	Small
B	Big
PB	Positive-Big
PM	Positive-Medium
PS	Positive-Small
ZO	(approximately) Zero
NS	Negative-Small
NM	Negative-Medium
NB	Negative-Big

With respect to Figure 5.5 and Figure 5.6, note that, the FGS's inputs $f_e(k)$ and $\dot{f}_e(k)$ both need to be normalized within the range of $[-1, +1]$ before being processed by the FGS system in Figure 5.5. However, the FGS's outputs (i.e., scheduling variables) α_P and α_I both are obtained within the range of $[-1, +1]$ and will be directly used in (5.6) and (5.7), respectively.

As it is presented in Tables 5.2 and 5.3, the mentioned rules in (5.8) are formulated according to expert's knowledge [33]. The rules attempt to represent the general facts about PID control. For example, to generate a strong control signal, the controller requires large proportional and integral gains, and a small derivative gain. It is worth mentioning that, in this paper, the logic AND operator is implemented using the *minimum* criterion. Moreover, to obtain the defuzzified outputs, *center of area* defuzzification method as defined in (5.9) and (5.10) is used, in which, α_{P_i} and α_{I_i} denote the values of α_P and α_I corresponding to the degree of membership μ_i for the *i*-th rule, respectively.

$$\alpha_P = \frac{\sum_{i=1}^{M} \mu_i \alpha_{P_i}}{\sum_{i=1}^{M} \mu_i} \tag{5.9}$$

$$\alpha_I = \frac{\sum_{i=1}^{M} \mu_i \alpha_{I_i}}{\sum_{i=1}^{M} \mu_i} \tag{5.10}$$

Table 5.2 Fuzzy rules for α_P

		$\dot{f}_e(k)$						
		NB	**NM**	**NS**	**ZO**	**PS**	**PM**	**PB**
$f_e(k)$	**NB**	B	B	B	B	B	B	B
	NM	S	B	B	B	B	B	S
	NS	S	S	B	B	B	S	S
	ZO	S	S	S	B	S	S	S
	PS	S	S	B	B	B	S	S
	PM	S	B	B	B	B	B	S
	PB	B	B	B	B	B	B	B

Table 5.3 Fuzzy rules for α_I

		$\dot{f}_e(k)$						
		NB	**NM**	**NS**	**ZO**	**PS**	**PM**	**PB**
$f_e(k)$	**NB**	B	B	B	B	B	B	B
	NM	B	B	S	S	S	B	B
	NS	B	B	B	S	B	B	B
	ZO	B	B	B	S	B	B	B
	PS	B	B	B	S	B	B	B
	PM	B	B	S	S	S	B	B
	PB	B	B	B	B	B	B	B

B) APC Based on Adaptive Pole Placement Control Approach

This subsection presents the APC scheme developed based on model-based adaptive pole placement control that can address the problem of control particularly where the parameters of the process under control are not sufficiently known, or that they change over time such as what happens in wind energy conversion systems.

Basically, since any plant-model represents an approximation to its corresponding real plant/process, model uncertainty, also known as plant-model mismatch, exists more or less in any case. The adaptive pole placement control employs an online model identification approach for obtaining the on–line mathematical description/model of the plant under control which can be affected by both uncertainty and faults. Once the time-varying parameters of the process are estimated online, then, the time-varying parameters of the controller will be computed online so

that the required control performance can be achieved. However, it should be noted that the quality of control performance also depends on the properties of the controlled system itself. For example, the quality of control behavior is sometimes severely limited in case of the so-called nonminimum phase systems, which have unstable zeros (i.e., the roots of the discrete transfer function numerator of the controlled system are located outside the unit circle in the z-complex plane). The nonminimum phase systems occur more frequently with a discrete description. In such a case, the properties of nonminimum phase conditions rely on not only the physical properties of the system but also on the sampling period.

Figure 5.7 shows the detailed structure of the APC scheme based on the adaptive pole placement control approach implemented in the network operator module shown in Figure 5.4.

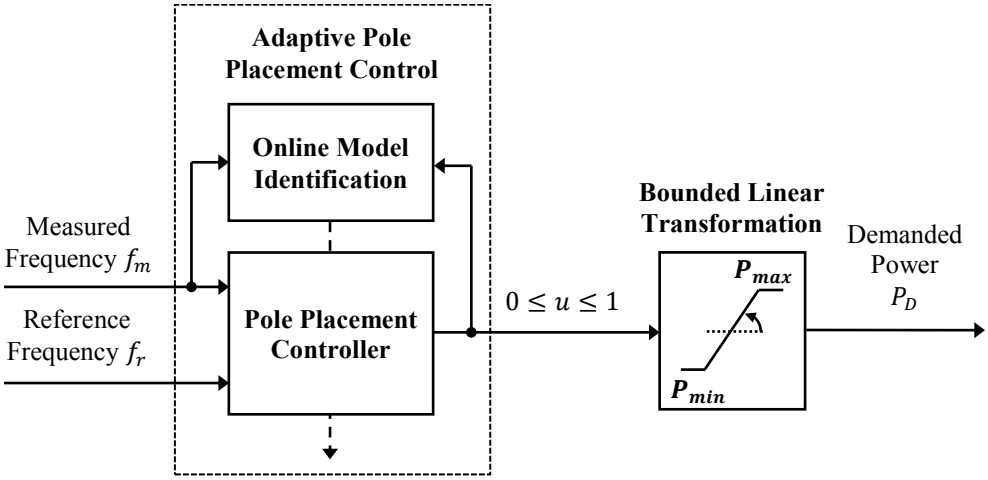

Figure 5.7 The APC scheme based on the adaptive pole placement control approach.

As it is shown in Figure 5.7, the active power demand P_D is determined using a simple linear transformation form as follows:

$$P_D = (P_{max} - P_{min})\, u + P_{min} \tag{5.11}$$

where $[P_{min}\,,\, P_{max}]$ are the prescribed minimum and maximum limits for the total power generated by the wind farm, and u is the normalized *scheduling* variable of demanded power within the range of $[0, +1]$. The scheduling variable u is determined online using a *single-input single-output (SISO)* adaptive control scheme based on an integrated *online model identification mechanism* and model-based *adaptive pole placement control system* (see Figure 5.7). In the

following two subsections, the online model identification and model-based adaptive pole placement control methods are described, respectively.

Online Model Identification for Control

The design of control strategy incorporates an online model identification approach for obtaining mathematical description of the plant model under control. There exists a wide variety of techniques for modelling and process identification in the literature. However, the online recursive identification technique based on the *Least Squares Method (LSM) with adaptive directional forgetting* discussed here [131] enables the most accurate identification of the given process. In comparison with classical LSM [103], and LMS with exponential forgetting [131] techniques, LSM with adaptive directional forgetting is the most sophisticated technique that is particularly useful for systems with time-varying parameters. In fact, the employed *signal weighting* process in LSM with adaptive directional forgetting technique makes it possible to finely modify/update a forgetting coefficient with respect to changes in input and output signals.

In the most general case, the purpose of LSM with adaptive directional forgetting technique is to identify online the unknown parameters a_i and b_j of a process described by the following transfer function:

$$G(z) = \frac{B(z^{-1})}{A(z^{-1})} = \frac{b_1 z^{-1} + b_2 z^{-2} + \cdots + b_m z^{-m}}{1 + a_1 z^{-1} + a_2 z^{-2} + \cdots + a_n z^{-n}}\ z^{-d} \tag{5.12}$$

in which m, n, and d are integers related to the structure of the model through defining the polynomials $A(z^{-1})$ and $B(z^{-1})$, whereas z is the so-called discrete-time complex variable.

As it is shown by (5.13), the estimated output of the process $\hat{y}_k$ at each time step k can be represented in the following vector form [103]:

$$\begin{gathered} \hat{y}_k = \mathbf{\Theta}_{k-1}^T \cdot \mathbf{\Phi}_k \\ \mathbf{\Theta}_{k-1} = \left[\hat{a}_1, \cdots, \hat{a}_n, \hat{b}_1, \cdots, \hat{b}_m\right]^T \\ \mathbf{\Phi}_k = [-y_{k-1}, \cdots, -y_{k-n}, u_{k-d-1}, \cdots, u_{k-d-m}]^T \end{gathered} \tag{5.13}$$

where the vector $\mathbf{\Theta}_{k-1}$ contains the model parameter estimates $\hat{a}_i$ and $\hat{b}_j$ computed at the time step $k-1$, and the vector $\mathbf{\Phi}_k$ contains the past process inputs u and outputs y data.

The recursive expression in (5.14) is used to update the process parameters at each time step:

$$\boldsymbol{\Theta}_k = \boldsymbol{\Theta}_{k-1} + \frac{\mathbf{C}_{k-1} \cdot \boldsymbol{\Phi}_k}{1 + \xi_k} \cdot (y_k - \boldsymbol{\Theta}_{k-1}^T \boldsymbol{\Phi}_k) \tag{5.14}$$

where,

$$\xi_k = \boldsymbol{\Phi}_k^T \cdot \mathbf{C}_{k-1} \cdot \boldsymbol{\Phi}_k \tag{5.15}$$

The matrix $\boldsymbol{C}$ is defined by:

$$\mathbf{C}_k = \begin{cases} \mathbf{C}_{k-1} - \dfrac{\mathbf{C}_{k-1} \cdot \boldsymbol{\Phi}_k \cdot \boldsymbol{\Phi}_k^T \cdot \mathbf{C}_{k-1}}{\varepsilon_k^{-1} + \xi_k} & , \quad \varepsilon_k > 0 \\ \mathbf{C}_{k-1} & , \quad \varepsilon_k = 0 \end{cases} \tag{5.16}$$

with

$$\varepsilon_k = \varphi_k - \frac{1 - \varphi_k}{\xi_{k-1}} \tag{5.17}$$

The forgetting coefficient φ_k and its auxiliary variables are updated as follows:

$$\varphi_k = \frac{1}{1 + (1 + \rho)\left\{ln(1 + \xi_{k-1}) + \left[\frac{(\nu_{k-1} + 1)\eta_{k-1}}{1 + \xi_{k-1} + \eta_{k-1}} - 1\right]\frac{\xi_{k-1}}{1 + \xi_{k-1}}\right\}} \tag{5.18}$$

where

$$\nu_k = \varphi_k(\nu_{k-1} + 1) \tag{5.19}$$

$$\eta_k = \frac{(y_k - \boldsymbol{\Theta}_{k-1}^T \boldsymbol{\Phi}_k)^T (y_k - \boldsymbol{\Theta}_{k-1}^T \boldsymbol{\Phi}_k)}{\lambda_k} \tag{5.20}$$

$$\lambda_k = \varphi_k \left[\lambda_{k-1} + \frac{(y_k - \hat{y}_k)^T (y_k - \hat{y}_k)}{1 + \xi_{k-1}}\right] \tag{5.21}$$

The start-up conditions are represented by a set of well-defined initial values for the parameters $\boldsymbol{\Theta_0}$, $\boldsymbol{C_0}$, φ_0, λ_0, ρ, and ν_0. In this way, the recursive identification technique recalled here computes the time-varying parameters of the discrete-time linear model as an approximation of the nonlinear plant/process. Accordingly, these parameters will be used by the adaptive controller described in the next subsection.

Pole Placement Two Degree-of-Freedom (DOF) Controller with Compensator for Third Order Processes

This subsection describes the adaptive controller used in connection with the online identification method already presented. In more detail, with respect to online determination of scheduling variable u in (5.11), a control scheme based on pole placement two DOF control with compensation for processes of third order ($n = 3$) is developed [132].

By substituting $n = m = 3$ and $d = 0$ in (5.12), the transfer function of the time-varying controlled system has the following form:

$$G(z) = \frac{B(z^{-1})}{A(z^{-1})} = \frac{b_1 z^{-1} + b_2 z^{-2} + b_3 z^{-3}}{1 + a_1 z^{-1} + a_2 z^{-2} + a_3 z^{-3}} \tag{5.22}$$

whose estimated parameter vector using the online identification approach is:

$$\boldsymbol{\Theta}_k = \left[\hat{a}_1, \hat{a}_2, \hat{a}_3, \hat{b}_1, \hat{b}_2, \hat{b}_3\right]^T \tag{5.23}$$

The two DOF control loop is depicted in Figure 5.8. In this figure, w_k, u_k and y_k are step reference signal, control signal and process output at the time step k, respectively.

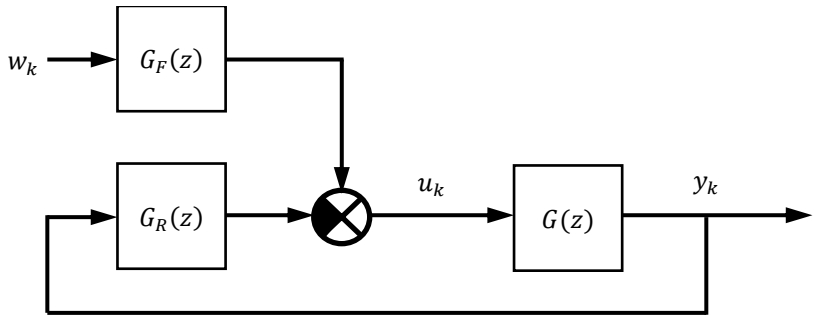

Figure 5.8 Closed-loop two DOF control system (This figure is based on [132]).

The feedback controller in Figure 5.8 can be written as:

$$G_R(z) = \frac{Q}{P\,K} = \frac{q_0 + q_1 z^{-1} + q_2 z^{-2} + q_3 z^{-3}}{(1 + p_1 z^{-1} + p_2 z^{-2})(1 - z^{-1})} \tag{5.24}$$

In addition to the above feedback controller, the feedforward control part in Figure 5.8 facilitates simpler and more efficient processing of reference signal. This feedforward controller for a step reference signal has the following form:

$$G_F(z) = \frac{R}{P\,K} = \frac{r_0}{(1 + p_1 z^{-1} + p_2 z^{-2})(1 - z^{-1})} \tag{5.25}$$

Characteristic polynomial of closed-loop system is defined as in (5.26):

$$A(z^{-1})\,P(z^{-1})\,K(z^{-1}) + B(z^{-1})\,Q(z^{-1}) = D(z^{-1}) \tag{5.26}$$

where the polynomial terms are as follows:

$$A(z^{-1}) = 1 + \hat{a}_1 z^{-1} + \hat{a}_2 z^{-2} + \hat{a}_3 z^{-3} \tag{5.27}$$

$$B(z^{-1}) = \hat{b}_1 z^{-1} + \hat{b}_2 z^{-2} + \hat{b}_3 z^{-3} \tag{5.28}$$

$$P(z^{-1}) = 1 + p_1 z^{-1} + p_2 z^{-2} \tag{5.29}$$

$$Q(z^{-1}) = q_0 + q_1 z^{-1} + q_2 z^{-2} + q_3 z^{-3} \tag{5.30}$$

$$K(z^{-1}) = 1 - z^{-1} \tag{5.31}$$

$$D(z^{-1}) = 1 + d_1 z^{-1} + \cdots + d_6 z^{-6} \tag{5.32}$$

The coefficients used in (5.32) are defined below:

$$d_1 = \begin{cases} -2e^{(-\xi\omega T_0)}\,cos\left(\omega T_0\sqrt{1-\xi^2}\right), & \xi \le 1 \\ -2e^{(-\xi\omega T_0)}\,cosh\left(\omega T_0\sqrt{\xi^2-1}\right), & \xi > 1 \end{cases} \tag{5.33}$$

$$d_2 = e^{(-2\xi\omega T_0)} \tag{5.34}$$

$$d_3 = d_4 = d_5 = d_6 = 0 \tag{5.35}$$

As it is shown in (5.33-5.35), the dynamic behaviour of closed-loop system is represented by two fundamental parameters ω and ξ which are the natural frequency and damping factor, respectively.

With respect to Figure 5.8, it is obvious that the control law corresponding to pole placement two DOF control with compensation for a third order process has the form:

$$P(z^{-1})K(z^{-1})u_k = R(z^{-1})w_k - Q(z^{-1})y_k \tag{5.36}$$

where u_k is the control signal at the time step k computed as follows:

$$u_k = r_0 w_k - q_0 y_k - q_1 y_{k-1} - q_2 y_{k-2} - q_3 y_{k-3} + \tag{5.37}$$

$$+(1-p_1)u_{k-1}+(p_1-p_2)u_{k-2}+p_2u_{k-3}$$

in which

$$r_0=\frac{1+d_1+d_2+d_3+d_4+d_5}{b_1+b_2+b_3} \tag{5.38}$$

As already mentioned, the control signal u_k computed by (5.37) will be used in (5.11) for smooth control of active power within its prescribed range.

5.4 Simulation Results and Discussion

In this section, simulation results are presented and discussed to evaluate the performance and effectiveness of the developed APC schemes in terms of their capability for tracking grid loads and tolerating occurrence of frequency events while considering practical safe operating limits of the turbines under the damaging structural loads induced by the control schemes. Simulation tests are performed in MATLAB/Simulink using the nonlinear benchmark model presented in Section 5.2. An offshore wind farm including 10 NREL 5MW turbines is created with the layout as shown in Figure 5.1. Simulations are conducted for a realistic wind field over 1000 seconds of run time. Figure 5.9 shows the wind speed profiles for each of the ten turbines in the farm.

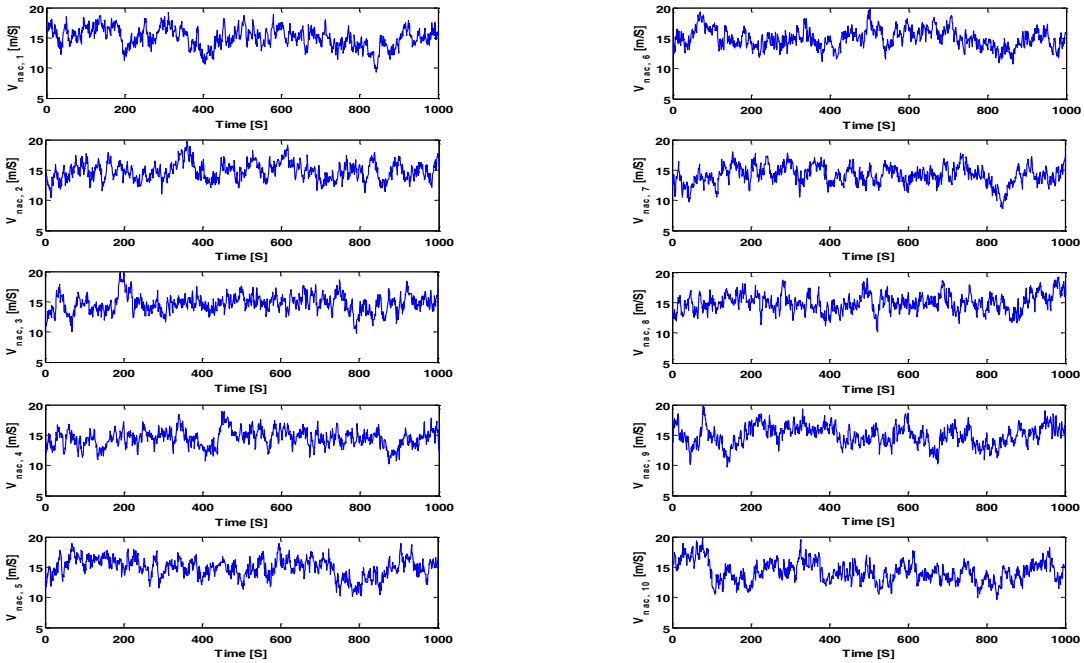

Figure 5.9 Nacelle wind speeds for the wind farm shown in Figure 5.1 (Note: $V_{nac,\,i}$ denotes nacelle wind speed for turbine T_i).

Tables 5.4 and 5.5 present the values of constant gains/coefficients as well as the start-up conditions used for APC schemes based on the proposed FGS PI control approach and adaptive pole placement control approach, respectively.

Table 5.4 Parameters used in fuzzy gain-scheduled PI control

	Parameter	Value
Proportional	K_{P_0}	11.5×10^7
	K_{P_1}	7×10^7
Integral	K_{I_0}	0.35×10^5
	K_{I_1}	0.4×10^5
	K_{I_2}	0.2×10^5

Table 5.5 Parameters used in adaptive pole placement control

	Parameter	Value
Identification	$\boldsymbol{\Theta_0}$	$[0.1, 0.2, 0.3, 0.4, 0.5, 0.6]^T$
	C_0	$10^9\ I_6$
	φ_0	1
	λ_0	10^{-3}
	ρ	99×10^{-2}
	ν_0	10^{-6}
Control	ω	1.1
	ξ	3

A) Performance of Active Power/Frequency Control

In order to demonstrate the nominal performance of active power/frequency control for the developed schemes, two different functions for the electrical grid load are defined and then separately applied to the wind farm. Figure 5.10(a), and (b) show the considered step, and smooth periodic functions for the grid load, respectively. The considered grid loads each is defined in a way to finely provide a reasonable possibility for challenging the nominal performance of APC schemes in a comparative framework while sufficient power is available from the wind. It is worth mentioning that, at initial time ($t = 0$), the load is assumed to be 0.0 MW. For example, in the case of the step-function load, the load has the following form:

$$L(t) = \begin{cases} 0 \ \ MW & t = 0 \\ 30 \ \ MW & t > 0 \end{cases} \tag{5.39}$$

Moreover, the initial active power generated by the wind farm is also assumed to be 0.0 MW since the wind farm starts from its idle mode. Consequently, the initial frequency is ideally assumed to be exactly equal to the reference frequency value of 50 Hz.

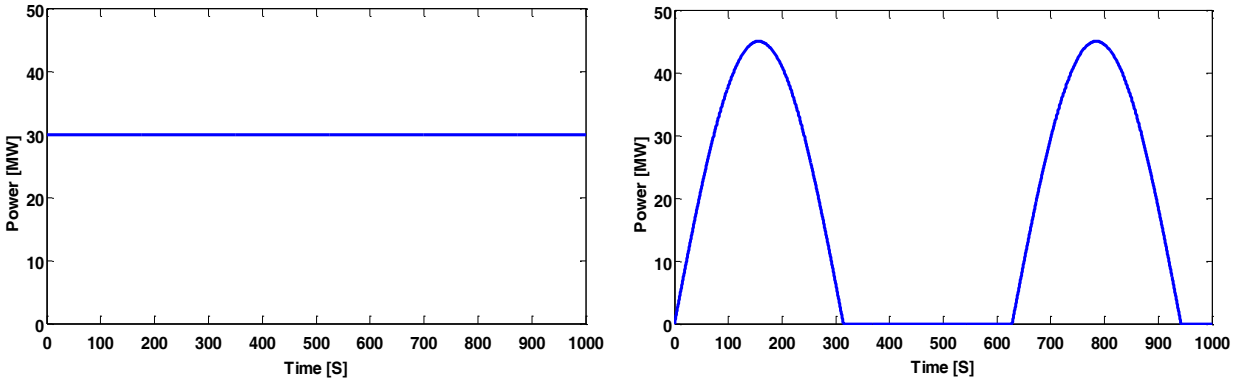

(a) (b)

Figure 5.10 Grid loads – (a) step, and (b) periodic.

Figure 5.11(a) and (b) provide performance illustrations of the wind farm APC schemes in response to the considered step, and periodic grid loads, respectively. The figures show active power responses obtained from all three APC schemes based on dead-band proportional gain control (baseline APC scheme in (5.2)), fuzzy gain-scheduled PI control, and adaptive pole placement control approaches.

In connection with Figure 5.11, to check the tracking accuracy of APC schemes required for matching the active power response and grid load, the *normalized root-mean-squared error (NRMSE)* is defined as follows:

$$NRMSE = \frac{\sqrt{\frac{1}{N}\sum_{k=1}^{N}(L_k - P_k)^2}}{\bar{L}} \tag{5.40}$$

where P_k, L_k, and $\bar{L}$ denote the kth active power sample, kth load sample, and the mean of the load, respectively. Table 5.6 presents a precise quantitative comparison between the APC schemes in terms of NRMSE defined in (5.40).

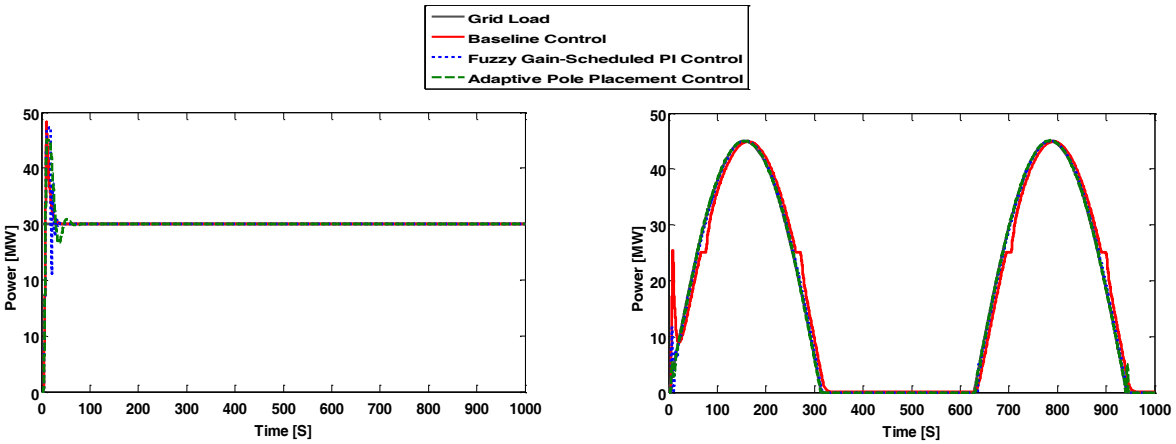

(a) (b)

Figure 5.11 Total active power response during (a) step grid load, and (b) periodic grid load.

Table 5.6 Quantitative comparison of APC schemes in terms of accuracy of active power response

Load	APC Scheme	NRMSE
Step	Baseline control	0.0857
	Fuzzy gain-scheduled PI control	0.0943
	Adaptive pole placement control	0.0946
Periodic	Baseline control	0.1383
	Fuzzy gain-scheduled PI control	0.0330
	Adaptive pole placement control	0.0188

To illustrate the ability of APC schemes in regulation of the grid frequency, Figure 5.12(a) and (b) show the grid frequency responses with respect to the considered step, and periodic grid loads, respectively. In connection with Figure 5.12, Table 5.7 quantitatively compares the obtained grid frequency responses in terms of mean, standard deviation (STD), and maximum deviation.

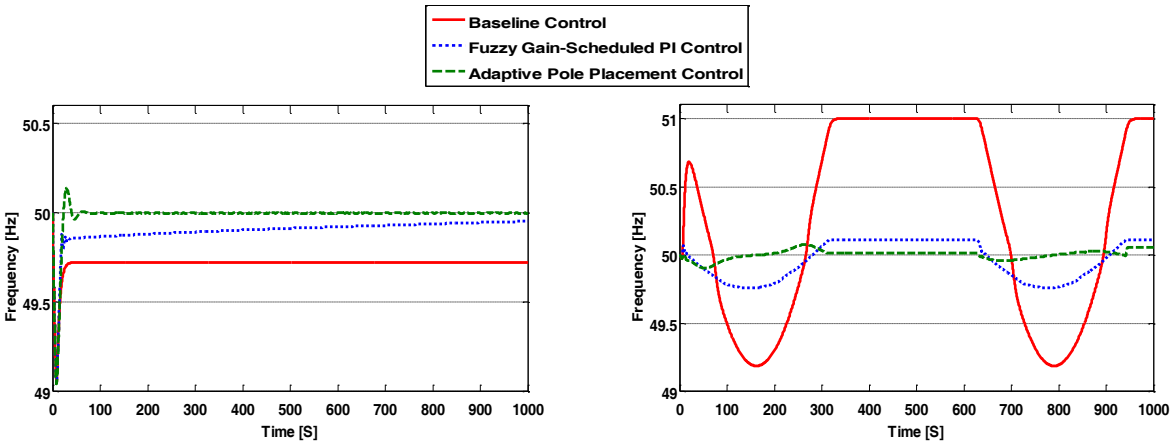

(a) (b)

Figure 5.12 Grid frequency response during (a) step grid load, and (b) periodic grid load.

Table 5.7 Quantitative comparison of APC schemes in terms of frequency regulation

Load	APC Scheme	Mean [Hz]	Standard Deviation [Hz]	Maximum Deviation [Hz]
Step	Baseline control	49.70	0.06	0.95
	Fuzzy gain-scheduled PI control	49.90	0.08	0.94
	Adaptive pole placement control	49.99	0.09	0.95
Periodic	Baseline control	50.26	0.72	1.01
	Fuzzy gain-scheduled PI control	49.96	0.14	0.24
	Adaptive pole placement control	50.01	0.03	0.10

With respect to the above results, in the case of step grid load, Figure 5.11(a) and Table 5.6 indicate that all APC schemes have almost similar performance in maintaining the required balance between the wind farm generation and grid load. However, based on Figure 5.12(a) and Table 5.7, the developed APC schemes based on fuzzy gain-scheduled PI control and adaptive pole placement control provide better frequency response during the step grid load simulation. In particular, the APC scheme based on adaptive pole placement control efficiently regulates frequency close to the reference frequency of 50 Hz. In the case of periodic grid load, all simulation results shown in Figure 5.11(b), Figure 5.12(b), and Tables 5.6 and 5.7, obviously, demonstrate superior performance of the developed APC schemes compared with the baseline APC scheme. Moreover, with respect to the developed APC schemes alone, the APC scheme based on adaptive pole placement control seems more effective than the APC scheme based on fuzzy gain-scheduled PI control.

B) Wind Farm Structural Loading/Fatigue

In addition to the evaluation of the performance and effectiveness of the developed APC schemes in terms of their capability for tracking grid loads and satisfactory regulation of grid frequency, it is necessary to assess the damaging structural loads induced on the turbines under the applied grid loads and APC schemes. Actually, to avoid any intense control command and thereby extreme structural loading on the wind turbines' actuators, the recommended rate and magnitude limiters are employed in the benchmark model under consideration. However, the high fidelity benchmark model described in Section 5.2 provides different structural loading measures such as rainflow counts and damage equivalent loads (DEL) for tower bending and main shaft torsion, such that the fatigue load of different APC schemes can be assessed. In fact, DEL computed based on MCrunch code (see [133]) is a convenient measure of the accumulation of load over a particular

load history that provides a single value representing fatigue over the duration of the simulation. With respect to the performed simulations, Table 5.8 and Table 5.9 present the DEL results for main shaft torsion and tower bending, respectively. Note that, the lower the DEL, the lower the fatigue and the better the APC has scored in terms of structural loading. The results presented in the table demonstrate that both the developed APC schemes have minimal impact on the wind turbine structural loading with respect to the results under baseline control approach. In fact, the developed APC schemes can provide more successful tracking of grid loads and satisfactory regulation of grid frequency through increased (more efficient) actuator usage without exceeding the safe operating limits of the turbines.

Table 5.8 Fatigue results (DEL – shaft torsion) for APC based on (A) baseline control (B) fuzzy gain-scheduled PI control (C) adaptive pole placement control

Load	APC Scheme	DEL – Shaft Torsion									
		T1	T2	T3	T4	T5	T6	T7	T8	T9	T10
Step	(A)	1.91×10^6	1.94×10^6	1.96×10^6	1.92×10^6	1.97×10^6	1.94×10^6	1.91×10^6	1.95×10^6	1.93×10^6	1.92×10^6
	(B)	1.93×10^6	1.89×10^6	1.94×10^6	2.02×10^6	1.97×10^6	1.90×10^6	1.86×10^6	1.89×10^6	1.87×10^6	1.93×10^6
	(C)	1.85×10^6	1.81×10^6	1.84×10^6	1.94×10^6	1.88×10^6	1.82×10^6	1.77×10^6	1.83×10^6	1.79×10^6	1.85×10^6
Periodic	(A)	2.13×10^6	2.16×10^6	2.13×10^6	2.13×10^6	2.14×10^6	2.16×10^6	2.17×10^6	2.16×10^6	2.14×10^6	2.14×10^6
	(B)	2.29×10^6	2.20×10^6	2.16×10^6	2.25×10^6	2.26×10^6	2.27×10^6	2.22×10^6	2.17×10^6	2.28×10^6	2.33×10^6
	(C)	2.26×10^6	2.18×10^6	2.15×10^6	2.25×10^6	2.25×10^6	2.26×10^6	2.18×10^6	2.16×10^6	2.28×10^6	2.31×10^6

Table 5.9 Fatigue results (DEL – tower bending) for APC based on (A) baseline control (B) fuzzy gain-scheduled PI control (C) adaptive pole placement control

Load	APC Scheme	DEL – Tower Bending									
		T1	T2	T3	T4	T5	T6	T7	T8	T9	T10
Step	(A)	5.80×10^7	3.57×10^7	3.66×10^7	5.60×10^7	4.91×10^7	5.47×10^7	3.98×10^7	3.80×10^7	5.78×10^7	6.22×10^7
	(B)	5.85×10^7	3.66×10^7	3.80×10^7	6.19×10^7	4.94×10^7	5.51×10^7	4.32×10^7	3.82×10^7	5.84×10^7	6.30×10^7
	(C)	6.04×10^7	3.53×10^7	3.67×10^7	6.21×10^7	5.09×10^7	5.71×10^7	3.97×10^7	3.81×10^7	6.11×10^7	6.68×10^7
Periodic	(A)	7.30×10^7	4.18×10^7	4.69×10^7	7.47×10^7	6.52×10^7	6.94×10^7	5.92×10^7	4.88×10^7	7.50×10^7	8.23×10^7
	(B)	8.07×10^7	4.32×10^7	5.16×10^7	8.41×10^7	7.28×10^7	7.64×10^7	6.62×10^7	5.42×10^7	8.31×10^7	9.26×10^7
	(C)	8.20×10^7	4.68×10^7	5.35×10^7	8.38×10^7	7.30×10^7	7.61×10^7	6.76×10^7	5.55×10^7	8.20×10^7	9.17×10^7

C) Tolerance against Frequency Events

In this subsection, the capability of the developed APC schemes in tolerating probable occurrence of a frequency event is investigated. As already mentioned, a frequency event may be caused under a wide variety of conditions, such as: sudden variations in electrical loads, new generation allocation, disconnection of generators, and disturbed generation due to faults and failures. Here, as it is presented in Table 5.10, a frequency event related to the disturbed generation

by turbines due to faults in their actuators is considered while a typical electrical grid load shown in Figure 5.13 is applied to the wind farm.

Table 5.10 Frequency events

Event	Time Period [S]
Disturbed generation due to occurrence of +2000 Nm torque offset faults in generator/converter actuators of T1, T2, T5, and T7 (see Figure 5.1)	[250-350]

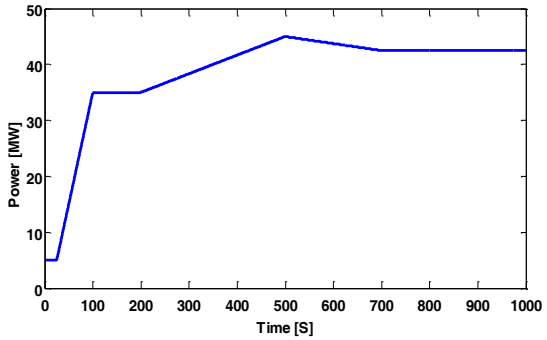

Figure 5.13 A typical grid load.

With respect to the frequency event mentioned in Table 5.10, Figure 5.14 demonstrates the total active power response of the wind farm during the load shown in Figure 5.13. As it is shown in Figure 5.14, although all APC schemes indicate passive fault tolerance capabilities against the considered frequency events in the wind farm, the developed APC schemes, in particular the APC scheme based on fuzzy gain-scheduled PI control, indicate better performance in terms of quick reaction and recovery against the frequency event.

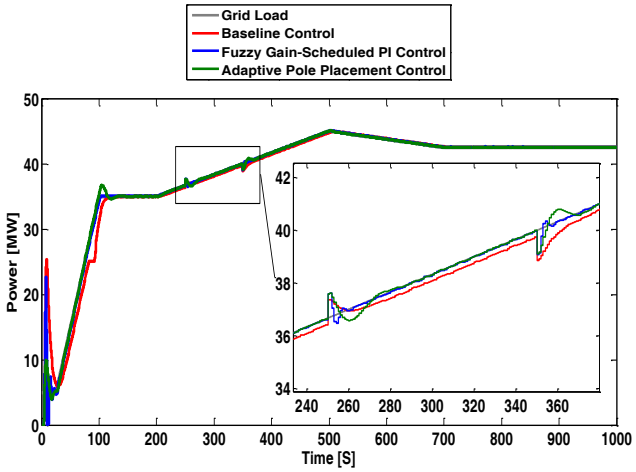

Figure 5.14 Total active power response during the frequency event.

D) Robustness

This subsection presents further evaluation of the developed APC schemes in terms of robustness to disturbances and measurement uncertainties. Actually, since wind energy conversion systems are composed of many subsystems and components that cannot be appropriately described by any analytical model derived via first principles, the analysis of Monte Carlo simulations represents a feasible solution. In the benchmark model, sensor models are updated as noise-contaminated, uncertain measurement systems. The robustness evaluation consists of extensive Monte Carlo simulations using different wind fields with mean wind speeds between 13-15 m/s and turbulence intensity values between 10-15%. In total, 100 Monte Carlo simulations have been carried out for each of the developed APC schemes. Moreover, to evaluate the robustness of the APC scheme based on model-based adaptive pole placement control against possible model-reality mismatch conditions (i.e., plant-model uncertainty), 5% error is considered in the online model identification process, and then, similar Monte Carlo simulations are carried out. In all simulations, the developed schemes were able to successfully perform the regulation of grid frequency with the best, average and worst values of performance measures reported in Tables 5.11 and 5.12. With respect to the results of Monte Carlo simulations reported in the both tables, all results confirm that both the developed APC schemes based on fuzzy gain-scheduled PI control and adaptive pole placement control are not only robust in the presence of disturbances, measurement uncertainties, and plant-model uncertainty, but also can successfully maintain grid frequency around its reference value.

Table 5.11 The results of Monte Carlo simulation studies under variations in wind fields with mean speeds within [13-15] m/s and turbulence intensity values between [10-15] % – (A) fuzzy gain-scheduled PI control (B) adaptive pole placement control

Load	**APC Scheme**	**Mean [Hz]**			**Standard Deviation [Hz]**			**Maximum Deviation [Hz]**		
		Best Case	Average Case	Worst Case	Best Case	Average Case	Worst Case	Best Case	Average Case	Worst Case
Step	(A)	49.93	49.92	49.88	0.073	0.085	0.092	0.891	0.972	0.101
	(B)	49.99	49.96	49.94	0.088	0.091	0.112	0.924	0.952	0.984
Periodic	(A)	49.98	49.93	49.89	0.121	0.132	0.165	0.213	0.252	0.261
	(B)	50.01	50.04	50.08	0.032	0.041	0.051	0.107	0.113	0.126

Table 5.12 The results of Monte Carlo simulation studies under plant-model uncertainty for adaptive pole placement control

Load	Mean [Hz]			Standard Deviation [Hz]			Maximum Deviation [Hz]		
	Best Case	Average Case	Worst Case	Best Case	Average Case	Worst Case	Best Case	Average Case	Worst Case
Step	49.98	49.94	49.89	0.110	0.124	0.132	1.04	1.09	1.12
Periodic	50.11	50.17	50.23	0.233	0.282	0.294	0.28	0.34	0.38

5.5 Conclusion

The increased penetration of wind power into the power grid have required wind farms to participate in grid frequency and voltage regulation through control of active and reactive power, respectively. This work has been only focused on the frequency regulation through control of active power. Generally speaking, there is little to no interconnection between the active and reactive power control loops in wind farm controls. In fact, while reactive power may be controlled through the turbine's power electronics (even when the turbine is offline), real power is regulated by changing the actual amount of power delivered to the utility grid through, for example, pitching of the blades of the wind turbines.

This paper exploits adaptive pole placement control and fuzzy gain-scheduled proportional-integral (PI) control approaches to address the design of active power control at an entire wind farm level. The active power control is conducted collectively across a wind farm to provide rapid power response while maintaining safe structural loading on turbines' components. The developed schemes not only ensure safe and reliable connection of a wind farm to the electrical grid in terms of frequency regulation but also tolerate probable occurrence of sudden imbalance between generation and loads. Simulations have been conducted using an advanced wind farm benchmark model in the presence of wind turbulences, measurement noises, plant-model uncertainty, and grid loads variations. Simulation results clearly indicate the effectiveness of the developed active power control schemes over the entire range of tested wind field under both nominal and frequency event conditions. In particular, the active power control scheme based on adaptive pole placement control provides more efficient regulation of grid frequency while the scheme based on fuzzy gain-scheduled PI control indicates quicker reaction and recovery against frequency event.

Basically, in comparison with active power control at an individual turbine level, performing such a control collectively across a wind farm can be advantageous in terms of faster response and

recovery to grid frequency deviations. However, to determine the full capabilities of active power control in wind turbines, developing more comprehensive schemes that consider both individual wind turbine and entire farm levels remains as an interesting open problem for future work. In addition, it is worth mentioning that employing more realistic and comprehensive benchmark models is important towards realistic controller design and practical applications, while the modeling of wind farms from its basic levels to grid integration level is still an active area of research, as none of the available models is completely suitable.

Chapter 6 Conclusions and Suggestions for Future Work

6.1 Summary and Conclusions

The aim of this research work was to design and develop novel condition monitoring, diagnosis and fault-tolerant control schemes with application to wind turbines at both individual wind turbine and entire wind farm levels. In general, there exist several different types of sensor, actuator, and system faults which occur in wind turbines most frequently. In this thesis work, among sensor faults, two important fault scenarios have been investigated: 1) scaling generator speed sensor, and 2) biased blade-pitch angle sensor. These two sensor faults are so significant on the effect to the behavior of the wind turbine control system. Among actuator faults, the torque offset faults in generator/converter has been investigated. This fault disturbs the torque control action with high severity. Consequently, serious problems arise with successful tracking of the maximum power point and rated power in partial and full load regions, respectively. Among system faults, decreased power generation fault caused by turbine blade erosion and debris build-up on the blades over time has been considered and investigated. In fact, most of the common faults in wind turbines can be handled at an individual wind turbine level. However, there some faults that are easier to be detected, diagnosed, and accommodated at wind farm level through comparing the performance of turbines operating under almost the same wind conditions. With respect to the mentioned fact, the sensor and actuator faults considered in this thesis work are all handled at an individual wind turbine level. While, the system fault is handled within a wind farm level. Moreover, in general, sensor, actuator, and system faults are of different nature in some aspects. Therefore, there exists usually no individual FDD and FTC strategy that can handle all types of faults, in particular for wind turbine which is a highly integrated system with many process parameters being interacted together exhibiting complex and nonlinear behaviors.

With respect to the sensor faults, this thesis work, first, proposes a FGS technique to enhance a simple gain-scheduled PI-controller (the baseline pitch controller) to a FGS PI-control system for robust and improved regulation of generator speed. Second, to add active fault tolerance capabilities to the FGS PI-control system, a model-based FDD scheme has been developed using

fuzzy modeling and identification method. The FDD system provides fault information to be used in an AFTCS based on a signal correction approach. Simulations and verifications indicate that the AFTCS does not affect the nominal performance of FGS PI-control system and provides acceptable performance in the presence of sensor faults, which cannot be achieved with baseline PI-controller and even FGS PI-control system alone.

With respect to the actuator fault, two FTC schemes are proposed for reliable regulation of generator torque load in a wind turbine. The first scheme is a PFTCS based on a fuzzy model reference adaptive control approach in which a fuzzy inference mechanism is used for parameter adaptation without any explicit knowledge of the potential faults in the system and without the need of a fault detection and diagnosis system. The second scheme is an AFTCS which exploits an automatic signal correction approach that itself relies on a FDD system. Numerical results and simulation studies clearly indicate the effectiveness and robustness of the proposed schemes over the entire range of tested wind profiles for both the fault-free and faulty conditions. Although both the FTC schemes are superior to a reference torque control system designed using classical methods, the fault-tolerance and nominal performance provided by the AFTCS will make it a practical choice if the faults change the system's behavior significantly. The PFTCS should be favored when faults are difficult to diagnose (e.g., due to their small impact on system performance), or there is no tolerance for false decisions in the fault detection and diagnosis system.

With respect to the system fault, two AFTC schemes are proposed that each employs a FDD system to provide accurate and timely diagnosis information to be used in an appropriate automatic signal correction algorithm for accommodation of fault(s) in a wind farm. The first scheme is based on a model-free FDD system that incorporates a rule-based threshold test technique for residual evaluation. Conversely, the second scheme is based on a model-based FDD system that incorporates data-driven models developed using fuzzy modelling and identification technique. All simulation studies and numerical results clearly indicate the effectiveness and robustness of the schemes over the entire range of tested wind profiles for both the fault-free and faulty conditions. The fault-tolerance and nominal performance provided by the AFTC schemes make them an efficient and practical choice for wind farms. In particular, the fact that the proposed schemes employ an automatic signal correction algorithm for fault accommodation, and hence they do not disturb the nominal performance of a wind farm under normal (fault-free) operating conditions is

a remarkable feature. This feature is particularly favorable in the case of any already designed wind farm control systems whose structures are well defined for optimizing power capture in a farm while achieving fault-tolerance capability without scarifying best performance of the wind farm.

This thesis has also considered the problem of frequency regulation through control of active power in large wind farms. Both adaptive pole placement control and fuzzy gain-scheduled proportional-integral (PI) control approaches are used to address the design of active power control at an entire wind farm level. The active power control is conducted collectively across a wind farm to provide rapid power response while maintaining safe structural loading on turbines' components. The developed schemes not only ensure safe and reliable connection of a wind farm to the electrical grid in terms of frequency regulation but also tolerate probable occurrence of sudden imbalance between generation and loads. Simulation results clearly indicate the effectiveness of the developed active power control schemes over the entire range of tested wind field under both nominal and frequency event conditions. In particular, the active power control scheme based on adaptive pole placement control provides more efficient regulation of grid frequency while the scheme based on fuzzy gain-scheduled PI control indicates quicker reaction and recovery against frequency event.

6.2 Scope for Research and Future Work

FDD methods integrated with novel FTC algorithms constitute an emerging approach for justifying further development and investment in wind turbine technology and wind power penetration. The merits of the performed research work can be reflected by an anticipated significant contribution to the realization of a new concept and technology of self-diagnosing and fault-tolerant wind turbines. More specifically, the schemes proposed here will significantly advance the reliability, availability and thereby power generation of modern wind turbines while reducing the cost of unscheduled maintenance. The knowledge gained in this research will be transferable and find many applications in not only wind power industries but also relevant sustainable smart power grids, all of which are important to meet our nation's 21st century power demands with optimal reliability, quality and cost, while addressing the environmental concerns. In particular, should the reader be interested, the research performed in this thesis can be continued and extended in the form of future works as suggested below:

- *Considering new faults from all types of sensor, actuator, and system component faults*: in this thesis work, only a limited number of faults have been considered and investigated. In fact, extending the presented FDD and FTC strategies to diagnosis and accommodation of other types of faults like new sensor, actuator, and system component faults remain as an interesting future research topic.

- *Investigation of a collective FDD and FTC framework for wind turbines*: Although this thesis work proposes different FDD and FTC schemes for each specific type of fault, the integration of all schemes in an appropriate way so that a collective FDD and FTC framework can be formed seems an interesting future topic due to highly integrated nature of the system with many process parameters being interacted together exhibiting complex and nonlinear behaviors.

- *Considering further requirements before practical implementation of proposed schemes*: In fact, all proposed schemes in this thesis have been investigated using high-fidelity wind turbine and wind farm simulation benchmark models that are already verified and validated even by using field test data in some individual components. However, in order to achieve a practical fault-tolerant control scheme, the fault detection and diagnosis system as well as real-time control system reconfiguration/adaptation should be designed along with techniques in fault-tolerant computing, and fault-tolerant communication networks followed by hardware-in-the-loop testing for thorough evaluation before real system tests.

- *Extension and investigation of proposed FDD and FTC schemes in higher level applications:* As a future work, the proposed schemes in this thesis can be effectively extended and applied to other levels of power generation, integration into grid, and distribution in Microgrids with sustainable distributed power systems, in particular wind power.

References

[1] WWEA, "World Wind Energy Report " 2012.

[2] B. Wu, Y. Lang, N. Zargari, and S. Kouro, *Power Conversion and Control of Wind Energy Systems*: Wiley-IEEE Press, 2011.

[3] P. Odgaard, J. Stoustrup, and M. Kinnaert, "Fault Tolerant Control of Wind Turbines - a Benchmark Model," in *the 7th IFAC Symposium on Fault Detection, Supervision and Safety of Technical Processes*, Spain, 2009, pp. 155–160.

[4] T. Esbensen and C. Sloth, "Fault Diagnosis and Fault-Tolerant Control of Wind Turbines," Master's Thesis, Aalborg University, Denmark, 2009.

[5] EWEA, "Wind Energy, the Facts, European Wind Energy Association (EWEA)," Brussels, Belgium, 2009.

[6] S. Faulstich, M. Durstewitz, B. Hahn, K. Knorr, and K. Rohrig, "German Wind Energy Report 2008," Institut für Solare Energieversorgungstechnik (ISET), Kassel, Germany, 2008.

[7] S. Faulstich, B. Hahn, and P. J. Tavner, "Wind Turbine Downtime and Its Importance for Offshore Deployment," *Wind Energy,* vol. 14, pp. 327-337, 2011.

[8] R. Isermann, *Fault-Diagnosis Systems: An Introduction from Fault Detection to Fault Tolerance*: Springer, 2006.

[9] M. Blanke, M. Kinnaert, J. Lunze, and M. Staroswiecki, *Diagnosis and Fault-Tolerant Control*. Germany: Springer, 2006.

[10] Y. M. Zhang and J. Jiang, "Bibliographical Review on Reconfigurable Fault-Tolerant Control Systems," *Annual Reviews in Control,* vol. 32, pp. 229-252, 2008.

[11] S. Pourmohammad and A. Fekih, "Fault-Tolerant Control of Wind Turbine Systems - A Review," in *IEEE Green Technologies Conference (IEEE-Green)*, Baton Rouge, LA, USA, 2011.

[12] Z. Hameed, Y. S. Hong, Y. M. Cho, S. H. Ahn, and C. K. Song, "Condition Monitoring and Fault Detection of Wind Turbines and Related Algorithms: A Review," *Renewable and Sustainable Energy Reviews,* vol. 13, pp. 1-39, 2009.

[13] B. Lu, Y. Li, X. Wu, and Z. Yang, "A Review of Recent Advances in Wind Turbine Condition Monitoring and Fault Diagnosis," in *IEEE Conference on Power Electronics and Machines in Wind Applications*, Lincoln, NE, USA, 2009, pp. 1-7.

[14] Y. Amirat, M. E. H. Benbouzid, B. Bensaker, and R. Wamkeue, "Condition Monitoring and Fault Diagnosis in Wind Energy Conversion Systems: A Review," in *IEEE International Electric Machines & Drives Conference*, Antalya, Turkey, 2007, pp. 1434-1439.

[15] J. F. Manwell, J. G. McGowan, and A. L. Rogers, *Wind Energy Explained: Theory, Design and Application*. UK: John Wiley & Sons Ltd, 2010.

[16] F. Bianchi, H. De Battista, and R. Mantz, *Wind Turbine Control Systems: Principles, Modelling and Gain Scheduling Design*. Germany: Springer Verlag, 2007.

[17] H. Badihi, Y. M. Zhang, and H. Hong, "A Review on Application of Monitoring, Diagnosis, and Fault-Tolerant Control to Wind Turbines," in *Proc. of International Conference on Control and Fault-Tolerant Systems (SysTol'13)*, Nice, France, 2013.

[18] R. W. Hyers, J. G. Mcgowan, K. L. Sullivan, J. F. Manwell, and B. C. Syrett, "Condition Monitoring and Prognosis of Utility Scale Wind Turbines," *Energy Materials,* vol. 1, 2006.

[19] X. Gong, "Online Nonintrusive Condition Monitoring and Fault Detection for Wind Turbines," Ph.D. Thesis, University of Nebraska, USA, 2012.

[20] J. Ribrant and L. M. Bertling, "Survey of Failures in Wind Power Systems with Focus on Swedish Wind Power Plants During 1997-2005," *IEEE Transactions on Energy Conversion,* vol. 22, pp. 167-173, 2007.

[21] S. Donders, "Fault Detection and Identication for Wind Turbine Systems: a Closed-Loop Analysis," Master's Thesis, Faculty of Applied Physics Systems and Control Engineering, University of Twente, 2002.

[22] X. Wei and M. Verhaegen, "Fault Detection of Large Scale Wind Turbine Systems: A Mixed H_∞=H- Index Observer Approach," in *Proceedings of 16th Mediterranean Conference on Control and Automation*, France, 2008, pp. 1675-1680.

[23] W. Chen, S. X. Ding, A. Haghani, A. Naik, A. Q. Khan, and S. Yin, "Observer-based FDI Schemes for Wind Turbine Benchmark," in *18th IFAC World Congress*, Italy, 2011.

[24] F. Kiasi, J. Prakash, S. L. Shah, and J. M. Lee, "Fault Detection and Isolation of a Benchmark Wind Turbine using the Likelihood Ratio Test," in *18th IFAC World Congress*, Italy, 2011.

[25] X. Zhang, Q. Zhang, S. Zhao, R. Ferrari, M. M. Polycarpou, and T. Parisini, "Fault Detection and Isolation of the Wind Turbine Benchmark: an Estimation-based Approach," in *18th IFAC World Congress*, Italy, 2011.

[26] J. Dong and M. Verhaegen, "Data Driven Fault Detection and Isolation of a Wind Turbine Benchmark," in *18th IFAC World Congress*, Italy, 2011.

[27] P. F. Odgaard and J. Stoustrup, "Unknown Input Observer Based Detection of Sensor Faults in a Wind Turbine," in *IEEE International Conference on Control Applications*, Japan, 2010, pp. 310-315.

[28] P. Pisu and B. Ayalew, "Robust Fault Diagnosis for a Horizontal Axis Wind Turbine," in *18th IFAC World Congress*, Italy, 2011.

[29] S. M. Tabatabaeipour, P. F. Odgaard, and T. Bak, "Fault Detection of a Benchmark Wind Turbine using Interval Analysis," in *Proc. of American Control Conference (ACC)*, Montreal, QC, 2012, pp. 4387–4392.

[30] S. M. Tabatabaeipour, P. F. Odgaard, T. Bak, and J. Stoustrup, "Fault Detection of Wind Turbines with Uncertain Parameters: A Set-Membership Approach," *Energies,* vol. 5, pp. 2424-2448, 2012.

[31] N. Laouti, N. Sheibat-Othman, and S. Othman, "Support Vector Machines for Fault Detection in Wind Turbines," in *18th IFAC World Congress*, Italy, 2011.

[32] S. Simani, P. Castaldi, and A. Tilli, "Data–Driven Approach for Wind Turbine Actuator and Sensor Fault Detection and Isolation," in *Proc. of the 18th IFAC World Congress*, Italy, 2011.

[33] H. Badihi, Y. M. Zhang, and H. Hong, "Fuzzy Gain-Scheduled Active Fault-Tolerant Control of a Wind Turbine," *Journal of the Franklin Institute,* vol. 351, pp. 3677–3706, 2014.

[34] H. Badihi, Y. M. Zhang, and H. Hong, "An Active Fault-Tolerant Control Approach to Wind Turbine Torque Load Control against Actuator Faults," in *Proc. of AIAA SciTech 2014*, Maryland, USA, 2014.

[35] S. Simani, P. Castaldi, and M. Bonfe, "Hybrid Model Based Fault Detection of Wind Turbine Sensors," in *Proc. of the 18th IFAC World Congress*, Italy, 2011.

[36] T. Burton, D. Sharpe, N. Jenkins, and E. Bossanyi, *Wind Energy Handbook*: John Wiley, 2001.

[37] M. A. Ayoubi and L.-C. Tai, "Intelligent Control of a Large Variable Speed Wind Turbine," *Journal of Solar Energy Engineering,* vol. 134, 2012.

[38] S. Simani, "Application of a Data-Driven Fuzzy Control Design to a Wind Turbine Benchmark Model," *Advances in Fuzzy Systems,* vol. 2012, 2012.

[39] F. Lescher, J.-Y. Zhao, and P. Borne, "Switching LPV Controllers for a Variable Speed Pitch Regulated Wind Turbine," *International Journal of Computers Communications & Control,* vol. 1, pp. 73-84, 2006.

[40] K. Z. Østergaard, J. Stoustrup, and P. Brath, "Linear Parameter Varying Control of Wind Turbines Covering Both Partial Load and Full Load Conditions," *International Journal of Robust and Nonlinear Control,* vol. 19, pp. 92-116, 2009.

[41] K. A. Stol and M. J. Balas, "Periodic Disturbance Accommodating Control for Blade Load Mitigation in Wind Turbines," *Journal of Solar Energy Engineering,* vol. 125, pp. 379-385, 2003.

[42] R. Santos, "Damage Mitigating Control for Wind Turbines," Ph.D. Thesis, University of Colorado at Boulder, USA, 2007.

[43] C. Sloth, T. Esbensen, and J. Stoustrup, "Robust and Fault-Tolerant Linear Parameter-Varying Control of Wind Turbines," *Mechatronics,* vol. 21, pp. 645-659, 2011.

[44] L. L. Fan and Y. D. Song, "Neuro-Adaptive Model-Reference Fault-Tolerant Control with Application to Wind Turbines," *IET Control Theory & Applications,* vol. 6, pp. 475-486, 2012.

[45] H. Badihi, Y. M. Zhang, and H. Hong, "Model Reference Adaptive Fault-Tolerant Control for a Wind Turbine against Actuator Faults," in *Proc. of International Conference on Control and Fault-Tolerant Systems (SysTol'13)*, Nice, France, 2013.

[46] S. Simani and P. Castaldi, "Active Actuator Fault-Tolerant Control of a Wind Turbine Benchmark Model," *International Journal of Robust and Nonlinear Control,* vol. 24, pp. 1283–1303, 2014.

[47] P. F. Odgaard and J. Stoustrup, "Fault Tolerant Control of Wind Turbines using Unknown Input Observers," in *8th IFAC Symposium on Fault Detection, Supervision and Safety of Technical Processes*, Mexico City, Mexico, 2012.

[48] P. Casau, P. Rosa, S. M. Tabatabaeipour, and C. Silvestre, "Fault Detection and Isolation and Fault Tolerant Control of Wind Turbines using Set-Valued Observers," in *8th IFAC Symposium on Fault Detection, Supervision and Safety of Technical Processes*, Mexico City, Mexico, 2012.

[49] D. Rotondo, F. Nejjari, V. Puig, and J. Blesa, "Fault Tolerant Control of the Wind Turbine Benchmark using Virtual Sensors/Actuators," in *8th IFAC Symposium on Fault Detection, Supervision and Safety of Technical Processes*, Mexico City, Mexico, 2012.

[50] X. Yang and J. M. Maciejowski, "Fault-tolerant Model Predictive Control of a Wind Turbine Benchmark," in *8th IFAC Symposium on Fault Detection, Supervision and Safety of Technical Processes*, Mexico City, Mexico, 2012.

[51] S. Simani and P. Castaldi, "Adaptive Fault-Tolerant Control Design Approach for a Wind Turbine Benchmark," in *Proc. of the 8th IFAC Symposium on Fault Detection, Supervision and Safety of Technical Processes*, Mexico City, Mexico, 2012.

[52] M. Sami and R. J. Patton, "Global Wind Turbine FTC via T-S Fuzzy Modelling and Control," in *8th IFAC Symposium on Fault Detection, Supervision and Safety of Technical Processes*, Mexico City, Mexico, 2012.

[53] M. Sami and R. J. Patton, "An FTC Approach to Wind Turbine Power Maximisation via T-S Fuzzy Modelling and Control," in *8th IFAC Symposium on Fault Detection, Supervision and Safety of Technical Processes*, Mexico City, Mexico, 2012.

[54] E. Kamal, A. Aitouche, R. Ghorbani, and M. Bayart, "Robust Fuzzy Fault-Tolerant Control of Wind Energy Conversion Systems Subject to Sensor Faults," *IEEE Transactions on Sustainable Energy,* vol. 3, pp. 231- 241, 2012.

[55] S. Simani and P. Castaldi, "Data–Driven Design of Fuzzy Logic Fault Tolerant Control for a Wind Turbine Benchmark," in *Proc. of the 8th IFAC Symposium on Fault Detection, Supervision and Safety of Technical Processes*, Mexico City, Mexico, 2012.

[56] K. E. Johnson and N. Thomas, "Wind Farm Control: Addressing the Aerodynamic Interaction among Wind Turbines," in *Proc. of American Control Conference (ACC)*, St. Louis, MO, 2009, pp. 2104-2109.

[57] L. Y. Pao and K. E. Johnson, "A Tutorial on the Dynamics and Control of Wind Turbines and Wind Farms," in *Proc. of American Control Conference (ACC)*, St. Louis, MO, 2009, pp. 2076-2089.

[58] M. Kristalny and D. Madjidian, "Decentralized Feedforward Control of Wind Farms: Prospects and Open Problems," in *Proc. of 50th IEEE Conference on Decision and Control and European Control Conference (CDC-ECC)*, Orlando, FL, 2011, pp. 3464-3469.

[59] V. Spudić, M. Jelavić, M. Baotić, and N. Perić, "Hierarchical Wind Farm Control for Power/Load Optimization," in *Proc. of Conf. of the Science of Making Torque from Wind*, Greece, 2010, pp. 681-692.

[60] V. Spudić, M. Jelavić, and M. Baotić, "Wind Turbine Power Control for Coordinated Control of Wind Farms," in *Proc. of the 18th International Conference on Process Control*, Slovakia, 2011, pp. 463–468.

[61] A. J. Brand, "A Quasi-Steady Wind Farm Control Model," in *Proc. of Eur. Wind Energy Conf.*, Belgium, 2011, pp. 1–40.

[62] M. Soleimanzadeh and R. Wisniewski, "Controller Design for a Wind Farm, Considering both Power and Load Aspects," *Mechatronics,* vol. 21, pp. 720-727, 2011.

[63] M. Soleimanzadeh, R. Wisniewski, and S. Kanev, "An Optimization Framework for Load and Power Distribution in Wind Farms," *Journal of Wind Engineering and Industrial Aerodynamics,* vol. 107–108, pp. 256-262, 2012.

[64] D. Madjidian and A. Rantzer, "A Stationary Turbine Interaction Model for Control of Wind Farms," in *Proc. of the 18th IFAC World Congress*, Italy, 2011, pp. 1–6.

[65] J. R. Marden, S. D. Ruben, and L. Y. Pao, "A Model-Free Approach to Wind Farm Control Using Game Theoretic Methods," *IEEE Transactions on Control Systems Technology,* vol. 21, pp. 1207-1214, 2013.

[66] J. Aho, A. Buckspan, J. Laks, Y. Jeong, F. Dunne, and L. Pao, "Tutorial of Wind Turbine Control for Supporting Grid Frequency through Active Power Control," in *American Control Conference*, Montreal, Canada, 2012.

[67] A. Kusiak and A. Verma, " A Data-Driven Approach for Monitoring Blade Pitch Faults in Wind Turbines," *IEEE Transactions on Sustainable Energy,* vol. 2, pp. 87–96, 2011.

[68] A. Kusiak and A. Verma, "A Data-Mining Approach to Monitoring Wind Turbines," *IEEE Transactions on Sustainable Energy,* vol. 3, pp. 150-157, 2012.

[69] P. F. Odgaard and K. E. Johnson, "Wind Turbine Fault Diagnosis and Fault Tolerant Control - an Enhanced Benchmark Challenge," in *Proc. of American Control Conference (ACC)*, Washington, DC, USA, 2013.

[70] J. Jonkman, S. Butterfield, W. Musial, and G. Scott, "Definition of a 5 MW Reference Wind Turbine for Offshore System Development," National Renewable Energy Laboratory, Colorado, USA, 2009.

[71] J. Jonkman and M. Buhl., "FAST User's Guide," National Renewable Energy Laboratory, Colorado, USA2005.

[72] http://www.awea.org.

[73] P. F. Odgaard and J. Stoustrup, "Results of a Wind Turbine FDI Competition," in *the 8th IFAC Symposium on Fault Detection, Supervision and Safety of Technical Processes*, Mexico City, Mexico, 2012.

[74] J. Liu, D. Xu, and X. Yang, "Sensor Fault Detection in Variable Speed Wind Turbine System Using H- /H∞ Method," in *the 7th World Congress on Intelligent Control and Automation*, Chongqing, 2008, pp. 4265-4269.

[75] P. F. Odgaard, J. Stoustrup, R. Nielsen, and C. Damgaard, "Observer Based Detection of Sensor Faults in Wind Turbines," presented at the European Wind Energy Conference, France, 2009.

[76] C. Svärd and M. Nyberg, "Automated Design of an FDI System for the Wind Turbine Benchmark," *Journal of Control Science and Engineering,* vol. 2012, 2012.

[77] X. Wei and M. Verhaegen, "Sensor and Actuator Fault Diagnosis for Wind Turbine Systems by Using Robust Observer and Filter," *Wind Energy,* vol. 14, pp. 491-516, 2011.

[78] T. Takagi and M. Sugeno, "Fuzzy Identification of Systems and Its Applications to Modeling and Control," *IEEE Transactions on Systems, Man, and Cybernetics,* vol. 15, pp. 116-132, 1985.

[79] G. Feng, "A Survey on Analysis and Design of Model-Based Fuzzy Control Systems," *IEEE Transactions on Fuzzy Systems,* vol. 14, pp. 676- 697, 2006.

[80] Q. Zhou, P. Shi, J. Lu, and S. Xu, "Adaptive Output-Feedback Fuzzy Tracking Control for a Class of Nonlinear Systems," *IEEE Transactions on Fuzzy Systems,* vol. 19, pp. 972-982, 2011.

[81] J. Qiu, G. Feng, and H. Gao, "Fuzzy-Model-Based Piecewise H∞ Static-Output-Feedback Controller Design for Networked Nonlinear Systems," *IEEE Transactions on Fuzzy Systems,* vol. 18, pp. 919-934, 2010.

[82] J. Qiu, G. Feng, and H. Gao, "Observer-Based Piecewise Affine Output Feedback Controller Synthesis of Continuous-Time T-S Fuzzy Affine Dynamic Systems Using Quantized Measurements," *IEEE Transactions on Fuzzy Systems,* vol. 20, pp. 1046-1062, 2012.

[83] G. Feng, *Analysis and Synthesis of Fuzzy Control Systems: A Model-Based Approach*. CRC Press, Boca Raton, FL, 2010.

[84] H. Li, H. Liu, H. Gao, and P. Shi, "Reliable Fuzzy Control for Active Suspension Systems With Actuator Delay and Fault," *IEEE Transactions on Fuzzy Systems,* vol. 20, pp. 342-357, 2012.

[85] B. Chen and X. Liu, "Reliable Control Design of Fuzzy Dynamic Systems with Time-Varying Delay," *Fuzzy Sets and Systems,* vol. 146, pp. 349–374, 2004.

[86] H. Wu and H. Zhang, "Reliable H∞ Fuzzy Control for Continuous-Time Nonlinear Systems with Actuator Failures," *IEEE Transactions on Fuzzy Systems,* vol. 14, pp. 609–618, 2006.

[87] S. Nguang, P. Shi, and S. Ding, "Fault Detection for Uncertain Fuzzy Systems: An LMI Approach," *IEEE Transactions on Fuzzy Systems,* vol. 15, pp. 1251–1262, 2007.

[88] V. Galdi, A. Piccolo, and P. Siano, "Designing an Adaptive Fuzzy Controller for Maximum Wind Energy Extraction," *IEEE Transactions on Energy Conversion,* vol. 23, pp. 559-569, 2008.

[89] C. Jauch, T. Cronin, P. Sørensen, and B. B. Jensen, "A Fuzzy Logic Pitch Angle Controller for Power System Stabilization," *Wind Energy,* vol. 10, pp. 19-30, 2007.

[90] W.-M. Lin, C.-M. Hong, and F.-S. Cheng, "Fuzzy Neural Network Output Maximization Control for Sensorless Wind Energy Conversion System," *Energy,* vol. 35, pp. 592-601, 2010.

[91] S. Simani, "Data–Driven Design of a PI Fuzzy Controller for a Wind Turbine Simulated Model," in *Proc. of the IFAC Conference on Advances in PID Control*, Brescia, Italy, 2012.

[92] S. Chiu, "Using Fuzzy Logic in Control Applications: Beyond Fuzzy PID Control," *Control Systems, IEEE,* vol. 18, pp. 100-104, 1998.

[93] Z.-Y. Zhao, M. Tomizuka, and S. Isaka, "Fuzzy Gain Scheduling of PID Controllers," *IEEE Transactions on Systems, Man and Cybernetics,* vol. 23, pp. 1392-1398, 1993.

[94] M. H. Hansen, A. Hansen, T. J. Larsen, S. Φye, P. Sørensen, and P. Fuglsang, "Control Design for a Pitch-Regulated, Variable Speed Wind Turbine," Roskilde, Denmark: Risø National Laboratory, 2005.

[95] J. G. Ziegler and N. B. Nichols, "Optimum Settings for Automatic Controllers," *Transactions of the ASME,* vol. 64, pp. 759-768, 1942.

[96] L. F. Mendonça, J. M. C. Sousa, and J. M. G. Sá da Costa, "An Architecture for Fault Detection and Isolation Based on Fuzzy Methods," *Expert Systems with Applications,* vol. 36, pp. 1092-1104, 2009.

[97] R. Babuska, *Fuzzy Modeling for Control*. Springer: Kluwer Academic Publishers, 1998.

[98] D. E. Gustafson and W. C. Kessel, " Fuzzy Clustering With a Fuzzy Covariance Matrix," in *IEEE Conference on Decision and Control*, San Diego, CA, USA, 1978, pp. 761–766.

[99] L. Y. Pao and K. E. Johnson, "Control of Wind Turbines; Approaches, Challenges, and Rescent Developments," *IEEE Control Systems Magazine,* April, 2011.

[100] A. D. Wright and L. J. Fingersh, "Advanced Control Design for Wind Turbines - Part I: Control Design, Implementation, and Initial Tests," National Renewable Energy Laboratory, Colorado, USA, 2008.

[101] P. F. Odgaard, J. Stoustrup, and M. Kinnaert, "Fault-Tolerant Control of Wind Turbines: A Benchmark Model," *IEEE Transactions on Control Systems Technology,* vol. 21, pp. 1168-1182, 2013.

[102] E. Kamal, A. Aitouche, R. Ghorbani, and M. Bayart, "Fuzzy Scheduler Fault-Tolerant Control for Wind Energy Conversion Systems," *IEEE Transactions on Control Systems Technology,* vol. 22, pp. 119-131, 2014.

[103] L. Ljung, *System Identification: Theory for the User*, 2nd ed. Englewood Cliffs, N.J.: Prentice-Hall, 1999.

[104] H. Badihi, Y. M. Zhang, and H. Hong, "Wind Turbine Fault Diagnosis and Fault-Tolerant Torque Load Control against Actuator Faults," *IEEE Transactions on Control Systems Technology,* vol. 23, pp. 1351-1372, 2015.

[105] A. Marvuglia and A. Messineo, "Monitoring of Wind Farms' Power Curves using Machine Learning Techniques," *Applied Energy,* vol. 98, pp. 574-583, 2012.

[106] P. F. Odgaard and J. Stoustrup, "Fault Tolerant Wind Farm Control — A Benchmark Model," in *Proc. of IEEE International Conference on Control Applications*, Hyderabad, India, 2013, pp. 412-417.

[107] S. Simani, S. Farsoni, and P. Castaldi, "Residual Generator Fuzzy Identification for Wind Farm Fault Diagnosis," in *Proc. of the 19th IFAC World Congress*, Cape Town, South Africa, 2014.

[108] E. Duviella, L. Serir, and M. Sayed-Mouchaweh, "An Evolving Classification Approach for Fault Diagnosis and Prognosis of a Wind Farm," in *Proc. of the 2nd Conference on Control Fault-Tolerant Systems*, Nice, France, 2013, pp. 377–382.

[109] J. Blesa, P. Jiménez, D. Rotondo, F. Nejjari, and Vicenç Puig, "An Interval NLPV Parity Equations Approach for Fault Detection and Isolation of a Wind Farm," *IEEE Transactions on Industrial Electronics,* vol. 62, pp. 3794-3805, 2015.

[110] A. B. Borcehrsen, J. A. Larsen, and J. Stoustrup, "Fault Detection and Load Distribution for the Wind Farm Challenge," in *Proc. of the 19th World Congress of the International Federation of Automatic Control*, Cape Town, South Africa, 2014.

[111] H. Badihi, Y. M. Zhang, and H. Hong, "Active Fault Tolerant Control in a Wind Farm with Decreased Power Generation Due to Blade Erosion/Debris Build-Up," *IFAC-PapersOnLine,* vol. 48, pp. 1369-1374, 2015.

[112] M. Soltani, T. Knudsen, and T. Bak, "Modeling and Simulation of Offshore Wind Farms for Farm Level Control," in *European Offshore Wind Conference and Exhibition (EOW)*, Stockholm, Sweden, 2009.

[113] L. Fingersh and P. Carlin, "Results from the NREL Variable-Speed Test Bed," in *Proc. of the 17th ASME Wind Energy Symp.*, NV, USA, 1998, pp. 233–237.

[114] F. Shi and R. J. Patton, "An Active Fault Tolerant Control Approach to an Offshore Wind Turbine Model," *Renewable Energy,* vol. 75, pp. 788–798, 2015.

[115] M. S. Shaker and R. J. Patton, "Active Sensor Fault Tolerant Output Feedback Tracking Control for Wind Turbine Systems via T–S Model," *Engineering Applications of Artificial Intelligence,* vol. 34, pp. 1-12, 2014.

[116] *Global Wind Energy Council [online], Available: www.gwec.net.*

[117] Hydro-Québec, "Technical Requirements for the Connection of Generation Facilites to the Hydro-Québec Transmission System: Supplementary Requirements for Wind Generation," Hydro-Québec, Montreal, Québec, Canada2005.

[118] H. Ma and B. Chowdhury, "Working Towards Frequency Regulation with Wind Plants: Combined Control Approaches," *IET Renewable Power Generation,* vol. 4, pp. 308–316, 2010.

[119] X. Juankorena, I. Esandi, J. Lopez, and L. Marroyo, "Method to Enable Variable Speed Wind Turbine Primary Regulation," in *International Conference on Power Engineering, Energy and Electrical Drives*, Lisbon, 2009, pp. 495–500.

[120] I. Gowaid, A. El-Zawawi, and M. El-Gammal, "Improved Inertia and Frequency Support from Grid-Connected DFIG Wind Farms," in *Power Systems Conference and Exposition*, Phoenix, AZ, 2011.

[121] J. Morren, S. d. Haan, W. Kling, and J. Ferreira, "Wind Turbines Emulating Inertia and Supporting Primary Frequency Control," *IEEE Transactions on Power Systems,* vol. 21, pp. 433–434, 2006.

[122] D. Gautam, L. Goel, R. Ayyanar, V. Vittal, and T. Harbour, "Control Strategy to Mitigate the Impact of Reduced Inertia Due to Doubly Fed Induction Generators on Large Power Systems," *IEEE Transactions on Power Systems,* vol. 26, pp. 214–224, 2011.

[123] A. Buckspan, J. Aho, P. Fleming, J. Yunho, and L. Pao, "Combining Droop Curve Concepts with Control Systems for Wind Turbine Active Power Control," in *Proc. of IEEE Power Electronics and Machines in Wind Applications*, Denver, CO, 2012, pp. 1-8.

[124] J. Aho, L. Pao, A. Buckspan, and P. Fleming, "An Active Power Control System for Wind Turbines Capable of Primary and Secondary Frequency Control for Supporting Grid Reliability," in *Proc. of the 51st AIAA Aerospace Sciences Meeting Including the New Horizons Forum and Aerospace Exposition*, TX, USA, 2013.

[125] X. Yuan, J. Chai, and Y. Li, "Control of Variable Pitch, Variable Speed Wind Turbine in Weak Grid Systems," in *Proc. of IEEE Energy Conversion Congress and Exposition*, Atlanta, GA, 2010, pp. 3778–3785.

[126] L.-R. Chang-Chien, C.-M. Hung, and Y.-C. Yin, "Dynamic Reserve Allocation for System Contingency by DFIG Wind Farms," *IEEE Transactions on Power Systems,* vol. 23, pp. 729–736, 2008.

[127] K. J. Åström and T. Hägglund, *PID Controllers: Theory, Design, and Tuning*, 2nd ed. North Carolina: Instrument Society of America, 1995.

[128] K. Jin-Sung, J. Jonghyun, and H. Hoon, "Design of adaptive PID for pitch control of large wind turbine generator," in *10th International Conference on Environment and Electrical Engineering*, Rome, Italy, 2011, pp. 1-4.

[129] S. Simani and P. Castaldi, "Data-Driven and Adaptive Control Applications to a Wind Turbine Benchmark Model," *Control Engineering Practice,* vol. 21, pp. 1678-1693, 2013.

[130] K. J. Åström and T. Hägglund, "Revisiting the Ziegler-Nichols Step Response Method for PID Control," *Journal of Process Control,* vol. 14, pp. 635-650, 2004.

[131] R. Kulhavý, "Restricted Exponential Forgetting in Real–time Identification," *Automatica,* vol. 23, pp. 589–600, 1987.

[132] V. Bobál, J. Böhm, J. Fessl, and J. Machácek, *Digital Self–Tuning Controllers: Algorithms, Implementation and Applications*, 1st ed.: Springer, 2005.

[133] M. Buhl, "MCrunch User's Guide for Version 1.00," National Renewable Energy Lab, Tech. Rep., 2008.